INFORMATION TO USERS

This manuscript has been reproduced from the microfilm master. UMI films the text directly from the original or copy submitted. Thus, some thesis and dissertation copies are in typewriter face, while others may be from any type of computer printer.

The quality of this reproduction is dependent upon the quality of the copy submitted. Broken or indistinct print, colored or poor quality illustrations and photographs, print bleedthrough, substandard margins, and improper alignment can adversely affect reproduction.

In the unlikely event that the author did not send UMI a complete manuscript and there are missing pages, these will be noted. Also, if unauthorized copyright material had to be removed, a note will indicate the deletion.

Oversize materials (e.g., maps, drawings, charts) are reproduced by sectioning the original, beginning at the upper left-hand corner and continuing from left to right in equal sections with small overlaps.

Photographs included in the original manuscript have been reproduced xerographically in this copy. Higher quality 6" x 9" black and white photographic prints are available for any photographs or illustrations appearing in this copy for an additional charge. Contact UMI directly to order.

ProQuest Information and Learning
300 North Zeeb Road, Ann Arbor, MI 48106-1346 USA
800-521-0600

UMI®

University of Alberta

Mechanistic Studies of an Enantioselective Hydrogenation Catalyzed by a Ruthenium–BINAP Complex

by

Jason Allan Wiles

A thesis submitted to the Faculty of Graduate Studies and Research in partial fulfillment of the requirements for the degree of Doctor of Philosophy

Department of Chemistry

Edmonton, Alberta

Spring 2000

University of Alberta

Library Release Form

Name of Author: Jason Allan Wiles

Title of Thesis: Mechanistic Studies of an Enantioselective Hydrogenation Catalyzed by a Ruthenium–BINAP Complex

Degree: Doctor of Philosophy

Year this Degree Granted: 2000

Jason Allan Wiles
#804, 11635 102 Avenue
Edmonton, AB T5K 0R4
Canada

Dec 20 1999

University of Alberta

Faculty of Graduate Studies and Research

The undersigned certify that they have read, and recommend to the Faculty of Graduate Studies and Research for acceptance, a thesis entitled *Mechanistic Studies of an Enantioselective Hydrogenation Catalyzed by a Ruthenium–BINAP Complex* submitted by Jason Allan Wiles in partial fulfillment of the requirements for the degree of Doctor of Philosophy.

Professor Steven H. Bergens

Professor Josef Takats

Professor Robert B. Jordan

Professor Mariusz Klobukowski

Professor Edward E. Knaus

Professor Brice Bosnich

Dec. 17 S.B. 1999

In loving memory of my father,

Allan Oswald Wiles

(1938–1999)

Abstract

[Ru((*R*)-BINAP)(1–3:5,6-η-C_8H_{11})(MeCN)]BF_4 (**1**; BINAP is 2,2'-bis(diphenylphosphino)-1,1'-binaphthyl) rapidly reacts with an excess of dihydrogen gas in solutions of weakly coordinating solvents to generate cyclooctane and [Ru((*R*)-BINAP)(H)-$(MeCN)_n(sol)_{3-n}$]BF_4 (**2**; n = 0–3, sol = acetone, methanol, or THF, depending on reaction medium). Complex **2** catalyzes the enantioselective hydrogenation of the olefinic substrate MAC (methyl α-acetamidocinnamate) to give (*R*)-$MAC(H)_2$ (*N*-acetylphenylalanine methyl ester) in up to 94% ee. The mechanism of this catalytic hydrogenation was investigated using in situ NMR spectroscopy, and by comparing the stereochemistry and regiochemistry of deuterium-labeling studies conducted on the catalytic reaction to those conducted on an isolated possible catalytic intermediate. This isolated species is the olefin–hydride insertion product [Ru((*R*)-BINAP)((*S*)-MAC(H))(MeCN)]BF_4 (($S_{C\alpha}$)-**3**) that is formed by both catalytic and stoichiometric reactions of the active catalyst **2** with the substrate MAC. Complex ($S_{C\alpha}$)-**3** is the only ruthenium species present in detectable amounts (by NMR) during the catalytic hydrogenation of MAC at room temperature. The absolute configuration (determined by X-ray diffraction) at the stereogenic α-carbon of MAC(H) in ($S_{C\alpha}$)-**3** is the same (assuming stereospecific replacement of ruthenium with hydrogen) as that of the major product enantiomer of the catalytic hydrogenation. The structure and the absolute configuration of the predecessor complex of ($S_{C\alpha}$)-**3**, the transient catalyst–substrate adduct [Ru((*R*)-BINAP)(H)(MAC)(MeCN)]BF_4 (*si*-**4**), was determined by low-temperature NMR methods. The hydrido–olefin species *si*-**4** is of the

same absolute configuration as ($S_{C\alpha}$)-**3**, and it undergoes direct first-order olefin–hydride insertion to generate ($S_{C\alpha}$)-**3**. Results obtained from the stoichiometric hydrogenolysis and deuteriolysis of ($S_{C\alpha}$)-**3**, from the catalytic deuteration of (*E*)-MAC and (*Z*)-MAC, and from the reaction of ($S_{C\alpha}$)-**3** with excess (*Z*)-MAC-CO_2CD_3 all indicate that formation of ($S_{C\alpha}$)-**3** is rapid and reversible prior to the irreversible hydrogenolysis of the ruthenium–carbon bond. The sum of the stereoselectivities and regioselectivities of the formation and hydrogenolysis of ($S_{C\alpha}$)-**3** equals the overall stereoselectivity and regioselectivity of the catalytic hydrogenation. Solvolysis of the ruthenium–carbon bond occurs to less than 4% during the catalytic hydrogenation conducted in methanol. Removal of MeCN from the catalyst system has no effect on the enantioselectivity of the catalytic hydrogenation, but causes a significant increase in rate.

Acknowledgment

The success of any research project relies heavily on the enthusiasm and cohesiveness of the people involved. This project was not an exception. The work described in this thesis would have been more difficult, and certainly less rewarding, without the assistance of, and the daily interaction with, numerous individuals.

I thank my advisor and mentor, Steve Bergens, for guidance and words of wisdom throughout this project. I wish to thank all of the group members (both past and present) and, in particular, Chris Daley for numerous chemical (and sporting) discussions, for many helpful suggestions, for being an energetic spirit in the laboratory, and for being a wonderful friend.

I sincerely appreciate the efforts of the talented people in the NMR Laboratory, Structure Determination Laboratory, Mass Spectrometry Laboratory, Spectral Services Laboratory, Microanalysis Laboratory, Glassblowing Shop, Electronic Instrument Services, and Machine Shop. I owe special thanks to the following three individuals of the NMR Laboratory: Gerdy Aarts, Glen Bigam, and Tom Nakashima. A large portion of the work presented in this thesis would not have been possible without the considerable skills of these three individuals. Specifically, I am indebted to Glen Bigam for his enthusiasm toward this project, and for always providing more than was ever requested of him. I must also thank Bob McDonald of the Structure Determination Laboratory for his assistance with calculations, database searches, and preparation of manuscripts. I also wish to thank Jackie Jorgenson for her help with preparation of manuscripts and other essential duties, regardless of insufficient notice.

I also thank the following great group of friends for providing five years of memorable lunch-time conversations, coffee conversations, weekend activities, and assorted fun times: Jason Cooke, Chris Daley, Steve Decker, Mike Ferguson, Greg Ferrence, Rob Lam, Chris Lee, Bryan Rowsell, Rich Schutte, Steve Trepanier, Sam Yan, and Yiming Yao. Although most of these individuals did not directly contribute to my project, I am certain that their influences somehow translated into my work.

I am especially grateful for having a loving family that has provided me with continuous encouragement and support. I have been blessed to have two caring, nurturing parents, who both taught me to work hard and to pursue the things that I enjoy. I am also privileged to have a devoted wife, Nicole, who has selflessly made considerable sacrifices for me, who has always lifted my spirits in difficult times, and who reminds me of the most important things in life.

Table of Contents

Chapter 1

Introduction

Definitions and General Principles of Catalysis 1

Catalytic Hydrogenation 3

Mechanism 4

Rhodium–Bis(phosphine)-Catalyzed Hydrogenation 5

Ruthenium–BINAP-Catalyzed Hydrogenation 9

Research Mission 15

References and Notes 17

Chapter 2

Syntheses, Characterization, and Reactivities of Ruthenium(II)–BINAP Complexes: A Versatile Catalyst System for Hydrogenation, Hydrosilylation, and Isomerization

Introduction 23

Results and Discussion 24

Syntheses and Characterization of Catalyst Precursors 24

Generation and Characterization of Catalysts 31

Catalysis 32

Catalysts and Catalyst Precursors Revisited 38

Conclusions 40

Experimental Section 40

Materials 40

Measurements 41

Syntheses 42

Catalytic Reactions 49

X-ray Crystallography 53

References and Notes 57

Chapter 3

The First Structure Determinations of Possible Intermediates in Ruthenium–BINAP-Catalyzed Hydrogenation with a Prochiral Group Bonded to Ruthenium

Introduction 64

Results and Discussion 65

Detection and Isolation of a Possible Catalytic Intermediate 65

X-ray Structure Determinations of Possible Intermediates 66

Hydrogenolysis of **2** 73

Conclusions 74

Experimental Section 74

Materials 74

Measurements 75

Syntheses 75

Hydrogenolysis of **2** 78

X-ray Crystallography 79

References and Notes 84

Chapter 4

Stoichiometric and Catalytic Isotope-Labeling Studies of Relevance to Ruthenium–BINAP-Catalyzed Enantioselective Hydrogenation

Introduction 89

Results and Discussion 91

Optimization of the Catalytic Hydrogenation 91

Mechanistic Investigations 92

Hydrogenolysis of ($S_{C\alpha}$)-**1** in Acetone 92

Reversibility of Formation of ($S_{C\alpha}$)-**1** 95

Deuterium Studies in Acetone 98

Stereoselectivity and Regioselectivity of the Catalytic Hydrogenation 104

Methanol as the Solvent 111

Conclusions 114

Experimental Section 115
Materials 115
Measurements 115
Syntheses 115
General Procedure for Catalytic Hydrogenations 116
General Procedure for Catalytic Deuterations 116
General Procedure for Hydrogenolysis and Deuteriolysis of ($S_{C\alpha}$)-**1** 118
Substrate Equilibrium with ($S_{C\alpha}$)-**1** 118
References and Notes 119

Chapter 5

The First Structure Determination of a Diastereomeric Hydrido–Olefin Putative Intermediate in Catalytic Enantioselective Hydrogenation

Introduction 124
Results and Discussion 125
Characterization of the Active Catalyst 125
Interception and Characterization of a Transient Intermediate 127
Conclusions 132
Experimental Section 133
Materials 133
Measurements 134
Syntheses 134
References and Notes 138

Chapter 6

Conclusions

Mechanism of Catalytic Hydrogenation 143
Rewards of Mechanistic Studies 146
Future Mechanistic Studies 153
References and Notes 156

List of Tables

Chapter 2

Table 2-1 Selected Bond Lengths (Å) and Angles (deg) for (*S*)-**2**·0.5$C_2H_4Cl_2$ ... 29

Table 2-2 Hydrosilylation and Isomerization Reactions Catalyzed by **4** ... 33

Table 2-3 Hydrogenation Reactions Catalyzed by **4** ... 35

Table 2-4 Catalytic Hydrogenation of MAC ... 37

Table 2-5 Crystallographic Experimental Details for (*S*)-**2**·0.5$C_2H_4Cl_2$ ... 55

Chapter 3

Table 3-1 Selected Bond Lengths (Å) and Angles (deg) for **2**·Et_2O ... 69

Table 3-2 Selected Bond Lengths (Å) and Angles (deg) for ($S_{C\alpha}$)-**4** ... 71

Table 3-3 Crystallographic Experimental Details for **2**·Et_2O ... 80

Table 3-4 Crystallographic Experimental Details for ($S_{C\alpha}$)-**4** ... 82

Chapter 4

Table 4-1 Hydrogenation of (*Z*)-MAC Catalyzed by **2** ... 91

List of Figures

Chapter 2

Figure 2-1 $^{15}N\{^1H\}$ NMR spectra of **2**-Me$C^{15}N$ (40.5 MHz, CD_2Cl_2) at 25 °C (top) and at –20 °C (bottom) 26

Figure 2-2 View of the complex cation of (*S*)-**2**·0.5$C_2H_4Cl_2$ showing the atom-labeling scheme 28

Figure 2-3 View of the complex cation of (*S*)-**2**·0.5$C_2H_4Cl_2$ illustrating the chiral environment of the (*R*)-BINAP ligand (MeCN and 1–3:5,6-η-C_8H_{11} ligands are omitted for clarity) 30

Figure 2-4 Plot of the chemical shifts (δ) of the (*R*)-MAC$(H)_2$·(+)-Eu$(tfc)_3$ and (*S*)-MAC$(H)_2$·(+)-Eu$(tfc)_3$ diastereomeric adducts in $CDCl_3$ (0.24 M) versus moles of (+)-Eu$(tfc)_3$ added 54

Chapter 3

Figure 3-1 View of one of the two crystallographically-independent complex cations of **2**·Et_2O (molecule 1) showing the atom-labeling scheme 67

Figure 3-2 View of the complex cation of ($S_{C\alpha}$)-**4** showing the atom-labeling scheme 70

Figure 3-3 Plausible bonding modes for transition-metal enolate complexes of esters 72

Chapter 4

Figure 4-1 $^{31}P\{^1H\}$ NMR spectrum of an operating catalytic hydrogenation of (*Z*)-MAC using **2** as the catalyst in acetone-d_6 93

Figure 4-2 The distribution of MAC$(H)_2$-d_n isotopomers from the deuteriolysis of ($S_{C\alpha}$)-**1** in acetone 99

Figure 4-3 The distribution of MAC$(H)_2$-d_n isotopomers from the catalytic deuteration of (*E*)-MAC when using **2** as the catalyst in acetone 106

Figure 4-4 The distribution of MAC(H)$_2$-d_n isotopomers from the deuteriolysis of ($S_{C\alpha}$)-**1** in methanol 113

Figure 4-5 Designations used for the ABX spin system in the ^{1}H NMR spectrum of MAC(H)$_2$ 117

Chapter 5

Figure 5-1 ^{31}P{^{1}H} NMR spectrum (161.9 MHz, THF-d_8, –40 °C) of a mixture containing **7** (75%), **1** (13%), and **2** (6%) recorded 1 h after mixing at –40 °C 128

Figure 5-2 Section of the ^{31}P–^{1}H HETCOR NMR spectrum (499.8 MHz, THF-d_8/CD_2Cl_2 (2:1 v/v), –40 °C) of **7** showing three ortho-type protons associated with each ^{31}P resonance 130

Figure 5-3 Observed NOE values that were used to determine the structure and absolute configuration of *si*-**7** 131

List of Schemes

Chapter 1

Scheme 1-1 The Curtin–Hammett Principle 2

Scheme 1-2 An Alternative to Ritalin®: (2*R*,3*R*)-Methylphenidate 4

Scheme 1-3 Common Products Prepared Via Enantioselective Catalytic Hydrogenation 6

Scheme 1-4 Proposed Mechanism for the Enantioselective Hydrogenation of MAC Catalyzed by $[Rh((R,R)\text{-DIPAMP})(MeOH)_2]BF_4$ 7

Scheme 1-5 Successful Bis(phosphine) Ligands Used In Ruthenium-Catalyzed Enantioselective Hydrogenation 9

Scheme 1-6 The First Syntheses of Ruthenium–BINAP Complexes 10

Scheme 1-7 Applications of Ruthenium–BINAP Catalyzed Hydrogenation 11

Scheme 1-8 Proposed Mechanism for the Enantioselective Hydrogenation of Tiglic Acid Catalyzed by $[Ru((R)\text{-BINAP})(CH_3CO_2)_2]$ 12

Scheme 1-9 Proposed Mechanism for the Enantioselective Hydrogenation of (*Z*)-α-Aminoacrylic Acids Catalyzed by a Ruthenium–BINAP Complex 14

Chapter 2

Scheme 2-1 Competing Hydrogenation and Isomerization of Geraniol 36

Chapter 4

Scheme 4-1 Proposed Sequence of Steps for the Reversible Formation of ($S_{C\alpha}$)-**1** and ($S_{C\alpha}$)-**1**-CO_2CD_3 97

Scheme 4-2 Proposed Sequence of Steps that Accounts for the Isotopomers of $MAC(H)_2$ Produced by the Stoichiometric Deuteriolysis of ($S_{C\alpha}$)-1 102

Scheme 4-3 Outcome of Stereoselective β-Deuteride and β-Hydride Elimination Within ($S_{C\alpha}$,$R_{C\beta}$)-β-d_1-**1** 104

Scheme 4-4 Sequence of Steps that Accounts for the Product Distribution from the Catalytic Deuteration of (*E*)-MAC 108

Scheme 4-5 A Plausible Route to Formation of Deuterium-Free (*Z*)-MAC During the Catalytic Deuteration of (*E*)-MAC 110

Chapter 5

Scheme 5-1 Formation of the Olefin–Catalyst Adduct *si*-**7** at Low Temperature and Its Conversion to **1** 126

Scheme 5-2 Proposed Major Diastereomeric Pathway for the Enantioselective Hydrogenation of MAC Catalyzed by **2** 133

Chapter 6

Scheme 6-1 Proposed Major Diastereomeric Pathway for the Enantioselective Hydrogenation of MAC Catalyzed by **2** 144

Scheme 6-2 Jasmonoid Compounds of Importance in the Fragrance Industry 146

Scheme 6-3 Components of Hedione® 147

Scheme 6-4 Industrial Synthesis of Hedione® 148

Scheme 6-5 Schrock's Catalyst and Its Chiral Variants 152

Scheme 6-6 Grubbs' Catalyst 152

List of Abbreviations and Symbols

anal.	analysis
atm	atmosphere(s)
BINAP	(*R*)- or (*S*)-2,2'-bis(diphenylphosphino)-1,1'-binaphthyl
calcd	calculated
COD	cycloocta-1,5-diene
COSY	correlated spectroscopy
COT	cycloocta-1,3,5-triene
Cp	cyclopentadienyl, C_5H_5
CP/MAS	cross-polarization/magic angle spinning
Cy	cyclohexyl, C_6H_{11}-
de	diastereomeric excess (% major diastereomer – % minor diastereomer)
DIOP	(2*R*,3*R*)- or (2*S*,3*S*)-*O*-isopropylidene-2,3-dihydroxy-1,4-bis(diphenylphosphino)butane
DIPAMP	(*R*,*R*)- or (*S*,*S*)-1,2-bis((*o*-methoxyphenyl)phenylphosphino)ethane
DIPHOS	1,2-bis(diphenylphosphino)ethane
E/*Z*	entgegen/zusammen (configurational)
ee	enantiomeric excess (% major enantiomer – % minor enantiomer)
equiv	equivalent(s)
ESI-MS	electrospray ionization mass spectrometry
Et	ethyl, CH_3CH_2-
(+)-Eu(tfc)$_3$	europium tris[3-(trifluoromethylhydroxymethylene)-(+)-camphorate]
δ	chemical shift relative to a standard (NMR)
fac	facial
g/mg	gram(s)/milligram(s)
GLC	gas–liquid chromatography
h	hour(s)
HETCOR	heteronuclear correlation
HMBC	heteronuclear multiple bond correlation

HMQC	heteronuclear multiple quantum coherence
HRMS (EI)	electron-impact high-resolution mass spectrometry
J	indirect spin-spin coupling constant
JOSIPHOS	(*R*)-1-[(*S*)-2-(diphenylphosphino)ferrocenyl]ethyldicyclohexylphosphine or (*S*)-1-[(*R*)-2-(diphenylphosphino)ferrocenyl]ethyldicyclohexylphosphine
m-	meta
m/z	mass-to-charge ratio
MAA	methyl α-acetamidoacrylate
$MAA(H)_2$	(*R*)- and/or (*S*)-*N*-acetylalanine methyl ester
MAC	methyl α-acetamidocinnamate
$MAC(H)_2$	(*R*)- and/or (*S*)-*N*-acetylphenylalanine methyl ester
MBA	(*S*)-α-methylbenzylamine
Me	methyl, CH_3-
MeCN	acetonitrile
Me-DuPHOS	1,2-bis((2*R*,5*R*)- or (2*S*,5*S*)-2,5-dimethylphospholano)benzene
M/mM	molar/millimolar
MeO-BIPHEP	(*R*)- or (*S*)-6,6'-dimethoxy-2,2'-bis(diphenylphosphino)-1,1'-biphenyl
MeOH	methanol
MHz	megahertz
min	minute(s)
mL/μL	millilitres/microlitres
mol	mole(s)
MTPA-Cl	(*R*)-α-methoxy-α-(trifluoromethyl)phenylacetyl chloride
NBD	norbornadiene or bicyclo[2.2.1]hepta-2,5-diene
NOE	nuclear Overhauser enhancement
ν	wavenumber (IR)
o-	ortho
p-	para
Ph	phenyl, C_6H_5-

pro-R/pro-S	stereochemical descriptors (enantiotopic faces or groups)
R/S	rectus/sinister (configurational)
rac	racemic
re/si	stereochemical descriptors (enantiotopic faces or groups)
rpm	revolutions per minute
s	second(s)
sol	solvent
t	time
T	temperature (°C)
THF	tetrahydrofuran
TOF	turnover frequency
TolBINAP	(*R*)- or (*S*)-2,2'-bis(di-*p*-tolylphosphino)-1,1'-binaphthyl
TON	turnover number

Chapter 1

Introduction

Definitions and General Principles of Catalysis. Asymmetric synthesis, or stereoselective synthesis, is any reaction in which one of a set of stereoisomers is predominantly, or exclusively, formed over the other.[1] An enantioselective reaction is an asymmetric reaction that preferentially transforms a prochiral substrate, possessing two enantiotopic atoms, faces, or groups, into one of two product enantiomers. The most efficient enantioselective reactions involve homogeneous, and to a much lesser extent, hetereogeneous catalysts.[2] Homogeneous catalysts, typically chiral transition-metal complexes[3] or enzymes,[4] promote a one-phase (solution) reaction that transforms a prochiral substrate into a chiral product (eq 1-1). The concentration of the catalyst enters into the kinetic equation (eq 1-2) but does not enter into the equilibrium constant for the reaction (eq 1-3); therefore, the catalyst does not modify the change in standard Gibbs energy, $\Delta G° = -RT \ln K$, for the reaction.[5] By definition, a catalyst is not consumed in a

$$\text{substrate} + \text{catalyst} \underset{k_{-1}}{\overset{k_1}{\rightleftharpoons}} \text{product} + \text{catalyst} \quad (1\text{-}1)$$

$$-d[\text{substrate}]/dt = k_1[\text{substrate}][\text{catalyst}] - k_{-1}[\text{product}][\text{catalyst}] \quad (1\text{-}2)$$

$$K = k_1/k_{-1} = [\text{product}]/[\text{substrate}] \quad (1\text{-}3)$$

reaction (less than stoichiometric amounts can, therefore, be used), and it cannot displace an equilibrium. Both the rates of the forward and reverse reactions are increased to the same extent, and, therefore, the ee of a reversible enantioselective catalytic reaction, such as that shown in eq 1-1, will be zero if the system is allowed to equilibrate. Catalysis is purely a kinetic phenomenon. The catalyst provides an alternative reaction pathway, a

catalytic cycle, in which the activation energy is lower, causing an increase in the rate of the reaction. Completion of one catalytic cycle is commonly known as a turnover. The turnover number (TON) is defined as the number of turnovers achieved by a catalyst (moles of product formed per mole of catalyst). The turnover frequency (TOF), or the productivity of the catalyst, is defined as the number of moles of product formed per mole of catalyst per unit time (TON $time^{-1}$, usually expressed as TON min^{-1}).[6]

For rapid preequilibrium enantioselective catalytic systems, where the rate of interconversion of diastereomeric intermediates (adducts of the chiral catalyst and a prochiral substrate; the simplest case is shown in Scheme 1-1, A and B) is considerably

Scheme 1-1. The Curtin–Hammett Principle

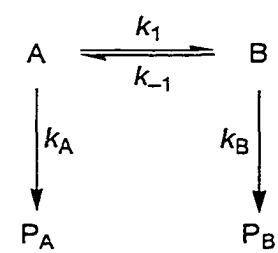

where k_1, k_{-1} >> k_A, k_B

greater than the rate of formation of the enantiomeric products (Scheme 1-1, P_A and P_B), the ratio of the enantiomeric products depends only on the difference in Gibbs energies of the transition states ($G_B^{\ddagger} - G_A^{\ddagger}$) for the two diastereomeric slow steps (k_A and k_B), as shown below (eq 1-4). This phenomenon is known as the Curtin–Hammett principle.[7] In

$$P_A/P_B = e^{(G_B^{\ddagger} - G_A^{\ddagger})/RT} \quad (1\text{-}4)$$

general, the ee of a product derived from a catalytic cycle is determined by the first irreversible step in the catalytic cycle involving diastereomeric transition states (corresponding to k_A and k_B for the respective diastereomeric pathways). This step is known as the enantioselective step.[8] The greater the difference in Gibbs energies of the

respective diastereomeric transition states, the greater the catalytic enantioselectivity. The difference need not be large to obtain high enantioselectivity; a difference of only 8 kJ mol^{-1} gives 92% ee at 300 K.

It is conceivable to model the two diastereomeric transition states, in an attempt to account for their difference in energies, based on structural data of the predecessor complexes (A and B). The Hammond postulate[9] states that for any single reaction step, the geometry of the transition state for that step resembles more the side of the reaction coordinate to which it is closer in Gibbs energy; thus, for an exergonic reaction, such as the conversion of A to P_A (and B to P_B), the transition state resembles the reactants more than products. Accumulation of A and B to detectable amounts that will allow their structural characterization, and possible transition-state modeling, can only be achieved if the conversion of A to P_A (and B to P_B) proceeds with the lowest rate constants in the catalytic cycle (and no side reactions consume the catalyst). Such a step is known as the turnover-limiting step. Note that for this simplest of examples, the enantioselective and the turnover-limiting steps coincide. This special case is not necessarily universal in enantioselective catalysis.

Transition-metal catalysts effect highly chemo-, diastereo-, enantio-, and regio-selective reactions with high efficiency—in some cases producing millions of chiral product molecules using only one molecule of a catalyst (chiral multiplication). Further, the minimization of waste and the reduction of raw material consumption is an attractive feature of all catalysts. Transition-metal catalysts also have advantages that complement biocatalysts (enzymes): (a) transition-metal catalysts can promote reactions using substrates that are not accepted by enzymes; (b) transition-metal catalysts can promote unnatural reactions such as hydroboration; (c) the structures and, therefore, the reactivities of transition-metal catalysts can be readily modified to augment the rates and the stereoselectivities of the reactions they catalyze; and (d) transition-metal catalysts are often used in non-aqueous media, allowing relatively easy separation and recovery of products.[10]

Catalytic Hydrogenation. Enantioselective catalytic hydrogenation is one of the most powerful synthetic approaches to producing chiral compounds that contain a

hydrogen atom at the stereogenic center. Catalytic enantioselective hydrogenation of prochiral unsaturated functional groups can be achieved using dihydrogen gas or a hydrogen donor (e.g., secondary alcohols or formic acid) as the hydrogen source. The latter method, known as transfer hydrogenation or the Meerwein–Ponndorf–Verley reaction, has only recently emerged as a practical alternative to the use of dihydrogen gas.[11] Enantioselective catalytic hydrogenation, using dihydrogen gas, is commonly effected by late transition-metal complexes (usually of ruthenium, rhodium, or iridium) that contain a chiral ligand (usually bis(phosphines)). This technique is now a standard synthetic tool for the organic chemist, and has especially found widespread use in the production of chiral organic molecules for biological applications such as agrochemicals[12] and pharmaceuticals.[13] These applications usually require the industrial syntheses to be highly enantioselective.[14] In biological systems, one enantiomer of a compound may give a desired effect through interactions with a natural binding site; however, its enantiomer may be inactive or it may have different, undesired reactivity. For example, Ritalin®, a drug used for the treatment of attention deficit disorder in children, is marketed in the United States by Novartis as the racemic threo diastereomer of methylphenidate hydrochloride. To avoid the side effects of insomnia and appetite suppression caused by Ritalin®, the pharmaceutical firm Celgene have recently developed methods to stereoselectively produce the innocuous and therapeutically active enantiomer, (2*R*,3*R*)-methylphenidate (Scheme 1-2).[15]

Scheme 1-2. An Alternative to Ritalin®: (2*R*,3*R*)-Methylphenidate

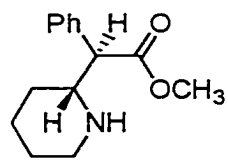

Mechanism. It is surprising, considering the fundamental importance of and the financial opportunities associated with enantioselective catalysis, that only a few enantioselective catalytic systems have been thoroughly studied to investigate their

mechanisms. The true origins of catalytic enantioselection can only be determined through detailed mechanistic investigations that include structure determinations of the diastereomeric intermediates responsible for the enantioselection during the enantio-selective step(s). Such studies are rare[16] because they require well-defined catalyst systems and they require either that the enantioselective step is turnover-limiting or that it precedes the turnover-limiting step. Rather than conducting detailed mechanistic studies of enantioselective reactions, it is more common that these reactions are optimized (rates and selectivities) through systematic modification of variables (metal, phosphine, substrate, solvent, temperature, etc.). In fact, combinatorial methods strive to automate this optimization process.[17]

The most detailed mechanistic studies of enantioselective catalysis are those of the hydrogenation of prochiral α-aminoacrylic acid derivatives using chiral rhodium(I)–bis(phosphine) catalysts, and the hydrogenation of prochiral α,β-unsaturated acids using ruthenium(II)–BINAP catalysts. It is appropriate that these systems were the subject of the first mechanistic studies as both represent the earliest successes in enantioselective hydrogenation of important classes of substrates. For example, the chiral products from hydrogenation of α-aminoacrylic acid derivatives are valuable for the preparation of peptides and peptidomimetic therapeutics. Specifically, this technology is used in the commercial production of (*S*)-DOPA and Aspartame by Monsanto and Enichem, respectively, using rhodium catalysts.[18] Also, the enantioselective hydrogenation of 2-arylacrylic acid derivatives using ruthenium–BINAP catalysts provides a low-cost route to analgesic profen drugs, namely (*S*)-Naproxen and (*S*)-Ibuprofen, in high enantiomeric purity[19] (Scheme 1-3).

Rhodium–Bis(phosphine)-Catalyzed Hydrogenation. An early advancement in the field of enantioselective catalysis was the development of the hydrogenation of prochiral olefins, albeit in modest ee, using chiral rhodium–phosphine complexes as catalysts in 1968.[20] These results initiated intense study by Knowles et al.[21] and Kagan et al.[22] that resulted in an attractive synthesis of natural and unnatural amino acid derivatives via α-aminoacrylic acids. Further development of the enantioselective hydrogenation of α-aminoacrylic acid derivatives showed that rhodium–bis(phosphine) catalysts, rather than

Scheme 1-3. Common Products Prepared Via Enantioselective Catalytic Hydrogenation

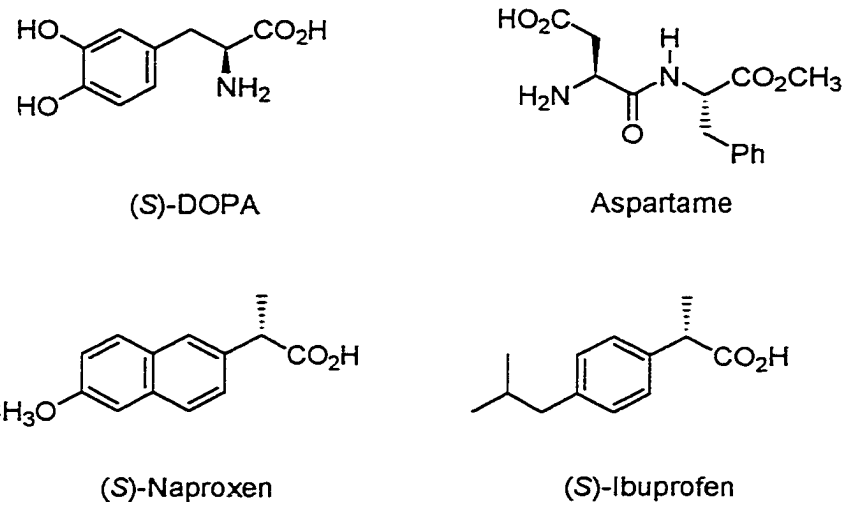

rhodium-phosphine catalysts, afforded high enantioselectivity.[23] It was not until the late 1970s that mechanistic studies of this reaction were initiated. The first studies focused on the spectroscopic detection and characterization of possible catalytic intermediates (under catalytic and stoichiometric conditions)[24] and on inference of mechanistic information from deuterium-labeling of the catalytic reactions.[25] Later studies included X-ray crystallographic characterization of intermediates,[26] inference of the structures of highly reactive rhodium intermediates through more stable iridium analogues,[27] determination of the mechanism of interconversion of intermediates,[28] kinetic measurements of key steps in the catalytic cycle,[29] and calculations that rationalize the relative reactivities of intermediates with dihydrogen gas.[30] Many workers have contributed significantly to the mechanistic understanding of this reaction, but Halpern[31] is the principal investigator attributed to discovering key aspects of the mechanism. The accepted mechanism[29b] for the enantioselective hydrogenation of MAC using [Rh((*R*,*R*)-DIPAMP)$(MeOH)_2$]BF_4 (**1**) as the catalyst is shown below (Scheme 1-4).[31b]

The catalytic cycle begins with binding of the substrate MAC to the catalyst **1** to reversibly form the catalyst–substrate adducts **2** and **2'**. The formation of **2** and **2'** is rapid and essentially complete even at moderate concentrations of MAC at ambient tempera-

Scheme 1-4. Proposed Mechanism for the Enantioselective Hydrogenation of MAC Catalyzed by [Rh((*R*,*R*)-DIPAMP)(MeOH)$_2$]BF$_4$

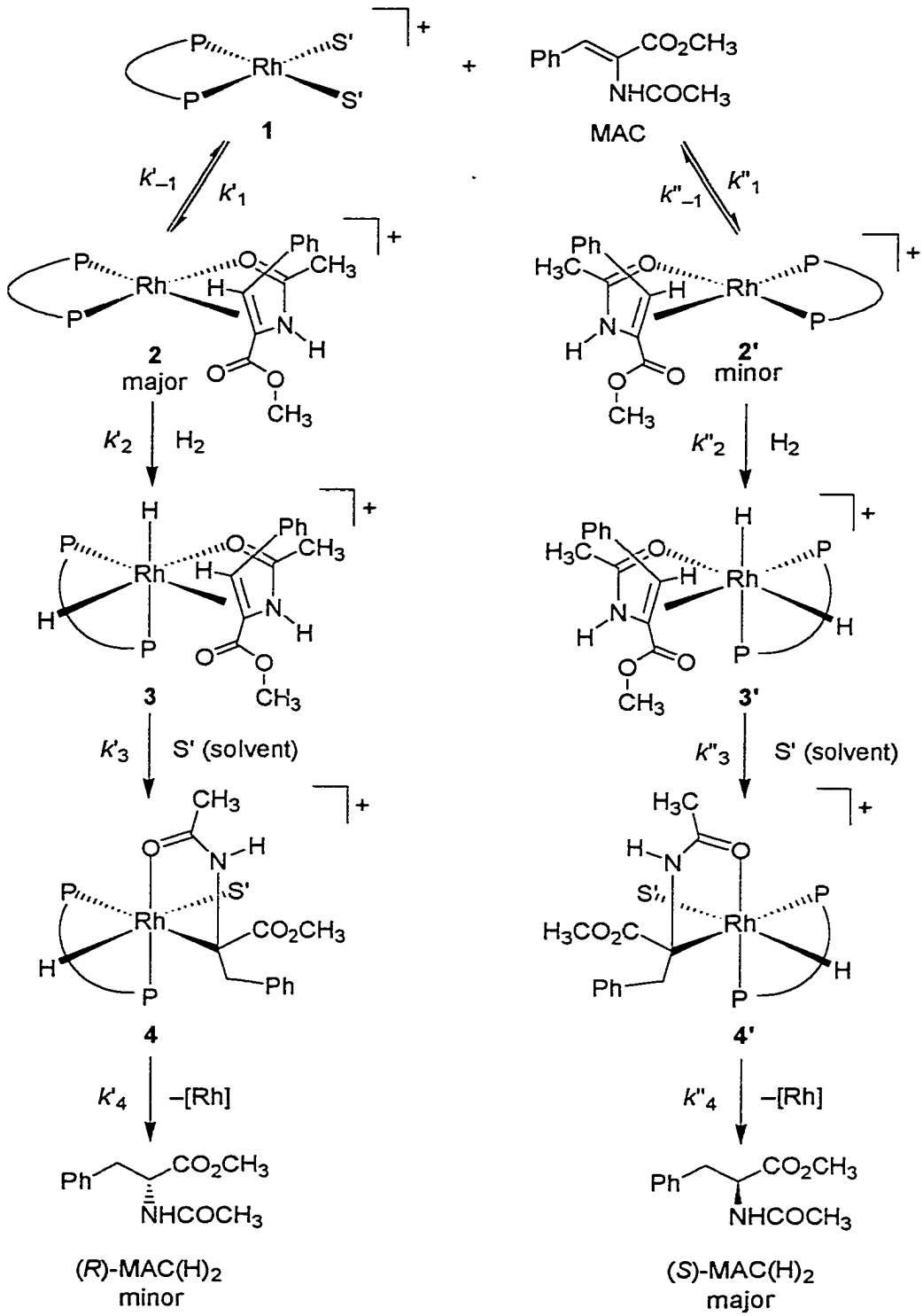

tures. At 25 °C, the equilibrium ratio of the two diastereomers is ≈11:1. It is the relatively high reactivity of the minor diastereomer (**2'**; less-favored binding mode) of the catalyst–substrate adduct toward dihydrogen gas, rather than the preferred initial binding of the substrate to the catalyst, that is responsible for the enantioselectivity of the reaction ($k''_2/k'_2 \approx 580$ at 25 °C). The predominant product enantiomer, (*S*)-MAC(H)$_2$, is therefore derived from the minor diastereomer (**2'**), not from the major diastereomer (**2**; more-favored binding mode). Oxidative addition of dihydrogen gas is the crucial step in the catalytic reaction, as it is the enantioselective step (first irreversible step in the catalytic cycle involving diastereomeric transition states) and, under ambient pressures and temperatures, the turnover-limiting step (step with the lowest rate constants in the catalytic cycle) in both diastereomeric pathways. Under ambient conditions, the system operates under Curtin–Hammett kinetics where a rapid preequilibrium of the diastereomeric catalyst–substrate adducts (corresponding to k'_1/k'_{-1} and k''_1/k''_{-1}) is established prior to the turnover-limiting step (corresponding to k'_2 and k''_2). The kinetic analysis of this system, therefore, required only the consideration of the substrate-binding and the oxidative-addition steps. At lower temperatures (ca. –40 °C), the turnover-limiting step becomes the reductive-elimination step (corresponding to k'_4 and k''_4), which allows the hydrido–alkyl intermediate **4'** to accumulate to detectable quantities. Under these conditions, only the prominent structural features of **4'** have been directly determined;[24c,24d,32] a more detailed structure has been inferred from structural data of a stable iridium analogue.[27c] The detailed structures and absolute configurations of both **4'** and the dihydrido intermediate **3'** must be directly determined before the structural study of the major product-forming pathway is complete. Only recently has a dihydrido intermediate similar to **4'** been detected, but not fully characterized, in a related system.[33] Although the mechanism for this reaction is understood, the true origins of enantioselection (involving the oxidative-addition step) are unclear. The origins for the observed thermodynamic diastereomeric ratio (**2**:**2'**) and why the minor diastereomeric catalyst–substrate adduct (**2'**) is more reactive toward dihydrogen gas than the major diastereomer (**2**) have been rationalized by calculations[30] based on steric interactions

alone; however, electronic factors have also been suggested using the ^{103}Rh nucleus as a probe.[34]

Ruthenium–BINAP-Catalyzed Hydrogenation. It was discovered shortly after the development of rhodium-catalyzed hydrogenation of α-aminoacrylic acid derivatives that complexes of ruthenium were also effective catalysts for enantioselective hydrogenation. The first example, disclosed by James et al.,[35] used a ruthenium complex of the chiral bis(phosphine) DIOP as the catalyst for the enantioselective hydrogenation of an α-aminoacrylic acid derivative. The low enantioselectivities observed for ruthenium–bis(phosphine) catalysts, compared to the corresponding rhodium catalysts, and the difficulty in their preparation (no universal synthesis) may account for the slow development of chiral ruthenium catalysts during this period that witnessed rapid advancements using rhodium catalysts. It was not until the inception of the bis(phosphine) ligand BINAP[36] that the potential of ruthenium catalysts, and enantioselective hydrogenation in general, was realized (Scheme 1-5). The first ruthenium–BINAP

Scheme 1-5. Successful Bis(phosphine) Ligands Used In Ruthenium-Catalyzed Enantioselective Hydrogenation

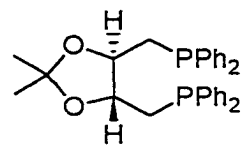

(2*R*,3*R*)-DIOP

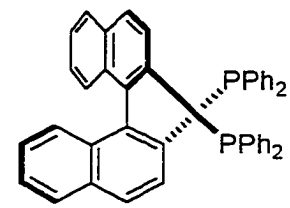

(*R*)-BINAP

complexes were described by Ikariya et al.[37] and Noyori et al.[38] in 1985 and 1986, respectively (Scheme 1-6). The performance of these ruthenium–BINAP catalysts in the enantioselective hydrogenation of α-aminoacrylic acid derivatives (and other enamides) were similar to, and in some cases superior to, that of the previously developed rhodium–BINAP system. Whereas rhodium–bis(phosphine) hydrogenation catalysts are mostly limited to α-aminoacrylic acid substrates, ruthenium–BINAP catalysts demonstrate

Scheme 1-6. The First Syntheses of Ruthenium–BINAP Complexes

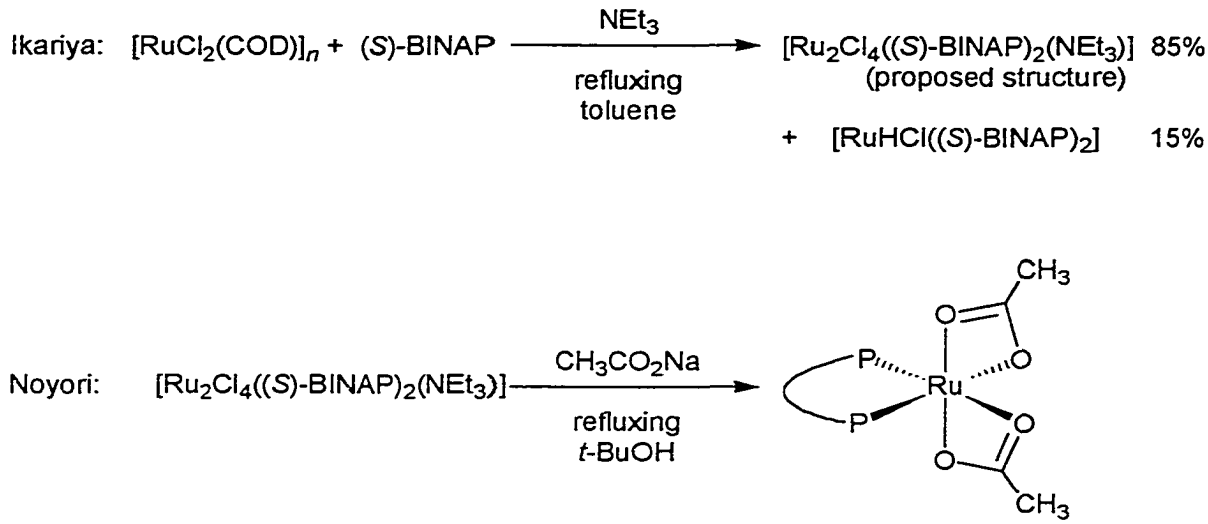

impressive generality and reactivity in enantioselective hydrogenation.[39] For example, many industrially feasible processes using ruthenium–BINAP catalyzed enantioselective hydrogenation have been developed (Scheme 1-7) that include: (1) hydrogenation of α,β-unsaturated acids used in the production of profen drugs[40] (e.g., Naproxen and Ibuprofen, see Scheme 1-3) and the core component of HIV protease inhibitors;[41] (2) hydrogenation of allylic alcohols used in the syntheses of carbapenem antibiotics,[42] prostaglandins,[43] and the side chain of α-tocopherol (vitamin E);[44] (3) hydrogenation of enamides in the production of Dextromethorphan[45] (a cough suppressant) and Clozylacon[12] (a fungicide). In addition, a recent report highlighted the remarkable TONs (up to 2.4×10^6) and TOFs (up to 5.63×10^5 h^{-1}) observed when using ruthenium–BINAP catalysts in the enantioselective hydrogenation of prochiral ketones to generate chiral secondary alcohols.[46]

Despite the importance of these reactions catalyzed by ruthenium–BINAP complexes, the only mechanism that has been studied in detail[47] is the enantioselective hydrogenation of α,β-unsaturated acids (specifically tiglic acid) catalyzed by [Ru((*R*)-BINAP)$(CH_3CO_2)_2$]. The accepted mechanism, as determined by Ashby and Halpern[48] and Ohta et al.,[49] is shown below (Scheme 1-8). Subsequent studies by Chan et al.[13c,50]

Scheme 1-7. Applications of Ruthenium–BINAP Catalyzed Hydrogenation

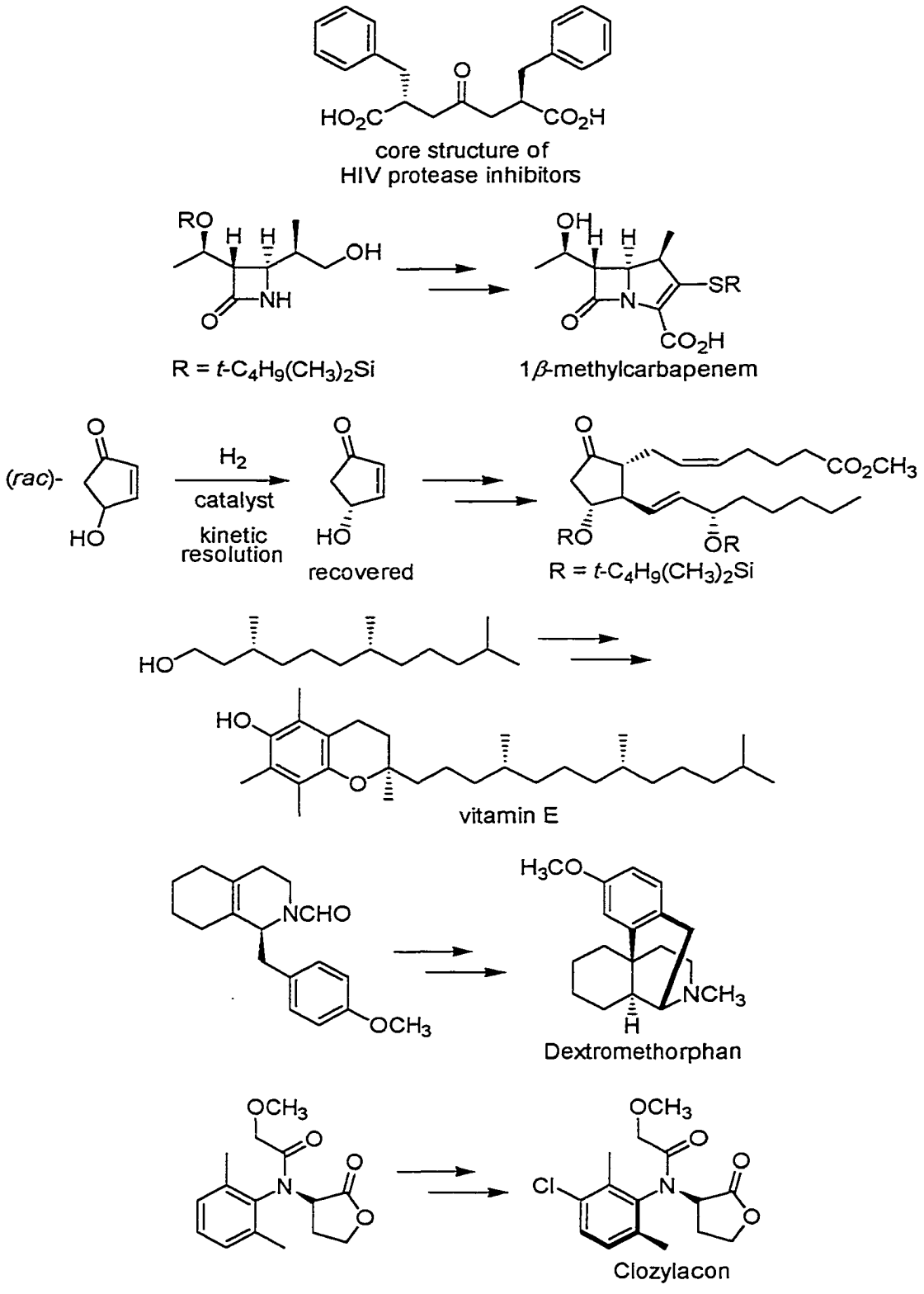

Scheme 1-8. Proposed Mechanism for the Enantioselective Hydrogenation of Tiglic Acid Catalyzed by [Ru((*R*)-BINAP)(CH_3CO_2)$_2$]

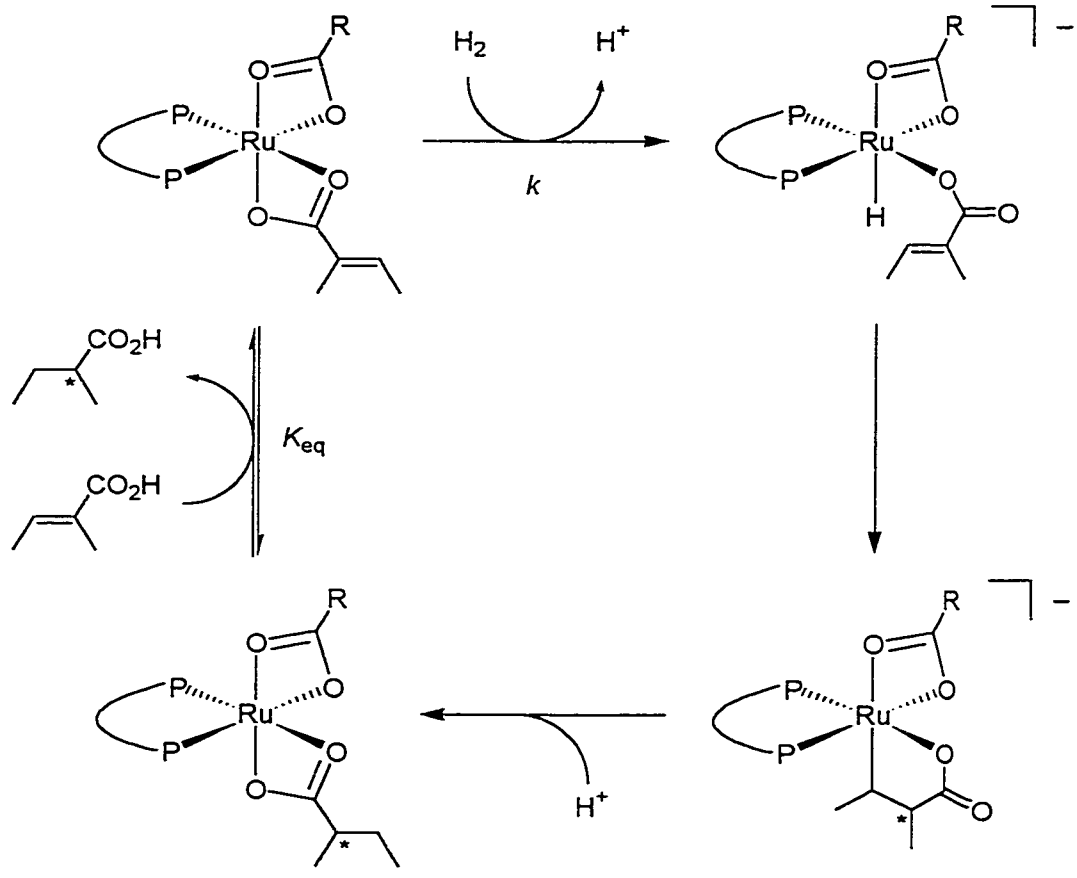

and Saburi et al.[51] support this proposal. Chan et al. and Ohta et al. have also postulated, in addition to the catalytic cycle shown, that hydrogenolysis of the ruthenium–alkyl intermediate also occurs when higher pressures of dihydrogen gas (>20 atm) are used. These claims are supported by an increase in hydrogen incorporation into the β-position of α,β-unsaturated acids with increasing pressure of dihydrogen gas in catalytic reactions carried out in CH_3OD.

Prior to entry into the catalytic cycle, the catalyst precursor [Ru((*R*)-BINAP)-(CH_3CO_2)$_2$] undergoes rapid carboxylate substitution with the substrate. It may be safely assumed that the catalyst precursor becomes [Ru((*R*)-BINAP)((CH_3)CH=C(CH_3)CO_2)$_2$] since (a) the concentration of [Ru((*R*)-BINAP)(CH_3CO_2)$_2$] and acetate are low compared

to the initial concentration of substrate, and (b) the acetate ligand and the conjugate bases of both the substrate and the product bind to ruthenium with comparable binding constants. The equilibration step is followed by turnover-limiting heterolytic cleavage of dihydrogen gas to generate a ruthenium dicarboxylate monohydrido species. This step is followed by insertion of the olefin group into the ruthenium–hydride bond to give a 5-membered metallaoxacycle where the ruthenium is bonded to the β-carbon of the substrate. Protonolysis of the ruthenium–carbon bond regenerates the ruthenium–dicarboxylate adduct, and the product is released from the catalyst by subsequent carboxylate exchange with the substrate. The detailed kinetic study of this system, however, could not provide information about the enantioselective step because it occurred after the turnover-limiting step. Further, the catalyst–substrate adduct, [Ru((*R*)-BINAP)($(CH_3)CH{=}C(CH_3)CO_2)_2$], was isolated and characterized by both X-ray crystallography and NMR spectroscopy; however, the prochiral olefin group was not bonded to the ruthenium center in the solid state or in solution.[52] The steric interactions that contribute to the enantioselectivity are, therefore, unknown. A subsequent structural study of a related ruthenium–BINAP catalyst–substrate adduct also showed that there was no interaction of the prochiral olefin group of the α,β-unsaturated acid substrate with the ruthenium center.[53] Although there have been reports of observations of unidentified species observed by NMR spectroscopy,[49,51,54] there are no reports of a structure determination (even by spectroscopy) of a possible catalytic intermediate with a prochiral group bonded to ruthenium. The structures, and the origins of enantioselectivity, are speculative as they have been inferred from indirect methods: stereochemical, isotope-labeling, and kinetic studies.

A further mechanistic study of the enantioselective hydrogenation of prochiral olefins using ruthenium–BINAP catalysts is warranted when considering the shortfalls of the previous studies described above. The purpose of this study is to expand our understanding of the role of ruthenium–BINAP complexes in enantioselective catalytic hydrogenation to include other substrates and to complement the previous studies regarding mechanism. This study will also test the validity of another mechanism that has been proposed by Kawano et al.[55] for the enantioselective hydrogenation of (*Z*)-α-

aminoacrylic acids catalyzed by a ruthenium–BINAP complex that involves reversibility in the catalytic cycle (Scheme 1-9). The reversible formation of the proposed catalyst–

Scheme 1-9. Proposed Mechanism for the Enantioselective Hydrogenation of (*Z*)-*α*-Aminoacrylic Acids Catalyzed by a Ruthenium–BINAP Complex

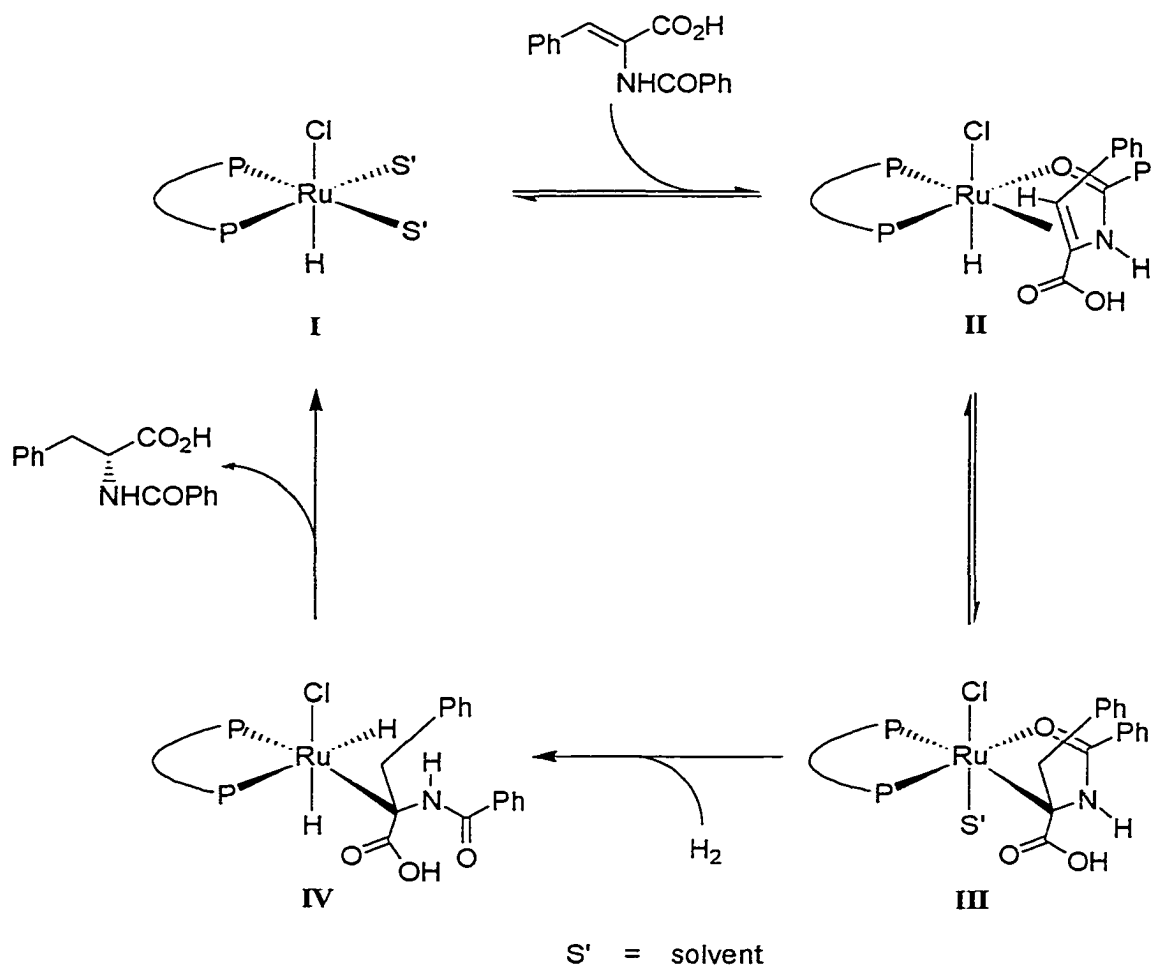

substrate adduct **II** and of the proposed ruthenium–alkyl species **III** was supported by formation of substantial amounts of (*Z*)-*α*-aminoacrylic acids during the catalytic hydrogenations of the corresponding less-stable (*E*)-isomers. This can be rationalized by stereoselective *β*-hydride elimination within **III** (formed via a species resembling **II** that contains an (*E*)-*α*-aminoacrylic acid) that favors the formation of the *Z* isomer of the substrate to generate **II**. There were no direct observations, however, of the proposed

intermediates **II**, **III**, and **IV**. Their existence and their structures were proposed exclusively from data obtained from the stereochemistry of the products derived from the catalytic hydrogenations of (*E*)- and (*Z*)-α-aminoacrylic acid derivatives.

Research Mission. The success of a mechanistic study often relies on the design and synthesis of a well-defined system that is amenable to such an investigation. It has been suggested that the catalytically active species in enantioselective hydrogenation catalyzed by ruthenium–bis(phosphine) complexes of BINAP[51,55] and DIOP[56] are ruthenium hydrides. An important objective, therefore, is to prepare a ruthenium–hydrido complex of BINAP from a robust ruthenium–BINAP catalyst precursor that will readily produce a ruthenium hydride in high concentration under mild conditions. The ruthenium hydride should also contain weakly coordinating solvento ligands (for late transition metals, these include acetone, methanol, and THF) that can be easily displaced by the substrate during catalysis. This will facilitate the detection and study of enantioselective catalyst–substrate interactions. Further, it is advantageous to use a benchmark substrate so that the results can be compared with other systems. A sensible choice is the prochiral olefin MAC because its hydrogenation was studied using rhodium catalysts and because the products derived from its hydrogenation are of practical importance. The strategies that will be used for studying the present catalytic mechanism include: (a) identification of the catalytically active species; (b) determination of the rate of the catalytic reaction and the stereochemistries of the hydrogenation products; (c) monitoring the catalytic reaction by in situ spectroscopic methods to detect and identify possible catalytic intermediates; (d) full characterization of possible catalytic intermediates (either isolated from the catalytic reaction or from the stoichiometric reaction of the catalytically active species and the substrate) that contain interactions between the prochiral group of the substrate and the ruthenium center; (e) determination of the rate of reaction of dihydrogen gas with the isolated possible intermediates and determination of the stereochemistries of the subsequent hydrogenation products; (f) investigation of the catalytic reaction and the reactivity of the isolated possible intermediates using isotope-labeling (dideuterium/dihydrogen gas and deuterated/protiated solvent) to determine the source of hydrogen (protonolysis/solvolysis or dihydrogen gas) incorporated in the hydrogenation products.

Only once a full study of a well-defined catalytic system is completed, which includes the isotope-labeling, kinetic, and stereochemical studies described above, can the origins of enantioselection be proposed. This thesis describes the strategies and methods used to study the mechanism of the enantioselective hydrogenation of MAC using a new ruthenium–hydrido complex of BINAP as the catalyst.

References and Notes

(1) *Asymmetric synthesis*; Aitken, R. A., Kilényi, S. N., Eds.; Chapman & Hall: London, 1992.

(2) Few heterogeneous catalytic systems have been developed. For successful examples that include the enantioselective hydrogenation of α-keto esters catalyzed by chinchona-modified Pt–Al_2O_3 and by tartaric acid/Raney–Ni/NaBr, see: (a) LeBlond, C.; Wang, J.; Liu, J.; Andrews, A. T.; Sun, Y.-K. *J. Am. Chem. Soc.* **1999**, *121*, 4920–4921. (b) Harada, T.; Izumi, Y. *Chem. Lett.* **1978**, 1195–1196.

(3) (a) Noyori, R. *Asymmetric Catalysis in Organic Synthesis*; Wiley: New York, 1994. (b) *Catalytic Asymmetric Synthesis*; Ojima, I., Ed.; VCH: New York, 1993.

(4) Wong, C.-H.; Whitesides, G. M. *Enzymes in Synthetic Organic Chemistry*; Pergamon: New York, 1994.

(5) Laidler, K. J. *Chemical Kinetics*, 3rd ed.; Harper & Row: New York, 1987.

(6) These definitions are frequently used by chemists involved with transition-metal-based catalysis. The following definitions apply to enzymatic reactions: (a) the turnover number (TN) is defined as the number of moles of product formed per mole of enzyme or cofactor per unit time; (b) the total turnover number (TTN) is the total number of moles of product formed per mole of enzyme or cofactor during the course of a complete reaction.[4]

(7) Seeman, J. I. *Chem. Rev.* **1983**, *83*, 83–134.

(8) *Asymmetric Catalysis*; Bosnich, B., Ed.; NATO ASI Series E, No. 103; Martinus Nijhoff: Dordrecht, 1986.

(9) (a) March, J. *Advanced Organic Chemistry: Reactions, Mechanisms, and Structure*, 4th ed.; Wiley: New York, 1992; p 216. (b) Lowry, T. H.; Richardson, K. S. *Mechanism and Theory in Organic Chemistry*, 3rd ed.; Harper & Row: New York, 1987; pp 212–214.

(10) Nugent, W. A.; RajanBabu, T. V.; Burk, M. J. *Science* **1993**, *259*, 479–483.

(11) Noyori, R.; Hashiguchi, S. *Acc. Chem. Res.* **1997**, *30*, 97–102.

(12) Ramos Tombo, G. M.; Bellus, D. *Angew. Chem., Int. Ed. Engl.* **1991**, *30*, 1193–1215.

(13) (a) Burk, M. J.; Gross, M. F.; Harper, T. G. P.; Kalberg, C. S.; Lee, J. R.; Martinez, J. P. *Pure Appl. Chem.* **1996**, *68*, 37–44. (b) Schmid, R.; Broger, E. A.; Cereghetti, M.; Crameri, Y.; Foricher, J.; Lalonde, M.; Müller, R. K.; Scalone, M.; Schoettel, G.; Zutter, U. *Pure Appl. Chem.* **1996**, *68*, 131–138. (c) Chan, A. S. C.; Laneman, S. A.; Miller, R. E. In *Selectivity in Catalysis*; Davis, M. E., Suib, S. L., Eds.; ACS Symposium Series 517; American Chemical Society: Washington, DC, 1993; Chapter 2.

(14) *Chirality in Industry II: Developments in the Manufacture and Applications of Optically Active Compounds*; Collins, A. N., Sheldrake, G. N., Crosby, J., Eds.; Wiley: Chichester, 1997.

(15) (a) Ramaswamy, S.; Khetani, V. U.S. Patent 5 965 734, 1999. (b) Dariani, M. M.; Zeitlin, A. L.; Zeldis, J. B. U.S. Patent 5 922 736, 1999. (c) Zeitlin, A. L.; Dariani, M. M.; Stirling, D. I. U.S. Patent 5 908 850, 1999.

(16) (a) Steinhagen, H.; Reggelin, M.; Helmchen, G. *Angew. Chem., Int. Ed. Engl.* **1997**, *36*, 2108–2110. (b) Brown, J. M.; Hulmes, D. I.; Guiry, P. J. *Tetrahedron* **1994**, *50*, 4493–4506. (c) Mackenzie, P. B.; Whelan, J.; Bosnich, B. *J. Am. Chem. Soc.* **1985**, *107*, 2046–2054.

(17) Bein, T. *Angew. Chem., Int. Ed. Engl.* **1999**, *38*, 323–326.

(18) Ojima, I.; Clos, N.; Bastos, C. *Tetrahedron* **1989**, *45*, 6901–6939.

(19) Chan, A. S. C. *CHEMTECH* **1993**, *23*, 46–51.

(20) (a) Knowles, W. S.; Sabacky, M. J. *J. Chem. Soc., Chem. Commun.* **1968**, 1445–1446. (b) Horner, L.; Siegel, H.; Büthe, H. *Angew. Chem., Int. Ed. Engl.* **1968**, *7*, 942.

(21) Knowles, W. S.; Sabacky, M. J.; Vineyard, B. D. *J. Chem. Soc., Chem. Commun.* **1972**, 10–11.

(22) Kagan, H. B.; Dang, T.-P. *J. Am. Chem. Soc.* **1972**, *94*, 6429–6433.

(23) (a) Ojima, I.; Kogure, T.; Yoda, N. *J. Org. Chem.* **1980**, *45*, 4728–4739. (b) Fryzuk, M. D.; Bosnich, B. *J. Am. Chem. Soc.* **1977**, *99*, 6262–6267. (c) Vineyard, B. D.;

Knowles, W. S.; Sabacky, M. J.; Bachman, G. L.; Weinkauff, D. J. *J. Am. Chem. Soc.* **1977**, *99*, 5946–5952.

(24) (a) Brown, J. M.; Murrer, B. A. *J. Chem. Soc., Perkin Trans. 2* **1982**, 489–497. (b) Brown, J. M.; Chaloner, P. A. *J. Am. Chem. Soc.* **1980**, *102*, 3040–3048. (c) Chan, A. S. C.; Halpern, J. *J. Am. Chem. Soc.* **1980**, *102*, 838–840. (d) Brown, J. M.; Chaloner, P. A. *J. Chem. Soc., Chem. Commun.* **1980**, 344–346. (e) Brown, J. M.; Chaloner, P. A. *J. Chem. Soc., Chem. Commun.* **1979**, 613–615. (f) Brown, J. M.; Chaloner, P. A. *Tetrahedron Lett.* **1978**, 1877–1880. (g) Brown, J. M.; Chaloner, P. A. *J. Chem. Soc., Chem. Commun.* **1978**, 321–322.

(25) (a) Detellier, C.; Gelbard, G.; Kagan, H. B. *J. Am. Chem. Soc.* **1978**, *100*, 7556–7561. (b) Koenig, K. E.; Knowles, W. S. *J. Am. Chem. Soc.* **1978**, *100*, 7561–7564. For subsequent studies, including the use of *para*-dihydrogen gas, see: (c) Harthun, A.; Selke, R.; Bargon, J. *Angew. Chem., Int. Ed. Engl.* **1996**, *35*, 2505–2507. (d) Burk, M. J.; Feaster, J. E.; Nugent, W. A.; Harlow, R. L. *J. Am. Chem. Soc.* **1993**, *115*, 10125–10138. (e) Brown, J. M.; Canning, L. R.; Downs, A. J.; Forster, A. M. *J. Organomet. Chem.* **1983**, *255*, 103–111.

(26) (a) McCulloch, B.; Halpern, J.; Thompson, M. R.; Landis, C. R. *Organometallics* **1990**, *9*, 1392–1395. (b) Chan, A. S. C. ; Pluth, J. J.; Halpern, J. *J. Am. Chem. Soc.* **1980**, *102*, 5952–5954. (c) Chan, A. S. C.; Pluth, J. J.; Halpern, J. *Inorg. Chim. Acta* **1979**, *37*, L477–L479.

(27) (a) Armstrong, S. K.; Brown, J. M.; Burk, M. J. *Tetrahedron Lett.* **1993**, *34*, 879–882. (b) Brown, J. M.; Maddox, P. J. *Chirality* **1991**, *3*, 345–354. (c) Brown, J. M.; Maddox, P. J. *J. Chem. Soc., Chem. Commun.* **1987**, 1276–1278. (d) Alcock, N. W.; Brown, J. M.; Derome, A. E.; Lucy, A. R. *J. Chem. Soc., Chem. Commun.* **1985**, 575–578.

(28) (a) Kless, A.; Börner, A.; Heller, D.; Selke, R. *Organometallics* **1997**, *16*, 2096–2100. (b) Bircher, H.; Bender, B. R.; von Philipsborn, W. *Magn. Res. Chem.* **1993**, *31*, 293–298. (c) Kadyrov, R.; Freier, T.; Heller, D.; Michalik, M.; Selke, R. *J. Chem. Soc., Chem. Commun.* **1995**, 1745–1746. (d) Brown, J. M.; Chaloner, P. A.; Morris, G. A. *J.*

Chem. Soc., Perkin Trans. 2 **1987**, 1583–1588. (e) Brown, J. M.; Chaloner, P. A.; Morris, G. A. *J. Chem. Soc., Chem. Commun.* **1983**, 644–666.

(29) (a) Chinn, M. S.; Eisenberg, R. *J. Am. Chem. Soc.* **1992**, *114*, 1908–1909. (b) Landis, C. R.; Halpern, J. *J. Am. Chem. Soc.* **1987**, *109*, 1746–1754.

(30) (a) Giovannetti, J. S.; Kelly, C. M.; Landis, C. R. *J. Am. Chem. Soc.* **1993**, *115*, 4040–4057. (b) Bosnich, B. *Pure Appl. Chem.* **1990**, *62*, 1131–1134. (c) Bogdan, P. L.; Irwin, J. J.; Bosnich, B. *Organometallics* **1989**, *8*, 1450–1453. (d) Brown, J. M.; Evans, P. L. *Tetrahedron* **1988**, *44*, 4905–4916.

(31) (a) Halpern, J. *Pure Appl. Chem.* **1983**, *55*, 99–106. (b) Halpern, J. *Science* **1982**, *217*, 401–407.

(32) Ramsden, J. A.; Claridge, T. D. W.; Brown, J. M. *J. Chem. Soc., Chem. Commun.* **1995**, 2469–2471.

(33) Harthun, A. ; Kadyrov, R.; Selke, R.; Bargon, J. *Angew. Chem., Int. Ed. Engl.* **1997**, *36*, 1103–1105.

(34) Bender, B. R.; Koller, M.; Nanz, D.; von Philipsborn, W. *J. Am. Chem. Soc.* **1993**, *115*, 5889–5890.

(35) James, B. R.; Wang, D. K. W.; Voigt, R. F. *J. Chem. Soc., Chem. Commun.* **1975**, 574–575.

(36) Miyashita, A.; Yasuda, A.; Takaya, H.; Toriumi, K.; Ito, T.; Souchi, T.; Noyori, R. *J. Am. Chem. Soc.* **1980**, *102*, 7932–7934.

(37) (a) Ikariya, T.; Ishii, Y.; Kawano, H.; Arai, T.; Saburi, M.; Yoshikawa, S.; Akutagawa, S. *J. Chem. Soc., Chem. Commun.* **1985**, 922–924. King and DiMichele subsequently collected NMR spectroscopic data that strongly suggested that the true structure of "$[Ru_2Cl_4(BINAP)(NEt_3)]$" is $Et_2NH_2[(RuCl(BINAP))_2(\mu\text{-}Cl)_3]$: (b) King, S. A.; DiMichele, L. In *Catalysis of Organic Reactions*; Scaros, M. G., Prunier, M. L., Eds.; Marcel Dekker: New York, 1995; Vol. 62, pp 157–166. Ohta et al. later confirmed the structural assignment of King and DiMichele by determining the solid-state structure of the (*R*)-*p*-MeO-BINAP analog by X-ray diffraction: (c) Ohta, T.; Tonomura, Y.; Nozaki, K.; Takaya, H.; Mashima, K. *Organometallics* **1996**, *15*, 1521–1523.

(38) Noyori, R.; Ohta, M.; Hsiao, Y.; Kitamura, M.; Ohta, T.; Takaya, H. *J. Am. Chem. Soc.* **1986**, *108*, 7117–7119.

(39) Naota, T.; Takaya, H.; Murahashi, S.-I. *Chem. Rev.* **1998**, *98*, 2599–2660.

(40) Ohta, T.; Takaya, H.; Kitamura, M.; Nagai, K.; Noyori, R. *J. Org. Chem.* **1987**, *52*, 3176–3178.

(41) Doi, T.; Hirabayashi, K.; Kokubo, M.; Komagata, T.; Yamamoto, K.; Takahashi, T. *J. Org. Chem.* **1996**, *61*, 8360–8361.

(42) Kitamura, M.; Nagai, K.; Hsiao, Y.; Noyori, R. *Tetrahedron Lett.* **1990**, *31*, 549–552.

(43) Kitamura, M.; Kasahara, I.; Manabe, K.; Noyori, R.; Takaya, H. *J. Org. Chem.* **1988**, *53*, 710–712.

(44) Takaya, H.; Ohta, T.; Sayo, N.; Kumobayashi, H.; Akutagawa, S.; Inoue, S.; Kasahara, I.; Noyori, R. *J. Am. Chem. Soc.* **1987**, *109*, 1596–1597.

(45) Kitamura, M.; Hsiao, Y.; Ohta, M.; Tsukamoto, M.; Ohta, T.; Takaya, H.; Noyori, R. *J. Org. Chem.* **1994**, *59*, 297–310.

(46) Doucet, H.; Ohkuma, T.; Murata, K.; Yokozawa, T.; Kozawa, M.; Katayama, E.; England, A. F.; Ikariya, T.; Noyori, R. *Angew. Chem., Int. Ed. Engl.* **1998**, *37*, 1703–1707.

(47) Brief accounts of parahydrogen-induced polarization (PHIP) in the hydrogenations of methyl acrylate, methyl propargyl ether, phenyl acetylene, and propargyl alcohol (to yield achiral products) catalyzed by [Ru((*R*)-BINAP)(CH_3CO_2)$_2$] have appeared in the literature. Enantioselective hydrogenation of prochiral substrates, including tiglic acid and methyl tiglate, catalyzed by [Ru((*R*)-BINAP)(CH_3CO_2)$_2$] proved to be too slow to be studied using this method: (a) Eisenberg, R.; Eisenschmid, T. C.; Chinn, M. S.; Kirss, R. U. In *Homogeneous Transition Metal Catalyzed Reactions*; Moser, W. R., Slocum, D. W., Eds.; Advances in Chemistry Series 230; American Chemical Society: Washington, DC, 1992; Chapter 4. (b) Eisenberg, R. *Acc. Chem. Res.* **1991**, *24*, 110–116. (c) Eisenschmid, T. C. Ph.D. Thesis, University of Rochester, 1989.

(48) Ashby, M. T.; Halpern, J. *J. Am. Chem. Soc.* **1991**, *113*, 589–594.

(49) Ohta, T.; Takaya, H.; Noyori, R. *Tetrahedron Lett.* **1990**, *31*, 7189–7192.

(50) Chan, A. S. C.; Chen, C. C.; Yang, T. K.; Huang, J. H.; Lin, Y. C. *Inorg. Chim. Acta* **1995**, *234*, 95–100.

(51) Saburi, M.; Takeuchi, H.; Ogasawara, M.; Tsukahara, T.; Ishii, Y.; Ikariya, T.; Takahashi, T.; Uchida, Y. *J. Organomet. Chem.* **1992**, *428*, 155–167.

(52) Ashby, M. T.; Khan, M. A.; Halpern, J. *Organometallics* **1991**, *10*, 2011–2015.

(53) Chen, C.-C.; Huang, T.-T.; Lin, C.-W.; Cao, R.; Chan, A. S. C.; Wong, W. T. *Inorg. Chim. Acta* **1998**, *270*, 247–251.

(54) King, S. A.; DiMichele, L. In *Catalysis of Organic Reactions*; Scaros, M. G., Prunier, M. L., Eds.; Marcel Dekker: New York, 1995; Vol. 62, pp 157–166.

(55) Kawano, H.; Ikariya, T.; Ishii, Y.; Saburi, M.; Yoshikawa, S.; Uchida, Y.; Kumobayashi, H. *J. Chem. Soc., Perkin Trans. 1* **1989**, 1571–1575.

(56) (a) James, B. R.; Wang, D. K. W. *Can. J. Chem.* **1980**, *58*, 245–250. (b) James, B. R.; McMillan, R. S.; Morris, R. H.; Wang, D. K. W. In *Transition Metal Hydrides*; Bau, R., Ed.; Advances in Chemistry Series 167; American Chemical Society: Washington, DC, 1978; Chapter 9.

Chapter 2†

Syntheses, Characterization, and Reactivities of Ruthenium(II)–BINAP Complexes: A Versatile Catalyst System for Hydrogenation, Hydrosilylation, and Isomerization

Introduction

Nearly all reported examples of enantioselective reactions catalyzed by chiral ruthenium(II)–bis(phosphine) complexes (the most common are of BINAP) are hydrogenations[1] and transfer hydrogenations (Meerwein–Ponndorf–Verley reaction)[2] of olefins or ketones. These reactions generally occur with high TOFs, TONs, and ee's.[3] Reports of other reductive-type additions to double bonds (transformations that usually involve oxidative additions, insertions, and reductive eliminations) catalyzed by ruthenium(II)–bis(phosphine) complexes are rare, and tend to require either reactive substrates or elevated temperatures.[4] Of the numerous reports describing ruthenium–BINAP or related catalysts, there are only two examples that describe enantioselective catalysis of such reactions: hydrosilylation of reactive nitrones[4c] and one isomerization of an olefin.[5] Both the enormous success of chiral ruthenium(II)–bis(phosphine) catalysts in enantioselective hydrogenations, and their near absence in other reductive-type additions to double bonds encouraged this research group to extend ruthenium(II)–BINAP chemistry to the catalyst system described here. This chapter will describe the development of moderately air-stable complexes of ruthenium(II) and (*R*)-BINAP that undergo facile hydrogenation to produce catalysts for hydrosilylation and hydrogenation of ketones; and for isomerization, intramolecular hydrosilylation, and hydrogenation of olefins.

---

† Reproduced in part with permission from Wiles, J. A.; Lee, C. E.; McDonald, R.; Bergens, S. H. *Organometallics* **1996**, *15*, 3782–3784. Copyright 1996 American Chemical Society.

Results and Discussion

Syntheses and Characterization of Catalyst Precursors. Schrock et al.[6] reported that reaction of *cis*-[Ru(MeCN)$_2$(COD)(η^3-C$_3$H$_5$)]BF$_4$ (**1**) with phosphines such as PPh$_3$, PPhMe$_2$, and DIPHOS yielded complex mixtures of products in which extensive replacement of COD had occurred. In this laboratory, it was found that reaction between **1** and (*R*)-BINAP in acetone did not result in displacement of COD, but rather, resulted in activation of an allylic C–H bond of COD, and subsequent formation of propene[7] and two equimolar diastereomers of [Ru((*R*)-BINAP)(1–3:5,6-η-C$_8$H$_{11}$)(MeCN)]BF$_4$ (**2**) (eq 2-1).[8]

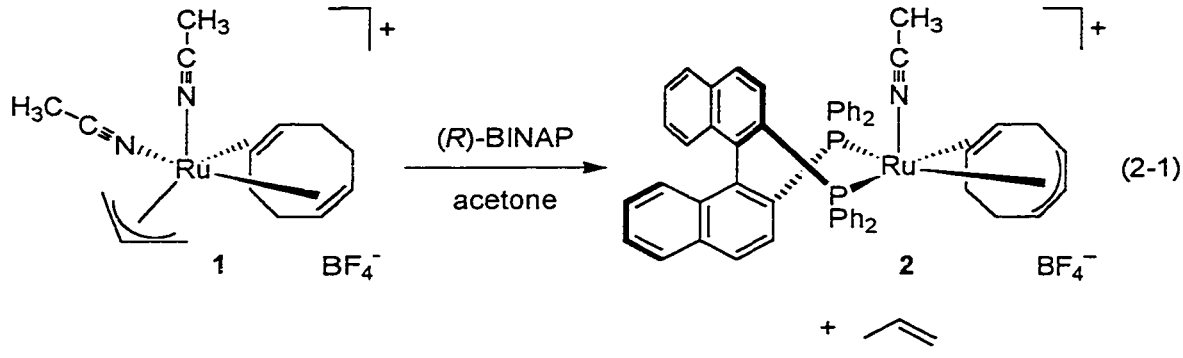

(2-1)

Complex **2** was isolated as moderately air-stable, lemon-yellow needles in 90% yield after recrystallization from diethyl ether and MeCN. This synthetic approach was also used for preparing the related complex [Ru((*R*)-TolBINAP)(1–3:5,6-η-C$_8$H$_{11}$)(MeCN)]BF$_4$ (**3**). Mass spectrometric data, multinuclear one- and two-dimensional NMR spectroscopic data, and elemental analyses data were all consistent with the formulation of two diastereomeric forms of **2**. The low-resolution positive-ion electrospray ionization mass spectrum displayed a signal of correct mass (m/z = 872.2) and isotope pattern for the molecular ion of **2** ((M – BF$_4$)$^+$). The ^{31}P{^{1}H} NMR spectrum showed an expected AB pattern for two inequivalent ^{31}P nuclei that occupy cis coordination sites ($^2J_{P-P}$ = 38.5 and 33.5 Hz) for each of the two diastereomers of **2**. The presence of both the 1–3:5,6-η-C$_8$H$_{11}$ and MeCN ligands was ascertained by ^{13}C{^{1}H} NMR spectroscopy. Two sets of five methine (CH) resonances ($\delta_{allylic}$ 31.1–90.0; $\delta_{olefinic}$ 62.9–117.3) and two sets of three

methylene (CH_2) resonances (δ 20.6–35.6) appeared in the $^{13}C\{^1H\}$ NMR spectrum of **2**, which are characteristic of the 1–3:5,6-η-C_8H_{11} ligand.[9] $^{13}C\{^1H\}$ NMR resonances at δ 4.8 and at δ 4.9 were ascribed to the methyl groups of the MeCN ligands of **2**. The ^1H NMR spectrum of **2** was poorly resolved (even at –80 °C) and, therefore, required two-dimensional techniques to obtain conclusive data. The connectivities in the framework of the 1–3:5,6-η-C_8H_{11} ligands were determined by ^1H–^1H COSY and ^1H–^{13}C HETCOR NMR experiments, and are consistent with the unconjugated η^5-assignment. Ranges for ^1H NMR resonances attributed to aliphatic, allylic, and olefinic groups of the 1–3:5,6-η-C_8H_{11} ligand are as follows: δ –0.21–3.26, δ 2.4–3.95, and δ 3.17–5.08, respectively. Full assignments for each of the diastereomers are listed in the Experimental Section.

The lability of the MeCN ligand in each of the diastereomers of **2** allowed the preparation of **2**-$MeC^{15}N$ by treating solutions of **2** with excess $MeC^{15}N$ at room temperature.[10] That only one signal was observed in the $^{15}N\{^1H\}$ NMR spectrum of **2**-$MeC^{15}N$ at room temperature (Figure 2-1) indicated that the $MeC^{15}N$ ligand of one of the two diastereomers (the labile diastereomer) was dissociating[11] at a rate that was similar to the timescale of the NMR technique (ca. 10^{-1}–10^{-6} s).[12] This conclusion is supported by the observation of one $^{15}N\{^1H\}$ NMR signal from each diastereomer at lower temperatures, where dissociation of $MeC^{15}N$ is suppressed. Further, the ^1H and $^{31}P\{^1H\}$ NMR signals from the labile diastereomer of **2** were broad at room temperature with respect to the corresponding signals at lower temperature. Unlike the $^{31}P\{^1H\}$ NMR signals from **2**-$MeC^{15}N$ at –20 °C, no $^2J_{P\text{-}N}$ was observed at room temperature. The magnitude of $^2J_{P\text{-}N}$ (2.5–4.0 Hz) for **2**-$MeC^{15}N$ at –20 °C indicated that the $MeC^{15}N$ ligand in each of the diastereomers occupy coordination sites cis to both phosphines. We believe that the two diastereomers of **2** have opposite absolute configurations about the sp^2 carbons in their respective 1–3:5,6-η-C_8H_{11} ligands. Crystals of one of the diastereomers of **2** suitable for X-ray analysis were obtained by slow liquid–liquid diffusion of methanol into a saturated 1,2-dichloroethane solution of **2** at room temperature. Crystals used for the X-ray analysis were not subsequently analyzed by NMR spectroscopy to assign signals to the diastereomer of **2** that was crystallographically characterized.

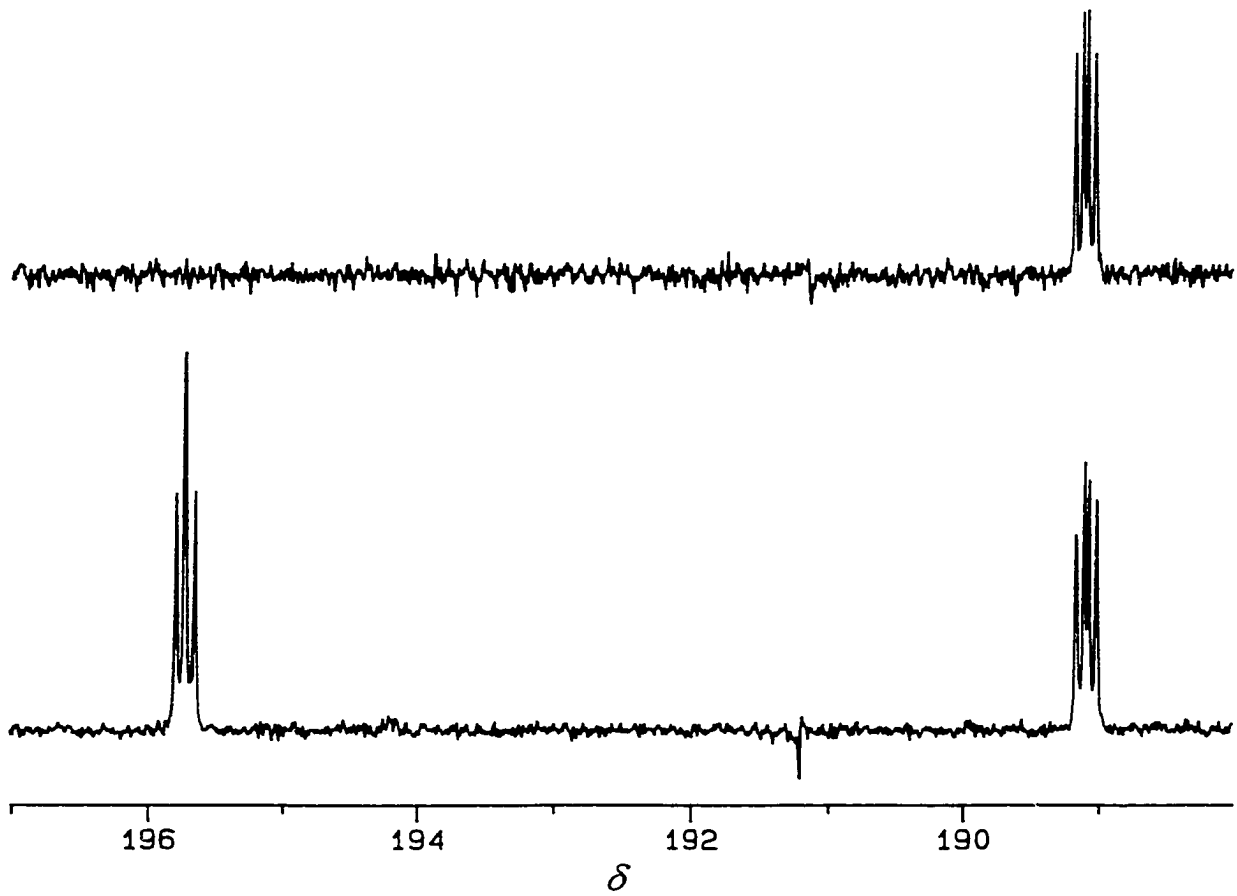

Figure 2-1. $^{15}N\{^{1}H\}$ NMR spectra of **2**-Me$C^{15}N$ (40.5 MHz, CD_2Cl_2) at 25 °C (top) and at –20 °C (bottom).

Figure 2-2 shows the molecular structure of (*S*)-**2**·0.5$C_2H_4Cl_2$ (*S* designates the absolute configuration of the central allylic carbon (C2) in 1–3:5,6-η-C_8H_{11}) as determined by single-crystal X-ray diffraction. Selected bond lengths and angles are listed in Table 2-1. Complex (*S*)-**2**·0.5$C_2H_4Cl_2$ is best described as a pseudo-octahedron about the ruthenium atom defined by the two phosphorus atoms of (*R*)-BINAP, by the nitrogen atom of the MeCN ligand, and by the facially coordinated 1–3:5,6-η-C_8H_{11} ligand. The dissymmetric (*R*)-BINAP ligand imposes a rigid λ conformation of the skewed seven-membered chelate ring that forces the phenyl substituents on the phosphorus atoms to be arranged in a chiral array. Figure 2-3 depicts this chiral environment where two of the phenyl groups (on opposite phosphorus atoms) are equatorially oriented and the remaining two phenyl groups are axially oriented with respect to the P–Ru–P plane. The Ru–P bond distances (Ru–P1, 2.332(2) Å; Ru–P2, 2.378(2) Å), the P1–Ru–P2 angle (91.20(8)°), and the dihedral angle between the two planes defined by the naphthalene rings (80.1(11)°) are all within the range reported for related ruthenium–BINAP complexes.[13] The Ru–N bond length (2.075(9) Å) is similar to those values reported for related ruthenium(II)–phosphine complexes.[10,14] Evidence against any π-backbonding component in the MeCN–Ru interaction is supported by the similarity of the N–C11 bond length (1.155(14) Å) to that determined for uncoordinated MeCN in the gas phase (1.157Å).[15] The 1–3:5,6-η-C_8H_{11} ligand is coordinated to the ruthenium atom through an olefin group (Ru–C5, 2.395(14) Å; Ru–C6, 2.402(12) Å) and through a nonsymmetric η^3-allylic interaction[9a,9c,16] (Ru–C1, 2.260(11) Å; Ru–C2, 2.165(11) Å; Ru–C3, 2.289(10) Å). That some of the C–C bond lengths in the cyclooctadienyl ligand are not chemically reasonable (C3–C4, 1.64(2) Å; C4–C5, 1.64(3) Å; C6–C7, 1.39(3) Å; C7–C8, 1.36(2) Å) and that the thermal ellipsoids for the some of the cyclooctadienyl ring carbons are severely elongated implies that disorder is present. The accuracy of this structure determination, as well as those reported in the literature, is also limited by data that were collected at room temperature; however, the structural information obtained is adequate for the purposes of confirming the bonding mode of the cyclooctadienyl ligand in (*S*)-**2**·0.5$C_2H_4Cl_2$ that was established by two-dimensional NMR spectroscopy.

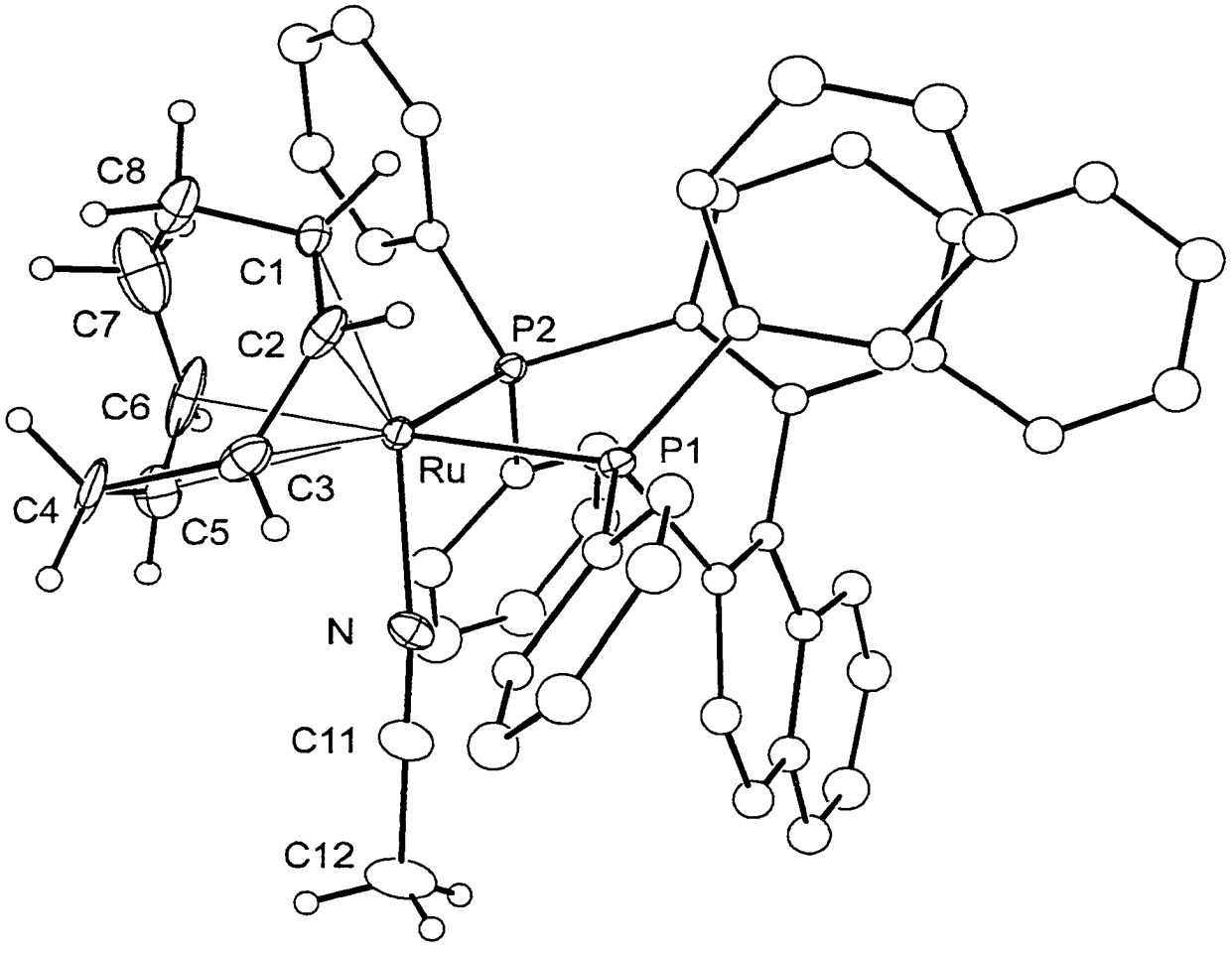

Figure 2-2. View of the complex cation of (*S*)-**2**·0.5$C_2H_4Cl_2$ showing the atom-labeling scheme.

Table 2-1. Selected Bond Lengths (Å) and Angles (deg) for (*S*)-2·0.5$C_2H_4Cl_2$

Ru–P1	2.332(2)	Ru–C5	2.395(14)	C4–C5	1.64(3)
Ru–P2	2.378(2)	Ru–C6	2.402(12)	C5–C6	1.23(2)
Ru–N	2.075(9)	C1–C2	1.41(2)	C6–C7	1.39(3)
Ru–C1	2.260(11)	C1–C8	1.50(2)	C7–C8	1.36(2)
Ru–C2	2.165(11)	C2–C3	1.41(2)	N–C11	1.155(14)
Ru–C3	2.289(10)	C3–C4	1.64(2)	C11–C12	1.46(2)
P1–Ru–P2	91.20(8)	C2–Ru–C1	37.2(4)	C2–Ru–C6	95.2(5)
N–Ru–P1	85.5(2)	C2–Ru–C3	36.8(4)	C1–Ru–C6	75.7(6)
N–Ru–P2	95.3(2)	C1–Ru–C3	66.7(4)	C3–Ru–C6	84.9(5)
N–Ru–C3	95.4(4)	C2–Ru–P2	134.8(3)	P1–Ru–C6	177.4(6)
C1–Ru–P1	103.5(3)	C1–Ru–P2	101.6(3)	C2–C1–C8	123.7(10)
C2–Ru–P1	85.4(3)	C3–Ru–P2	167.0(3)	C3–C2–C1	124.8(11)
C3–Ru–P1	97.0(3)	N–Ru–C5	76.7(5)	C2–C3–C4	126.7(10)
C3–Ru–P1	97.0(3)	C2–Ru–C5	90.1(5)	C5–C4–C3	100.4(9)
C5–Ru–P2	110.5(5)	C1–Ru–C5	88.3(5)	C6–C5–C4	125.9(17)
C6–Ru–P2	86.6(5)	C3–Ru–C5	65.1(6)	C5–C6–C7	128.9(19)
N–Ru–C2	129.1(4)	P1–Ru–C5	152.9(5)	C8–C7–C6	117.5(22)
N–Ru–C1	160.6(3)	N–Ru–C6	96.0(7)	C7–C8–C1	121.3(15)

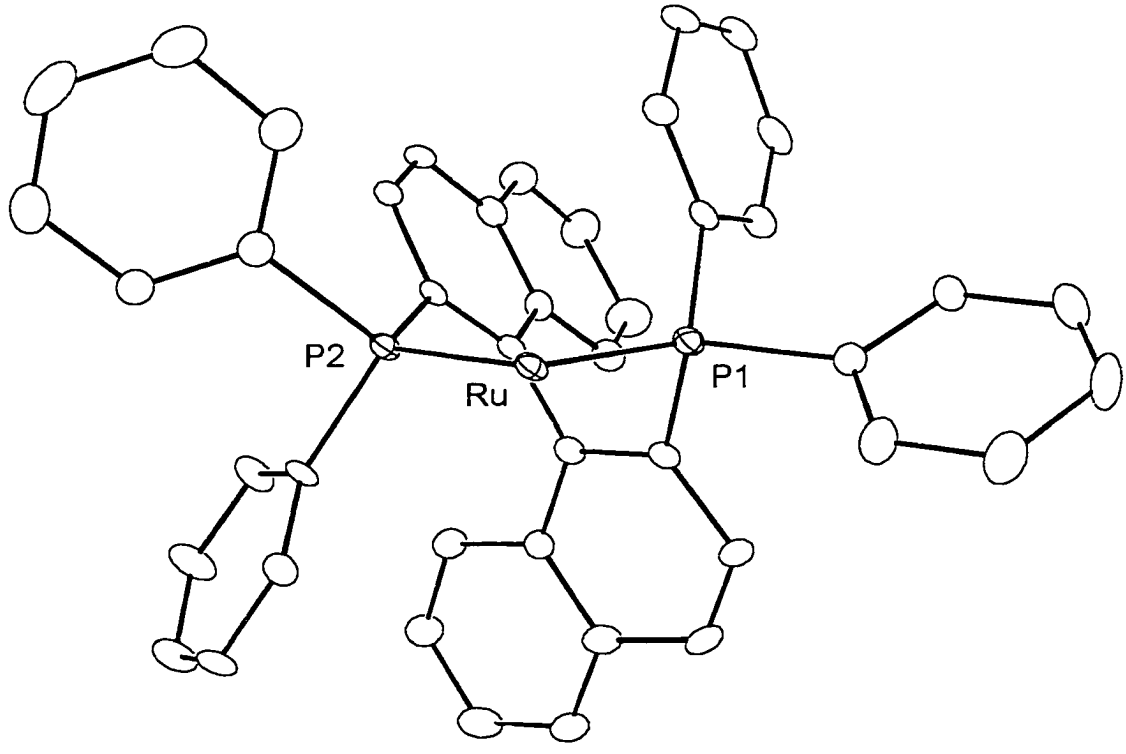

Figure 2-3. View of the complex cation of (*S*)-**2**·0.5$C_2H_4Cl_2$ illustrating the chiral environment of the (*R*)-BINAP ligand (MeCN and 1–3:5,6-η-C_8H_{11} ligands are omitted for clarity).

Generation and Characterization of Catalysts. Complex **2** reacted with an excess of dihydrogen gas under mild conditions (pressure of dihydrogen gas ≈ 1 atm, room temperature) in solutions of acetone, methanol, or THF[17] to yield cyclooctane[18] and the extremely air-sensitive hydride, [Ru((*R*)-BINAP)(H)(MeCN)$_n$(sol)$_{3-n}$]BF$_4$ (**4**, sol = acetone, methanol, or THF; n = 0–3, depending on reaction medium) (eq 2-2).[19] Further

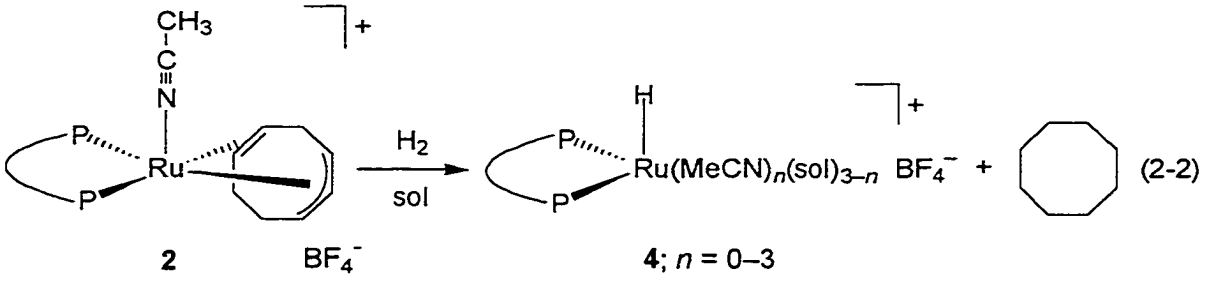

sol = acetone, methanol, or THF

reaction between **4** and dihydrogen gas under these conditions was not detected by NMR spectroscopy. Solutions of **4** do, however, readily react with dideuterium gas (even at –78 °C) to generate **4**-*d* with concomitant formation of HD gas. No detectable quantities of η^2-dihydrogen complexes were observed. It is believed that hydrogenolysis of **2** requires dissociation of MeCN prior to reaction with dihydrogen gas as the labile diastereomer (containing the more labile MeCN ligand) reacts faster than the non-labile diastereomer. Consistent with this hypothesis is that reaction of both diastereomers of **2** with dihydrogen gas is impeded by the presence of excess MeCN in solution. Exchange of the MeCN ligand between all the solvento coordination sites of **4** was rapid at room temperature in all solvents. This exchange slows upon cooling to give a static mixture of 8 hydrides ranging from *fac*-[Ru((*R*)-BINAP)(H)(acetone)$_3$]BF$_4$ to *fac*-[Ru((*R*)-BINAP)(H)-(MeCN)$_3$]BF$_4$ at –80 °C in acetone. These complexes all contain the hydrido ligand in a coordination site cis to both phosphorus centers as shown by the magnitude of the coupling between the phosphorus atoms and the hydride ($^2J_{P-H}$ = 24–30 Hz). The mutually cis disposition of the coordinated hydride and phosphorus centers presumably results from the high trans influence commonly observed for both of these ligands.[20] In THF

solution, the system exists mainly as one diastereomer of [Ru((*R*)-BINAP)(H)(MeCN)-(THF)$_2$]BF$_4$.[21] In MeCN solution, or when ≥2 equiv of MeCN are added to solutions of **4**, the system exists solely as *fac*-[Ru((*R*)-BINAP)(H)(MeCN)$_3$]BF$_4$ (**5**). Likewise, [Ru((*R*)-TolBINAP)(H)(MeCN)$_n$(sol)$_{3-n}$]BF$_4$ (**6**, sol = acetone, methanol, or THF; n = 0–3, depending on reaction medium) and *fac*-[Ru((*R*)-TolBINAP)(H)(MeCN)$_3$]BF$_4$ (**7**) can be prepared from **3** using the above methodology.

Catalysis. The availability of a hydrido ligand and at least two coordination sites (containing labile solvento ligands) makes **4** an attractive candidate for enantioselective catalysis. These features also distinguish **4** from other ruthenium–BINAP catalysts that have appeared in the literature. The versatility of **4** as a catalyst was evaluated using test reactions that are common in enantioselective catalysis. Tables 2-2, 2-3, and 2-4 summarize the reactions effected using 1–2 mol % **4** as the catalyst.

Reaction of (*rac*)-3-buten-2-ol ((*rac*)-**8**) with **4** (eq 2-3; Table 2-2, entry 1) resulted in a stereoselective isomerization to generate significant quantities of the simple enol, (*Z*)-2-buten-2-ol (**9**; maximum concentration ≈0.055 M). (*E*)-2-Buten-2-ol was not

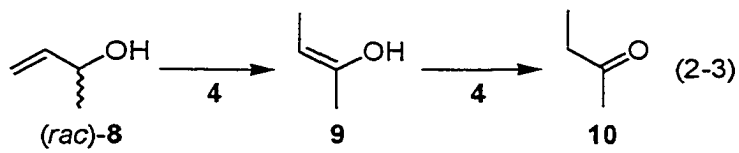

detected in solution by NMR spectroscopy. Although **9** was previously generated via isomerization of (*rac*)-**8** using rhodium–bis(phosphine) catalysts,[22] the rhodium catalysts were less stereoselective than **4**, and generated the enol as a mixture of the *E* and *Z* stereoisomers. A partial kinetic resolution of the *R* and *S* enantiomers of (*rac*)-**8** occurred during the isomerization catalyzed by **4**. The ee of **8** was 42% (*S*) at 50% conversion (t = 60 min; reaction mixture composition: 50% **8**, 42% **9**, 8% 2-butanone (**10**)). The rate of isomerization of **9** to **10** (eq 2-3; Table 2-2, entry 2) varied little over the course of the reaction.

Reaction of dimethyl(2-propen-1-oxy)silane (**11**)[23] with **4** (eq 2-4; Table 2-2, entry 3) resulted in competing intramolecular hydrosilylation and isomerization to generate (*Z*)-

Table 2-2. Hydrosilylation and Isomerization Reactions Catalyzed by 4[a]

entry	substrate	product	TOF, min^{-1} (time, h)[b]	yield, %	ee, %	abs conf
1[c]	(*rac*)-**8**	**9**	2.2[d]	50	42	*S*
2[c]	**9**	**10**	0.1	100	—	—
3	**11**	**12/13**	1.6	94[e]	—	—
4[f]	**12/13**	**14**[g]	(48)	100	—	—
5[f]	**15**[h]	**17**[i]	0.6 (1.5)	100	7	*R*

[a] Reactions conditions: 2 mol % **4**; [**4**] = 2.6 mM in THF unless stated otherwise. Complex **4** was generated before addition of substrate by hydrogenolysis of **2** (pressure of dihydrogen gas ≈ 1 atm, $t \approx 2$ min) followed by bubbling of the solution with argon gas (1 min). [b] The value in parentheses is the time required for complete reaction. [c] Reaction carried out in a mixture of THF and methylene chloride (≈20:1). [d] Initial rate of isomerization. [e] 87% **12** and 13% **13**. The remaining product (6%) was **14**. [f] Reaction carried out at 60 °C. [g] Generated as a mixture of monomer and polymer.[23] [h] Excess chlorodimethylsilane (3 equiv) was added to minimize the effect of its loss from evaporation on the hydrosilylation reaction. [i] Obtained by hydrolysis of **16** with potassium carbonate in methanol.[4d]

dimethyl(1-propen-1-oxy)silane (**12**; 81%), (*E*)-dimethyl(1-propen-1-oxy)silane (**13**; 13%), and 2,2-dimethyl-1-oxa-2-silacyclopentane (**14**; 6%, resulting from intramolecular hydrosilylation). Both **12** and **13** underwent intramolecular hydrosilylation to generate **14** upon heating to 60 °C (eq 2-4; Table 2-2, entry 4). The hydrosilylation of the silyl enol ethers, **12** and **13**, most likely proceeded via reverse isomerization to **11** followed by hydrosilylation of **11** to generate **14**.

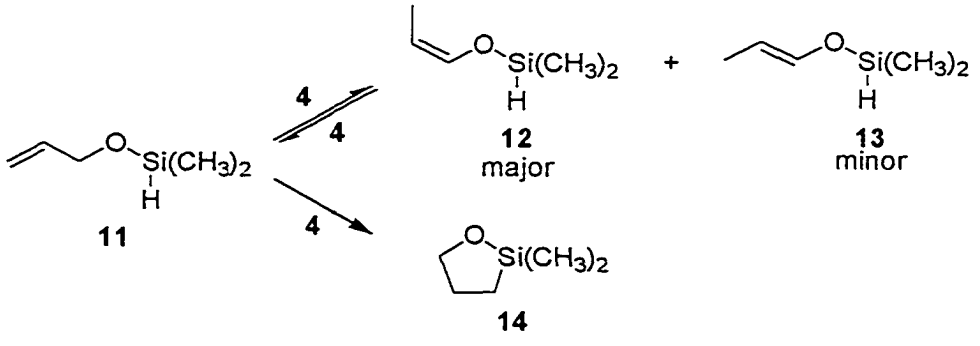

(2-4)

The hydrosilylation of ethyl acetoacetate (**15**) by chlorodimethylsilane (eq 2-5; Table 2-2, entry 5) using **4** as the catalyst proceeded at a reasonable rate to generate the corresponding silylated β-hydroxy ester (**16**). Subsequent hydrolysis of **16** with potassium carbonate in methanol afforded ethyl (*R*)-3-hydroxybutyrate ((*R*)-**17**) in 7% ee. Although the observed enantioselectivity for this reaction was poor, the above hydrosilylations of an olefin, **11**, and a ketone, **15**, are the first examples of such reactions to be catalyzed by a ruthenium–BINAP complex.

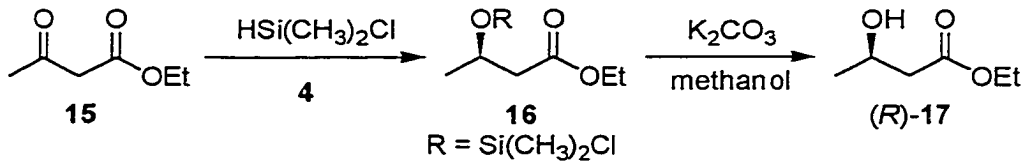

(2-5)

The hydrogenation of **15** to give (*S*)-**17** (eq 2-6; Table 2-3, entry 1) proceeded in a quantitative fashion, but with poor enantioselectivity (15% ee). Mashima et al. reported that addition of 2 equiv of HX (i.e., X = Cl or Br) to [Ru(BINAP)(CH_3CO_2)$_2$], followed by removal of all volatile components in vacuo, generated highly enantioselective catalysts for the hydrogenation of various β-keto esters, giving the corresponding secondary alcohols in >98% ee.[13e] Addition of 10 equiv of LiCl to **1** (Table 2-3; entry 2) marginally increased the enantioselectivity, but generated the opposite enantiomer as major product (20% ee (*R*)). The role of LiCl is unclear.

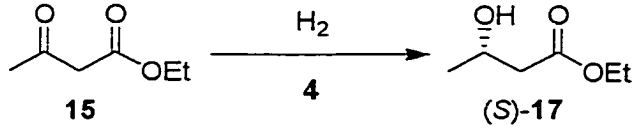

(2-6)

The hydrogenation of tiglic acid (**18**) was quantitative under mild conditions giving (*R*)-2-methylbutyric acid ((*R*)-**19**) in 90% ee (eq 2-7; Table 2-3, entry 3). The enantioselectivity observed for this particular substrate is among the highest reported for ruthenium–BINAP catalysts.[24] As is common with other ruthenium–BINAP catalysts,[25]

Table 2-3. Hydrogenation Reactions Catalyzed by 4[a]

entry	substrate	product	$P(H_2)$,[b] atm	T, °C	time, h	ee, %
1	**15**	(*S*)-**17**	100	50	24	15
2[c]	**15**	(*R*)-**17**	100	50	24	20
3	**18**	(*R*)-**19**	3	25	9.5	90
4	**18**	(*R*)-**19**	55	25	17.5	72
5	**20**	(*R*)-**21**	1	25	5	21
6	**20**	(*S*)-**21**	4	25	5	70
7	**20**	(*S*)-**21**	100	25	0.25	86

[a] Reaction conditions: 1 mol % **4**; [**4**] = 3.0 mM in methanol; stir rate = 1100 rpm; 100% conversion of reactants to products. [b] Pressures of dihydrogen gas are quoted as gauge pressure plus 1 atm. [c] LiCl (10 equiv) was added.

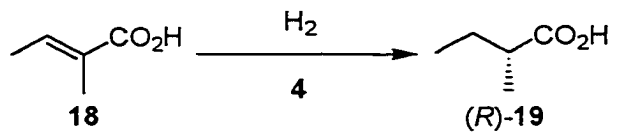

(2-7)

the ee for the hydrogenation of tiglic acid catalyzed by **4** decreased when the initial pressure of dihydrogen gas was increased (Table 2-3, entry 4).

The enantioselectivity for the hydrogenation of geraniol (**20**) catalyzed by **4** to generate β-citronellol (**21**) was also highly dependent on the pressure of dihydrogen gas (eq 2-8). The enantioselectivity inverted and its magnitude increased when the pressure of

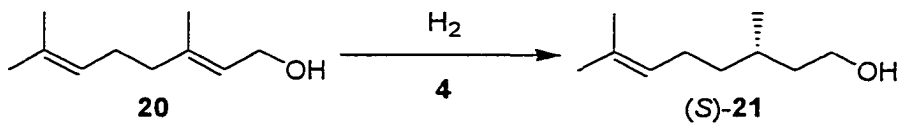

(2-8)

dihydrogen gas was increased from 1 atm to 4 atm (Table 2-3, entries 5 and 6). Compound (*S*)-**21** was obtained in 86% ee when the pressure of dihydrogen gas was elevated to 100 atm (Table 2-3, entry 7). Takaya et al. reported increases in ee from 70 to 98% (*S*) when the pressure of dihydrogen gas was increased from 4 to 100 atm using

[Ru((*R*)-BINAP)(CH_3CO_2)$_2$] as the catalyst precursor.[26] Blackmond and co-workers determined that the isomerization of **20** to γ-geraniol occured at a rate that was similar to that of the hydrogenation when using Et_2NH_2[(RuCl((*S*)-TolBINAP))$_2$(μ-Cl)$_3$] as the catalyst precursor (Scheme 2-1).[5,27] The enantioselectivity for the direct hydrogenation of

Scheme 2-1. Competing Hydrogenation and Isomerization of Geraniol

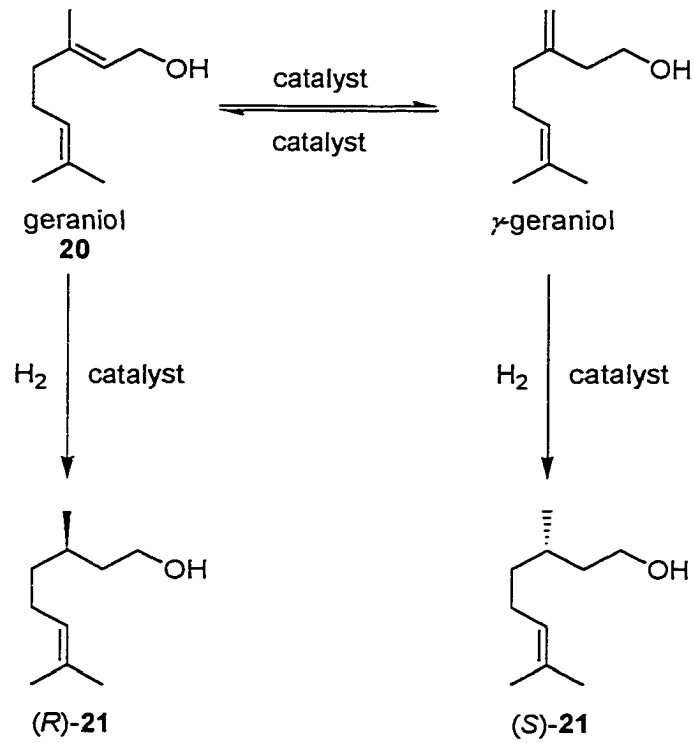

20 was found to be opposite to that for the direct hydrogenation of γ-geraniol, resulting in an inversion of enantioselectivity over the course of the catalytic hydrogenation. The results from the present study indicate that similar behavior occurs when **4** is the catalyst. It should be noted, however, that reaction of **20** with catalytic amounts of **4** in the absence of dihydrogen gas results in a complex mixture of olefin isomerization products rather than the exclusive formation of γ-geraniol as noted by Blackmond and co-workers.

The enantioselectivity observed for the hydrogenation of MAC (Table 2-4, entry 1) in methanol (87% ee (*R*)) catalyzed by **4** is comparable to values reported for other ruthenium–((*R*)-BINAP) catalysts.[1g,19c,28] Higher enantioselectivity (92% ee (*R*)) and TOF

Table 2-4. Catalytic Hydrogenation of MAC[a]

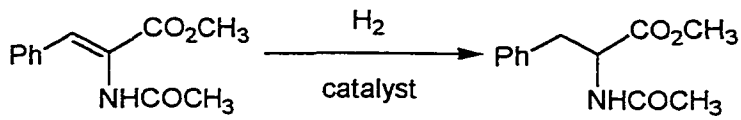

entry	solvent	catalyst	$P(H_2)$, atm	TOF,[b] min^{-1}	ee,[c] %	abs conf[c]
1	methanol	**4**	4	2.7×10^{-2}	87	*R*
2	acetone	**4**	4	0.9	92	*R*
3	acetone	**6**	4	—	87	*R*
4	acetone	**22**	4	—	33	*S*
5	methanol	**22**	4	2.7	19	*S*
6	MeCN	**4**	50	no reaction	—	—
7	acetone	**24**	4	—	92	*R*
8[d]	acetone	**24**	1	11.9	96	*R*
9[d]	acetone	**4**	1	0.1	—	—
10[d]	acetone	**22**	1	9.8	—	—

[a] Reaction conditions: 2 mol % catalyst; [catalyst] = 2.6 mM; stir rate = 1100 rpm; T = 30 °C except where noted otherwise. [b] The TOFs were determined by setting up and taking down the pressure reactor as quickly as possible during a hydrogenation. Their values are, therefore, to be taken as approximate. [c] Hydrogenations were allowed to react for 48 h to ensure complete conversion of reactants to products before the absolute configurations and the ee's of the products were determined. [d] Reaction carried out at 25 °C.

(ca. 0.9 min^{-1}) were obtained in acetone (Table 2-4, entry 2) than in the traditional solvent methanol (TOF ≈ 2.7×10^{-2} min^{-1}). The (*R*)-TolBINAP catalyst **6** was less enantioselective than **4** in acetone, leading to the hydrogenation product (*R*)-MAC$(H)_2$ in 87% ee (Table 2-4, entry 3). The enantioselectivity of **4** and **6** are significantly higher than that found for the benchmark catalyst precursor [Rh((*R*)-BINAP)(NBD)](ClO_4) (**22**). Hydrogenation of MAC in acetone and in methanol using **22** (Table 2-4, entries 4 and 5) as the catalyst precursor generated MAC$(H)_2$ in low ee and with the opposite enantioface selection (33% ee (*S*) and 19% ee (*S*), respectively). The TOF when using **22**, however, was greater than that when using **4** by approximately two orders of magnitude. A factor

contributing to this difference in TOF may be the presence of MeCN in **4**. Strong evidence that supports this argument is that no hydrogenation product was detected when the hydrogenation of MAC was performed in MeCN solution using **4** (effectively **5**) as catalyst even under forcing conditions (Table 2-4, entry 6). Other workers have also recognized that MeCN, and other nitriles, are strong inhibitors of ruthenium-catalyzed reactions.[11,13c,29] We anticipated that a ruthenium–BINAP catalyst without an MeCN ligand (i.e., *fac*-[Ru((*R*)-BINAP)(H)(sol)$_3$]BF$_4$, sol = acetone, methanol, or THF, depending on reaction medium) would provide TOFs that are similar to those found for **22**, while maintaining the high enantioselectivity exhibited by **4**.

Catalysts and Catalyst Precursors Revisited. Recent experiments showed that heating solutions of **2** in *n*-propanol results in isomerization of the 1–3:5,6-η-C_8H_{11} ligand[30] and loss of MeCN to generate **23** (eq 2-9) that contains a BINAP ligand formally acting as 6-electron donor (η^2-κ^2-biaryl coordination).[31] Both mass spectrometric data

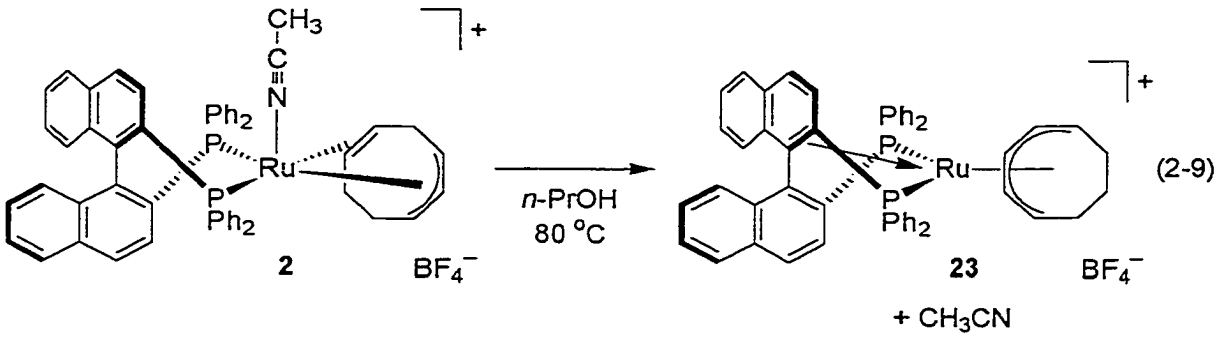

and multinuclear one- and two-dimensional NMR spectroscopic data are consistent with the formulated structure of **23**. The high-resolution positive-ion electrospray mass spectrum displayed a signal of correct mass (*m/z* = 831.188043) and isotope pattern for the molecular ion of **23** ((M – BF$_4$)$^+$, exact mass calcd for $C_{52}H_{43}P_2Ru$ 831.188351). The presence of the 1–5-η-C_8H_{11} ligand was unequivocally determined by ^{1}H and ^{13}C NMR spectroscopy. Initial inspection of the ^{1}H NMR spectrum of **23** revealed a high-field apparent quartet (δ –0.15 (J = 15.0 Hz, 1H, exo H-7)) that is typical for 1–5-η-C_8H_{11} ligands.[9c,30a,32] Subsequent ^{1}H–^{1}H COSY and ^{1}H–^{13}C HMQC NMR measurements confirmed this assignment, yielding data that are very similar to those obtained for the

related biaryl bis(phosphine) complex [Ru((*S*)-MeO-BIPHEP)(1–5-η-C_8H_{11})]BF_4.[31b] The $^{31}P\{^1H\}$ NMR spectrum of **23** showed a typical AX pattern for two inequivalent ^{31}P nuclei that occupy cis coordination sites (δ –6.0 (d) and δ 63.9 (d), $^2J_{P-P}$ = 44.5 Hz), with one of the ^{31}P nuclei suspiciously resonating at higher field than is commonly associated with a coordinated phosphine. Widely dispersed ^{31}P chemical shifts are now recognized as an indicator of the unconventional η^2-κ^2-biaryl bis(phosphine) coordination. The ^{13}C chemical shifts for the coordinated biaryl double bond (an expected upfield shift upon coordination), however, is a more reliable criterion. The ^1H–^{13}C HMBC NMR spectrum of **23** shows correlations that locate resonances from the coordinated biaryl double bond carbons[33] at δ 64.0 (d, J_{P-C} = 35.0 Hz, BINAP C-2) and δ 97.8 (dd, J_{P-C} = 5.5 Hz, 4.0 Hz, BINAP C-1). These data fully support the proposed structure of **23** and are in accord with the values reported for other genuine ruthenium–η^2-κ^2-BINAP complexes.[13c,31a]

Analogous to **2**, complex **23** rapidly reacted with an excess of dihydrogen gas in solutions of acetone to yield cyclooctane and *fac*-[Ru((*R*)-BINAP)(H)(acetone)$_3$]BF_4 (**24**; eq 2-10). Complexes **4** and **24** were found to catalyze the hydrogenation of MAC (Table

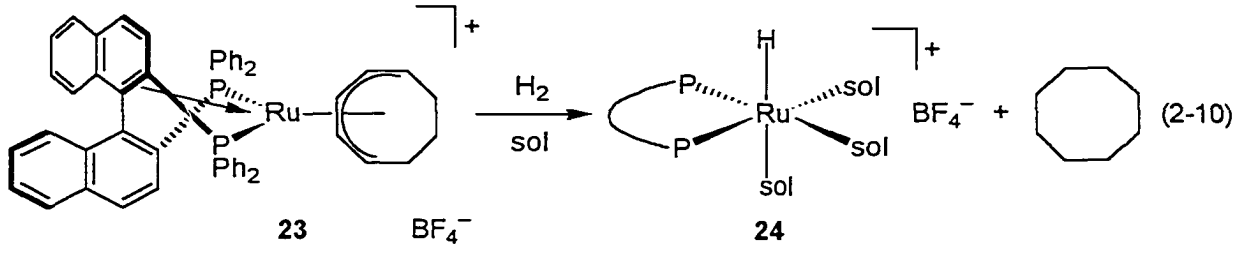

sol = acetone, methanol, or THF

2-4, entries 7 and 8) with equally high enantioselectivities (92% ee (*R*); T = 30 °C, pressure of dihydrogen gas = 4 atm); however, a substantial improvement in TOF was observed when **24** was the catalyst (**24**: ca. 11.9 min^{-1}; **4**: ca. 0.1 min^{-1}, T = 25 °C, pressure of dihydrogen gas = 1 atm). In comparison to **24**, the hydrogenation of MAC catalyzed by the benchmark catalyst [Rh((*R*)-BINAP)(acetone)$_2$](ClO_4) (Table 2-4, entry 10) proceeds with similar TOF (ca. 9.8 min^{-1}), but with much lower enantioselectivity and with an opposite sense of asymmetric induction (33% ee (*S*)).

Conclusions

Two diastereomeric forms of the catalyst precursor **2** were readily prepared by reaction of **1** with one equiv of (*R*)-BINAP. Thermally induced isomerization of the 1–3:5,6-η-C_8H_{11} ligand of **2** and loss of MeCN generates the highly reactive catalyst precursor **23**. Complexes **4** and **24** are most likely the active catalysts generated by reaction of **2** and **23**, respectively, with dihydrogen gas. Complex **24** is the most reactive (MeCN-free) form of **4**. The facile substitution of the solvento ligands in **4** (assuming that MeCN is displaced during catalysis), and the ability of the hydrido ligand to undergo insertion and elimination reactions, allows the ruthenium center to present the equivalent of four vacant coordination sites during catalysis. Further, **4** is not sterically hindered, the ruthenium center is in a low-oxidation state, and it apparently undergoes oxidative additions, insertions, and reductive eliminations. The combination of these abilities distinguishes **4** from previously reported ruthenium–bis(phosphine) complexes and accounts for the activity of **4** towards the catalytic reactions presented in this chapter. Finally, this catalyst system lends itself well to mechanistic investigations because the active catalyst can be easily generated in high concentrations.

Experimental Section

Materials. Argon gas (Praxair, 99.998%) was dried by passage through a column containing 3 Å molecular sieves and phosphorus pentoxide before use. Dihydrogen gas (Praxair, 99.99%) was passed through an Alltech Oxy-Trap to remove trace amounts of oxygen before use. Dideuterium gas (Aldrich, 99.8%; Praxair, 99.7%) was used as received. All protiated solvents (Anachemia, Caledon, and Fisher Scientific) and deuterated solvents (99.5–99.9% D, Cambridge Isotope Laboratories) were distilled from appropriate drying agents[34] under an atmosphere of argon gas before use , except absolute ethanol (200 proof) which was used as received. Unless stated otherwise, all reagents were used as received from Aldrich. The following reagents were distilled before use

under an atmosphere of argon gas or under vacuum (ca. 10 mm Hg), depending on their boiling points: (*rac*)-3-buten-2-ol, allyl alcohol, allyl chloride, chlorodimethylsilane, COD, ethyl acetoacetate, and geraniol. $[Ph_3C]BF_4$ was recrystallized from MeCN before use.[35] Triethylamine (Fisher Scientific) and pyridine (Fisher Scientific) were distilled from calcium hydride before use. (*R*)-BINAP (Strem) was recrystallized by established procedures before use.[36] $[Ru(COD)Cl_2]_n$,[37] $[Ru(COD)(\eta^3\text{-}C_3H_5)_2]$,[37] dimethyl(2-propen-1-oxy)silane,[23] (*R*)-MTPA-Cl,[38] (*R*)-MTPA esters,[38] and [Rh((*R*)-BINAP)(NBD)](ClO_4)[28b] were prepared as previously described. MAC was prepared by the esterification of α-acetamidocinnamic acid (recrystallized 5 times from boiling ethanol/*n*-hexanes) using diazomethane.[39] (*rac*)-MAC$(H)_2$ was obtained by hydrogenation of MAC using [Rh-(NBD)(DIPHOS)](ClO_4)[40] as the catalyst. (*S*)-MAC$(H)_2$ was used as received from Serva. Florisil (60–100 mesh) was supplied by Fisher Scientific.

Measurements. One-dimensional NMR spectra were recorded using a Bruker AM-400 spectrometer (^{1}H at 400.1 MHz, ^{13}C at 100.6 MHz, ^{15}N at 40.5 MHz, and ^{31}P at 161.9 MHz). Two-dimensional NMR spectra were recorded using a Varian Unity 500 spectrometer (^{1}H at 499.8 MHz and ^{13}C at 125.7 MHz). The chemical shifts for ^{1}H and ^{13}C are reported in parts per million (δ) relative to external tetramethylsilane and were referenced to signals of residual protons in the deuterated solvent. The chemical shifts for ^{15}N and ^{31}P are reported in parts per million (δ) relative to external liquid ammonia and external 85% phosphoric acid, respectively. NMR abbreviations used: br = broad, s = singlet, d = doublet, dd = doublet of doublet, ddd = doublet of doublet of doublets, t = triplet, q = quartet, dq = doublet of quartets, dt = doublet of triplets, and m = multiplet. Mass spectrometric analyses of **2** (in MeCN) and **23** (in methanol) were performed by positive-ion mode electrospray ionization (ESI-MS (pos)) on a Micromass ZabSpec Hybrid Sector-TOF spectrometer. Calculated *m/z* values refer to the isotopes ^{12}C, ^{1}H, ^{14}N, ^{16}O, ^{31}P, and ^{102}Ru. GLC–IR experiments were conducted on a Hewlett–Packard 5965IRD instrument, employing a J&W Scientific column DB5 (30 m × 0.32 mm internal diameter) having a film thickness of 1.00 μm. The carrier gas was helium and operated at a flow rate of 1.6 mL/min. Optical rotations were measured with a Perkin—Elmer 241

polarimeter at 589 nm using 1.0 dm cells. Elemental analyses were performed at the University of Alberta Microanalysis Laboratory.

Syntheses. All reactions requiring the exclusion of oxygen and/or water were carried out in dry solvents under an atmosphere of a dry argon gas using standard Schlenk and glovebox techniques.[34] All glassware and syringes were successively treated with ethanolic ammonium hydroxide solution and acetone, and oven-dried before use. Organometallic products were isolated in a glovebox filled with dinitrogen gas and were stored at –30 °C for prolonged periods.

(A) 1. Complex **1** was more conveniently prepared using $HBF_4 \cdot Et_2O$ as the electrophile instead of the originally reported electrophile $[Ph_3C]BF_4$.[6] The modified procedure is as follows. A diethyl ether solution (54% wt) of tetrafluoroboric acid (318 μL, 2.31 mmol) was added to a stirred solution of freshly sublimed $[Ru(COD)(\eta^3\text{-}C_3H_5)_2]$ (748.0 mg, 2.57 mmol, sublimed under dynamic vacuum (ca. 0.05 mm Hg) at 70 °C) in diethyl ether (5.0 mL) and MeCN (5.0 mL) at 0 °C. The resulting yellow solution was stirred for 5 min at 0 °C, and stirred an additional 2 min while warming to room temperature. The reaction mixture was evaporated under reduced pressure and the resulting yellow residue was washed with diethyl ether (5 × 5.0 mL). Slow addition of diethyl ether (5.0 mL over a 2 h period) to a saturated solution of the crude product in MeCN (1.3 mL) afforded yellow microcrystals. The product was washed with diethyl ether (3 × 5.0 mL) and dried in vacuo to yield 631.8 mg of **1** (65% yield based on tetrafluoroboric acid). The spectroscopic properties of this material matched those reported in the literature for **1**.

(B) 2. A 500-mL Schlenk flask was charged with **1** (0.8412 g, 2.01×10^{-3} mol), finely ground (*R*)-BINAP (1.2496 g, 2.01×10^{-3} mol), and acetone (100 mL). The resulting suspension (partially dissolved (*R*)-BINAP) was stirred at room temperature for 3 h to generate a dark yellow solution. Removal of the solvent under reduced pressure gave a yellow solid discolored by a brown residue. The crude product was dissolved in MeCN (20 mL), and the resulting solution was passed through a filter-paper-tipped cannula to remove trace amounts of particulate. Slow addition of diethyl ether (250 mL) to the filtered solution at room temperature afforded lemon-yellow needles. The product

was collected by filtration and was washed with diethyl ether (3 × 10 mL). Drying the solid in vacuo for 38 h at room temperature yielded 1.7394 g (90%) of **1**·0.4Et_2O. NMR spectroscopic data indicated that **1**·0.4Et_2O was isolated as a mixture of a labile and a non-labile diastereomer in a ratio of 1:1. The asterisks (*) denote resonances attributed to the labile diastereomer. ^{1}H NMR (400.1 MHz, CD_2Cl_2, 25 °C): δ –0.21 (m, 1H, H-7*), 1.05 (m, 1H, H-7'*), 1.41 (m, 1H, H-8*), 1.6–1.9 (m, 2H, H-8'* and H-8), 1.73 (s, 3H, CH_3CN*), 1.95 (m, 4H, H-8' and CH_3CN), 2.16 (m, 1H, H-4), 2.4–2.6 (m, 3H, H-3*, H-4*, and H-7), 2.69 (m, 1H, H-4'), 2.87 (m, 1H, H-7'), 3.17 (m, 2H, H-1 and H-5), 3.26 (m, 2H, H-2* and H-4'*), 3.40 (m, 1H, H-3), 3.53 (m, 2H, H-2 and H-5*), 3.95 (m, 1H, H-1*), 4.89 (m, 1H, H-6*), 5.08 (m, 1H, H-6), 5.6–8.1 (aromatic). ^{13}C{^{1}H} NMR (100.6 MHz, CD_2Cl_2, 25 °C): δ 4.8 (s, CH_3CN*), 4.9 (s, CH_3CN), 20.6 (s, C-4*), 21.2 (s, C-4), 24.9 (s, C-8), 25.3 (s, C-7*), 31.1 (s, C-3), 31.6 (s, C-8*), 35.6 (s, C-7), 36.7 (d, J_{P-C} = 14.5 Hz, C-3*), 55.8 (s, C-1*), 62.9 (s, C-5*), 66.2 (s, C-1), 71.2 (d, J_{P-C} = 27.5 Hz, C-5), 85.4 (s, C-2), 90.0 (s, C-2*), 99.3 (d, J_{P-C} = 12.0 Hz, C-6*), 117.3 (d, J_{P-C} = 8.5 Hz, C-6), 125–142 (aromatic, CH_3CN, and CH_3CN*). ^{31}P{^{1}H} NMR (161.9 MHz, CD_2Cl_2, 25 °C): δ 32.8 (d, $^2J_{P-P}$ = 33.5 Hz, 1P, P(A)), 35.7 (br d, $^2J_{P-P}$ = 38.5 Hz, 1P, P(A')*), 45.6 (br d, $^2J_{P-P}$ = 38.5 Hz, 1P, P(B')*), 46.9 (d, $^2J_{P-P}$ = 33.5 Hz, 1P, P(B)). ESI-MS (pos): *m/z* 872.2 ($(M - BF_4)^+$, exact mass calcd for $C_{54}H_{46}NP_2Ru$ 872.2). Anal. Calcd for $C_{54}H_{46}BF_4NP_2Ru$·0.4Et_2O: C, 67.56; H, 5.10; N, 1.42. Found: C, 67.21; H, 4.92; N, 1.54.

2-MeC^{15}N. MeC^{15}N (300 μL, 5.71 mmol) was added to a stirred solution of **2** (138.0 mg, 0.144 mmol) in methylene chloride (3.0 mL) at room temperature under argon gas. The reaction mixture was stirred at room temperature for 2 h, and then diethyl ether (200 mL) was slowly added to give a yellow solid. The product was collected by filtration and washed with diethyl ether (5 × 10 mL) to give 120.0 mg (87%) of **3**-MeC^{15}N (>95% ^{15}N-enriched). The asterisks (*) denote resonances attributed to the labile isomer. ^{31}P{^{1}H} NMR (161.9 MHz, CD_2Cl_2, –20 °C): δ 33.0 (dd, $^2J_{P-P}$ = 33.5 Hz, $^2J_{P-N}$ = 2.5 Hz, 1P), 35.5* (dd, $^2J_{P-P}$ = 39.0 Hz, $^2J_{P-N}$ = 3.0 Hz, 1P), 45.6* (dd, $^2J_{P-P}$ = 39.0 Hz, $^2J_{P-N}$ = 3.0 Hz, 1P), 46.8 (dd, $^2J_{P-P}$ = 33.5 Hz, $^2J_{P-N}$ = 4.0 Hz, 1P). ^{15}N{^{1}H} NMR (40.5 MHz, CD_2Cl_2, –20 °C): δ 189.1 (dd, $^2J_{P-N}$ = 4.0 Hz, $^2J_{P-N}$ = 2.5 Hz), 195.7* (apparent t, $^2J_{P-N}$ =

3.0 Hz). $^{15}N\{^1H\}$ NMR (40.5 MHz, CD_2Cl_2, 25 °C): δ 189.1 (dd, $^2J_{P(B)-N}$ = 4.0 Hz, $^2J_{P(A)-N}$ = 2.5 Hz). The corresponding $^{15}N\{^1H\}$ resonance for the labile diastereomer was not observed at 25 °C.

(C) 3. The method used for the preparation of **3** was the same as that used for **2** with substitution of (*R*)-TolBINAP for (*R*)-BINAP. The only procedural modifications were that **3** was recrystallized from a methylene chloride/diethyl ether solvent mixture and that the product was dried in vacuo for 12 h. Yield: 75%. NMR spectroscopic data indicated that **3** was isolated as a solvated mixture (**3**·0.8Et_2O·0.3CH_2Cl_2) of a labile and a non-labile diastereomer in a ratio of 1:1. The asterisks (*) denote resonances attributed to the labile isomer. ^1H NMR (400.1 MHz, CD_2Cl_2, 25 °C): δ –0.10 (m, 1H), 1.06 (m, 1H), 1.40 (m, 1H), 1.5–2.0 (m, 3H), 1.76 (br s, 3H, CH_3), 1.95 (br s, 3H, CH_3), 1.97 (s, 3H, CH_3), 1.98 (s, 3H, CH_3), 2.0–2.3 (m, 1H), 2.13 (s, 3H, CH_3), 2.16 (br s, 3H, CH_3), 2.3–2.6 (m, 3H), 2.43 (s, 3H, CH_3), 2.44 (s, 3H, CH_3), 2.48 (s, 6H, 2 × CH_3 overlapping), 2.67 (m, 1H), 2.84 (m, 1H), 3.19 (m, 4H), 3.36 (m, 1H), 3.46 (m, 2H), 3.91 (m, 1H), 4.84 (m, 1H), 5.02 (m, 1H), 5.7–8.6 (aromatic). $^{13}C\{^1H\}$ NMR (100.6 MHz, CD_2Cl_2, 25 °C): δ 4.8 (br, CH_3CN*), 5.0 (s, CH_3CN), 20.5 (br, C-4*), 21.0 (s, $C_6H_4CH_3$), 21.1 (s, $C_6H_4CH_3$), 21.2 (s, C-4), 21.4 (s, 2 × $C_6H_4CH_3$ overlapping), 24.9 (d, J_{P-C} = 3.5 Hz, C-8), 25.4 (d, J_{P-C} = 5.5 Hz, C-7*), 30.5 (s, C-3), 31.6 (s, C-8*), 35.6 (d, J_{P-C} = 7.0 Hz, C-7), 36.2 (d, J_{P-C} = 9.0 Hz, C-3*), 55.5 (br, C-1*), 62.5 (br, C-5*), 66.2 (s, C-1), 70.8 (d, J_{P-C} = 26.5 Hz, C-5), 85.4 (s, C-2), 90.0 (br, C-2*), 98.8 (br, C-6*), 116.3 (d, J_{P-C} = 9.0 Hz, C-6), 122–142 (aromatic, CH_3CN, and CH_3CN*). $^{31}P\{^1H\}$ NMR (161.9 MHz, CD_2Cl_2, 25 °C): δ 31.1 (d, $^2J_{P-P}$ = 33.5 Hz, 1P), 34.0 (br d, $^2J_{P-P}$ = 38.5 Hz, 1P*), 43.9 (br d, $^2J_{P-P}$ = 38.5 Hz, 1P*), 45.2 (d, $^2J_{P-P}$ = 33.5 Hz, 1P). ESI-MS (pos): *m/z* 928.3 ($(M - BF_4)^+$, exact mass calcd for $C_{58}H_{54}NP_2Ru$ 928.3). Anal. Calcd for $C_{58}H_{54}BF_4NP_2Ru$·0.8-Et_2O·0.3CH_2Cl_2: C, 67.17; H, 5.74; N, 1.27, Cl, 1.93. Found: C, 66.98; H, 5.55; N, 1.48, Cl, 2.13.

(D) 4 (Sol = Acetone-d_6). Complex **1** (19.5 mg, 2.03 × 10^{-5} mol) was partially dissolved in acetone-d_6 in an NMR tube under an atmosphere of argon gas. At room temperature, the headspace of the tube was flushed with dihydrogen gas, pressurized (1–2 atm), and shaken until a deep yellow-orange solution was generated (ca. 5 min). The

atmosphere of dihydrogen gas was replaced by argon gas and the resulting, highly air-sensitive solution was analyzed by ^{1}H and $^{31}P\{^{1}H\}$ NMR spectroscopy at –80 °C (to obtain well-resolved spectra). NMR spectroscopic analysis indicated a mixture of 8 ruthenium–hydrido species ([Ru((*R*)-BINAP)(H)(MeCN)$_n$(acetone-d_6)$_{3-n}$]BF_4, n = 0–3) and cyclooctane formed. At –80 °C, dideuterium gas (5.0 mL) was injected into the headspace of the NMR tube via syringe. The NMR tube was removed from the cooling bath, shaken for ca. 15 s, and then immediately placed in a precooled (–80 °C) NMR probe. Although the $^{31}P\{^{1}H\}$ NMR spectrum at –80 °C remained unchanged, the ^{1}H NMR spectrum indicated that exchange of all ruthenium–hydrido species with dideuterium gas (to form ruthenium–deuterio species) had occurred with concomitant formation of HD gas. NMR spectroscopic data for the hydrides (A–H): ^{1}H (400.1 MHz, acetone-d_6, –80 °C): δ –19.87 (br, A), –19.60 (apparent t, $^{2}J_{P-H}$ = 30.0 Hz, B), –19.45 (br, C), –19.26 (apparent t, $^{2}J_{P-H}$ = 30.0 Hz, D), –13.50 (apparent t, $^{2}J_{P-H}$ = 25.0 Hz, E), –13.20 (apparent t, $^{2}J_{P-H}$ = 25.0 Hz, F), –13.15 (dd, $^{2}J_{P-H}$ = 28.0 Hz, 24.0 Hz, G), –12.88 (apparent t, $^{2}J_{P-H}$ = 27.0 Hz, H), 1.6–2.4 (12 s, 12 × C*H*$_3$CN–Ru), 6.0–8.5 (aromatic). $^{31}P\{^{1}H\}$ (161.9 MHz, acetone-d_6, –80 °C): δ 59.4 (d, $^{2}J_{P-P}$ = 43.0 Hz, A), 60.8 (d, $^{2}J_{P-P}$ = 46.5 Hz, B), 63.2 (d, $^{2}J_{P-P}$ = 44.0 Hz, F), 63.6 (d, $^{2}J_{P-P}$ = 40.5 Hz, E), 66.0 (d, $^{2}J_{P-P}$ = 43.0 Hz, A), 68.2 (d, $^{2}J_{P-P}$ = 46.0 Hz, C),‡ 69.6 (d, $^{2}J_{P-P}$ = 40.5 Hz, E), 71.2 (d, $^{2}J_{P-P}$ = 49.5 Hz, D), 71.5 (d, $^{2}J_{P-P}$ = 43.0 Hz, G), 74.2 (d, $^{2}J_{P-P}$ = 47.0 Hz, H), 75.4 (d, $^{2}J_{P-P}$ = 43.0 Hz, G), 76.5 (d, $^{2}J_{P-P}$ = 46.5 Hz, B), 79.3 (d, $^{2}J_{P-P}$ = 49.5 Hz, D), 80.3 (d, $^{2}J_{P-P}$ = 44.0 Hz, F), 82.7 (d, $^{2}J_{P-P}$ = 47.0 Hz, H). The approximate distribution of ruthenium–hydrido species was 3% A, 14% B, 5% C, 22% D, 15% E, 15% F, 11% G, and 15% H. Although we have been unable to assign individual structures for each hydride, we have independently prepared *fac*-[Ru((*R*)-BINAP)(H)(MeCN)$_3$]BF_4 (**5**) and *fac*-[Ru((*R*)-BINAP)(H)(acetone-d_6)$_3$]BF_4 (**7**) that corresponded to hydrides E and D, respectively (vide infra).

‡ The corresponding $^{31}P\{^{1}H\}$ NMR signal was obscured by resonances attributed to hydrides D and G ca. δ 71.3.

4 (Sol = Methanol-d_4). Complex **1** (28.3 mg, 2.95 × 10^{-5} mol) was partially dissolved in methanol-d_4 (0.6 mL) and reacted with dihydrogen gas as outlined above for the synthesis of **4** (sol = acetone-d_6). ^{1}H NMR (400.1 MHz, methanol-d_4, –60 °C): δ –

20.22 (br), –13.10 (br), –12.93 (br apparent t, $^2J_{P-H}$ = 27.5 Hz, major, ca. 50% of total ruthenium species present), 1.65–2.40 (overlapping s, C*H*$_3$CN–Ru), 5.9–8.6 (br, aromatic). $^{31}P\{^1H\}$ NMR (161.9 MHz, methanol-d_4, –60 °C): δ 60.0 (br), 61.3 (apparent t, $^2J_{P-P}$ = 48.0 Hz), 64.1 (br d, $^2J_{P-P}$ = 43.5 Hz), 66.0 (d, $^2J_{P-P}$ = 43.5 Hz), 67.6 (d, $^2J_{P-P}$ = 43.5 Hz), 69.7 (d, $^2J_{P-P}$ = 43.5 Hz), 71.2 (d, $^2J_{P-P}$ = 43.5 Hz), 74.1 (br d, $^2J_{P-P}$ = 52.5 Hz), 75.4 (d, $^2J_{P-P}$ = 48.0 Hz, major, ca. 50%), 79.9 (d, $^2J_{P-P}$ = 46.0 Hz), 81.0 (apparent t, $^2J_{P-P}$ = 48.0 Hz), 82.3 (d, $^2J_{P-P}$ = 49.0 Hz, major, ca. 50%).

4 (Sol = THF-d_8). Complex **1** (10.7 mg, 1.16 × 10^{-5} mol) was dissolved in a mixture of THF-d_8 (0.5 mL) and CD_2Cl_2 (0.1 mL) in an NMR tube under an atmosphere of argon gas to generate a yellow solution. At room temperature, dihydrogen gas (5.0 mL, 2.0 × 10^{-4} mol) was injected into the headspace of the tube via syringe, and the mixture was shaken for 2 min with intermittent cooling (–78 °C) to give a dark yellow solution. Cooling was necessary to prevent the degradation of **4** that is rapid in the presence of methylene chloride at room temperature. The distribution of ruthenium species as determined by NMR spectroscopy at –80 °C was 44% [Ru((*R*)-BINAP)-(H)(MeCN)(THF)$_2$]BF$_4$, 15% [Ru((*R*)-BINAP)(H)(MeCN)$_2$(THF)]BF$_4$, and 41% **1** (non-labile diastereomer). The presence of cyclooctene and cyclooctane was determined by ^{1}H NMR spectroscopy (cyclooctene:cyclooctane ≈ 1:3) and confirmed by GLC–IR. Further addition of dihydrogen gas (5.0 mL) and shaking at room temperature for 2 min caused complete hydrogenation of cyclooctene to cyclooctane. The distribution of ruthenium species detected in solution were 59% [Ru((*R*)-BINAP)(H)(MeCN)(THF)$_2$]BF$_4$, 14% [Ru((*R*)-BINAP)(H)(MeCN)$_2$(THF)]BF$_4$, 27% **1** (non-labile diastereomer), and two other species in amounts too low to accurately integrate (we assign one as *fac*-[Ru((*R*)-BINAP)(H)(MeCN)$_3$]BF$_4$ (**5**)). The solution was warmed to room temperature and MeCN (3.6 mL, 6.9 × 10^{-5} mol) was added via syringe, causing the yellow color to lighten. The solution was cooled to –80 °C for further ^{1}H and $^{31}P\{^1H\}$ NMR spectroscopic analyses. The solution contained a product identified by NMR spectroscopy as **5** (78%), and the non-labile diastereomer of **1** (22%). **4** ([Ru((*R*)-BINAP)(H)(MeCN)-(THF)$_2$]BF$_4$): ^{1}H NMR (400.1 MHz, THF-d_8/CD_2Cl_2 (5:1 v/v), –80 °C): δ –13.05 (apparent t, $^2J_{P-H}$ = 28.0 Hz, 1H, Ru–*H*), 2.74 (s, 3H, C*H*$_3$CN), 6.0–8.7 (aromatic,

overlapping with [Ru((*R*)-BINAP)(H)(MeCN)$_2$(THF)]BF$_4$). ^{31}P{^{1}H} NMR (161.9 MHz, THF-d_8/CD$_2$Cl$_2$ (5:1 v/v), –80 °C): δ 72.2 (d, $^2J_{P-P}$ = 49.5 Hz, 1P, overlapping with [Ru((*R*)-BINAP)(H)(MeCN)$_2$(THF)]BF$_4$), 81.3 (d, $^2J_{P-P}$ = 49.5 Hz, 1P). **4** ([Ru((*R*)-BINAP)(H)(MeCN)$_2$(THF)]BF$_4$): ^{1}H NMR (400.1 MHz, THF-d_8/CD$_2$Cl$_2$ (5:1 v/v), –80 °C): δ –12.98 (Ru–*H*, overlapping with [Ru((*R*)-BINAP)(H)(MeCN)(THF)$_2$]BF$_4$), 1.96 (s, 3H, C*H*$_3$CN), 2.17 (s, 3H, C*H*$_3$CN), 6.0–8.7 (aromatic, overlapping with [Ru((*R*)-BINAP)(H)(MeCN)(THF)$_2$]BF$_4$). ^{31}P{^{1}H} NMR (161.9 MHz, THF-d_8/CD$_2$Cl$_2$ (5:1 v/v), –80 °C): δ 72.2 (1P, overlapping with [Ru((*R*)-BINAP)(H)(MeCN)(THF)$_2$]BF$_4$), 76.9 (d, $^2J_{P-P}$ = 42.5 Hz, 1P). **5**: ^{1}H NMR (400.1 MHz, THF-d_8/CD$_2$Cl$_2$ (5:1 v/v), –80 °C): δ –13.48 (apparent t, $^2J_{P-H}$ = 24.0 Hz, 1H, Ru–*H*), 1.84 (s, 3H, C*H*$_3$CN), 1.87 (s, 3H, C*H*$_3$CN), 2.22 (s, 3H, C*H*$_3$CN), 6.0–8.9 (aromatic). ^{31}P{^{1}H} NMR (161.9 MHz, THF-d_8/CD$_2$Cl$_2$ (5:1 v/v), –80 °C): δ 64.2 (d, $^2J_{P-P}$ = 40.0 Hz, 1P), 69.9 (d, $^2J_{P-P}$ = 40.0 Hz, 1P).

(E) 6 (Sol = Acetone-d_6). Complex **3** (25.3 mg, 2.49 × 10^{-5} mol) was dissolved in acetone-d_6 (0.6 mL) and reacted with dihydrogen gas as outlined above for the synthesis of **4** (sol = acetone-d_6). NMR spectroscopic data for the hydrides (A–H): ^{1}H (400.1 MHz, acetone-d_6, –80 °C): δ –20.14 (apparent t, $^2J_{P-H}$ = 28.0 Hz, A), –19.80 (apparent t, $^2J_{P-H}$ = 30.0 Hz, C), –19.77 (apparent t, $^2J_{P-H}$ = 30.0 Hz, B), –19.55 (apparent t, $^2J_{P-H}$ = 30.0 Hz, D), –13.77 (dd, $^2J_{P-H}$ = 26.5 Hz, 24.0 Hz, E), –13.53 (apparent t, $^2J_{P-H}$ = 27.0 Hz, F), –13.34 (dd, $^2J_{P-H}$ = 29.0 Hz, 24.0 Hz, G), –13.14 (apparent t, $^2J_{P-H}$ = 27.0 Hz, H), 1.6–2.5 (overlapping s, C*H*$_3$), 5.8–8.2 (aromatic). ^{31}P{^{1}H} (161.9 MHz, acetone-d_6, –80 °C): δ 56.8 (d, $^2J_{P-P}$ = 43.5 Hz, A), 59.0 (d, $^2J_{P-P}$ = 48.0 Hz, B), 60.8 (d, $^2J_{P-P}$ = 44.5 Hz, F), 60.9 (d, $^2J_{P-P}$ = 41.0 Hz, E), 63.7 (d, $^2J_{P-P}$ = 43.5 Hz, A), 65.8 (d, $^2J_{P-P}$ = 48.5 Hz, C), 66.8 (d, $^2J_{P-P}$ = 41.0 Hz, E), 68.2 (d, $^2J_{P-P}$ = 48.5 Hz, C), 68.9 (d, $^2J_{P-P}$ = 43.5 Hz, G), 69.3 (d, $^2J_{P-P}$ = 50.0 Hz, D), 72.2 (d, $^2J_{P-P}$ = 47.5 Hz, H), 73.1 (d, $^2J_{P-P}$ = 43.5 Hz, G), 74.7 (d, $^2J_{P-P}$ = 48.0 Hz, B), 76.8 (d, $^2J_{P-P}$ = 50.0 Hz, D), 77.7 (d, $^2J_{P-P}$ = 44.5 Hz, F), 80.0 (d, $^2J_{P-P}$ = 47.5 Hz, H). The approximate distribution of ruthenium–hydrido species was 4% A, 19% B, 4% C, 29% D, 11% E, 15% F, 7% G, and 11% H. Although we have been unable to assign individual structures for each hydride, we have independently

prepared **7** (by addition of 2 equiv of MeCN to a solution of **6** in acetone-d_6) that corresponded to hydride E.

(F) 23. Complex **2** (100.7 mg, 0.105 mmol) was partially dissolved in *n*-propanol (40.0 mL) under an atmosphere of argon gas. The reactor was sealed and the mixture was stirred with heating (80 °C) for 40 min to generate an amber solution. The solvent was removed under reduced pressure with heating (80 °C) to give a yellow solid. Slow addition of *n*-pentane (80 mL) to a methylene chloride solution (2.0 mL) of the product afforded a yellow powder. The purified product was collected by filtration, washed with *n*-pentane (2 × 20 mL), and dried in vacuo for 90 h to yield 55.6 mg (58%) of **23**.[41] ^{1}H NMR (599.9 MHz, CD_2Cl_2, 25 °C): δ –0.15 (apparent q, J = 15.0 Hz, 1H, exo H-7), 0.07 (apparent t, J = 15.0 Hz, 1H, H-6), 0.84 (apparent t, J = 15.0 Hz, 2H, overlapping H-4 and endo H-7), 1.00 (br, 1H, H-6'), 1.54 (apparent t, J = 15.0 Hz, 1H, H-8), 1.86 (br, 1H, H-8'), 2.20 (br, 1H, H-5), 4.65 (br, 1H, H-1), 5.46 (br, 2H, overlapping H-2 and H-3), 6.0–8.3 (aromatic). ^{13}C{^{1}H} NMR (100.6 MHz, CD_2Cl_2, 25 °C): δ 18.9 (s, C-7), 23.2 (d, J_{P-C} = 2.0 Hz, C-6), 27.3 (s, C-8), 58.5 (apparent t, J_{P-C} = 3.5 Hz, C-1), 64.0 (d, J_{P-C} = 35.0 Hz, BINAP C-2), 71.6 (dd, J_{P-C} = 20.0 Hz, 2.0 Hz, C-5), 91.0 (s, C-2), 96.2 (s, C-4), 97.8 (dd, J_{P-C} = 5.5 Hz, 4.0 Hz, BINAP C-1), 114.1 (d, J_{P-C} = 9.5 Hz, C-3), 123–148 (aromatic). ^{31}P{^{1}H} NMR (161.9 MHz, CD_2Cl_2, 25 °C): δ –6.0 (d, $^2J_{P-P}$ = 44.5 Hz, 1P), 63.9 (d, $^2J_{P-P}$ = 44.5 Hz, 1P). Satisfactory elemental analyses could not be obtained for **23** after repeated attempts on several recrystallized samples that were solvent-free and of >95% purity as determined by NMR spectroscopy. Typically, carbon analyzed 2–3% lower than that calculated for **23**, although hydrogen analysis data were in good agreement with the calculated values. It is plausible that the low carbon analysis resulted from incomplete oxidation of carbon caused by the formation of ruthenium carbides upon thermal decomposition of **23**. The molecular weight determined by HRMS is provided in lieu of elemental analyses. High-resolution ESI-MS (pos): *m/z* 831.188043 ($(M - BF_4)^+$, exact mass calcd for $C_{52}H_{43}P_2Ru$ 831.188351).

(G) 24 (Sol = Acetone-d_6). Complex **23** (16.0 mg, 1.74 × 10^{-5} mol) was dissolved in acetone-d_6 (0.6 mL) and reacted with dihydrogen gas as outlined above for the synthesis of **4** (sol = acetone-d_6). ^{1}H NMR (400.1 MHz, acetone-d_6, 25 °C): δ –19.80

(apparent t, $^2J_{P-H}$ = 30.5 Hz). $^{31}P\{^1H\}$ NMR (161.9 MHz, acetone-d_6, 25 °C): δ 71.2 (d, $^2J_{P-P}$ = 49.5 Hz, 1P), 79.7 (d, $^2J_{P-P}$ = 49.5 Hz, 1P).

24 (Sol = THF-d_8). Complex **23** (25.0 mg, 2.72 × 10^{-5} mol) was dissolved in THF-d_8 (0.6 mL) and reacted with dihydrogen gas as outlined above for the synthesis of **4** (sol = acetone-d_6). ^1H NMR (400.1 MHz, THF-d_8, –40 °C): δ –19.45 (br, Ru–*H*), 6.0–8.5 (aromatic). $^{31}P\{^1H\}$ NMR (161.9 MHz, THF-d_8, –40 °C): δ 74.1 (br d, $^2J_{P-P}$ = 50.0 Hz, 1P), 82.0 (br, 1P).

Catalytic Reactions. Small-scale hydrosilylation and isomerization reactions were conducted in 5-mm NMR tubes and were monitored by ^1H NMR spectroscopy to calculate TOF values and chemical yields (see Table 2-2). TOF values for hydrogenation reactions were determined by setting up and taking down the pressure reactor as quickly as possible during a hydrogenation. Their values are, therefore, to be taken as approximate. The ee for each reaction was determined by repeating the experiment on a larger scale and analyzing the products as described below.

(A) Procedure for Small-Scale Catalytic Hydrosilylation and Isomerization Reactions. Typically, complex **2** (1.2 mg, 1.25 × 10^{-6} mol) was vigorously mixed with THF-d_8 (0.48 mL) for several minutes to generate a light yellow solution. Dihydrogen gas (5.0 mL, 2.0 × 10^{-4} mol) was injected into the headspace of the NMR tube via syringe and the mixture was shaken for ca. 2 min at room temperature to generate a dark yellow solution. The solution was slowly bubbled with argon gas (1 min) and the substrate (50 equiv, 6.25 × 10^{-5} mol) was then added via syringe.

(B) Procedure for Large-Scale Catalytic Reactions. These reactions were performed in a manner similar to that described for small-scale experiments, except that quantities of reactants were increased by a factor of 15, and non-deuterated solvents were used. Generation of the catalytically active solution for hydrosilylation and isomerization reactions was accomplished by bubbling dihydrogen gas through a stirring solution (2.6 mM) of **2** in a Schlenk flask at room temperature for ca. 2 min, followed by bubbling the solution with argon gas for 1 min. The substrate was then added via syringe, and the reaction was carried out under the conditions given in Table 2-2. A glass pressure reactor (Lab Glass) was employed for hydrogenation reactions where the pressure of dihydrogen

gas was ≤4 atm. For reactions requiring elevated pressures, a Parr cell-disruption bomb was used. For hydrogenation reactions, the appropriate pressure reactor was charged with substrate and catalyst precursor under an atmosphere of argon gas. The reaction vessel was purged with dihydrogen gas and its contents were dissolved in the appropriate deoxygenated solvent. The reactor was pressurized and heated to the desired levels, and the reaction was stirred at 1100 rpm. Reaction conditions are given in Tables 2-3 and 2-4.

(C) Workups and Analyses. The solvents were removed at the end of the reaction by use of either a rotary evaporator or by distillation at atmospheric pressure, depending on the boiling points of the products. The specific workups and product analyses are outlined below.

The isomerization of (*rac*)-3-buten-2-ol ((*rac*))-**8** in THF-d_8/CD_2Cl_2 (≈20:1 v/v) was monitored by ^{1}H NMR spectroscopy. (*Z*)-2-Buten-2-ol (**9**) was identified by comparison to a literature spectrum.[23] 2-Butanone (**10**) was identified by ^{1}H NMR spectroscopy and by GLC–IR (the IR spectrum was identical to that of an authentic sample). The ee of the remaining **8** was determined as follows. An aliquot (5 mL) was removed via cannula from a large-scale reaction mixture 60 min after the addition of substrate, and the catalyst was deactivated in the aliquot by bubbling carbon monoxide gas (1 atm) through the solution for 30 s. The aliquot was mixed with *n*-pentane (20 mL), and passed through a Florisil plug to remove the catalyst. The solvent was removed by distillation under argon gas (T_{bath} = 70 °C), and the residue was reacted with (*R*)-MTPA-Cl. The ee was determined by comparison of the ^{1}H NMR spectrum of the derivatized residue to that of the (*R*)-MTPA ester of an authentic sample of (*S*)-**8**.[42] (*R*)-MTPA ester of (*S*)-**8** (*R*,*S* diastereomer): ^{1}H NMR ($CDCl_3$, 400.1 MHz, 25 C°): δ 1.44 (d, J = 6.5 Hz, 3H, CH_3CH), 3.58 (d, J = 1.5 Hz, 3H, OCH_3), 5.16 (apparent dt, J = 10.5 Hz, 1.5 Hz, 1H, *cis*-CH_2=CH), 5.25 (apparent dt, J = 17.5, 1.5 Hz, 1H, *trans*-CH_2=CH), 5.59 (m, 1H, CH_3CH, overlapping with the *R*,*R* diastereomer), 5.81 (ddd, J = 17.5 Hz, 10.5 Hz, 4.5 Hz, 1H, CH_2=CH), 7.3–7.7 (aromatic, overlapping with the *R*,*R* diastereomer). (*R*)-MTPA ester of (*R*)-**8** (*R*,*R* diastereomer): ^{1}H NMR ($CDCl_3$, 400.1 MHz, 25 C°): δ 1.37 (d, J = 6.5 Hz, 3H, CH_3CH), 3.56 (d, J = 1.5 Hz, 3H, OCH_3), 5.22 (apparent dt, J = 10.5, 1.5 Hz, 1H, *cis*-CH_2=CH), 5.35 (apparent dt, J = 17.5, 1.5 Hz, 1H, *trans*-CH_2=CH), 5.59 (m,

1H CH_3CH, overlapping with the *R,S* diastereomer), 5.90 (ddd, J = 17.5 Hz, 10.5 Hz, 4.5 Hz, 1H, CH_2=CH), 7.3–7.7 (aromatic, overlapping with the *R,S* diastereomer).

The isomerization and intramolecular hydrosilylation of dimethyl(2-propen-1-oxy)silane (**11**) in THF-d_8 was monitored by ^{1}H NMR spectroscopy. Compounds **12**, **13**, **14**, and poly-**14** were identified by comparison to literature spectra.[43] **12**: ^{1}H NMR (400.1 MHz, THF-d_8, 25 °C): δ 0.25 (d, J = 3.0 Hz, 6H, $SiH(CH_3)_2$), 1.52 (dd, J = 6.5, 1.5 Hz, 3H, CH_3CH=CH), 4.50 (dq, J = 6.5 Hz, 1.5 Hz, 1H, CH_3CH=CH), 4.69 (heptet, J = 3.0 Hz, 1H, $SiH(CH_3)_2$), 6.17 (dq, J = 6.5 Hz, 1.5 Hz, 1H, CH_3CH=CH). **13**: ^{1}H NMR (400.1 MHz, THF-d_8, 25 °C): δ 0.23 (d, J = 3.0 Hz, 6H, $SiH(CH_3)_2$), 1.49 (dd, J = 6.5, 2.0 Hz, 3H, CH_3CH=CH), 4.99, (m, 1H, CH_3CH=CH), 4.61 (heptet, J = 3.0 Hz, 1H, $SiH(CH_3)_2$), 6.21 (dq, J = 12.0, 2.0 Hz, 1H, CH_3CH=CH). **14**: ^{1}H NMR (400.1 MHz, THF-d_8, 25 °C): δ 0.12 (s, 6H, $Si(CH_3)_2$), 0.70 (t, J = 7.5 Hz, 2H, $SiCH_2CH_2CH_2O$), 1.82 (tt, J = 7.5 Hz, 6.5 Hz, 2H, $SiCH_2CH_2CH_2O$), 3.74 (t, J = 6.5 Hz, 2H, $SiCH_2CH_2CH_2O$). Poly-**14**: ^{1}H NMR (400.1 MHz, THF-d_8, 25 °C): δ 0.09 (m, 6H, $Si(CH_3)_2$), 0.87 (m, 2H, $SiCH_2CH_2CH_2O$), 1.50 (m, 2H, $SiCH_2CH_2CH_2O$), 3.24–3.87 (m, 2H, $SiCH_2CH_2CH_2O$).

The material obtained from hydrosilylation of ethyl acetoacetate (**15**) by chlorodimethylsilane in THF was hydrolyzed as described in the literature.[4d] The identity of the resulting **17** was confirmed by comparison of both its ^{1}H NMR spectrum, and its GLC–IR to those of an authentic sample (Aldrich). The residue obtained from the hydrolysis was reacted with (*R*)-MTPA-Cl. The ee and absolute configuration were determined by comparison of the ^{1}H NMR spectrum of the derivatized residue to that of the (*R*)-MTPA esters of (*rac*)-**17** and authentic (*R*)-**17** (Aldrich), respectively. (*R*)-MTPA ester of (*R*)-**17** (*R,R* diastereomer): ^{1}H NMR (400.1 MHz, $CDCl_3$, 25 °C): δ 1.23 (t, J = 7.0 Hz, 3H, OCH_2CH_3), 1.34 (d, J = 6.5 Hz, 3H, $CH_3C(O)H$), 2.57 (dd, J = 16.0, 5.0 Hz, 1H, CH_2CO), 2.72 (dd, J = 16.0, 8.5 Hz, 1H, CH_2CO), 3.49 (br s, 3H, OCH_3), 4.13 (qd, J = 7.0, 1.5 Hz, 2H, OCH_2CH_3), 5.57 (m, 1H, $CH_3C(O)H$), 7.3–7.7 (m, 5H, Ph). (*R*)-MTPA ester of (*S*)-**17** (*R,S* diastereomer): ^{1}H NMR (400.1 MHz, $CDCl_3$, 25 °C): δ 1.19 (t, J = 7.0 Hz, 3H, OCH_2CH_3), 1.43 (d, J = 6.5 Hz, 3H, $CH_3C(O)H$), 2.53 (dd, J = 16.0, 5.0 Hz, 1H, CH_2CO), 2.68 (dd, J = 16.0, 8.5 Hz, 1H, CH_2CO), 3.55 (br s, 3H), 4.06 (q, J = 7.1 Hz, 2H), 5.57 (m, 1H), 7.3–7.7 (m, Ph, overlapping with the *R,R* diastereomer).

The product residue from the hydrogenation of ethyl acetoacetate (**15**) in methanol was purified by flash distillation. The ee and absolute configuration of the product were determined as described above for the hydrosilylation of **15**.

The product residue from the hydrogenation of tiglic acid (**18**) in methanol was dissolved in methylene chloride and passed through a Florisil plug to remove the catalyst. The solvent was then removed under reduced pressure, and the remaining residue was converted to the corresponding diastereomeric amides of (*S*)-MBA.[44] The ee and absolute configuration were determined by comparison of the ^{1}H NMR spectrum of the derivatized residue to that of the corresponding amide derivatives prepared from (*rac*)-**19** and authentic (*S*)-**19** (Lancaster), respectively. (*S*)-MBA amide of (*S*)-**19** (*S,S* diastereomer): ^{1}H (400.1 MHz, $CDCl_3$, 25 °C): δ 0.84 (t, J = 7.0 Hz, 3H), 1.13 (d, J = 7.0 Hz, 3H), 1.39 (m, 1H), 1.46 (d, J = 7.0 Hz, 3H), 1.64 (m, 1H), 2.10 (apparent sextet, J = 7.0 Hz, 1H), 5.14 (apparent quintet, J = 7.0 Hz, 1H), 5.89 (br s, 1H,), 7.1–7.4 (m, 5H, Ph). (*S*)-MBA amide of (*R*)-**19** (*S,R* diastereomer): ^{1}H (400.1 MHz, $CDCl_3$, 25 °C): δ 0.92 (t, J = 7.0 Hz, 3H), 1.10 (d, J = 7.0 Hz, 3H), 1.38 (m, 1H, overlapping with the *S,S* diastereomer), 1.47 (d, J = 7.0 Hz, 3H), 1.64 (m, 1H, overlapping with the *S,S* diastereomer), 2.09 (apparent sextet, J = 7.0 Hz, 1H, overlapping with the *S,S* diastereomer), 5.13 (apparent quintet, J = 7.0 Hz, 1H, overlapping with the *S,S* diastereomer), 5.89 (br s, 1H, overlapping with the *S,S* diastereomer), 7.1–7.4 (Ph, overlapping with the *S,S* diastereomer).

The product residue from the hydrogenation of geraniol (**20**) in methanol was purified by flash distillation and reacted with (*R*)-MTPA-Cl. The ee was determined by ^{1}H NMR spectroscopic analyses of the diastereomeric (*R*)-MTPA esters. The ratio of the methyl peaks at δ 0.91 (d, J = 6.5 Hz, *R,R* diastereomer) and δ 0.90 (d, J = 6.5 Hz, *R,S* diastereomer) were used to determine the ee. The ratio of these peaks was 1:1 for the (*R*)-MTPA esters derived from (*rac*)-**21**. The absolute configuration of the product was determined by comparison of its rotation with the reported optical rotation of (*R*)-**21** ($[\alpha]^{25}_D$= +5.12°, c = 21.0, $CHCl_3$).[45] NMR spectroscopic data for the diastereomeric esters: ^{1}H (400.1 MHz, $CDCl_3$, 25 °C): δ 0.90 (d, J = 6.3 Hz, 3H, CH_3, *R,S* diastereomer), 0.91 (d, J = 6.5 Hz, 3H, CH_3, *R,R* diastereomer), 1.19 (m, 2H), 1.33 (m,

2H), 1.51 (m, 4H), 1.59 (s, 6H), 1.68 (s, 6H), 1.74 (m, 2H), 1.95 (m, 4H), 3.50 (br s, 3H; *R,S* diastereomer), 3.56 (br s, 3H; *R,R* diastereomer), 4.37 (m, 4H), 5.06 (m, 2H), 7.35–7.70 (m, 10H, aromatic). ^{1}H NMR signals for individual diastereomers were assigned when overlap did not occur.

MAC(H)$_2$ was the only material detected by ^{1}H NMR spectroscopy in the residue obtained from the hydrogenation of MAC. The residue was analyzed without purification. The ee's were spectroscopically determined (^{1}H NMR) via chiral lanthanide shift reagent[46] (typically 0.4–0.6 equiv (+)-Eu(tfc)$_3$) in $CDCl_3$ (see Figure 2-4). The ratio of the methoxy signals (ca. δ 4; 1:1 for (*rac*)-MAC(H)$_2$) was used to quantify all ee's. In all cases, addition of (*S*)-MAC(H)$_2$ caused a decrease in ee, indicating the absolute configuration of the major enantiomer was *R*. The catalyst residue was removed before polarimetry by passing an ethyl acetate solution of the reaction mixture through a column of Florisil. The ee and absolute configuration of the major enantiomer for this mixture were determined as described above, and were confirmed by the magnitude and the sign of the optical rotation,[47] respectively, from polarimetric measurements.

X-ray Crystallography. Crystals of (*S*)-**2**·0.5$C_2H_4Cl_2$ suitable for structure determination by X-ray diffraction were obtained by slow liquid–liquid diffusion of methanol into a saturated solution of **2** in 1,2-dichloroethane at room temperature. Data collection, structure solution, and structure refinement for (*S*)-**2**·0.5$C_2H_4Cl_2$ were performed by Dr. Robert McDonald, Faculty Service Officer, Structure Determination Laboratory, Department of Chemistry, University of Alberta. See Table 2-1 for selected bond lengths and angles for (*S*)-**2**·0.5$C_2H_4Cl_2$. See Table 2-5 for a summary of crystal data, X-ray data collection, structure solution, and structure refinement information for (*S*)-**2**·0.5$C_2H_4Cl_2$.

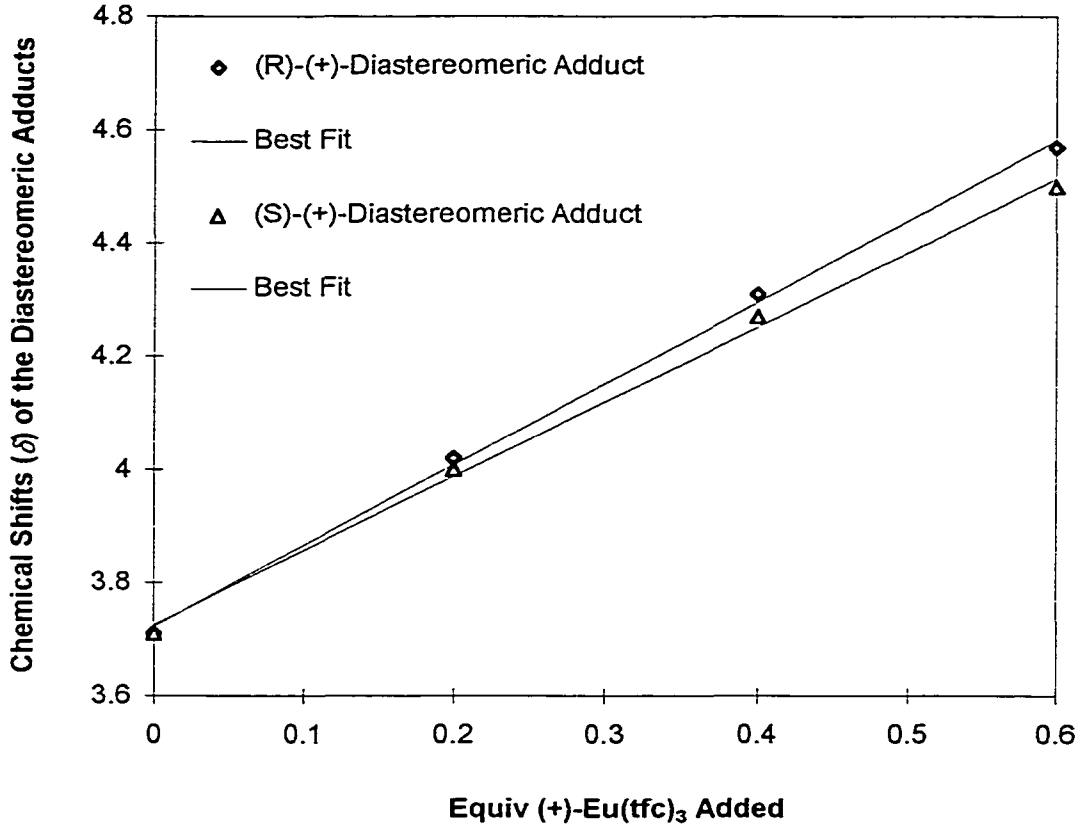

Figure 2-4. Plot of the chemical shifts (δ) of the (R)-MAC(H)$_2$·(+)-Eu(tfc)$_3$ and (S)-MAC(H)$_2$·(+)-Eu(tfc)$_3$ diastereomeric adducts in $CDCl_3$ (0.24 M) versus moles of (+)-Eu(tfc)$_3$ added.

Table 2-5. Crystallographic Experimental Details for (*S*)-2·0.5$C_2H_4Cl_2$

A. Crystal Data	
formula	$C_{55}H_{48}BClF_4NP_2Ru$
formula weight	1008.21
crystal dimensions (mm)	0.56 × 0.08 × 0.06
crystal system	monoclinic
space group	$P2_1$ (No. 4)
unit cell parameters[a]	
a (Å)	12.8559(8)
b (Å)	13.0675(8)
c (Å)	14.9401(9)
α (deg)	90
β (deg)	91.678(6)
γ (deg)	90
V (Å^3)	2508.8(3)
Z	2
ρ_{calcd} (g cm^{-3})	1.335
μ (mm^{-1})	4.040
B. Data Collection and Refinement	
diffractometer	Siemens P4/RA[b]
radiation (λ [Å])	Cu Kα (1.54178)
monochromator	incident-beam, graphite crystal
temperature (°C)	22
scan type	θ–2θ
data collection 2θ limit (deg)	110.0
total data collected	3486 ($0 \le h \le 13$, $0 \le k \le 13$, $-15 \le l \le 15$)
independent reflections	3315
number of observations (NO)	3178 [$F_o^2 \ge 2\sigma(F_o^2)$]
structure solution method	direct methods (SHELXS–86[c])
refinement method	full-matrix least-squares on F^2 (SHELXL–93[d])
absorption correction method	semiempirical (ψ scans)
range of transmission factors	0.4003–0.3182
data/restraints/parameters	3315 [$F_o^2 \ge -3\sigma(F_o^2)$] / 1 / 374
Flack absolute structure parameter[e]	0.007 (16)
goodness-of-fit (S)[f]	1.076 [$F_o^2 \ge -3\sigma(F_o^2)$]
final R indices[g]	
R_1 [$F_o^2 > 2\sigma(F_o^2)$]	0.0483
wR_2 [$F_o^2 \ge -3\sigma(F_o^2)$]	0.1306
largest difference peak and hole	0.878 and –0.579 e Å^{-3}

[a] Obtained from least-squares refinement of 25 reflections with 53.7° < 2θ < 56.0°. [b] Programs for diffractometer operation, data collection, data reduction, and absorption correction were those supplied

by Siemens. [c] Sheldrick, G. M. *Acta Crystallogr.* **1990**, *A46*, 467–473. [d] Sheldrick, G. M. SHELXL-93 Program for Crystal Structure Determination; Universität Göttingen, Göttingen, Germany, 1993. Refinement on F_o^2 for all reflections (all of these having $F_o^2 \geq -3\sigma(F_o^2)$). Weighted R-factors wR_2 and all goodnesses of fit S are based on F_o^2; conventional R-factors R_1 are based on F_o, with F_o set to zero for negative F_o^2. The observed criterion of $F_o^2 > 2\sigma(F_o^2)$ is used only for calculating R_1, and is not relevant to the choice of reflections for refinement. R-factors based on F_o^2 are statistically about twice as large as those based on F_o, and R-factors based on ALL data will be even larger. [e] Flack, H. D. *Acta Crystallogr.* **1983**, *A39*, 876–881. The Flack parameter will refine to a value near zero if the structure is in the correct configuration and will refine to a value near one for the inverted configuration. [f] $S = [\Sigma w(F_o^2 - F_c^2)^2/(n - p)]^{1/2}$ (n = number of data; p = number of parameters varied; $w = [\sigma^2(F_o^2) + (0.0771P)^2 + 5.5988P]^{-1}$ where $P = [\max(F_o^2, 0) + 2F_c^2]/3$). [g] $R_1 = \Sigma||F_o| - |F_c||/\Sigma|F_o|$; $wR_2 = [\Sigma w(F_o^2 - F_c^2)^2/\Sigma w(F_o^4)]^{1/2}$.

References and Notes

(1) For reviews, see: (a) Ratovelomanana-Vidal, V; Genêt, J. -P. *J. Organomet. Chem.* **1998**, *567*, 163–171. (b) Genêt, J. P. In *Reductions in Organic Synthesis: Recent Advances and Practical Applications*; Abdel-Magid, A. F., Ed.; ACS Symposium Series 641; American Chemical Society: Washington, DC, 1996; Chapter 2. (c) Ager, D. J.; Laneman, S. A. *Tetrahedron: Asymmetry* **1997**, *8*, 3327–3355. (d) Noyori, R. *Acta Chem. Scand.* **1996**, *50*, 380–390. (e) Kumobayashi, H. *Recl. Trav. Chim. Pays-Bas* **1996**, *115*, 201–210. (f) Akutagawa, S. *Applied Catalysis A: General* **1995**, *128*, 171–207. (g) Noyori, R. *Asymmetric Catalysis in Organic Synthesis*; Wiley: New York, 1994. (h) Noyori, R. *Tetrahedron* **1994**, *50*, 4259–4292. (i) Takaya, H.; Ohta, T.; Noyori, R. In *Catalytic Asymmetric Synthesis*; Ojima, I., Ed.; VCH: New York, 1993; Chapter 1. (j) Takaya, H.; Ohta, T.; Mashima, K. In *Homogeneous Transition Metal Catalyzed Reactions*; Moser, W. R., Slocum, D. W., Eds.; Advances in Chemistry Series 230; American Chemical Society: Washington, DC, 1992; Chapter 8. (k) Noyori, R. *CHEMTECH* **1992**, *22*, 360–367. (l) Noyori, R. In *Organic Synthesis in Japan Past, Present, and Future*; Noyori, R., Ed.; Tokyo Kagaku Dozin: Tokyo, 1992; pp 301–307. (m) Noyori, R. *Science* **1990**, *248*, 1194–1199. (n) Noyori, R.; Takaya, H. *Acc. Chem. Res.* **1990**, *23*, 345–350. (o) Noyori, R. *Chem. Soc. Rev.* **1989**, *18*, 187–208. (p) Noyori, R.; Kitamura, M. In *Modern Synthetic Methods 1989*; Scheffold, R., Ed.; Springer–Verlag: Berlin, 1989; pp 115–198.

(2) (a) Ohkuma, T.; Doucet, H.; Pham, T.; Mikami, K.; Korenaga, T.; Terada, M.; Noyori, R. *J. Am. Chem. Soc.* **1998**, *120*, 1086–1087. (b) Ohkuma, T.; Ikehira, H.; Ikariya, T.; Noyori, R. *Synlett* **1997**, 467–468. (c) Gao, J. -X.; Ikariya, T.; Noyori, R. *Organometallics* **1996**, *15*, 1087–1098. (d) Genêt, J.-P.; Ratovelomanana-Vidal, V.; Pinel, C. *Synlett* **1993**, 478–480. (e) Saburi, M.; Ohnuki, M.; Ogasawara, M.; Takahashi, T.; Uchida, Y. *Tetrahedron Lett.* **1992**, *33*, 5783–5786. (f) Brown, J. M.; Brunner, H.; Leitner, W.; Rose, M. *Tetrahedron: Asymmetry* **1991**, *2*, 331–334.

(3) For recent examples, see: (a) Ohkuma, T.; Koizumi, M.; Doucet, H.; Pham, T.; Kozawa, M.; Murata, K.; Katayama, E.; Yokozawa, T.; Ikariya, T.; Noyori, R. *J. Am.*

Chem. Soc. **1998**, *120*, 13529–13530. (b) Doucet, H.; Ohkuma, T.; Murata, K.; Yokozawa, T.; Kozawa, M.; Katayama, E.; England, A. F.; Ikariya, T. Noyori, R. *Angew. Chem., Int. Ed. Engl.* **1998**, *37*, 1703–1707.

(4) The discussion is limited to bis(phosphine) ligands because of the high success obtained with their use in homogeneous catalysis, and because, in general, multidentate chiral ligands are required to obtain high ee's. For examples of high enantioselectivity obtained using monodentate chiral phosphine ligands, see: (a) Hayashi, T.; Niizuma, S.; Kamikawa, T.; Suzuki, N.; Uozumi, Y. *J. Am. Chem. Soc.*, **1995**, *117*, 9101–9102. For examples of reactions catalyzed by ruthenium–(bis(phosphine)) complexes other than hydrogenations, see the following. For isomerization of olefins: (b) Frauenrath, H.; Kaulard, M. *Synlett*, **1994**, 517–518. (c) Frauenrath, H.; Philipps, T. *Angew. Chem., Int. Ed. Engl.* **1986**, *25*, 274. For intramolecular hydrosilylation of ketones: (d) Burk, M. J.; Feaster, J. E. *Tetrahedron Lett.* **1992**, *33*, 2099–2102. For hydrosilylation of nitrones: (e) Murahashi, S.-I.; Watanabe, S.; Shiota, T. *J. Chem. Soc., Chem. Commun.* **1994**, 725–726.

(5) Sun, Y.; LeBlond, C.; Wang, J.; Blackmond, D. G.; Laquidara, J.; Sowa, J. R., Jr. *J. Am. Chem. Soc.* **1995**, *117*, 12647–12648.

(6) Schrock, R. R.; Johnson, B. F. G.; Lewis, J. *J. Chem. Soc., Dalton Trans.* **1974**, 951–959.

(7) Propene was identified, but not quantified, in a reaction monitored by ^{1}H NMR spectroscopy.

(8) Small amounts (2–3% of each) of two other species formed as well as **2**. One species is tentatively assigned as $[Ru(MeCN)_2((R)\text{-BINAP})(\eta^3\text{-}C_3H_5)]BF_4$ on the basis of uncoordinated COD observed in the ^{1}H NMR spectrum of an in situ reaction ($^{31}P\{^1H\}$ NMR (161.9 MHz, CD_2Cl_2, 25°C): δ 39.0 (d, $^2J_{P\text{-}P}$ = 35.0 Hz, 1P), 57.8 (d, $^2J_{P\text{-}P}$ = 35.0 Hz, 1P). Complex **2** was purified by recrystallization from a solution of MeCN by slow addition of diethyl ether (resulting in isolation of **2**·0.4Et_2O). $[Ru(MeCN)_2((R)\text{-BINAP})\text{-}(\eta^3\text{-}C_3H_5)]BF_4$ was not detected in recrystallized **2**. The amount of the other unidentified impurity ($^{31}P\{^1H\}$ NMR (161.9 MHz, CD_2Cl_2, 25 °C): δ 27.7 (d, $^2J_{P\text{-}P}$= 36.5 Hz, 1P), 40.3 (d, $^2J_{P\text{-}P}$ = 36.5 Hz, 1P)) did not change, even after several recrystallizations of **2**. It

is notable that hydrogenolysis of **2** (containing these impurities) in acetone-d_6, followed by addition of excess MeCN yielded *fac*-[Ru((*R*)-BINAP)(H)(MeCN)$_3$]BF$_4$ (**5**) as the only product detected by ^{1}H and ^{31}P{^{1}H} NMR spectroscopy.

(9) (a) Bennett, M. A.; Willis, A. C.; Goh, L. Y.; Chen, W. *Polyhedron* **1996**, *15*, 3559–3567. (b) Cox, D. N.; Roulet, R. *J. Chem. Soc., Chem. Commun.* **1988**, 951–953. (c) Ashworth, T. V.; Chalmers, A. A.; Liles, D. C.; Meintjies, E.; Singleton, E. *Organometallics* **1987**, *6*, 1543–1552 and references therein.

(10) The lability of MeCN ligands in a ruthenium(II)–phosphine complex has been previously demonstrated by ligand exchange with CD$_3$CN: Siedle, A. R.; Newmark, R. A.; Pignolet, L. H. *Inorg. Chem.* **1986**, *25*, 1345–1351.

(11) NMR spectroscopic evidence for nitrile-dissociated species of [Ru(BINAP)-(RCN)$_2$Cl$_2$] (R = Ph, 2-furan, and C$_6$F$_5$) has been reported: Shao, L.; Takeuchi, K; Ikemoto, M.; Kawai, T.; Ogasawara, M.; Takeuchi, H.; Kawano, H.; Saburi, M. *J. Organomet. Chem.* **1992**, *435*, 133–147.

(12) Crabtree, R. H. *The Organometallic Chemistry of the Transition Metals*; Wiley: New York, 1988; pp. 220–224.

(13) (a) MacFarlane, K. S.; Rettig, S. J.; Liu, Z.; James, B. R. *J. Organomet. Chem.* **1998**, *557*, 213–219. (b) Chen, C. -C.; Huang, T. -T.; Lin, C. -W.; Cao, R.; Chan, A. S. C.; Wong, W. T. *Inorg. Chim. Acta* **1998**, *270*, 247–251. (c) Pathak, D. D.; Adams, H.; Bailey, N. A.; King, P. J.; White, C. *J. Organomet. Chem.* **1994**, *479*, 237–245. (d) Hoke, J. B.; Hollis, L. S.; Stern, E. W. *J. Organomet. Chem.* **1993**, *455*, 193–196. (e) Mashima, K.; Hino, T.; Takaya, H. *J. Chem. Soc., Dalton Trans.* **1992**, 2099–2107. (f) Kawano, H.; Ikariya, T.; Ishii, Y.; Kodama, T.; Saburi, M.; Yoshikawa, S.; Uchida, Y.; Akutagawa, S. *Bull. Chem. Soc. Jpn.* **1992**, *65*, 1595–1602. (g) Ashby, M. T.; Khan, M. A.; Halpern, J. *Organometallics* **1991**, *10*, 2011–2015. (h) Mashima, K.; Kusano, K.; Ohta, T.; Noyori, R.; Takaya, H. *J. Chem. Soc., Chem. Commun.* **1989**, 1208–1210. (i) Ohta, T.; Takaya, H.; Noyori, R. *Inorg. Chem.* **1988**, *27*, 566–569. (j) Kawano, H.; Ishii, Y.; Kodama, T.; Saburi, M.; Uchida, Y. *Chem. Lett.* **1987**, 1311–1314.

(14) (a) Han, S. -H.; Sung, K. -M.; Huh, S.; Jun, M. -J.; Whang, D.; Kim, K. *Polyhedron* **1996**, *15*, 3811–3820. (b) Morandini, F.; Consiglio, G.; Ciani, G.; Sironi, A. *Inorg. Chim. Acta* **1984**, *82*, L27–L28.

(15) Costain, C. C. *J. Chem. Phys.* **1958**, *29*, 864–874.

(16) (a) Steed, J. W.; Tocher, D. A.; Rogers, R. D. *J. Chem. Soc., Chem. Commun.* **1996**, 1598–1590. (b) Ashworth, T. V.; Nolte, M. J.; Reimann, R. F.; Singleton, E. *J. Chem. Soc., Chem. Commun.* **1977**, 937–939.

(17) Mixtures of THF and methylene chloride were used. Solutions of THF required small quantities of methylene chloride (THF:methylene chloride ≈ 5:1) to dissolve **2** at high enough concentrations to obtain satisfactory NMR spectra of **4**. Complex **4** rapidly decomposes in the presence of methylene chloride at room temperature. It was therefore necessary to keep these solutions of **4** at –78 °C as much as possible. The catalytic reactions were carried out at lower concentrations of **4** (see Tables 2-2, 2-3, and 2-4) and, except for one reaction (Table 2-2, entries 1 and 2), in the absence of methylene chloride.

(18) Cyclooctane was identified and quantified by ^{1}H NMR spectroscopy and by GLC (retention time confirmed by comparison to an authentic sample). ^{1}H NMR spectra measured of solutions early in the hydrogenolysis of **2** showed the presence of cyclooctene (ca. 30% versus cyclooctane), indicating that cyclooctene is initially formed by hydrogenation of 1–3:5,6-η-C_8H_{11} in **2**.

(19) The rapid exchange of solvento ligands did not allow the isolation of **4**. Complex **4** was characterized by low-temperature ^{1}H and ^{31}P{^{1}H} NMR spectroscopy. A related chiral hydrido–solvent complex of ruthenium(II) has been crystallographically characterized: (a) Currao, A.; Feiken, N.; Macchioni, A.; Nesper, R.; Pregosin, P. S.; Trabesinger, G. *Helv. Chim. Acta* **1996**, *79*, 1587–1591. Three ruthenium–hydrido complexes of BINAP ([RuH((*R*)-BINAP)$_2$]PF$_6$, [RuH(η^2-H$_2$)((*R*)-BINAP)$_2$]PF$_6$, and [RuHCl((*R*)- or (*S*)-BINAP)$_2$]) have been previously characterized: (b) Tsukahara, T.; Kawano, H.; Ishii, Y.; Takahashi, T.; Saburi, M.; Uchida, Y.; Akutagawa, S. *Chem. Lett.* **1988**, 2055–2058. (c) Ikariya, T.; Ishii, Y.; Kawano, H.; Arai, T.; Saburi, M.; Yoshikawa, S.; Akutagawa, S. *J. Chem. Soc., Chem. Commun.* **1985**, 922–924.

(20) Miessler, G. L.; Tarr, D. A. *Inorganic Chemistry*; Prentice Hall: Englewood Cliffs, NJ, 1991; pp 397–398.

(21) See Chapter 5 for a full discussion regarding the unambiguous solution structures of **4** in THF derived from ^{15}N-labeling experiments.

(22) Bergens, S. H.; Bosnich, B. *J. Am. Chem. Soc.* **1991**, *113*, 958–967.

(23) Massol, M.; Barrau, J.; Satge, J.; Bouyssieres, B. *J. Organomet. Chem.* **1974**, *80*, 47–69.

(24) Daley, C. J. A.; Wiles, J. A.; Bergens, S. H. *Can. J. Chem.* **1998**, *76*, 1447–1456.

(25) Ohta, T.; Takaya, H.; Kitamura, M.; Nagai, K.; Noyori, R. *J. Org. Chem.* **1987**, *52*, 3176–3178.

(26) Takaya, H.; Ohta, T.; Inoue, S.; Tokunaga, M.; Kitamura, M.; Noyori, R. In *Organic Syntheses*; Coffen, D. L., Ed.; Wiley: New York, 1995; Vol. 72, pp 74–85.

(27) Sun, Y.; Wang, J.; LeBlond, C.; Reamer, R. A.; Laquidara, J.; Sowa, J. R., Jr.; Blackmond, D. G. *J. Organomet. Chem.* **1997**, *548*, 65–72.

(28) (a) Noyori, R.; Ikeda, T.; Ohkuma, T.; Widhalm, M.; Kitamura, M.; Takaya H.; Akutagawa, S.; Sayo, N.; Saito, T.; Taketomi, T.; Kumobayashi, H. *J. Am. Chem. Soc.* **1989**, *111*, 9134–9135. For the rhodium–BINAP catalyzed hydrogenation of the corresponding acid, see: (b) Miyashita, A.; Takaya, H.; Souchi, T. Noyori, R. *Tetrahedron* **1984**, *40*, 1245–1253.

(29) Murahashi, S. -I.; Naota, T.; Ito, K.; Maeda, Y.; Taki, H. *J. Org. Chem.* **1987**, *52*, 4319–4327.

(30) Thermally induced isomerizations of [Ru(1–3:5,6-η-$C_8H_{11})_2$] to generate [Ru(1–6-η-C_8H_{10})(1,2:5,6-η-C_8H_{12})] and of [Ru(1–6-η-C_8H_{10})(1,2:5,6-η-C_8H_{12})] to generate [Ru(1–5-η-$C_8H_{11})_2$] have been reported: (a) Itoh, K.; Nagashima, H.; Ohshima, T.; Oshima, N.; Nishiyama, H. *J. Organomet. Chem.* **1984**, *272*, 179–188. (b) Pertici, P.; Vitulli, G.; Paci, M.; Porri, L. *J. Chem. Soc., Dalton Trans.* **1980**, 1961–1964.

(31) For discussions of BINAP and MeO-BIPHEP ligands acting as 6-electron donors in ruthenium(II) complexes, see: (a) Feiken, N.; Pregosin, P. S.; Trabesinger, G.; Albinati, A.; Evoli, G. L. *Organometallics* **1997**, *16*, 5756–5762. (b) Feiken, N.; Pregosin, P. S.; Trabesinger, G.; Scalone, M. *Organometallics* **1997**, *16*, 537–543 and reference 13c.

Recently, triphenylphosphine was shown to function as a chelating 4-electron donor ligand, with a C=C bond of one phenyl group bonded to a molybdenum(II) center: (c) Cheng, T.-Y.; Szalda, D. J.; Bullock, R. M. *J. Chem. Soc., Chem. Commun.* **1999**, 1629–1630. MeO-BIPHEP ligands acting as 8-electron donors in ruthenium(II) complexes (in which only one phosphine group is coordinated together with an η^6-C_6H_3 group derived from one of the biaryl rings) have been reported: (d) den Reijer, C. J.; Ruegger, H.; Pregosin, P. S. *Organometallics* **1998**, *17*, 5213–5215 and references therein.

(32) (a) Bouachir, F.; Chaudret, B.; Dahan, F.; Agbossou, F.; Tkatchenko, I. *Organometallics* **1991**, *10*, 455–462. (b) Cox, D. N.; Roulet, R. *J. Chem. Soc., Chem. Commun.* **1988**, 951–953. (c) Stebler-Röthlisberger, M.; Salzer, A.; Bürgi, H. B.; Ludi, A. *Organometallics* **1986**, *5*, 298–302. (d) Bouachir, F.; Chaudret, B.; Tkatchenko, I. *J. Chem. Soc., Chem. Commun.* **1986**, 94–96.

(33) In general, quaternary carbons have long spin-lattice relaxation times as a result of no attached protons to assist in dipole–dipole relaxation. Observing ^{13}C signals from these carbons is, therefore, often difficult without the aid of two-dimensional NMR spectroscopy which takes advantage of both ^{13}C and ^{1}H magnetization.

(34) (a) Leonard, J.; Lygo, B.; Procter, G. *Advanced Practical Organic Chemistry*, 2nd ed.; Chapman & Hall: London, 1995. (b) *Experimental Organometallic Chemistry: A Practicum in Synthesis and Characterization*; Wayda, A. L., Darensbourg, M. Y., Eds.; ACS Symposium Series 357; American Chemical Society: Washington, DC, 1987.

(35) Dauben, H. J., Jr.; Honnen, L. R.; Harmon, K. M. *J. Org. Chem.* **1960**, *25*, 1442–1445.

(36) Takaya, H.; Akutagawa, S.; Noyori, R. In *Organic Syntheses*; Smart, B. E., Ed.; Wiley: New York, 1989; Vol. 67, pp 20–32.

(37) Albers, M. O.; Singleton, E.; Yates, J. E. In *Inorganic Syntheses*; Kaesz, H. D., Ed.; Wiley: New York, 1989; Vol. 26, pp 249–258.

(38) Dale, J. A.; Dull, D. L.; Mosher, H. S. *J. Org. Chem.* **1969**, *34*, 2543–2549.

(39) (a) Leonard, J.; Lygo, B.; Procter, G. *Advanced Practical Organic Chemistry*, 2nd ed.; Chapman & Hall: London, 1995; pp 103–106. (b) Vineyard, B. D.; Knowles, W.

S.; Sabacky, M. J.; Bachman, G. L.; Weinkauff, D. J. *J. Am. Chem. Soc.* **1977**, *99*, 5946–5952.

(40) Schrock, R. R.; Osborn, J. A. *J. Am. Chem. Soc.* **1971**, *93*, 2397–2407.

(41) A small amount (5%) of [Ru((*R*)-BINAP)(1–3:5,6-η-C_8H_{11})]BF_4 also formed ($^{31}P\{^1H\}$ NMR (161.9 MHz, CD_2Cl_2, 25 °C): δ –12.8 (d, $^2J_{P-P}$ = 32.0 Hz, 1P), 71.8 (d, $^2J_{P-P}$ = 32.0 Hz, 1P)). This assignment is supported by the observation that addition of excess MeCN to solutions of **9** in methylene chloride at room temperature generates **2** (5%) and a new fluxional species that is tentatively assigned as [Ru((*R*)-BINAP)(MeCN)-(1–5-η-C_8H_{11})]BF_4 (95%).

(42) Resolution outlined in: (a) Young, W. G.; Caserio, F. F., Jr. *J. Org. Chem.* **1961**, *26*, 245–246. (b) Kenyon, J.; Snellgrove, D. R. *J. Chem. Soc.* **1925**, 1169–1181.

(43) Compared to ^1H NMR spectra[22,23] of (*E*)- and (*Z*)-1-propen-1-ol, (*E*)- and (*Z*)-trimethylsilyl-1-propen-1-ol, and **14** and poly-**14** (B. Bosnich, personal communication).

(44) Shioiri, T.; Yokoyama, Y.; Kasai, Y.; Yamada, S. *Tedrahedron* **1976**, *32*, 2211–2217.

(45) Takaya, H.; Ohta, T.; Sayo, N.; Kumobayashi, H.; Akutagawa, S.; Inoue, S. Kasahara, I.; Noyori, R. *J. Am. Chem. Soc.* **1987**, *109*, 1596–1597.

(46) (a) Parker, D. *Chem. Rev.* **1991**, *91*, 1441–1457. (b) Alcock, N. W.; Brown, J. M.; Maddox, P. J. *J. Chem. Soc., Chem. Commun.* **1986**, 1532–1534.

(47) Burk, M. J.; Feaster, J. E.; Nugent, W. A.; Harlow, R. L. *J. Am. Chem. Soc.* **1993**, *115*, 10125–10138.

Chapter 3†

The First Structure Determinations of Possible Intermediates in Ruthenium–BINAP-Catalyzed Hydrogenation with a Prochiral Group Bonded to Ruthenium

Introduction

Complexes of ruthenium(II) and BINAP comprise the most effective catalyst systems developed for the enantioselective hydrogenation of prochiral olefins and ketones. Numerous reports[1] describing such reactions, including several industrial syntheses, have appeared since the first examples were disclosed in 1985 and 1986.[2] Despite the intense study of these systems, there are no reports of structural characterization (even using spectroscopy) of a species with a prochiral olefin or ketone bonded to a ruthenium center.[3] The structures of the catalytic intermediates, and therefore the origins of enantioselection by these systems, are speculative as they must be extrapolated from indirect methods: stereochemical, isotope-labeling, and kinetic studies.[3,4]

The synthesis and the catalytic activity of $[Ru((R)\text{-BINAP})(H)(MeCN)_n(sol)_{3-n}]$-$BF_4$ (**1**; n = 0–3, sol = acetone, methanol, or THF, depending on reaction medium) was recently reported by this research group.[5] Complex **1** is a highly enantioselective catalyst system for the hydrogenation of prochiral olefinic substrates. In particular, **1** catalyzes the hydrogenation of MAC in solutions of acetone to generate (R)-$MAC(H)_2$ in 92% ee (eq 3-1). This enantioselectivity is comparable to those of other ruthenium–(BINAP) catalysts reported in the literature.[2b,4g,6] This chapter describes the first isolation, structural characterization, and reaction with dihydrogen gas of the major ruthenium-containing species present in solution during a catalytic olefin hydrogenation.

---

† Reproduced in part with permission from Wiles, J. A.; Bergens, S. H.; Young, V. G. *J. Am. Chem. Soc.* **1997**, *119*, 2940–2941. Copyright 1997 American Chemical Society.

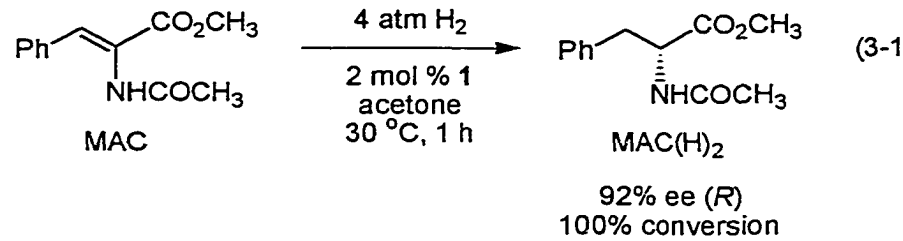

(3-1)

Results and Discussion

Detection and Isolation of a Possible Catalytic Intermediate. Stoichiometric reaction between MAC and **1** in acetone (and in other weakly coordinating solvents, e.g., methanol and THF) at room temperature resulted in the rapid formation of a predominant ruthenium species (**2**, >99%) in solution (eq 3-2). $^{31}P\{^{1}H\}$ NMR spectra recorded under

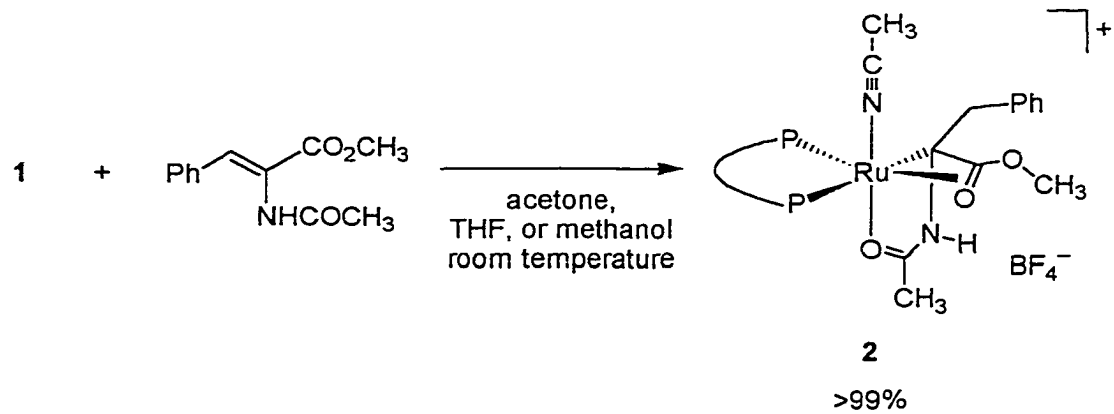

(3-2)

conditions similar to those of the catalytic reaction (pressure of dihydrogen gas ≈ 2 atm, 2 mol % **1**, methanol solution, room temperature) showed that **2** was the predominant species in solution during the catalytic hydrogenation.[7] NMR spectroscopic data indicated that **2** resulted from olefin–hydride insertion with transfer of the hydrido ligand in **1** to the β-olefinic carbon of MAC and transfer of ruthenium to the α-carbon to form a 5-membered metallacycle.[8] Further, the signal in the $^{13}C\{^{1}H\}$ NMR spectrum of **2** for the α-carbon showed cis and trans coupling (δ 67.3 (dd, $^{2}J_{P1-C(cis)}$ = 4.0 Hz, $^{2}J_{P2-C(trans)}$ = 42.0 Hz)) to the phosphorus nuclei, suggesting that the α-carbon was coordinated to ruthenium

in the plane containing the phosphine groups. The $^{13}C\{^1H\}$ NMR signals for the amido and the ester carbonyl groups were also coupled to the phosphorus nuclei (δ 179.7 (d, J_{P2-C} = 7.0 Hz, NH*C*OCH$_3$), 160.8 (d, J_{P2-C} = 3.5 Hz, *C*O$_2$CH$_3$)), suggesting that these groups were coordinated to ruthenium as well.[9]

X-ray Structure Determinations of Possible Intermediates. Crystals of **2** suitable for structure determination by X-ray diffraction were obtained by slow liquid–liquid diffusion of diethyl ether into a saturated 1,2-dichloroethane solution of the complex at room temperature. Figure 3-1 shows the molecular structure of **2**·Et$_2$O as determined by single-crystal X-ray diffraction. The positions of the signals in the solid-state ^{13}C CP/MAS NMR spectrum of **2** were nearly identical to those in the solution $^{13}C\{^1H\}$ NMR spectrum, implying that the solid-state structure was representative of the solution structure. As predicted from the NMR spectroscopic data, MAC(H) was bonded to the ruthenium center via the α-carbon and the amido and ester groups. The most important information—at least for the present study—obtained from the structure determination of **2**·Et$_2$O is the absolute configuration (*S*) at the α-carbon (C3) of the MAC(H) ligand. Stereospecific replacement of ruthenium by a hydrogen atom would generate (*R*)-MAC(H)$_2$, which is the same absolute configuration as the major enantiomer of the catalytic hydrogenation. Further, the regiochemistry of the olefin–hydride insertion step to produce **2**·Et$_2$O is the same as that observed for the catalytic hydrogenation.

Similar tridentate (facial) bonding of MAC(H) to a metal center was identified spectroscopically at low temperatures by Brown and Chaloner for [Rh((*R*,*R*)-DIPAMP)(MAC(H))(H)]BF$_4$ (**3**).[10] Unlike **3**, however, the amido carbonyl of **2**·Et$_2$O occupied a coordination site that was cis to both phosphines, and the ester carbonyl occupied a coordination site that was in the plane containing the phosphines. Molecular models indicated that exchange of coordination sites by the ester and the amide groups of **2** (to resemble **3**) would result in severe steric repulsions between an equatorial phenyl group of (*R*)-BINAP and the benzyl group of MAC(H) for both absolute configurations at C3. It should also be noted that the MeCN ligand of **2**·Et$_2$O is trans to the amido carbonyl, and that it remains cis to both phosphines as it was for the precursor complex [Ru((*R*)-BINAP)(1–3:5,6-η-C$_8$H$_{11}$)(MeCN)]BF$_4$.

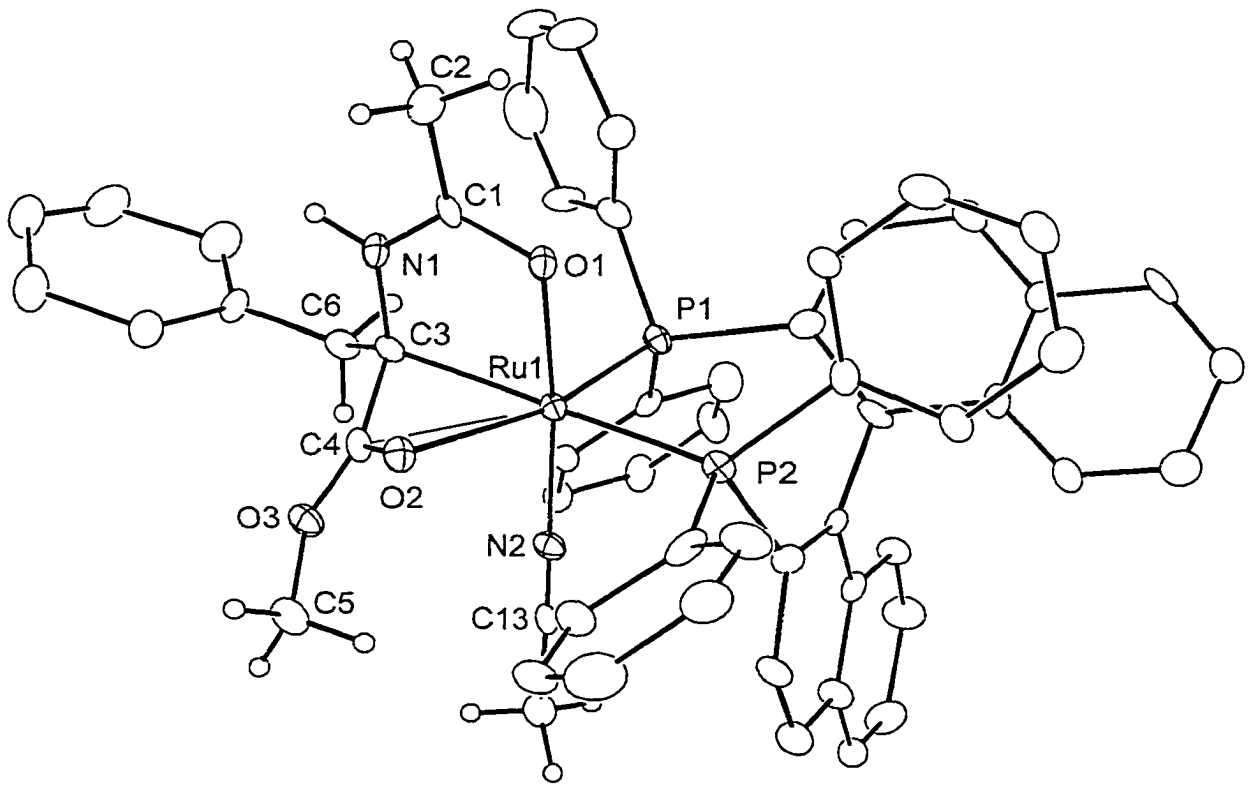

Figure 3-1. View of one of the two crystallographically-independent complex cations of **2**·Et_2O (molecule 1) showing the atom-labeling scheme.

Crystals of **2**·Et_2O quickly desolvated upon exposure to air causing rapid deterioration of the sample. This sensitivity required the crystals to be quickly mounted at low temperature. The analyzed crystal contained a large amount of disordered solvent molecules that caused diffuse scattering. The result is that the two crystallographically independent (but chemically identical) cation–anion pairs in the asymmetric unit have variations in bond lengths, bond angles, and torsional angles (see Table 3-1). More accurate X-ray structural data were obtained from the study of the MAA(H) species **4**.

Reaction of **1** with 1 equiv of MAA in acetone at room temperature immediately generated (>99% by NMR analysis) a mixture of two ruthenium species in a ratio of 72:28. NMR spectroscopy, ESI-MS, and elemental analyses indicated that these species were two diastereomeric forms of the complex [Ru((*R*)-BINAP)(MAA(H))(MeCN)]BF_4 (**4**) that resulted from olefin–hydride insertion between MAA and **1**. In accord with **2**, the olefin–hydride insertion reaction of **1** with MAA was regioselective, with transfer of the hydride to the β-olefinic carbon in MAA and transfer of ruthenium to the α-carbon in both diastereomers of **4**. NMR chemical shifts and coupling constants for both diastereomers of **4** were similar to those found for **2**. For example, the $^{13}C\{^1H\}$ NMR signals from the coordinated amido and the ester carbonyls, as well as from the α-carbon (that σ-bonded to ruthenium) were similar to those of **2**. These similarities strongly suggest that the two diastereomers of **3** differ by the absolute configuration at the α-carbon of MAA(H) (($S_{C\alpha}$)-**4** and ($R_{C\alpha}$)-**4**). The absolute configuration of the major (72%) diastereomer of **4** was determined as follows.

Slow liquid–liquid diffusion of *n*-dibutyl ether into a 1,2-dimethoxyethane solution of **4** (72:28) at room temperature produced X-ray quality crystals. Diffraction data were collected from two separate crystals. In both cases, the molecular structure of the isolated species was of ($S_{C\alpha}$)-**4**, as shown in Figure 3-2. To determine if ($S_{C\alpha}$)-**4** was the major or minor diastereomer, the crystal used for one of the two structure determinations was dissolved at –78 °C in CD_2Cl_2. The ^1H NMR spectrum of the resulting solution at –80 °C revealed a 95:5 (major:minor) mixture of the diastereomers of **4** within the crystal.[11] This ratio did not change upon warming to 25 °C, showing that interconversion between the

Table 3-1. Selected Bond Lengths (Å) and Angles (deg) for 2·Et_2O

		molecule 1			
Ru1–N2	2.009(9)	Ru1–C4	2.353(9)	C4–O2	1.267(11)
Ru1–P1	2.269(3)	O1–C1	1.272(11)	C4–O3	1.309(11)
Ru1–P2	2.369(3)	C1–C2	1.525(15)	O3–C5	1.409(11)
Ru1–O1	2.075(7)	C1–N1	1.313(12)	C3–C6	1.526(14)
Ru1–O2	2.260(7)	N1–C3	1.466(13)	N2–C13	1.156(12)
Ru1–C3	2.257(10)	C3–C4	1.540(14)	C13–C14	1.454(15)
O1–Ru1–C3	79.9(3)	O2–Ru1–N2	90.4(3)	Ru1–C3–C6	132.7(7)
O1–Ru1–O2	82.2(2)	O2–Ru1–P2	104.1(2)	N1–C3–C4	111.1(9)
O1–Ru1–P1	95.7(2)	N2–Ru1–P1	91.4(2)	N1–C3–C6	114.6(8)
O1–Ru1–P2	93.0(2)	N2–Ru1–P2	88.5(2)	C4–C3–C6	118.1(8)
C3–Ru1–O2	64.8(3)	P1–Ru1–P2	93.62(10)	C3–C4–O2	118.9(9)
C3–Ru1–N2	97.3(3)	Ru1–C3–N1	99.7(6)	C3–C4–O3	116.2(9)
C3–Ru1–P1	97.4(3)	Ru1–C3–C4	73.9(5)	O2–C4–O3	124.5(10)
		molecule 2			
Ru2–N4	1.991(8)	Ru2–C62	2.333(10)	C62–O5	1.251(11)
Ru2–P3	2.267(3)	O4–C59	1.276(11)	C62–O6	1.345(11)
Ru2–P4	2.376(3)	C59–C60	1.474(14)	O6–C63	1.465(11)
Ru2–O4	2.062(6)	C59–N3	1.327(12)	C61–C64	1.526(13)
Ru2–O5	2.292(7)	N3–C61	1.523(12)	N4–C71	1.136(12)
Ru2–C61	2.195(10)	C61–C62	1.412(13)	C71–C72	1.48(2)
O4–Ru2–C61	81.5(3)	O5–Ru2–N4	91.6(3)	Ru2–C61–C64	134.0(7)
O4–Ru2–O5	80.3(2)	O5–Ru2–P4	106.1(2)	N3–C61–C62	111.4(8)
O4–Ru2–P3	95.9(2)	N4–Ru2–P3	92.2(2)	N3–C61–C64	109.2(7)
O4–Ru2–P4	91.6(2)	N4–Ru2–P4	89.3(2)	C62–C61–C64	119.6(9)
C61–Ru2–O5	62.2(3)	P3–Ru2–P4	93.31(10)	C61–C62–O5	121.0(9)
C61–Ru2–N4	96.1(3)	Ru2–C61–N3	101.3(5)	C61–C62–O6	116.8(9)
C61–Ru2–P3	98.1(3)	Ru2–C61–C62	77.2(6)	O5–C62–O6	121.7(8)

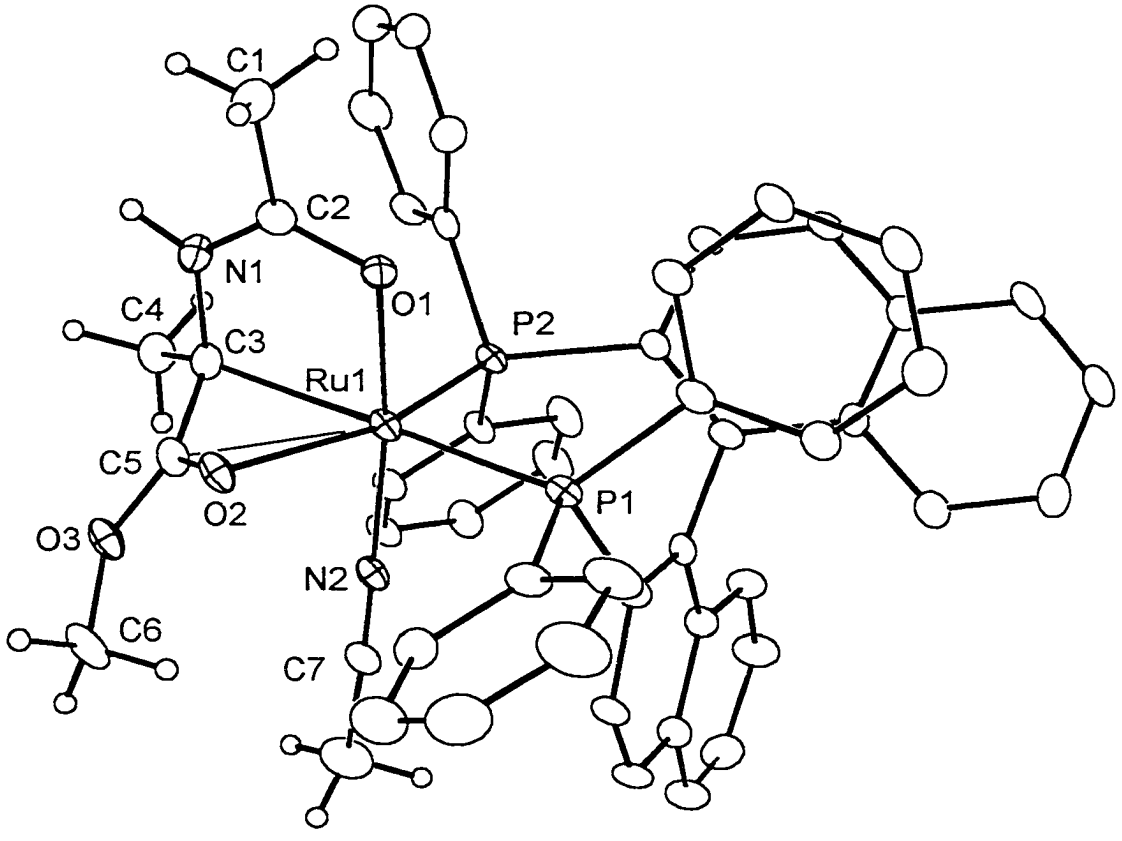

Figure 3-2. View of the complex cation of ($S_{C\alpha}$)-**4** showing the atom-labeling scheme.

diastereomers of **4** does not occur under these conditions. These X-ray and NMR data show that the major diastereomer of **4**, formed by reaction of MAA and **1**, is ($S_{C\alpha}$)-**4**. Crystals of the minor diastereomer suitable for X-ray diffraction were not obtained.

Selected bond lengths and angles derived from the X-ray structure determination of ($S_{C\alpha}$)-**4** are listed in Table 3-2. The Ru–P bond distances (Ru1–P1, 2.3525(13) Å;

Table 3-2. Selected Bond Lengths (Å) and Angles (deg) for ($S_{C\alpha}$)-4

Ru1–N2	1.995(4)	Ru1–C5	2.345(5)	C5–O2	1.278(5)
Ru1–P2	2.2640(11)	O1–C2	1.259(5)	C5–O3	1.364(6)
Ru1–P1	2.3525(13)	C2–C1	1.520(6)	O3–C6	1.434(6)
Ru1–O1	2.072(3)	C2–N1	1.302(6)	C3–C4	1.515(7)
Ru1–O2	2.278(3)	N1–C3	1.469(6)	N2–C7	1.145(6)
Ru1–C3	2.230(5)	C3–C5	1.437(7)	C7–C8	1.469(8)
O1–Ru1–C3	80.0(2)	O2–Ru1–N2	88.88(13)	Ru1–C3–C4	132.0(3)
O1–Ru1–O2	82.69(11)	O2–Ru1–P1	105.97(9)	N1–C3–C5	112.1(4)
O1–Ru1–P2	95.65(9)	N2–Ru1–P2	92.62(11)	N1–C3–C4	111.4(4)
O1–Ru1–P1	93.20(9)	N2–Ru1–P1	88.27(11)	C5–C3–C4	119.1(4)
C3–Ru1–O2	63.4(2)	P2–Ru1–P1	92.32(4)	C3–C5–O2	121.5(4)
C3–Ru1–N2	97.0(2)	Ru1–C3–N1	101.4(3)	C3–C5–O3	117.5(4)
C3–Ru1–P2	98.31(13)	Ru1–C3–C5	76.1(3)	O2–C5–O3	120.6(4)

Ru1–P2, 2.2640(11) Å), the P–Ru–P angle (P1–Ru1–P2, 92.32(4)°), the Ru–N bond length (Ru1–N2, 1.995(4)Å), and the dihedral angle between the two planes defined by the naphthalene rings (C21–C30–C31–C40, 74.9(6)°) for ($S_{C\alpha}$)-**4** are similar to values reported for [Ru((*R*)-BINAP)(1–3:5,6-η-C_8H_{11})(MeCN)]BF_4.[5,12] As was predicted from the solution NMR spectroscopic data, MAA(H) was bonded to the ruthenium center via the α-carbon (C3), the amido carbonyl, and the ester carbonyl groups. The Ru–O_{acyl} (Ru1–O1, 2.072(3) Å), C–O_{acyl} (C2–O1, 1.259(5) Å), and Ru–Cα (Ru1–C3, 2.230(5) Å) bond lengths are similar to a related ruthenium complex reported by Vahrenkamp and co-workers that also contains a MAA(H) ligand with an O-bonded amido group and a σ-

bonded α-carbon.[8a,b] The C3–C4 bond of ($S_{C\alpha}$)-**4** has lost all of its double bond character (1.515(7) Å); however, C3 is not fully pyramidalized as would be expected for a σ-bonded (sp^3) carbon (the sum of the angles C5–C3–N1, C5–C3–C4, and N1–C3–C4 being ca. 342°). Other transition-metal enolate complexes related to ($S_{C\alpha}$)-**4** that contain α-metal–alkyl bonds that are supported by metal–carbonyl (ester) interactions (Figure 3-3, **I** and **II**) show a similar extent of pyramidalization.[13] Alternatively, the bonding of the α-carbon

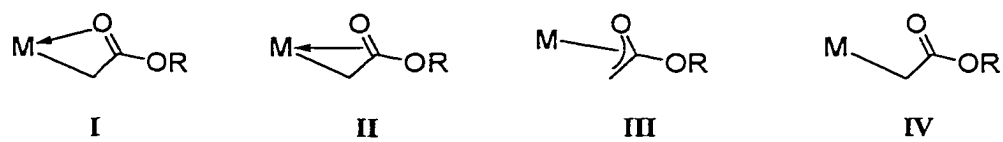

Figure 3-3. Plausible bonding modes for transition-metal enolate complexes of esters.

and the ester group could be collectively considered as an η^3-oxaallyl interaction (**III**) since the ester group appears to be π-bonded to the ruthenium center. This bonding situation would require a significant amount of conjugation (double bond character) between the α-carbon and the ester carbonyl carbon, which is not observed (C3–C5, 1.437(7) Å). For comparison, the C3–C5 bond length of ($S_{C\alpha}$)-**4** is similar to those found for the η^1-enolate (**IV**) complex [$Cp(CO)_3W(CH_2CO_2Et)$] (1.441(6) Å)[14] and the η^1,κ^1-*O*-bonded ester enolate (**I**) of [$W(CH(t\text{-}Bu)CH_2CH(CO_2CH_3))(N(2,6\text{-}(i\text{-}Pr)_2C_6H_3)(OCMe_2\text{-}(CF_3))_2$] (1.42(1) Å).[15] Further evidence against an η^3-oxaallyl formulation is that the transannular distance between ruthenium and the carbonyl carbon of the ester group (Ru1–C5, 2.345(5) Å) is significantly longer than Ru–Cα (Ru1–C3, 2.230(5) Å) bond length. This is visually demonstrated in Figure 3-2 by the dihedral angle between the two planes defined by C3–Ru1–O2 and C3–C5–O2 (121.2°). In contrast, most η^3-oxaallyl[16] and η^3-allyl[17] complexes contain a central carbon that is closer to the metal center than the terminal carbon(s). The most appropriate way of viewing the bonding of the enolate moiety of MAA(H) (and the MAC(H)) ligand is as a ruthenium–alkyl complex supported by an α-CO_2CH_3 group that interacts with the ruthenium center through the carbonyl group in a π-fashion (**II**). The Ru1–O2 and C5–O2 bond lengths for ($S_{C\alpha}$)-**4** (2.278(3) Å

and 1.278(5) Å, respectively) are similar to values reported for ruthenium(II) complexes in the literature[18] that contain O-bonded esters; however, the ν(C=O) band (1522 cm^{-1}) assigned to the ester carbonyl in the IR spectrum of ($S_{C\alpha}$)-**4**, the upfield shift of the ester carbonyl carbon ($\Delta\delta$ −12.4 versus MAA(H)$_2$) in the $^{13}C\{^1H\}$ NMR spectrum of ($S_{C\alpha}$)-**4**, and the proximity of the ester carbonyl carbon to the ruthenium center support a weak π-interaction of the ester carbonyl with the ruthenium center.[19]

Hydrogenolysis of 2. The most important information obtained from the structure determinations of **2** and **4** are the absolute configurations at the α-carbons of the MAC(H) and MAA(H) ligands, respectively. The absolute configuration at the α-carbon of the MAC(H) ligand in **2**·Et_2O is *S*. Stereospecific replacement of ruthenium by a hydrogen atom would generate (*R*)-MAC(H)$_2$, which is the same absolute configuration as the major enantiomer of the catalytic hydrogenation. The stoichiometric reaction of **2** with dihydrogen gas under conditions similar[20] to those of the catalytic hydrogenation resulted in formation of MAC(H)$_2$ and [Ru((*R*)-BINAP)(H)(η^6-MAC(H)$_2$)]BF_4 (**5**), in which MAC(H)$_2$ was bonded to ruthenium as an η^6-arene ligand.[21] The remainder of the ruthenium compounds were unidentifiable, and presumably resulted from decomposition of **1** under these conditions in the absence of MAC. MAC(H)$_2$ was liberated from **5** by refluxing in MeCN solution (to generate *fac*-[Ru((*R*)-BINAP)(H)(MeCN)$_3$]BF_4) (eq 3-3).[22] The ee of the combined portions of MAC(H)$_2$ was 83% (*R*).[23] Assuming that direct

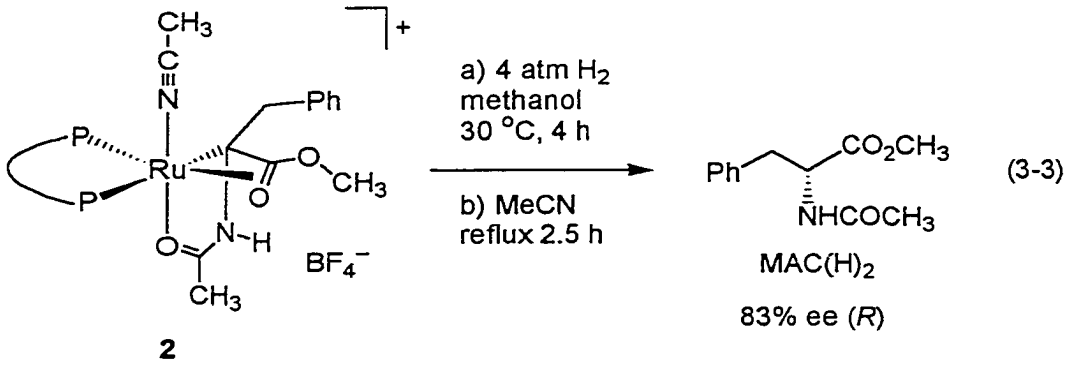

(3-3)

reaction of **2** with dihydrogen gas results in a stereospecific replacement of ruthenium by hydrogen,[24] these results show that formation of **2** was to some extent reversible under the

conditions of the catalytic hydrogenation.[25] Vahrenkamp and co-workers have also shown that the regio- and stereoselective insertion of MAA into ruthenium–hydride bonds of chiral clusters is reversible;[8a,b] however, these ruthenium–alkyl complexes do not react with dihydrogen gas. Further, a mechanism involving reversible formation of an intermediate similar to **2** was also proposed to account for the isomerization of (*E*)-α-benzamidocinnamic acid to (*Z*)-α-benzamidocinnamic acid observed during a hydrogenation catalyzed by $Et_2NH_2[(RuCl((R)\text{-BINAP}))_2(\mu\text{-}Cl)_3]$.[4g]

Conclusions

Hydrogenolysis of a ruthenium–carbon bond in which the carbon center is stereogenic has been proposed as a key step in several hydrogenations catalyzed by ruthenium–BINAP complexes, and may be the enantioselective step of the present catalytic hydrogenations.[4] Further investigation is required to determine whether **2** and **4** are actual intermediates in their respective catalytic cycles, and whether the chiral interactions in **2** and **4** are relevant to the origins of enantioselection. It is notable, however, that formation of complexes **2** and **4** were rapid relative to the overall rates of the catalytic hydrogenations, that **2** and **4** are the predominant ruthenium species in solution during catalysis, and that the rate of reaction of **2** with dihydrogen gas was similar to that of the catalytic reaction in methanol solution.[26]

Experimental Section

Materials. Gases and solvents were purified as outlined in Chapter 2. All reagents were used as received from Aldrich unless stated otherwise. $[Ru((R)\text{-BINAP})(1\text{–}3{:}5,6\text{-}\eta\text{-}C_8H_{11})(MeCN)]BF_4$, MAC, (*rac*)-$MAC(H)_2$, and (*S*)-$MAC(H)_2$ were obtained by methods described in Chapter 2. MAA was purified by column chromatography on neutral alumina (acetone) before use. (*rac*)-$MAA(H)_2$ and (*S*)-$MAA(H)_2$ were prepared

by the esterification of *N*-acetylalanine and *N*-acetylalanine, respectively, using diazomethane.[27] Florisil (60–100 mesh) was supplied by Fisher Scientific.

Measurements. All instrumentation used were as described in Chapter 2 unless stated otherwise. The ^{13}C CP/MAS NMR spectrum of **2** was recorded using a Bruker AM-R-300 spectrometer operating at 75.5 MHz. Mass spectrometric analyses (ESI-MS (pos)) of **2**, **4**, and **5** were performed in MeCN solution. IR spectra were recorded on a Nicolet Magna-IR 750 spectrometer as solutions (methylene chloride) using a cell having KCl windows of 0.1 mm spacing. IR abbreviations used: s = strong and m = medium.

Syntheses. All techniques used were as described in Chapter 2.

(A) 2. [Ru((*R*)-BINAP)(1–3:5,6-η-C_8H_{11})(MeCN)]BF_4 (547.5 mg, 0.571 mmol) was partially dissolved in acetone (20.0 mL) under an atmosphere of dry argon gas and subjected to 3 freeze–pump–thaw cycles. The reactor was backfilled with dihydrogen gas (20 psig) at room temperature and vigorously shaken for 10 min to generate a clear, dark orange solution. This extremely air-sensitive solution was subjected to 2 freeze–pump–thaw cycles and backfilled with argon gas. To this solution at room temperature, an acetone solution (5.0 mL) of MAC (125.2 mg, 0.571 mmol) was added. The resulting dark amber solution was shaken for 1 min, and the solvent was removed under reduced pressure to give a yellow solid discolored by a brown residue. Slow addition of diethyl ether (80 mL) to a solution of the product in methylene chloride (2.5 mL) afforded a yellow powder. This powder was collected by filtration, washed with diethyl ether (5 × 10 mL), and dried under dynamic vacuum (16 h). Yield: 534.1 mg (87%). IR (CH_2Cl_2): ν(NCO) 1588 s, ν(NH) 1553 m, $\nu(CO_2)$ 1522 m cm^{-1}. ESI-MS (pos): *m/z* 985.2 ($(M - BF_4)^+$, exact mass calcd for $C_{58}H_{49}N_2O_3P_2Ru$ 985.2). Anal. Calcd for $C_{58}H_{49}BF_4N_2O_3P_2$-Ru: C, 64.99; H, 4.61; N, 2.61. Found: C, 63.85; H, 4.65; N, 2.86. ^1H NMR (400.1 MHz, CD_2Cl_2, 25 °C): δ 1.71 (s, 3H, CH_3CN), 1.95 (s, 3H, $NHCOCH_3$), 2.70 (dd, $^2J_{H-H}$ = 14.0 Hz, $^4J_{P-H}$ = 4.5 Hz, 1H, *pro-R*-CH_2Ph), 3.98 (s, 3H,CO_2CH_3), 4.15 (d, $^2J_{H-H}$ = 14.0 Hz, 1H, *pro-S*-CH_2Ph), 5.87 (br d, $^5J_{P-H}$ = 2.5 Hz, 1H, $NHCOCH_3$), 6.4–8.0 (aromatic). $^{31}P\{^1H\}$ NMR (161.9 MHz, CD_2Cl_2, 25 °C): δ 33.6 (d, $^2J_{P-P}$ = 24.0 Hz, 1P), 59.7 (d, $^2J_{P-P}$ = 24.0 Hz, 1P). $^{13}C\{^1H\}$ NMR (100.6 MHz, CD_2Cl_2, 25 °C): δ 4.7 (s, CH_3CN), 20.9 (s, $NHCOCH_3$), 38.5 (s, CH_2Ph), 53.3 (s, CO_2CH_3), 67.3 (dd, $^2J_{P-C(trans)}$ = 42.0 Hz, $^2J_{P-C(cis)}$ =

4.0 Hz, Ru–*C*), 126–142 (aromatic and CH_3CN), 160.8 (d, J_{P-C} = 3.5 Hz, CO_2CH_3), 179.7 (d, J_{P-C} = 7.0 Hz, $NHCOCH_3$). ^{13}C CP/MAS NMR (75.5 MHz, 25 °C): δ 6, 21, 39, 56, 69, 128, 134, 161, 181. Complex **2** (($S_{C\alpha}$)-**2**) is the only species observed in NMR spectra recorded at room temperature. Subsequent spectra recorded at low temperature shows the presence (ca. 8%) of the other diastereomer ($R_{C\alpha}$)-**2**. Selected NMR spectroscopic data for ($S_{C\alpha}$)-**2** and ($R_{C\alpha}$)-**2** (the asterisks denote resonances attributed to the minor diastereomer (($R_{C\alpha}$)-**2**): $^{13}C\{H\}$ (100.6 MHz, CD_2Cl_2, –40 °C): δ 36.1 (s, $PhCH_2C$–Ru*), 37.8 (s, $PhCH_2C$–Ru), 66.9 (dd, $^2J_{P(B)-C}$ = 42.0 Hz, $^2J_{P(A)-C}$ = 3.5 Hz, Ru–*C*), 70.0 (dd, $^2J_{P(B')-C}$ = 42.0 Hz, $^2J_{P(A')-C}$ = 3.5 Hz, Ru–*C**), 157.9 (br, CO_2CH_3*), 159.7 (d, $J_{P(B)-C}$ = 3.0 Hz, CO_2CH_3), 179.6 (d, $J_{P(B)-C}$ = 7.0 Hz, $NHCOCH_3$), 179.9 (d, $J_{P(B')-C}$ = 7.0 Hz, $NHCOCH_3$*). $^{15}N\{H\}$ (40.5 MHz, CD_2Cl_2, –40 °C): δ 184.4 (dd, $^2J_{P(A)-N}$ = 4.5 Hz, $^2J_{P(B)-N}$ = 3.0 Hz, $CH_3C^{15}N$–Ru). The corresponding $^{15}N\{^1H\}$ resonance for ($R_{C\alpha}$)-**2** was not observed; however, the $^{31}P\{^1H\}$ NMR spectrum of ($R_{C\alpha}$)-**2** prepared using $CH_3C^{15}N$ displayed $^2J_{P(A')-N}$ = 4.5 Hz and $^2J_{P(B')-N}$ = 3.0 Hz. $^{31}P\{H\}$ (161.9 MHz, CD_2Cl_2, –40 °C): δ 32.9 (d, $^2J_{P-P}$ = 23.5 Hz, 1P, P(B)), 40.1 (d, $^2J_{P-P}$ = 24.0 Hz, 1P, P(B')*), 55.2 (d, $^2J_{P-P}$ = 24.0 Hz, 1P, P(A')*), 59.4 (d, $^2J_{P-P}$ = 23.5 Hz, 1P, P(A)).

(B) 4. The method used for the preparation of **4** was the same as that used for **2** with substitution of MAA for MAC. Yield: 92%. NMR spectroscopic analysis showed the product contained a diastereomeric mixture of ($S_{C\alpha}$)-**4** and ($R_{C\alpha}$)-**4** (72:28). An in situ reaction monitored by NMR spectroscopy displayed the same ratio of diastereomers. IR (CH_2Cl_2): ν(NCO) 1591 s, ν(NH) 1568 m, $\nu(CO_2)$ 1527 m cm^{-1}. ESI-MS (pos): *m/z* 909.2 ($(M - BF_4)^+$, exact mass calcd for $C_{52}H_{45}N_2O_3P_2Ru$ 909.2). Anal. Calcd for $C_{52}H_{45}BF_4N_2O_3P_2Ru$: C, 62.72; H, 4.56; N, 2.81. Found: C, 62.35; H, 4.88; N, 2.64. NMR spectroscopic data for **4** (the asterisks denote resonances attributed to the minor diastereomer (($R_{C\alpha}$)-**4**): ^1H (400.1 MHz, acetone-d_6, 25 °C): δ 1.17 (d, $^4J_{P-H}$ = 5.0 Hz, 3H, Ru–C–CH_3*), 1.61 (d, $^4J_{P-H}$ = 5.0 Hz, 3H, Ru–C–CH_3), 1.83 (s, 3H, CH_3CN), 1.92 (s, 3H, CH_3CN*), 2.04 (s, 3H, $NHCOCH_3$), 2.17 (s, 3H, $NHCOCH_3$*) 3.77 (s, 3H, CO_2CH_3*), 3.85 (s, 3H, CO_2CH_3), 6.4–8.1 (aromatic), 8.38 (br s, 1H, $NHCOCH_3$), 9.02 (br s, 1H, $NHCOCH_3$*). ^1H (400.1 MHz, acetone-d_6, –40 °C): δ 0.99 (d, $^4J_{P-H}$ = 5.0 Hz, 3H, Ru–C–CH_3*), 1.55 (d, $^4J_{P-H}$ = 5.0 Hz, 3H, Ru–C–CH_3), 1.84 (s, 3H, CH_3CN), 1.89

(s, 3H, CH_3CN*), 2.03 (s, 3H, $NHCOCH_3$), 2.17 (s, 3H, $NHCOCH_3$*), 3.74 (s, 3H, CO_2CH_3*), 3.82 (s, 3H, CO_2CH_3), 6.4–8.1 (aromatic), 8.69 (br s, 1H, $NHCOCH_3$), 9.28 (br s, 1H, $NHCOCH_3$*). $^{13}C\{^1H\}$ (100.6 MHz, CD_2Cl_2, 25 °C): δ 4.2 (s, CH_3CN–Ru*), 4.5 (s, CH_3CN–Ru), 17.4 (br s, Ru–C–CH_3*),18.8 (s, Ru–C–CH_3),19.7 (s, $NHCOCH_3$*), 20.4 (s, $NHCOCH_3$), 52.6 (s, CO_2CH_3*), 52.9 (s, CO_2CH_3), 63.3 (dd, $^2J_{P-C(trans)}$ = 44.0 Hz, $^2J_{P-C(cis)}$ = 4.0 Hz, Ru–*C*), 66.4 (br d, $^2J_{P-C(trans)}$ = 43.0 Hz, Ru–*C**), 126–142 (overlapping aromatic, CH_3CN, and CH_3CN*), 161.5 (d, J_{P-C} = 3.0 Hz, overlapping ($S_{C\alpha}$)-**4** and ($R_{C\alpha}$)-**4**, CO_2CH_3), 179.3 (d, J_{P-C} = 7.0 Hz, $NHCOCH_3$), 179.9 (d, J_{P-C} = 7.0 Hz, $NHCOCH_3$*). $^{13}C\{^1H\}$ (100.6 MHz, CD_2Cl_2, –40 °C): δ 4.1 (s, CH_3CN–Ru*), 4.3 (s, CH_3CN–Ru), 16.9 (s, Ru–C–CH_3*), 18.2 (s, Ru–C–CH_3), 19.5 (s, $NHCOCH_3$*), 20.1 (s, $NHCOCH_3$), 52.4 (s, CO_2CH_3*), 52.6 (s, CO_2CH_3), 63.0 (dd, $^2J_{P-C(trans)}$ = 43.5 Hz, $^2J_{P-C(cis)}$ = 4.0 Hz, Ru–*C*), 66.8 (dd, $^2J_{P-C(trans)}$ = 44.5 Hz, $^2J_{P-C(cis)}$ = 3.0 Hz Ru–*C**), 124–141 (overlapping aromatic, CH_3CN, and CH_3CN*), 159.1 (s, CO_2CH_3*), 160.1 (s, CO_2CH_3), 178.6 (d, J_{P-C} = 7.0 Hz, $NHCOCH_3$), 179.1 (d, J_{P-C} = 6.5 Hz, $NHCOCH_3$*). $^{15}N\{^1H\}$ (40.5 MHz, acetone-d_6, 25 °C): δ 183.1 (dd, $^2J_{P(A)-N}$ = 4.5 Hz, $^2J_{P(B)-N}$ = 3.0 Hz, CH_3CN–Ru), 184.8 (dd, $^2J_{P(A)-N}$ = 4.0 Hz, $^2J_{P(B)-N}$ = 3.0 Hz, CH_3CN–Ru*). $^{15}N\{^1H\}$ (40.5 MHz, acetone-d_6, –40 °C): δ 181.9 (br apparent t, $^2J_{P(A)-N}$ = $^2J_{P(B)-N}$ = 3.5 Hz, $CH_3C^{15}N$–Ru), 183.5 (br, $CH_3C^{15}N$–Ru*). $^{31}P\{^1H\}$ (161.9 MHz, acetone-d_6, 25 °C): δ 33.8 (d, $^2J_{P-P}$ = 22.0 Hz, 1P, P(B)), 38.8 (br d, $^2J_{P-P}$ = 21.0 Hz, 1P, P(B')*), 58.5 (br d, $^2J_{P-P}$ = 21.0 Hz, 1P, P(A')*), 59.7 (d, $^2J_{P-P}$ = 22.0 Hz, 1P, P(A)). $^{31}P\{^1H\}$ (161.9 MHz, acetone-d_6, –40 °C): δ 33.4 (d, $^2J_{P-P}$ = 23.0 Hz, 1P, P(B)), 38.7 (d, $^2J_{P-P}$ = 22.0 Hz, 1P, P(B')*), 57.1 (d, $^2J_{P-P}$ = 22.0 Hz, 1P, P(A')*), 59.4 (d, $^2J_{P-P}$ = 23.0 Hz, 1P, P(A)).

(C) 5. (*rac*)-$MAC(H)_2$ (15.1 mg, 0.068 mmol) and [Ru((*R*)-BINAP)(1–3:5,6-η-C_8H_{11})(MeCN)]BF_4 (65.5 mg, 0.068 mmol) were dissolved in acetone (8.0 mL) under an atmosphere of argon gas and subjected to 3 freeze–pump–thaw cycles. The reactor was backfilled with dihydrogen gas (20 psig) at room temperature and shaken for 10 min. The resulting solution was concentrated to ca. 1 mL under reduced pressure. Addition of diethyl ether (100 mL) followed by filtration afforded a yellow powder. The product was washed with diethyl ether (5 × 10 mL) and dried under dynamic vacuum (24 h). Yield: 39.4 mg (56%). A reaction mixture monitored by ^1H and $^{31}P\{^1H\}$ NMR spectroscopy

confirmed that the two diastereomeric complexes were formed in quantitative yield. The individual diastereomer [Ru((*R*)-BINAP)(H)(η^6-(*S*)-MAC(H)$_2$)]BF_4 ((*R*,*S*)-**5**) was prepared using (*S*)-MAC(H)$_2$ in a manner analogous to that described above. NMR spectroscopic data for (*R*,*S*)-**5**: ^{1}H (400.1 MHz, CD_2Cl_2, 25 °C): δ –9.14 (dd, $^2J_{P-H}$ = 40.5 Hz, $^2J_{P-H}$ = 29.5 Hz, 1H, Ru–*H*), 1.83 (s, 3H, NHCOC*H*$_3$), 2.51 (dd, $^2J_{H\beta-H\beta'}$ = 14.0 Hz, $^3J_{H\alpha-H\beta}$ = 5.0 Hz, 1H, $C_6H_5CH_2CH$ (Hβ)), 2.82 (dd, $^2J_{H\beta-H\beta'}$ = 14.0 Hz, $^3J_{H\alpha-H\beta'}$ = 8.0 Hz, 1H, $C_6H_5CH_2CH$ (Hβ')), 3.62 (s, 3H, CO_2CH_3), 4.40 (d, $^3J_{H-H}$ = 6.0 Hz, 1H, $C_6H_5CH_2CH$), 4.47 (d of apparent t, $^3J_{H\alpha-H\beta'}$ = $^3J_{H\alpha-H(NH)}$ = 8.0 Hz, $^3J_{H\alpha-H\beta}$ = 5.0 Hz, 1H, $C_6H_5CH_2CH$ (Hα)), 4.55 (apparent t, $^3J_{H-H}$ = 6.0 Hz, 1H, $C_6H_5CH_2CH$), 5.45 (d, $^3J_{H-H}$ = 6.0 Hz, 1H, $C_6H_5CH_2CH$), 5.78 (apparent t, $^3J_{H-H}$ = 6.0 Hz, 1H, $C_6H_5CH_2CH$), 6.03 (apparent t, $^3J_{H-H}$ = 6.0 Hz, 1H, $C_6H_5CH_2CH$), 6.1–8.2 (aromatic, BINAP). $^{31}P\{^1H\}$ (161.9 MHz, CD_2Cl_2, 25 °C): δ 50.4 (d, $^2J_{P-P}$ = 45.5 Hz, 1P), 51.5 (d, $^2J_{P-P}$ = 45.5 Hz, 1P). NMR spectroscopic data for (*R*,*R*)-**5**: ^{1}H (400.1 MHz, CD_2Cl_2, 25 °C): δ –9.06 (dd, $^2J_{P-H}$ = 36.0 Hz, $^2J_{P-H}$ = 33.5 Hz, 1H, Ru–*H*), 1.88 (s, 3H, NHCOC*H*$_3$), 2.56 (dd, $^2J_{H\beta-H\beta'}$ = 14.0 Hz, $^3J_{H\alpha-H\beta}$ = 8.0 Hz, 1H, $C_6H_5CH_2CH$ (Hβ)), 2.98 (dd, $^2J_{H\beta-H\beta'}$ = 14.0 Hz, $^3J_{H\alpha-H\beta'}$ = 5.0 Hz, 1H, $C_6H_5CH_2CH$ (Hβ'), 3.62‡ (s, CO_2CH_3), 4.43‡ ($C_6H_5CH_2CH$ (Hα)), 4.89 (d, $^3J_{H-H}$ = 6.0 Hz, 1H, $C_6H_5CH_2CH$), 4.95 (apparent t, $^3J_{H-H}$ = 6.0 Hz, 1H, $C_6H_5CH_2CH$), 5.06 (d, $^3J_{H-H}$ = 6.0 Hz, 1H, $C_6H_5CH_2CH$), 5.60 (apparent t, $^3J_{H-H}$ = 6.0 Hz, 1H, $C_6H_5CH_2CH$), 6.03 (apparent t, $^3J_{H-H}$ = 6.0 Hz, 1H, $C_6H_5CH_2CH$), 6.0–8.2 (aromatic, BINAP). $^{31}P\{^1H\}$ (161.9 MHz, CD_2Cl_2, 25 °C): δ 51.1 (d, $^2J_{P-P}$ = 45.0 Hz, 1P), 51.4 (d, $^2J_{P-P}$ = 45.0 Hz, 1P). ESI-MS (pos): *m/z* 946.2 ((M – BF_4)$^+$, exact mass calcd for $C_{56}H_{48}NO_3P_2Ru$ 946.2). Anal. Calcd for $C_{56}H_{48}BF_4NO_3P_2Ru$: C, 65.12; H, 4.68; N, 1.36. Found: C, 64.39; H, 4.67; N, 1.68.

‡ Overlapping with resonances of (*R*,*S*)-**5**.

Hydrogenolysis of 2. In a glass pressure reactor (Lab Glass), a deoxygenated solution of **2** (137.2 mg, 0.128 mmol) in methanol (12.8 mL) was allowed to react with dihydrogen gas (4 atm) at 30 °C for 4 h while stirring at 1100 rpm. The final reaction mixture was a red–orange solution containing a red–orange solid precipitate. This solid readily dissolved in methylene chloride. Removal of all volatile components in vacuo, followed by ^{1}H and $^{31}P\{^1H\}$ NMR spectroscopic analyses indicated that a mixture of **5** and

MAC(H)$_2$ was present (**5**:MAC(H)$_2$ ≈ 1:2). The remainder of the "Ru((*R*)-BINAP)" existed as numerous unidentified species, each in very low concentration (amount of each was too low too accurately quantify by ^{31}P{^{1}H} NMR spectroscopy). The solvent was removed in vacuo and the remaining residue was refluxed in MeCN (5.0 mL) for 2.5 h under an atmosphere of argon gas. Complete liberation of MAC(H)$_2$ from **5** was established by ^{1}H and ^{31}P{^{1}H} NMR spectroscopy. After evaporation of the solvent, the solid residue was washed with ethyl acetate (25 mL) and the solution was passed through a Florisil plug to remove the ruthenium–BINAP species. Evaporation of the solvent yielded a white powder (pure MAC(H)$_2$ by ^{1}H NMR spectroscopy). The ee was determined by mixing MAC(H)$_2$ and (+)-Eu(tfc)$_3$ (0.4 equiv) in $CDCl_3$ and recording the ^{1}H NMR spectrum of the resulting solution (see Chapter 2). The ratio of the methoxy signals (ca. δ 4; 1:1 for a solution containing (*rac*)-MAC(H)$_2$) was 10.8:1, corresponding to 83% ee. Addition of (*S*)-MAC(H)$_2$ to this solution caused a decrease in ee, indicating the major enantiomer was *R*.

X-ray Crystallography. Crystals of **2**·Et$_2$O suitable for structure determination by X-ray diffraction were obtained by slow liquid–liquid diffusion of diethyl ether into a saturated solution of the complex in 1,2-dichloroethane at room temperature. Suitable crystals of ($S_{C\alpha}$)-**4** were obtained by slow liquid–liquid diffusion of *n*-dibutyl ether into a saturated solution of **4** in 1,2-dimethoxyethane at room temperature. Data collections, structure solutions, and structure refinements for **2**·Et$_2$O and ($S_{C\alpha}$)-**4** were performed by Dr. Victor G. Young, Jr., X-Ray Crystallographic Laboratory, Department of Chemistry, University of Minnesota, Minneapolis. See Tables 3-1 and 3-2 for selected bond lengths and angles for **2**·Et$_2$O and ($S_{C\alpha}$)-**4**, respectively. See Tables 3-3 and 3-4 for summaries of crystal data, X-ray data collection, structure solution, and structure refinement information for **2**·Et$_2$O and ($S_{C\alpha}$)-**4**, respectively.

Table 3-3. Crystallographic Experimental Details for 2·Et_2O

A. Crystal Data	
formula	$C_{62}H_{59}BF_4N_2O_4P_2Ru$
formula weight	1145.93
crystal dimensions (mm)	0.45 × 0.25 × 0.12
crystal habit, color	plate, yellow
crystal system	monoclinic
space group	$P2_1$ (No. 4)
unit cell parameters[a]	
a (Å)	15.3846(1)
b (Å)	18.9635(3)
c (Å)	21.8056(1)
α (deg)	90
β (deg)	101.856(1)
γ (deg)	90
V (Å^3)	6225.98(11)
Z	4
ρ_{calcd} (g cm^{-3})	1.223
μ (mm^{-1})	0.359
F_{000}	2368
B. Data Collection	
diffractometer	Siemens SMART Platform CCD[b]
radiation (λ [Å])	Mo Kα (0.71073)
temperature (°C)	−100
data collection 2θ range (deg)	2.70–50.20
total data collected	31332
	($-18 \geq h \geq 17$, $-16 \geq k \geq 22$, $0 \geq l \geq 25$)
independent reflections	16214 (R_{int} = 0.0513)
number of observations (NO)	10610 ($F_o^2 \geq 2\sigma(F_o^2)$)
C. Structure Solution and Refinement	
program system	Siemens SHELXTL-Plus V5.0
structure solution method	direct methods
refinement method	full-matrix least-squares on F^2
absorption correction method	SADABS
range of absorption correction factors	1.000–0.816
data/restraints/parameters	16214 [$F_o^2 \geq -3\sigma(F_o^2)$]/34[c]/1369
Flack absolute structure parameter[d]	0.03 (4)
goodness-of-fit (S)[e]	0.955 [$F_o^2 \geq -3\sigma(F_o^2)$]
final R indices[f]	
R_1 [$F_o^2 \geq 2s(F_o^2)$]	0.0685
wR_2 [$F_o^2 \geq -3s(F_o^2)$]	0.1733
largest difference peak and hole	0.814 and −0.523 e Å^{-3}

[a] Obtained from least-squares refinement of 8192 strong reflections from the data collection. [b] Programs for diffractometer operation and data collection were those supplied by Siemens. [c] Restraints were applied to allow the solvent diethyl ether molecules to be refined with similar geometries and displacement parameters. [d] Flack, H. D. *Acta Crystallogr.* **1983**, *A39*, 876–881. The Flack parameter will refine to a value near zero if the structure is in the correct configuration and will refine to a value near one for the inverted configuration. [e] $S = [\Sigma w(F_o^2 - F_c^2)^2/(n - p)]^{1/2}$ (n = number of data; p = number of parameters varied; $w = [\sigma^2(F_o^2) + (0.0932P)^2]^{-1}$ where $P = [\max(F_o^2, 0) + 2F_c^2]/3$). [f] $R_1 = \Sigma||F_o| - |F_c||/\Sigma|F_o|$; $wR_2 = [\Sigma w(F_o^2 - F_c^2)^2/\Sigma w(F_o^4)]^{1/2}$.

Table 3-4. Crystallographic Experimental Details for ($S_{C\alpha}$)-4

A. Crystal Data	
formula	$C_{52}H_{45}BF_4N_2O_3P_2Ru$
formula weight	995.72
crystal dimensions (mm)	0.40 × 0.25 × 0.13 mm
crystal habit, color	irregular plate, yellow
crystal system	orthorhombic
space group	$C222_1$
unit cell parameters[a]	
a (Å)	21.4849(2)
b (Å)	29.7175(2)
c (Å)	18.8513(2)
α (deg)	90
β (deg)	90
γ (deg)	90
V (Å^3)	12036.1(2)
Z	8
ρ_{calcd} (g cm^{-3})	1.099
μ (mm^{-1})	0.361
F_{000}	4080
B. Data Collection	
diffractometer	Siemens SMART Platform CCD[b]
radiation (λ [Å])	Mo Kα (0.71073)
temperature (°C)	–100
data collection 2θ range (deg)	2.34–50.08
total data collected (index ranges)	36587 ($-25 \leq h \leq 25$, $0 \leq k \leq 35$, $0 \leq l \leq 22$)
independent reflections	10589 (R_{int} = 0.0568)
number of observations (NO)	8758 ($F_o^2 \geq 2\sigma(F_o^2)$)
C. Structure Solution and Refinement	
program system	Siemens SHELXTL-V5.0
structure solution method	direct methods
refinement method	full-matrix least-squares on F^2
absorption correction method	SADABS
range of absorption correction factors	1.000–0.641
data/restraints/parameters	10587 [$F_o^2 \geq -3\sigma(F_o^2)$]/40/636
Flack absolute structure parameter[c]	0.00(3)
goodness-of-fit (S)[d]	1.041 [$F_o^2 \geq -3\sigma(F_o^2)$]
final R indices[e]	
R_1 [$F_o^2 \geq 2\sigma(F_o^2)$]	0.0480
wR_2 [$F_o^2 \geq -3\sigma(F_o^2)$]	0.1261
largest difference peak and hole	0.682 and –0.468 e Å^{-3}

[a] Obtained from least-squares refinement of 8192 strong reflections from the data collection. [b] Programs for diffractometer operation and data collection were those supplied by Siemens. [c] Flack, H. D. *Acta Crystallogr.* **1983**, *A39*, 876–881. The Flack parameter will refine to a value near zero if the structure is in the correct configuration and will refine to a value near one for the inverted configuration. [d] $S = [\Sigma w(F_o^2 - F_c^2)^2/(n - p)]^{1/2}$ (n = number of data; p = number of parameters varied; $w = [\sigma^2(F_o^2) + (0.0727P)^2]^{-1}$ where $P = [\max(F_o^2, 0) + 2F_c^2]/3$). [e] $R_1 = \Sigma||F_o| - |F_c||/\Sigma|F_o|$; $wR_2 = [\Sigma w(F_o^2 - F_c^2)^2/\Sigma w(F_o^4)]^{1/2}$.

References and Notes

(1) For reviews, see: (a) Ratovelomanana-Vidal, V; Genêt, J. -P. *J. Organomet. Chem.* **1998**, *567*, 163–171. (b) Genêt, J. P. In *Reductions in Organic Synthesis: Recent Advances and Practical Applications*; Abdel-Magid, A. F., Ed.; ACS Symposium Series 641; American Chemical Society: Washington, DC, 1996; Chapter 2. (c) Ager, D. J.; Laneman, S. A. *Tetrahedron: Asymmetry* **1997**, *8*, 3327–3355. (d) Noyori, R. *Acta Chem. Scand.* **1996**, *50*, 380–390. (e) Kumobayashi, H. *Recl. Trav. Chim. Pays-Bas* **1996**, *115*, 201–210. (f) Akutagawa, S. *Applied Catalysis A: General* **1995**, *128*, 171–207. (g) Noyori, R. *Asymmetric Catalysis in Organic Synthesis*; Wiley: New York, 1994. (h) Noyori, R. *Tetrahedron* **1994**, *50*, 4259–4292. (i) Takaya, H.; Ohta, T.; Noyori, R. In *Catalytic Asymmetric Synthesis*; Ojima, I., Ed.; VCH: New York, 1993; Chapter 1. (j) Takaya, H.; Ohta, T.; Mashima, K. In *Homogeneous Transition Metal Catalyzed Reactions*; Moser, W. R., Slocum, D. W., Eds.; Advances in Chemistry Series 230; American Chemical Society: Washington, DC, 1992; Chapter 8. (k) Noyori, R. *CHEMTECH* **1992**, *22*, 360–367. (l) Noyori, R. In *Organic Synthesis in Japan Past, Present, and Future*; Noyori, R., Ed.; Tokyo Kagaku Dozin: Tokyo, 1992; pp 301–307. (m) Noyori, R. *Science* **1990**, *248*, 1194–1199. (n) Noyori, R.; Takaya, H. *Acc. Chem. Res.* **1990**, *23*, 345–350. (o) Noyori, R. *Chem. Soc. Rev.* **1989**, *18*, 187–208. (p) Noyori, R.; Kitamura, M. In *Modern Synthetic Methods 1989*; Scheffold, R., Ed.; Springer–Verlag: Berlin, 1989; pp 115–198. For recent examples see: (q) Doucet, H.; Ohkuma, T.; Murata, K.; Yokozawa, T.; Kozawa, M.; Katayama, E.; England, A. F.; Ikariya, T.; Noyori, R. *Angew. Chem., Int. Ed. Engl.* **1998**, *37*, 1703–1707. (r) Ohkuma, T.; Koizumi, M.; Doucet, H.; Pham, T.; Kozawa, M.; Murata, K.; Katayama, E.; Yokozawa, T.; Ikariya, T.; Noyori, R. *J. Am. Chem. Soc.* **1998**, *120*, 13529–13530.

(2) (a) Noyori, R.; Ohta, M.; Hsiao, Y.; Kitamura, M.; Ohta, T.; Takaya, H. *J. Am. Chem. Soc.* **1986**, *108*, 7117–7119. (b) Ikariya, T.; Ishii, Y.; Kawano, H.; Arai, T.; Saburi, M.; Yoshikawa, S.; Akutagawa, S. *J.Chem. Soc., Chem. Commun.* **1985**, 992–924.

(3) There have been reports of observations of unidentified species by NMR spectroscopy: (a) King, S. A.; DiMichele, L. In *Catalysis of Organic Reactions*; Scaros, M. G., Prunier, M. L., Eds.; Marcel Dekker: New York, 1995; Vol. 62, pp 157–166. (b) Saburi, M.; Takeuchi, H.; Ogasawara, M.; Tsukahara, T.; Ishii, Y.; Ikariya, T.; Takahashi, T.; Uchida, Y. *J. Organomet. Chem.* **1992**, *428*, 155–167. (c) Ohta, T.; Takaya, H.; Noyori, R. *Tetrahedron Lett.* **1990**, *31*, 7189–7192. For X-ray structure determinations of putative ruthenium–BINAP intermediates in enantioselective hydrogenation of α,β-unsaturated carboxlic acids, see: (d) Chen, C.-C.; Huang, T.-T.; Lin, C.-W.; Cao, R.; Chan, A. S. C.; Wong, W. T. *Inorg. Chim. Acta* **1998**, *270*, 247–251. (e) Ashby, M. T.; Khan, M. A.; Halpern, J. *Organometallics* **1991**, *10*, 2011–2015. These studies showed that the prochiral olefin groups were not bonded to the ruthenium centers in these complexes.

(4) (a) Shaharuzzaman, M.; Braddock-Wilking, J.; Chickos, J. S.; Tam, C, N,; Silva, R. A. G. D.; Keiderling, T. A. *Terahedron: Asymmetry* **1998**, *9*, 1111–1114. (b) Brown, J. M.; Rose, M.; Knight, F. I.; Wienand, A. *Recl. Trav. Chim. Pays-Bas* **1995**, *114*, 242–251. (c) Chan, A. S. C.; Chen, C. C.; Yang, T. K.; Huang, J. H.; Lin, Y. C. *Inorg. Chim. Acta* **1995**, *234*, 95–100. (d) Brown, J. M. *Chem. Soc. Rev.* **1993**, 25–41. (e) Chan, A. S. C.; Laneman, S. A.; Miller, R. E. In *Selectivity in Catalysis*; Davis, M. E., Suib, S. L., Eds.; ACS Symposium Series 517; American Chemical Society: Washington, DC, 1993; Chapter 2. (f) Ashby, M. T.; Halpern, J. *J. Am. Chem. Soc.* **1991**, *113*, 589–594. (g) Kawano, H.; Ikariya, T.; Ishii, Y.; Saburi, M.; Yoshikawa, S.; Uchida, Y.; Kumobayashi, H. *J. Chem. Soc., Perkin Trans. 1* **1989**, 1571–1575. For mechanistic studies of enantioselective hydrogenations using other ruthenium complexes as catalysts, see: (h) Fehr, M. J.; Consiglio, G.; Scalone, M.; Schmid, R. *New. J. Chem.* **1998**, 1499–1504. (i) Haack, K.-J.; Hashiguchi, S.; Fujii, A.; Ikariya, T.; Noyori, R. *Angew. Chem., Int. Ed. Engl.* **1997**, *36*, 285–288. (j) Mezzetti, A.; Tschumper, A.; Consiglio, G. *J. Chem. Soc., Dalton Trans.* **1995**, 49–56. (k) James, B. R.; Wang, D. K. W. *Can. J. Chem.* **1980**, *58*, 245–250.

(5) Wiles, J. A.; Lee, C. E.; McDonald, R.; Bergens, S. H. *Organometallics* **1996**, *15*, 3782–3784.

(6) (a) Noyori, R.; Ikeda, T.; Ohkuma, T.; Widhalm, M.; Kitamura, M.; Takaya H.; Akutagawa, S.; Sayo, N.; Saito, T.; Taketomi, T.; Kumobayashi, H. *J. Am. Chem. Soc.* **1989**, *111*, 9134–9135. For the hydrogenation of the corresponding acid catalyzed by a rhodium–BINAP complex, see: (b) Miyashita, A.; Takaya, H.; Souchi, T. Noyori, R. *Tetrahedron* **1984**, *40*, 1245–1253.

(7) The low concentration of the catalyst necessitated the acquisition of ca. 5000 scans to obtain a $^{31}P\{^{1}H\}$ NMR spectrum with a satisfactory signal-to-noise ratio. A spectrum recorded 1.5 h after mixing (after approximately 8 turnovers) showed **2** was the predominant ruthenium species in solution.

(8) Similar regio- and stereoselective insertion of MAA into ruthenium–hydride bonds of chiral clusters has been previously described by others; however, these ruthenium–hydride cluster complexes do not catalyze the the hydrogenation of MAA, and these isolated insertion complexes do not react with dihydrogen gas: (a) Mani, D.; Schacht, H.-T.; Powell, A. K.; Vahrenkamp, H. *Chem. Ber.* **1989**, *122*, 2245–2251. (b) Mani, D.; Schacht, H.-T.; Powell, A.; Vahrenkamp, H. *Organometallics* **1987**, *6*, 1360–1361. Structures of other α-metallated amino acids have been recently reported: (c) Kayser, B.; Missling, C.; Knizek, J.; Nöth, H.; Beck, W. *Eur. J. Inorg. Chem.* **1998**, 375–379. (d) Kayser, B.; Nöth, H.; Schmidt, M.; Steglich, W.; Beck, W. *Chem. Ber.* **1996**, *129*, 1617–1620.

(9) This observation is indicative, but it is not conclusive evidence for coordination. For examples of uncoordinated esters carbonyls that display J_{P-C} in metal complexes of amino acid derivatives, see: Brown, J. M.; Chaloner, P. A. *J. Am. Chem. Soc.* **1980**, *102*, 3040–3048 and reference 8c.

(10) Brown, J. M.; Chaloner, P. A. *J. Chem. Soc., Chem. Commun.* **1980**, 344–346.

(11) Both the dissolution of the crystal and the analysis of the resulting solution were performed at low temperature to prevent any diastereomeric interconversion that may occur. This precaution was not necessary as $^{31}P\{^{1}H\}$ NMR spectroscopic analysis of **4** (72:28 and 95:5 major:minor diastereomeric ratios) in acetone-d_6 over a range of temperatures (–80 °C to 25 °C) showed invariable diastereomeric ratios. The 95:5 ratio

observed in the particular crystal analyzed by X-ray diffraction was the same ratio found for the entire crop of crystals (bulk sample).

(12) For X-ray structure determinations of related ruthenium–BINAP complexes, see: (a) MacFarlane, K. S.; Rettig, S. J.; Liu, Z.; James, B. R. *J. Organomet. Chem.* **1998**, *557*, 213–219. (b) Pathak, D. D.; Adams, H.; Bailey, N. A.; King, P. J.; White, C. *J. Organomet. Chem.* **1994**, *479*, 237–245. (c) Hoke, J. B.; Hollis, L. S.; Stern, E. W. *J. Organomet. Chem.* **1993**, *455*, 193–196. (d) Mashima, K.; Hino, T.; Takaya, H. *J. Chem. Soc., Dalton Trans.* **1992**, 2099–2107. (e) Kawano, H.; Ikariya, T.; Ishii, Y.; Kodama, T.; Saburi, M.; Yoshikawa, S.; Uchida, Y.; Akutagawa, S. *Bull. Chem. Soc. Jpn.* **1992**, *65*, 1595–1602. (f) Mashima, K.; Kusano, K.; Ohta, T.; Noyori, R.; Takaya, H. *J. Chem. Soc., Chem. Commun.* **1989**, 1208–1210. (g) Ohta, T.; Takaya, H.; Noyori, R. *Inorg. Chem.* **1988**, *27*, 566–569. (h) Kawano, H.; Ishii, Y.; Kodama, T.; Saburi, M.; Uchida, Y. *Chem. Lett.* **1987**, 1311–1314 and references 3d and 3e.

(13) (a) Cameron, P. A.; Britovsek, G. J. P.; Gibson, V. C.; Williams, D. J.; White, A. J. P. *J. Chem. Soc., Chem. Commun.* **1998**, 737–738. (b) Agh-Atabay, N. M.; Carlton, L.; Davidson, J. L.; Douglas, G.; Muir, K. W. *J. Chem. Soc., Dalton Trans.* **1996**, 999–1011.

(14) Burkhardt, E. R.; Doney, J. J.; Bergman, R. G.; Heathcock, C. H. *J. Am. Chem. Soc.* **1987**, *109*, 2022–2039.

(15) Feldman, J.; Murdzek, J. S.; Davis, W. M.; Schrock, R. R. *Organometallics* **1989**, *8*, 2260–2265.

(16) See reference 14 and references therein.

(17) (a) Schoonover, M. W.; Kubiak, C. P.; Eisenberg, R. *Inorg. Chem.* **1978**, *17*, 3050–3055. (b) Smith, A. E. *Inorg. Chem.* **1972**, *11*, 2306–2310.

(18) (a) Torres, M. R.; Vegas, A.; Santos, A.; Ros, J. *J. Organomet. Chem.* **1987**, *326*, 413–421. (b) Komiya, S.; Ito, T.; Cowie, M.; Yamamoto, A.; Ibers, J. A. *J. Am. Chem. Soc.* **1976**, *98*, 3874–3884.

(19) Schmidt, T.; Goddard, R. *J. Chem. Soc., Dalton Trans.* **1995**, 1563–1568.

(20) The dihydrogen pressure, temperature, and solvent were the same as the catalytic reaction, but the concentration of **2** for the stoichiometric reaction was ca. 3 times higher

than the initial concentration of **1** for the catalytic reaction.

(21) Complex **5** was identified by NMR spectroscopy. The η^6-arene adducts of (*rac*)-MAC(H)$_2$ and (*S*)-MAC(H)$_2$ were synthesized for comparison. Related ruthenium(II)–(η^6-arene) complexes of phenylalanine derivatives have been reported: (a) Wolff, J. M.; Sheldrick, W. S. *Chem. Ber.* **1997**, *130*, 981–988. (b) Wolff, J. M.; Sheldrick, W. S. *J. Organomet. Chem.* **1997**, *531*, 141–149. (c) Moriarty, R. M.; Ku, Y.-Y.; Gill, U. S. *J. Chem. Soc., Chem. Commun.* **1987**, 1837–1838.

(22) Displacement of η^6-arene ligands by nitriles in ruthenium–BINAP complexes have been previously described: Shao, L.; Takeuchi, K.; Ikemoto, M.; Kawai, T.; Ogasawara, M.; Takeuchi, H.; Kawano, H.; Saburi, M. *J. Organomet. Chem.* **1992**, *435*, 133–147 and reference 12d.

(23) The ee of MAC(H)$_2$ was spectroscopically determined (^{1}H NMR) using a chiral shift reagent ((+)-Eu(tfc)$_3$) in $CDCl_3$ after separation from *fac*-[Ru((*R*)-BINAP)-(H)(MeCN)$_3$]BF$_4$ by column chromatography on Florisil (ethyl acetate). The absolute configuration of the major enantiomer was determined by comparison to authentic (*S*)-MAC(H)$_2$.

(24) Another possibility is that solvolysis of the ruthenium–carbon bond may also have occurred under these conditions. To clarify this issue, the reaction of **2** with Brønsted–Lowry acids in methanol, with dideuterium gas in methanol, and with dihydrogen gas in methanol-d_4 are being investigated in this laboratory.

(25) Low-temperature reaction of **1** and MAC generated two isomers of [Ru((*R*)-BINAP)(H)(MAC)(MeCN)]BF$_4$ (MAC is bonded through the amide carbonyl group and through an olefin–ruthenium π-bond) and one other non-hydrido complex. The solution structures and kinetics of these complexes are being investigated in this laboratory to further understand the mechanism of this hydrogenation.

(26) The stoichiometric reaction was 92% complete after 1.25 h.

(27) (a) Leonard, J.; Lygo, B.; Procter, G. *Advanced Practical Organic Chemistry*, 2nd ed.; Chapman & Hall: London, 1995; pp 103–106. (b) Vineyard, B. D.; Knowles, W. S.; Sabacky, M. J.; Bachman, G. L.; Weinkauff, D. J. *J. Am. Chem. Soc.* **1977**, *99*, 5946–5952.

Chapter 4†

Stoichiometric and Catalytic Isotope-Labeling Studies of Relevance to Ruthenium–BINAP-Catalyzed Enantioselective Hydrogenation

Introduction

Complexes of ruthenium(II) and BINAP are among the most successful catalyst systems for the enantioselective hydrogenation of prochiral olefins and ketones.[1] Despite the high ee's and TONs that often distinguish these systems, the asymmetric interactions that are responsible for their enantioselection are unknown.[2,3] Among the reasons that enantioselective interactions have not been elucidated for these hydrogenations is that all reported observations of putative catalytic intermediates are either incomplete,[4] providing little information about how the substrate is bonded to ruthenium, or they are of species in which the substrate is not bonded to ruthenium through a prochiral functionality.[5] Recently, this research group reported[6] the first observation and structural characterization of a ruthenium–BINAP complex with a substrate bonded to ruthenium through a stereogenic carbon center derived from the prochiral functionality of the substrate. The complex, [Ru((*R*)-BINAP)((*S*)-MAC(H))(MeCN)]BF_4 (($S_{C\alpha}$)-**1**), results from the stoichiometric or catalytic (excess substrate) reaction between (*Z*)-MAC and the catalyst system [Ru((*R*)-BINAP)(H)$(MeCN)_n(sol)_{3-n}$]BF_4 (**2**; n = 0–3, sol = acetone or methanol, depending on reaction medium)[7] at room temperature. Complex ($S_{C\alpha}$)-**1** is the product of olefin–hydride insertion with placement of ruthenium at the α-olefin carbon of (*Z*)-MAC (eq 4-1). To identify with reasonable certainty that ($S_{C\alpha}$)-**1** or any species observed during an enantioselective catalytic reaction is a catalytic intermediate leading to the major enantiomer of the product, the following criteria must be satisfied: (1) the absolute

---

† Reproduced with permission from Wiles, J. A.; Bergens, S. H. *Organometallics* **1998**, *17*, 2228–2240. Copyright 1998 American Chemical Society.

configuration of the putative intermediate must directly extrapolate to that of the major enantiomer of the product. Although satisfaction of this criterion does not constitute proof of the authenticity of the putative intermediate, failure to satisfy this criterion is

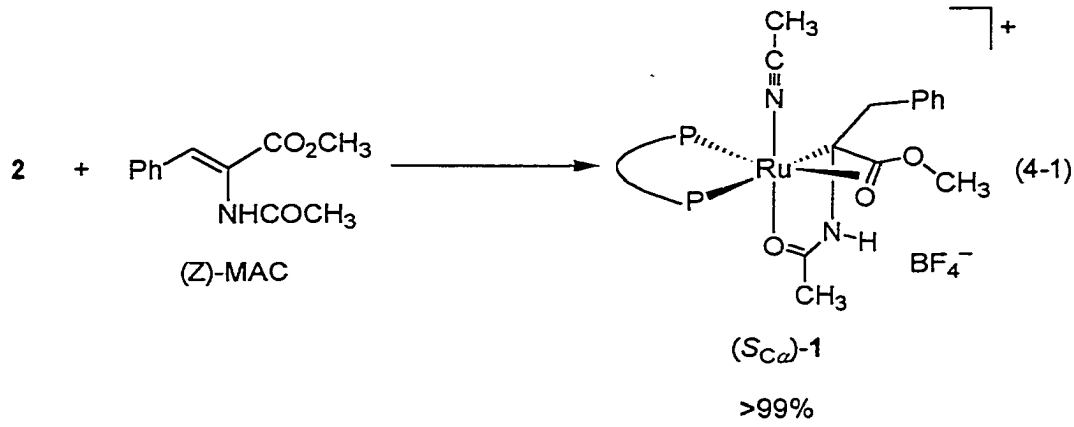

proof that the species is not an intermediate leading to the major enantiomer. (2) The stereoselectivities and regioselectivities (as determined by isotope labeling or other probes) of the stoichiometric reactions forming the putative intermediate and of the reactions converting it to product (and free catalyst) must summate to give the overall stereoselectivity and regioselectivity of the catalytic reaction. (3) The kinetics of the stoichiometric reactions forming the putative intermediate and those of the reactions converting it to product (and free catalyst) must comprise at least a component of the overall kinetics of the catalytic cycle. In addition to this information, the identities and kinetics of the enantioselective step(s) must be obtained to determine if the asymmetric interactions in the putative intermediate are relevant to the origins of enantioselection by the catalytic reaction. As part of an ongoing effort to determine if ($S_{C\alpha}$)-**1** is an authentic catalytic intermediate, the stereoselectivity and regioselectivity of the olefin–hydride insertion to form ($S_{C\alpha}$)-**1**, the stereoselectivity and regioselectivity of the reverse β-hydride elimination, and the extent to which formation of ($S_{C\alpha}$)-**1** is reversible prior to hydrogenolysis of the ruthenium–carbon bond have been investigated by this research group. These results will be compared to the stereoselectivity and regioselectivity of the catalytic hydrogenation. The extent of solvolysis of the ruthenium–carbon bond during

catalytic hydrogenations carried out in methanol solution and the effect of removing MeCN from the system on the catalytic enantioselectivity will also be reported.

Results and Discussion

Optimization of the Catalytic Hydrogenation. The pressure of dihydrogen gas, the solvent, and the temperature were varied to optimize the hydrogenation of (*Z*)-MAC using **2** as the catalyst. Table 4-1 summarizes the results. Among the solvents surveyed,

Table 4-1. Hydrogenation of (*Z*)-MAC Catalyzed by 2[a]

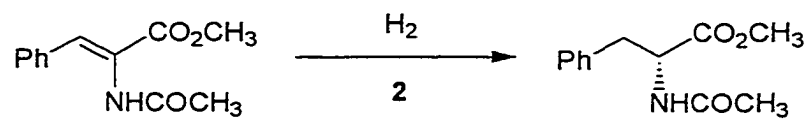

entry	$P(H_2)$,[b] atm	solvent	T, °C	ee, %
1	2	acetone	30	94
2	4	acetone	30	92
3	20	acetone	30	83
4	50	acetone	30	75
5	4	acetone	50	92
6	4	acetone	10	93
7	4	methanol	30	87
8	4	THF	30	85
9	4	CH_2Cl_2	30	64
10	50	MeCN	30	no reaction

[a] Reaction conditions: 2 mol % **2**; [**2**] = 2.6 mM; stir rate = 1100 rpm; t = 48 h; 100% conversion except where noted otherwise. [b] Pressures of dihydrogen gas are quoted as gauge pressure plus 1 atm.

the highest ee was obtained in acetone. This ee was even higher than that obtained in methanol—the most common solvent for hydrogenations using ruthenium–BINAP catalyst systems.[1] The TOF[8] was higher in acetone (ca. 0.9 min^{-1}) than in methanol (ca. 2.7×10^{-2}

min^{-1})[7] as well. Although the maximum TON in acetone was not determined, 980 turnovers in 91% ee (*R*) were achieved after 4 days at 30 °C under 4 atm of dihydrogen gas.

The ee in acetone solution decreased as the dihydrogen pressure was increased (Table 4-1). Inverse relationships between ee and dihydrogen pressure have been reported for other catalyst–substrate systems.[1g] Barring mass-transfer effects,[9] an inverse relationship between ee and pressure of dihydrogen gas often implies that the identity of the enantioselective step changed with the increase in dihydrogen pressure.

The ee in acetone increased slightly as the temperature was decreased from 50 °C to 10 °C; however, the TOF was too low to be of practical use below 10 °C. It is concluded from these results that the optimum conditions for hydrogenation of (*Z*)-MAC when using **2** as the catalyst are acetone solution, 30 °C, and 4 atm dihydrogen gas.

Mechanistic Investigations. Figure 4-1 shows a $^{31}P\{^{1}H\}$ NMR spectrum recorded of an operating catalytic hydrogenation of (*Z*)-MAC after 8 turnovers under conditions (acetone, pressure of dihydrogen gas ≈ 1 atm, 25 °C, 4 mol % **2**) similar to the optimum conditions described in the previous section.[10] Complex ($S_{C\alpha}$)-**1** was the only detectable ruthenium species in solution at room temperature.[11] Similar results were obtained using methanol, THF, and methylene chloride as solvent.[12] Deuterium labeling and other experiments will show (vide infra) that it is extremely unlikely that the formation of ($S_{C\alpha}$)-**1** is an irreversible kinetic trap under these conditions. Further, the catalytic hydrogenation of (*Z*)-MAC using isolated ($S_{C\alpha}$)-**1** as the catalyst occurs at the same rate and ee as when **2** is used as the catalyst. Its relatively high concentration during catalysis is therefore good evidence that ($S_{C\alpha}$)-**1**, whether a catalytic intermediate or not, is the most stable ruthenium complex in solution under these conditions.

Hydrogenolysis of ($S_{C\alpha}$)-1 in Acetone. The absolute configuration at the carbon center bonded to ruthenium in ($S_{C\alpha}$)-**1** is *S*. Stereospecific replacement of ruthenium by hydrogen will form (*R*)-MAC$(H)_2$, the major enantiomer formed by the catalytic hydrogenation. As reported earlier, the stoichiometric reaction of ($S_{C\alpha}$)-**1** with dihydrogen gas in methanol solution generated MAC$(H)_2$ at a similar rate and ee as the catalytic hydrogenation in methanol.[6] It is now reported that although the stoichiometric hydrogenolysis of ($S_{C\alpha}$)-**1** in acetone solution also produces MAC$(H)_2$ in similar ee to the catalytic

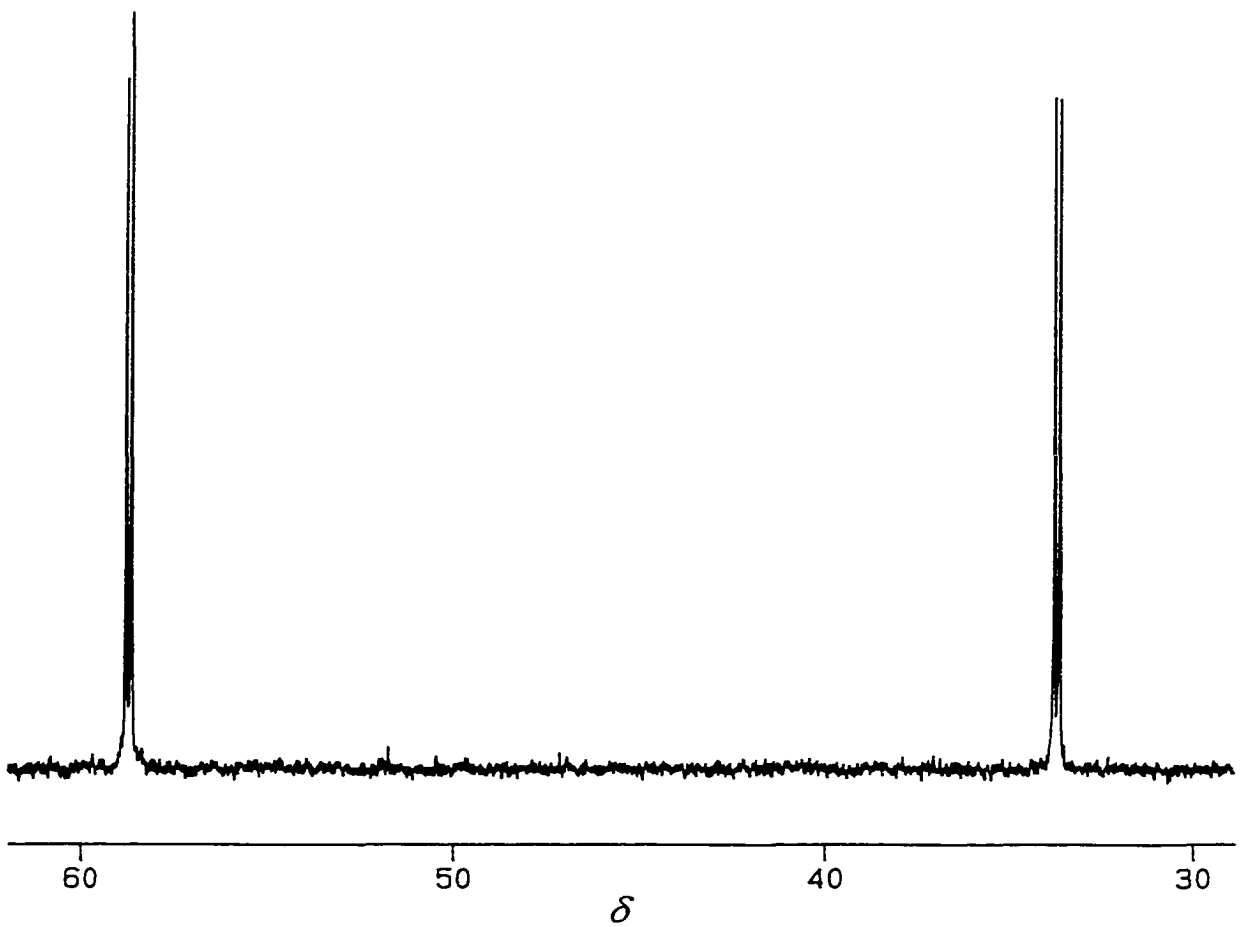

Figure 4-1. $^{31}P\{^{1}H\}$ NMR spectrum of an operating catalytic hydrogenation of (*Z*)-MAC using **2** as the catalyst in acetone-d_6.

hydrogenation (stoichiometric, 89% (*R*) (eq 4-2); catalytic, 92% ee (*R*)), the rate of the stoichiometric hydrogenolysis slows over the course of the reaction in this solvent.

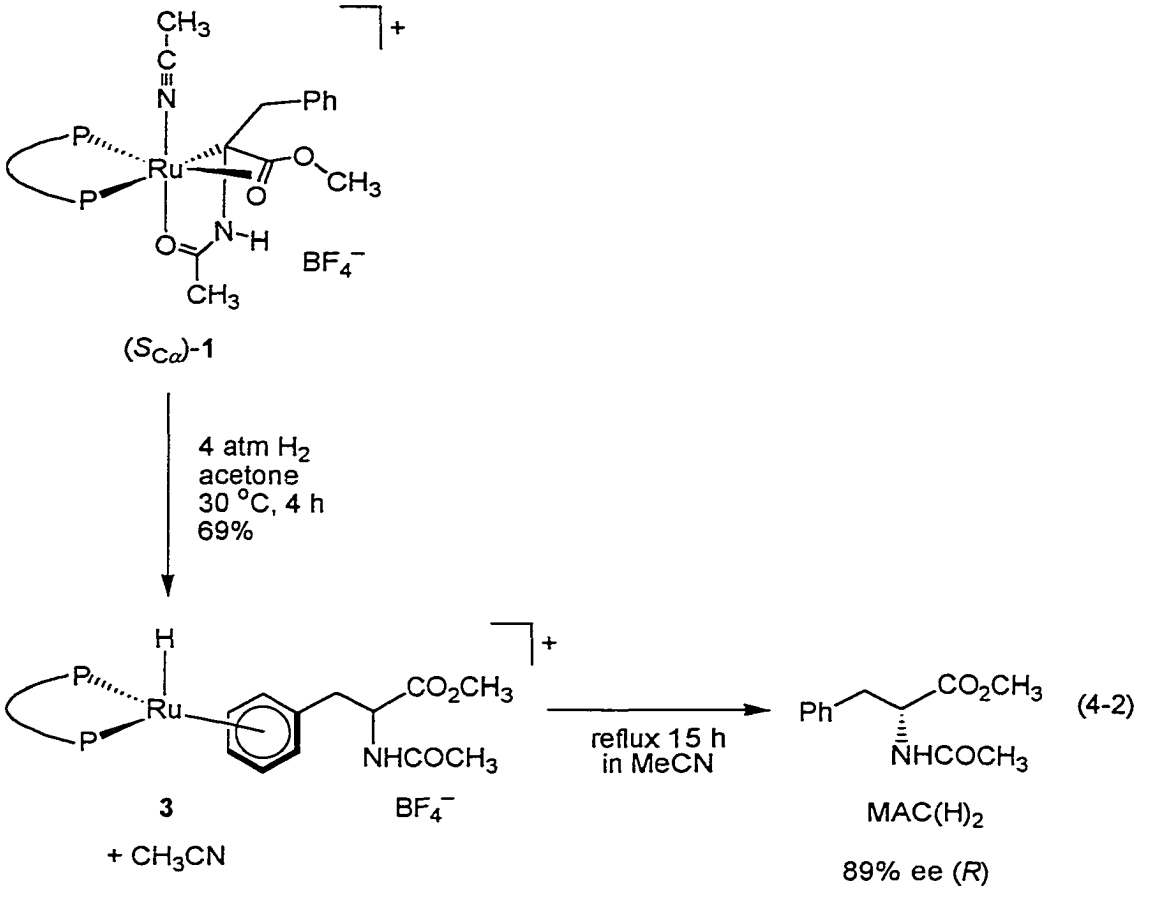

The product distribution after 4 h was 31% ($S_{C\alpha}$)-**1**, 58% [Ru((*R*)-BINAP)(H)(η^6-MAC(H)$_2$)]BF$_4$ (**3**; MAC(H)$_2$ is bonded to ruthenium as an η^6-ligand through the arene ring),[6] and 11% MAC(H)$_2$.[13] The hydrogenolysis was 97% complete after 24 h. MAC(H)$_2$ was liberated from **3** by refluxing the mixture in MeCN solution before the ee was determined. The conditions for the stoichiometric hydrogenolysis in acetone were the same as the catalytic hydrogenation in acetone except that excess (*Z*)-MAC was absent and that the concentration of ($S_{C\alpha}$)-**1** was approximately 4-fold higher for the stoichiometric hydrogenolysis than for the catalytic hydrogenation. Hydrogenolyses of ruthenium–carbon bonds in coordinatively saturated 18-electron ruthenium(II) complexes has been shown to require prior ligand dissociation to generate a 16-electron intermediate.

For example, the hydrogenolysis of the ruthenium–acyl bond in $[RuCl(COC_7H_9)(CO)_2(PPh_3)_2]$ requires prior dissociation of a triphenylphosphine ligand.[14] It is quite likely that hydrogenolysis of ($S_{C\alpha}$)-**1** proceeds via prior dissociation of the MeCN ligand to generate the 16-electron intermediate [Ru((*R*)-BINAP)((*S*)-MAC(H))]BF_4, which may contain a weakly coordinating acetone ligand. Since MeCN binds well to ruthenium(II) complexes such as ($S_{C\alpha}$)-**1**,[15] the decrease in rate as the hydrogenolysis proceeded in acetone solution most likely arose from the increase in the concentration of MeCN which occurred as complex **3** accumulated in solution (eq 4-2). Kinetic investigations of the stoichiometric hydrogenolysis and of the catalytic hydrogenation of (*Z*)-MAC are underway, and their results will be compared in due course. It is notable that although added MeCN is a strong inhibitor of the catalytic hydrogenation of (*Z*)-MAC when using **2** as the catalyst, free MeCN does not build up to detectable levels during the catalytic reaction because the excess (*Z*)-MAC in solution reacts with **2** to generate ($S_{C\alpha}$)-**1**, thereby preventing formation of **3** (see Figure 4-1). Further, the dissociation of MeCN prior to the hydrogenolysis of ($S_{C\alpha}$)-**1** or of a related species does not contribute to the enantioselection of the catalytic reaction; the ee for the catalytic hydrogenation of (*Z*)-MAC when using [Ru((*R*)-BINAP)(H)(η^6-(*rac*)-MAC(H)$_2$)]BF_4 as the catalyst in methanol was 86% (*R*) (eq 4-3), in accord with that obtained when using ($S_{C\alpha}$)-**1** and **2** as the catalysts (each giving 87% ee (*R*)).

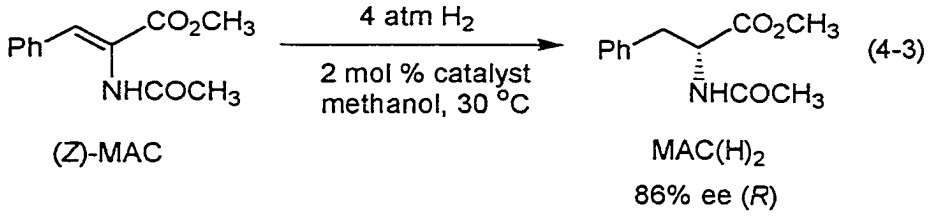

catalyst = [Ru((*R*)-BINAP)(H)(η^6-(*rac*)-MAC(H)$_2$)]BF_4

Reversibility of Formation of ($S_{C\alpha}$)-1. Reaction of diastereomerically pure ($S_{C\alpha}$)-**1** with dihydrogen gas generated (*R*)-MAC(H)$_2$ in ee's similar to those of the catalytic reactions in methanol and in acetone. The similar ee's for the catalytic and stoichiometric

reactions indicate that the formation of ($S_{C\alpha}$)-**1** was to some extent reversible, and that the other diastereomer(s) of ($S_{C\alpha}$)-**1** reacted to form (*S*)-MAC(H)$_2$. To confirm that its formation is reversible, complex ($S_{C\alpha}$)-**1** was reacted with 2.8 equiv of (*Z*)-MAC-CO_2CD_3 in acetone solution at 35 °C (eq 4-4). The system achieved equilibrium (assuming

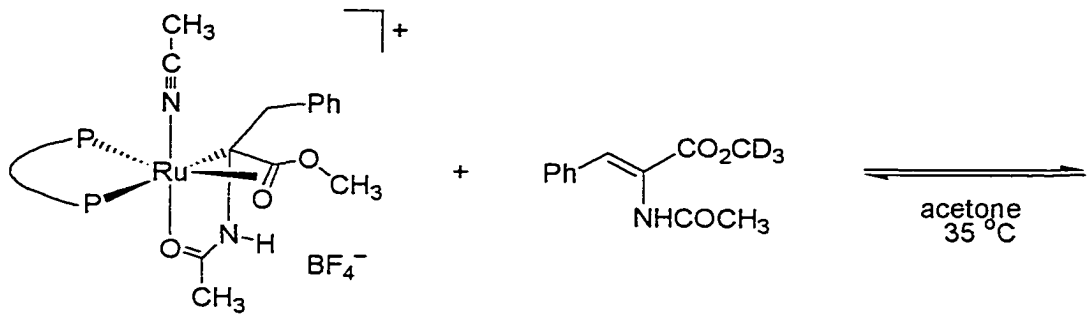

($S_{C\alpha}$)-**1** (*Z*)-MAC-CO_2CD_3

Initial: 1 (equiv) 2.8
Final: 0.26 2.06

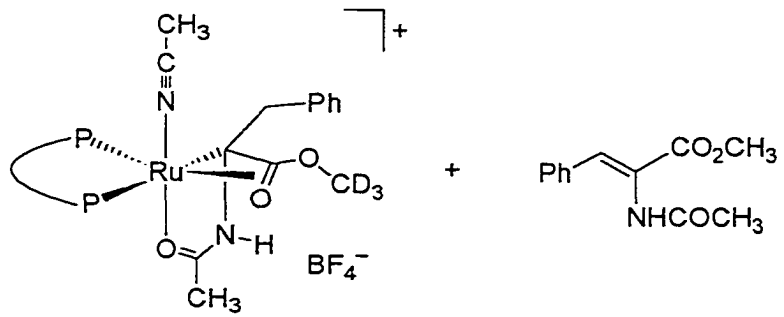

(4-4)

($S_{C\alpha}$)-**1**-CO_2CD_3 (*Z*)-MAC

0 0
0.74 0.74

K_{eq} = 1), demonstrating that formation of ($S_{C\alpha}$)-**1** was reversible. Complexes ($S_{C\alpha}$)-**1** and ($S_{C\alpha}$)-**1**-CO_2CD_3 were the only ruthenium species detected in solution. Scheme 4-1 shows a proposed sequence of steps for the reversible formation of ($S_{C\alpha}$)-**1** and ($S_{C\alpha}$)-**1**-CO_2CD_3 via **2** reacting with (*Z*)-MAC or with (*Z*)-MAC-CO_2CD_3, respectively, assuming the reverse of formation of ($S_{C\alpha}$)-**1** proceeds via a β-hydride elimination. β-Hydride elim-

Scheme 4-1. Proposed Sequence of Steps for the Reversible Formation of ($S_{C\alpha}$)-1 and ($S_{C\alpha}$)-1-CO_2CD_3[a]

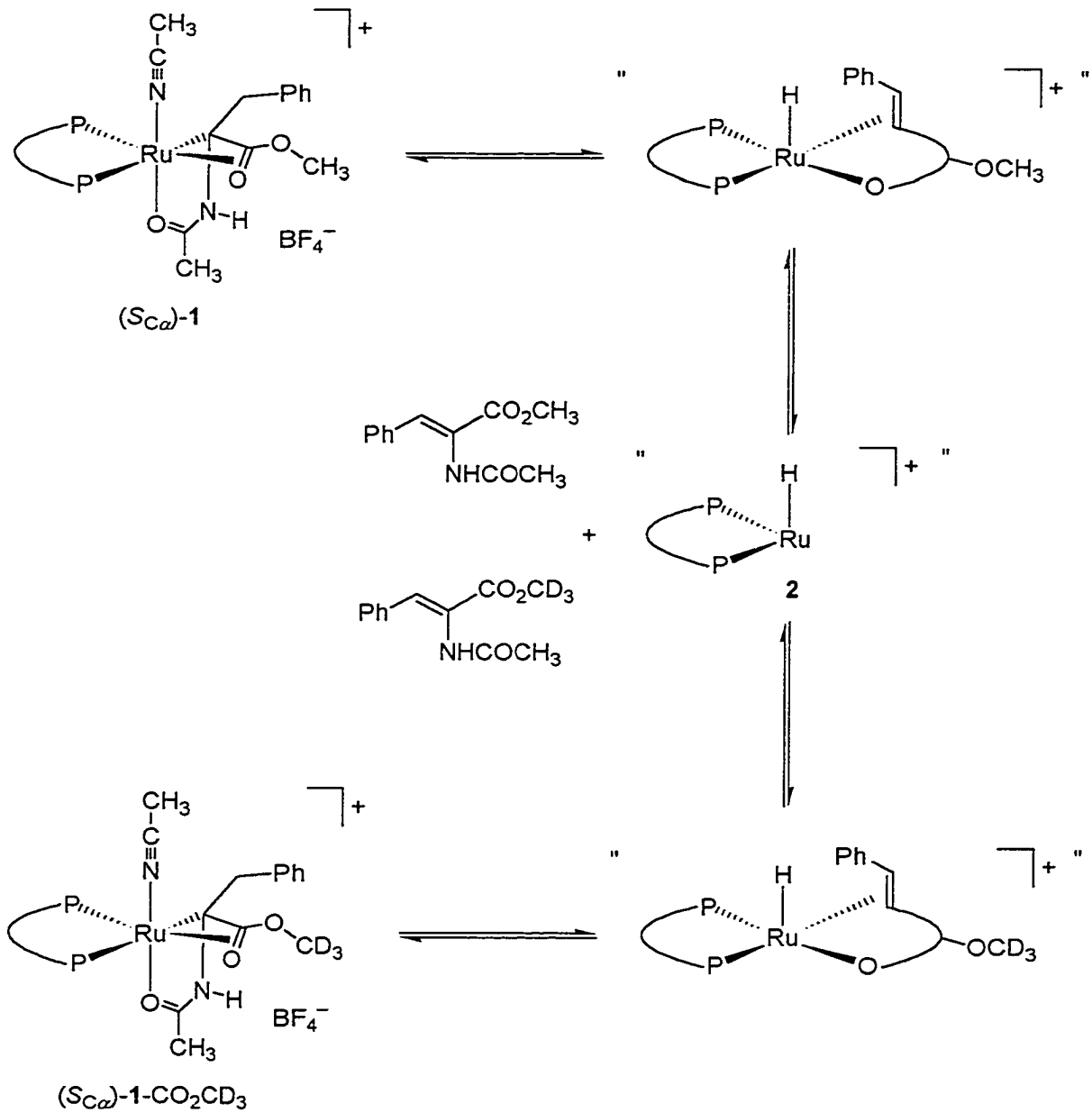

[a] Species shown in quotation marks are approximate representations of the true species in solution.

ination within ($S_{C\alpha}$)-**1** followed by dissociation of (*Z*)-MAC would generate **2**, which can either react with (*Z*)-MAC or with (*Z*)-MAC-CO_2CD_3 to generate the corresponding isotopomers of ($S_{C\alpha}$)-**1**. A consequence of the formation of ($S_{C\alpha}$)-**1** being to some extent reversible via a β-hydride elimination on the timescale of the hydrogenolysis is that stoichiometric deuteriolysis of ($S_{C\alpha}$)-**1** must form some MAC$(H)_2$ with deuterium at the β-position. This condition on the proposed mechanism for the reverse process is investigated in the next section.

Deuterium Studies in Acetone. The stoichiometric deuteriolysis of ($S_{C\alpha}$)-**1** carried out in acetone solution slowed after ca. 76% conversion (eq 4-5). Figure 4-2

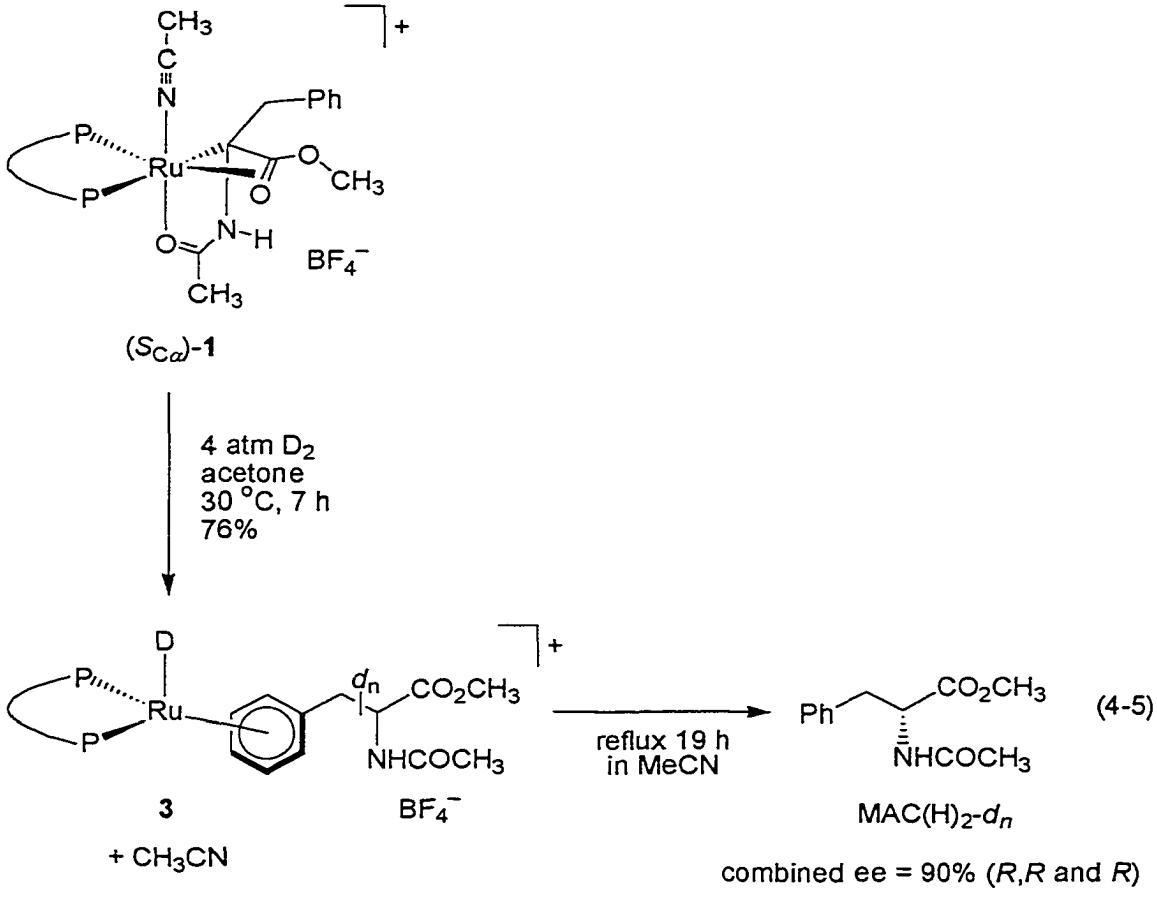

shows the composition of the reduced MAC after the deuteriolysis had slowed ((*R*,*R* and *S*,*S*)-MAC$(H)_2$-α,β-d_2,[16,17] 80%; MAC$(H)_2$-α-d_1, 12%; (*R*,*R* and *S*,*S*)-MAC$(H)_2$-β-d_1, 6%;

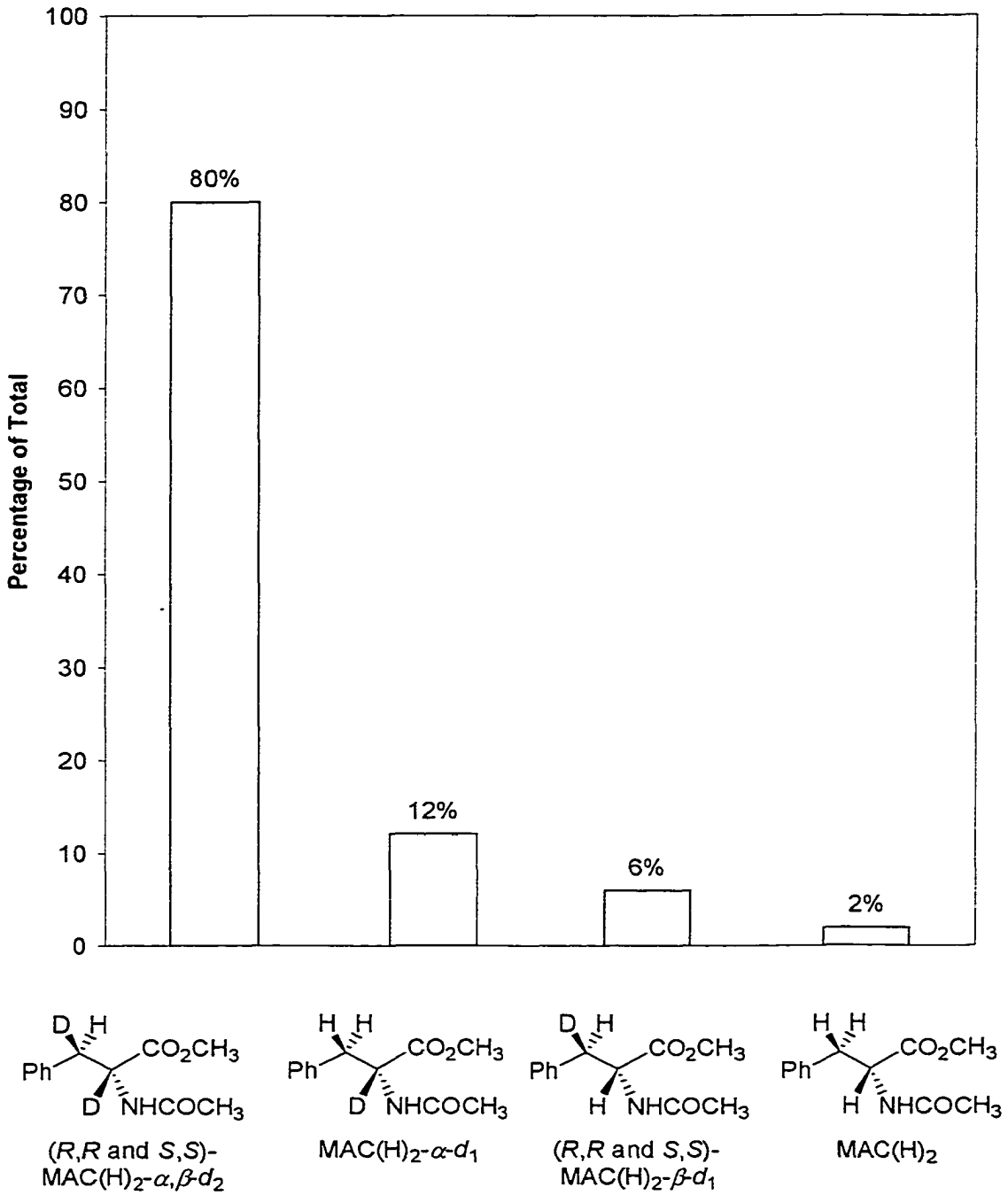

Figure 4-2. The distribution of MAC(H)$_2$-d_n isotopomers from the deuteriolysis of ($S_{C\alpha}$)-**1** in acetone.

and MAC(H)$_2$, 2%). The combined ee was 90% (*R*,*R* and *R*), which is similar to that of the catalytic hydrogenation of (*Z*)-MAC in acetone (92% (*R*)). MAC(H)$_2$ labeled with deuterium at the β-position formed as predicted by the β-hydride-elimination mechanism for the reverse of formation of ($S_{C\alpha}$)-**1** (Scheme 4-1). It is necessary to determine the reactivity of **2** towards dideuterium gas to more fully interpret these results.

Further reaction between **2** and dihydrogen gas (1 atm) was not detected by NMR spectroscopy in acetone solution over temperatures ranging from –80 °C to 25 °C. Reaction with dideuterium gas (1 atm), however, resulted in the immediate formation of **2**-*d* even at temperatures well below 0 °C (eq 4-6).[18] Under dihydrogen gas, complex **2** is

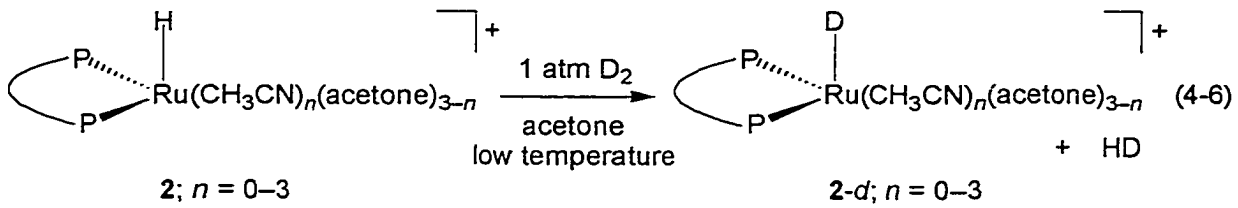

(4-6)

therefore in rapid equilibrium with small concentrations of the ruthenium(IV) trihydride [Ru((*R*)-BINAP)(H)$_3$(MeCN)$_x$(acetone)$_y$]BF$_4$ (**4**) (or the corresponding ruthenium(II) hydrido-η^2-dihydrogen species), resulting in the observed H–D exchange with dideuterium gas. An equilibrium between **2** and **4** would, in principle, favor **2** because **4** must contain at least one mutually *trans*-disposition of a phosphine and a hydrido ligand—an unfavorable situation as both these ligands have strong trans influences.[19] Any free **2** generated in solution during the stoichiometric deuteriolysis of **1** is likely to quickly react with dideuterium gas to generate **2**-*d*.

In all probability, the MAC(H)$_2$-α-d_1 (12%) produced by the stoichiometric deuteriolysis (Figure 4-2) resulted from the deuteriolysis of the ruthenium–carbon bond in ($S_{C\alpha}$)-**1**. The product which formed in large excess (80%) was (*R*,*R* and *S*,*S*)-MAC(H)$_2$-α,β-d_2, with deuterium at both the α- and β-positions. This product is that of a net syn addition of dideuterium gas to the carbon–carbon double bond of (*Z*)-MAC; its presence is strong evidence for the formation of ($S_{C\alpha}$)-**1** being reversible via a β-hydride elimination.

Another possibility, a stereoselective C–H activation at the β-position of MAC(H)$_2$-α-d_1, is ruled out by our finding that reaction of MAC(H)$_2$ with **2**-*d* under dideuterium gas does not result in H–D exchange at the α- or β-positions of MAC(H)$_2$. Scheme 4-2 shows the sequence of steps involving olefin–hydride insertion and β-hydride elimination that accounts for the isotopomers of MAC(H)$_2$-d_n produced by the stoichiometric deuteriolysis of ($S_{C\alpha}$)-**1** in acetone. Elimination of the *pro-R*-β-hydride in ($S_{C\alpha}$)-**1** followed by olefin dissociation generates (*Z*)-MAC and **2**. The stereochemistry of the β-hydride elimination will be discussed in more detail below where it will be shown that elimination of the *pro-S*-β-hydride within ($S_{C\alpha}$)-**1** is highly unlikely. Complex **2**, generated via the β-hydride elimination, will quickly react with the excess dideuterium gas in the reactor to produce **2**-*d* (eq 4-6). Coordination of (*Z*)-MAC to **2**-*d* through the *si*-olefin face followed by insertion into the ruthenium–deuteride bond will generate ($S_{C\alpha}$,$R_{C\beta}$)-β-d_1-**1** (of *R* absolute configuration at the deuterated β-carbon center). Strong support for this sequence of steps is that placement of acetone solutions of ($S_{C\alpha}$)-**1** under lower pressures of dideuterium gas (1 atm) results in H–D exchange with the *pro-R*-β-hydride. Further, **2**-*d* (made by reaction of **2** with dideuterium gas (eq 4-6)) reacts with (*Z*)-MAC to produced ($S_{C\alpha}$,$R_{C\beta}$)-β-d_1-**1** as the only detectable ruthenium species in solution. The stereochemistry of the olefin–hydride insertion results in a net syn addition of ruthenium and hydrogen across the carbon–carbon double bond of (*Z*)-MAC. Assuming retention of configuration at the α-carbon, deuteriolysis of the ruthenium–carbon bond in ($S_{C\alpha}$,$R_{C\beta}$)-β-d_1-**1** will produce (*R*,*R*)-MAC(H)$_2$-α,β-d_2, the product of net syn addition of dideuterium to the carbon–carbon double bond of (*Z*)-MAC. (*S*,*S*)-MAC(H)$_2$-α,β-d_2 would result from coordination of (*Z*)-MAC to **2**-*d* via the *re*-olefin face followed by deuteriolysis of the ruthenium–carbon bond.

As discussed above, β-hydride elimination and dissociation of (*Z*)-MAC from **1** during the stoichiometric deuteriolysis will produce (*Z*)-MAC and **2** in the presence of excess dideuterium gas (Scheme 4-2). Complex **2** in this mixture can either react with (*Z*)-MAC to regenerate ($S_{C\alpha}$)-**1** (leading to MAC(H)$_2$-α-d_1 after deuteriolysis of the ruthenium–carbon bond) or it can react with dideuterium gas to produce **2**-*d* (leading

Scheme 4-2. Proposed Sequence of Steps that Accounts for the Isotopomers of MAC(H)$_2$ Produced by the Stoichiometric Deuteriolysis of ($S_{C\alpha}$)-1

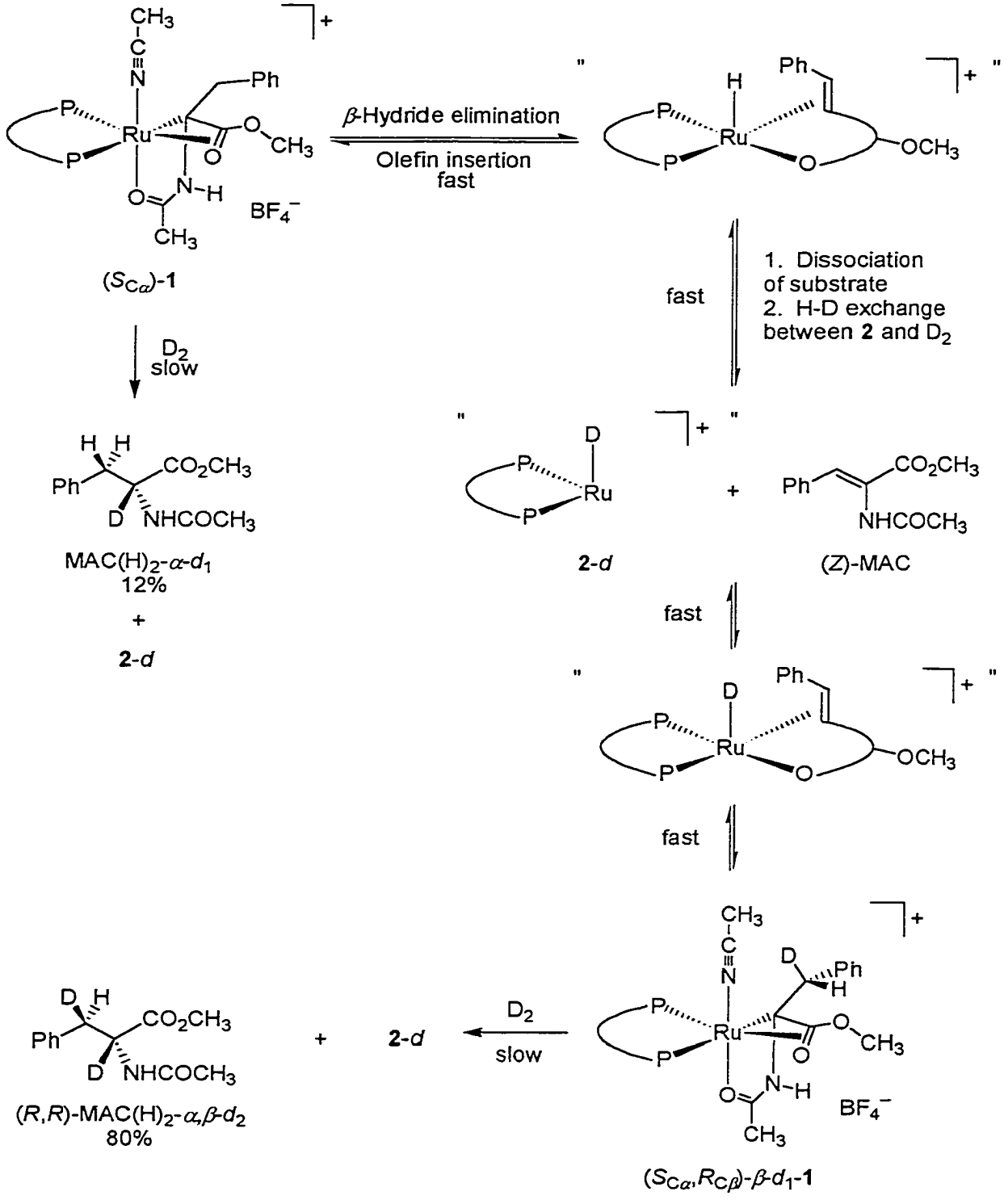

eventually to (*R*,*R* and *S*,*S*)-MAC(H)$_2$-α,β-d_2). Since the relative rate of formation of ($S_{C\alpha}$)-**1** versus that of **2**-*d* in this mixture is unknown, the 85:15 ratio of (*R*,*R* and *S*,*S*)-MAC(H)$_2$-α,β-d_2 to MAC(H)$_2$-α-d_1 represents the lower limit to the extent of reversibility of formation of ($S_{C\alpha}$)-**1** during the deuteriolysis. It was not possible to isolate MAC(H)$_2$-α-d_1 in order to determine its ee, which would be 100% (*R*) if it formed from direct deuteriolysis of ($S_{C\alpha}$)-**1** without prior formation of **2** and (*Z*)-MAC. Since the lower limit to the extent to which formation of ($S_{C\alpha}$)-**1** reversed is ca. 85%, equilibration between ($S_{C\alpha}$)-**1**, **2**, and (*Z*)-MAC must be relatively rapid and nearly complete before deuteriolysis of the ruthenium–carbon bond occurs under these conditions.

Only the (*R*,*R*) and (*S*,*S*) diastereomers of MAC(H)$_2$-α,β-d_2 were produced by the deuteriolysis of ($S_{C\alpha}$)-**1**. This stereoselectivity is a consequence of the direct relationship between whether β-hydride or β-deuteride elimination occurred within ($S_{C\alpha}$,$R_{C\beta}$)-β-d_1-**1** and the stereochemistry of the resulting MAC. This relationship also exists in the opposite diastereomer ($R_{C\alpha}$,$S_{C\beta}$)-β-d_1-**1**. As shown in Scheme 4-3, (*Z*)-MAC will result from β-deuteride elimination, and the less stable isomer (*E*)-MAC-β-d_1 will result from β-hydride elimination. Reaction of (*E*)-MAC-β-d_1 with **2**-*d* followed by deuteriolysis of the ruthenium–carbon bond must generate MAC(H)$_2$-α,β,β-d_3.[20] Since MAC(H)$_2$-α,β,β-d_3 was not detected among the products, we conclude that β-hydride elimination within ($S_{C\alpha}$)-**1** is highly stereoselective, favoring the *pro-R*-β-hydride in ($S_{C\alpha}$)-**1** (this position is occupied by deuterium in ($S_{C\alpha}$,$R_{C\beta}$)-β-d_1-**1**) and the *pro-S*-β-hydride in ($R_{C\alpha}$)-**1** (this position is occupied by deuterium in ($R_{C\alpha}$,$S_{C\beta}$)-β-d_1-**1**). This stereoselectivity likely originates from the unfavorability of formation of (*E*)-MAC over formation of (*Z*)-MAC. Similar control over the stereoselectivity of a β-hydride elimination was observed during the intramolecular hydrosilylation of olefins catalyzed by [Rh((*S*)-BINAP)-(acetone)$_2$](ClO$_4$).[21] It is possible, however, that elimination of the *pro-S*-β-hydride does occur within ($S_{C\alpha}$)-**1**, but the resulting (*E*)-MAC does not dissociate from ruthenium but rather reinserts into the ruthenium–hydride bond to regenerate ($S_{C\alpha}$)-**1**. The stoichiometric deuteriolysis of ($S_{C\alpha}$)-**1** is mute regarding this issue because *E*-stereoselective β-hydride elimination within ($S_{C\alpha}$,$R_{C\beta}$)-β-d_1-**1** will be of no net consequence if the resulting

Scheme 4-3. Outcome of Stereoselective β-Deuteride and β-Hydride Elimination Within ($S_{C\alpha}$,$R_{C\beta}$)-β-d_1-1

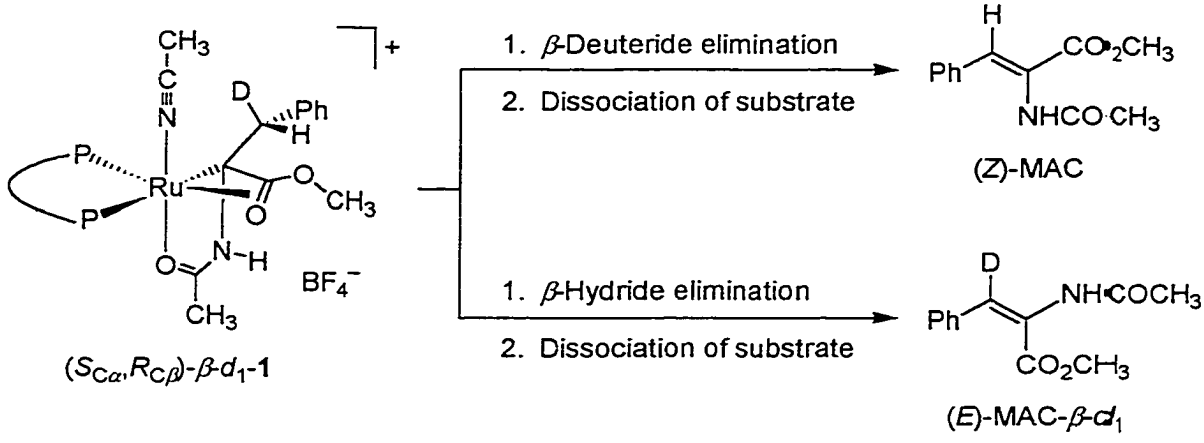

(*E*)-MAC-β-d_1 reinserts into the ruthenium–hydride bond without prior olefin dissociation. It is unlikely, however, that (*Z*)-MAC will dissociate from ruthenium but (*E*)-MAC will not.

The most likely explanation for formation of the other minor products of the stoichiometric deuteriolysis, (*R*,*R*)-MAC(H)$_2$-β-d_1 (6%) and MAC(H)$_2$ (2%), is solvolysis of the ruthenium–carbon bonds in ($S_{C\alpha}$,$R_{C\beta}$)-β-d_1-**1** and ($S_{C\alpha}$)-**1**, respectively, by adventitious water or by acetone.[22]

It is concluded from the predominant formation of (*R*,*R* and *S*,*S*)-MAC(H)$_2$-α,β-d_2 by the stoichiometric deuteriolysis of ($S_{C\alpha}$)-**1** that olefin coordination, olefin–hydride insertion, and their reverse transformations are rapid relative to the hydrogenolysis of the ruthenium–carbon bond under these reaction conditions (which include an accumulation of MeCN in solution as the reaction proceeds). It is also concluded that β-hydride elimination within ($S_{C\alpha}$)-**1** is highly stereoselective, favoring formation of the more stable olefin isomer (*Z*)-MAC. The catalytic deuteration of (*E*)-MAC and (*Z*)-MAC were carried out to investigate the stereoselectivity of the catalytic hydrogenation.

Stereoselectivity and Regioselectivity of the Catalytic Hydrogenation. The catalytic deuteration of (*Z*)-MAC in acetone generated (*R*,*R* and *S*,*S*)-MAC(H)$_2$-α,β-d_2 as the only detectable diastereomers in 92% ee (*R*,*R*) (eq 4-7). Although the net syn addition

of dideuterium gas across (*Z*)-MAC is consistent with the stereochemistry of the stoichiometric deuteriolysis of ($S_{C\alpha}$)-**1**, it is also consistent with any mechanism involving olefin–hydride insertion followed by reductive elimination of a carbon–hydrogen bond. The net syn addition implies, however, that if the catalytic hydrogenation proceeds through ($S_{C\alpha}$)-**1** or a similar species, any β-hydride elimination which occurred was highly stereoselective, favoring formation of (*Z*)-MAC.

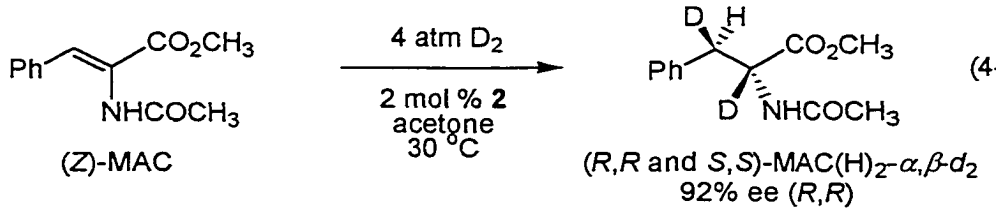

(4-7)

The catalytic hydrogenation and deuteration of (*E*)-MAC were carried out to investigate if formation of ($S_{C\alpha}$)-**1** (Figure 4-1) or of a similar species is reversible during the catalytic hydrogenation (eq 4-4). The catalytic hydrogenation of (*E*)-MAC in acetone produced $MAC(H)_2$ in 91% ee (*R*), which is similar to the ee for hydrogenation of (*Z*)-MAC (92% (*R*)). The similar ee's indicate that both of these hydrogenations proceed through the same olefin geometry, implying that the hydrogenation of (*E*)-MAC proceeds via a rapid prior isomerization to (*Z*)-MAC.[23]

The catalytic deuteration of (*E*)-MAC was carried out to determine if olefin isomerization occurs prior to formation of $MAC(H)_2$. Insertion of (*E*)-MAC into a ruthenium–deuteride bond with placement of ruthenium at the α-carbon, followed by β-elimination favoring the *Z* isomer will form (*Z*)-MAC-β-d_1 with deuterium at the β-position. Deuteration of (*Z*)-MAC-β-d_1 would then lead to $MAC(H)_2$-α,β,β-d_3. Figure 4-3 shows the distribution of isotopomers produced by the catalytic deuteration of (*E*)-MAC in acetone ($MAC(H)_2$-α,β,β-d_3, 69%; (*R*,*R* and *S*,*S*)-$MAC(H)_2$-α,β-d_2, 20%; $MAC(H)_2$-β,β-d_2, 4%; (*R*,*S* and *S*,*R*)-$MAC(H)_2$-α,β-d_2, 4%; (*R*,*R* and *S*,*S*)-$MAC(H)_2$-β-d_1, 1%; and $MAC(H)_2$-α-d_1, 2%). The combined ee of the products was 92% (*R*,*R* and *R*). $MAC(H)_2$-α,β,β-d_3 amounted to 69% of the product mixture, which is strong evidence that prior isomerization of (*E*)-MAC to (*Z*)-MAC occurred during the catalytic

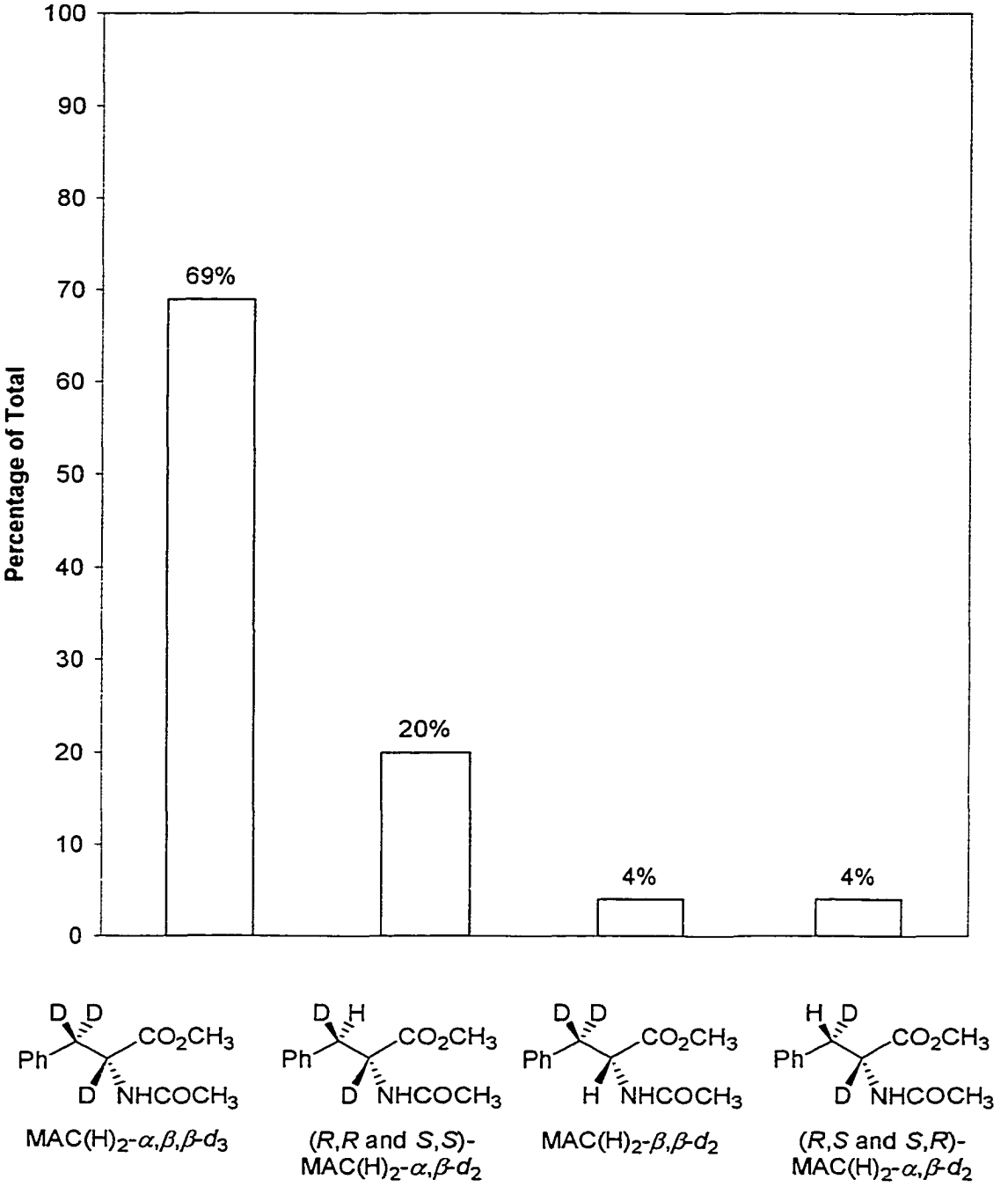

Figure 4-3. The distribution of MAC(H)$_2$-d_n isotopomers from the catalytic deuteration of (*E*)-MAC when using **2** as the catalyst in acetone. The isotopomers (*R*,*R* and *S*,*S*)-MAC(H)$_2$-β-d_1 and MAC(H)$_2$-α-d_1 (combined 3% of total mixture) are not shown.

deuteration. Scheme 4-4 shows the sequence of steps that accounts for this distribution of isotopomers via a rapid formation of ($S_{C\alpha}$)-**1**, or a related species, which is reversible via a stereoselective β-hydride elimination. Coordination of (*E*)-MAC to **2**-*d* through the *re* face or the *si* face followed by olefin–hydride insertion generates ($R_{C\alpha}$,$R_{C\beta}$)-β-d_1-**1** or ($S_{C\alpha}$,$S_{C\beta}$)-β-d_1-**1**, respectively (Scheme 4-4, upper left). Stereoselective β-hydride elimination within ($R_{C\alpha}$,$R_{C\beta}$)-β-d_1-**1** or ($S_{C\alpha}$,$S_{C\beta}$)-β-d_1-**1** to favor formation of (*Z*)-MAC followed by olefin dissociation generates (*Z*)-MAC-β-d_1, **2**, and subsequently **2**-*d* (by reaction of **2** with dideuterium (eq 4-6)). Deuteration of (*Z*)-MAC-β-d_1 using **2**-*d* as catalyst generates MAC(H)$_2$-α,β,β-d_3, the predominant product of the catalytic deuteration (69%; Scheme 4-4, upper right). An initial isomerization of (*E*)-MAC to (*Z*)-MAC via the same sequence of steps likely accounts for the catalytic hydrogenations of (*E*)-MAC and (*Z*)-MAC occurring with similar ee's. The formation of MAC(H)$_2$-α,β,β-d_3 is strong evidence that at least 69% of (*E*)-MAC underwent isomerization to (*Z*)-MAC-β-d_1 via the reversible formation of ($S_{C\alpha}$)-**1**, or of a structurally related species, during the catalytic reaction (although not necessarily as part of the catalytic cycle). Further, a rapid and reversible formation of ($S_{C\alpha}$)-**1** via stereoselective β-hydride elimination is also consistent with formation of (*R*,*R* and *S*,*S*)-MAC(H)$_2$-α,β-d_2 as the only detectable product from the catalytic deuteration of (*Z*)-MAC (eq 4-7).

The amount of MAC(H)$_2$-α,β,β-d_3 in the product mixture (69%) is the lower limit to the extent of isomerization of (*E*)-MAC to (*Z*)-MAC prior to deuteration because (*R*,*R* and *S*,*S*)-MAC(H)$_2$-α,β-d_2 (20%) may also have arisen from such a process. As discussed previously, (*R*,*R* and *S*,*S*)-MAC(H)$_2$-α,β-d_2 (20%) results from a net syn addition of dideuterium to (*Z*)-MAC (eq 4-7). It is believed that deuterium-free (*Z*)-MAC was produced during the catalytic deuteration of (*E*)-MAC through reaction of (*E*)-MAC with **2**, which resulted from the stereoselective β-hydride elimination within ($R_{C\alpha}$,$R_{C\beta}$)-β-d_1-**1** or ($S_{C\alpha}$,$S_{C\beta}$)-β-d_1-**1** (Scheme 4-4, top, and as discussed in the previous paragraph). It is reasonable to propose that rather than reacting with dideuterium gas to generate **2**-*d*, some of **2** reacted with (*E*)-MAC (which is in up to 50-fold excess under *catalytic* conditions) to generate a *deuterium-free* diastereomer of ($S_{C\alpha}$)-**1** or a structurally related

Scheme 4-4. Sequence of Steps that Accounts for the Product Distribution from the Catalytic Deuteration of (*E*)-MAC

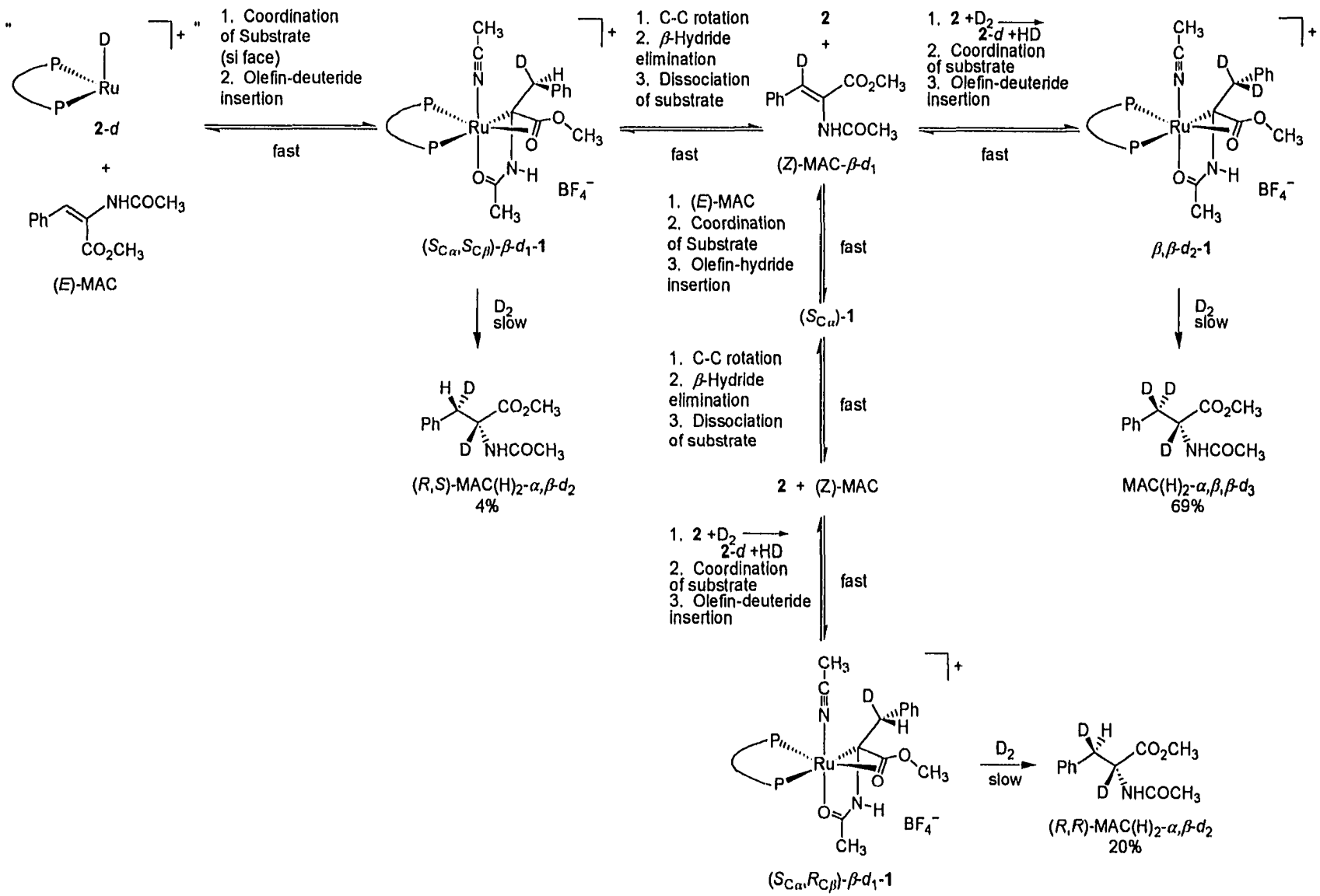

species (Scheme 4-4, middle). *Z*-Stereoselective β-hydride elimination followed by substrate dissociation will generate **2** and deuterium-free (*Z*)-MAC. Deuteration of (*Z*)-MAC then generates (*R,R* and *S,S*)-MAC(H)$_2$-α,β-d_2 (20%).

Scheme 4-5 shows another conceivable route to formation of deuterium-free (*Z*)-MAC during the catalytic deuteration of (*E*)-MAC.[3h,3i] In this sequence, **2**-*d* activates the N–H bond of (*E*)-MAC to generate the corresponding amido–allyl complex **5**. A π–σ–π rearrangement through formation of a ruthenium–carbon σ bond at the β-position would form the amido–allyl complex **5'** which could eliminate (*Z*)-MAC-*N*-*d*. Deuteration of (*Z*)-MAC-*N*-*d* will generate (*R,R* and *S,S*)-MAC(H)$_2$-α,β,N-d_3. As previously discussed,[17] varying amounts of product deuterated at nitrogen were observed in all reactions carried out under deuterium gas in acetone solution. Control experiments show that **2** catalyzes the H–D exchange between dideuterium and the N–H group of MAC(H)$_2$ and (by extension) presumably also of MAC. The formation of N–D products by the catalytic reaction under deuterium gas therefore cannot be used as direct evidence for involvement of amido–allyl (**5**, **5'**) or related species in the catalytic hydrogenation. There is no experimental evidence that *conclusively* distinguishes between reaction of **2** with (*E*)-MAC to form ($S_{C\alpha}$)-**1** (Scheme 4-4, middle) or formation of an amido–allyl species (Scheme 4-5, **5** and **5'**) to account for formation of (*Z*)-MAC during the catalytic deuteration. Evidence against an amido–allyl species, however, is that little, if any, H–D exchange between nitrogen and the α-carbon or β-carbon centers occurs during the catalytic deuteration of (*Z*)-MAC in methanol solvent (vide infra, eq 4-8). It is reasonable to expect amido–allyl species such as **5** and **5'** to undergo some deuteride addition to the β-carbon-forming species such as **6** and **6'** (Scheme 4-5). Among other things, these sequences of steps would allow H–D exchange between nitrogen and the β-carbon. The lack of an observable amount of such exchange during the catalytic deuteration of (*Z*)-MAC in methanol favors formation of (*Z*)-MAC via reaction of **2** with (*E*)-MAC (Scheme 4-4, middle) over an amido–allyl route.

The major product of the catalytic deuteration of (*E*)-MAC, MAC(H)$_2$-α,β,β-d_3 (69%), resulted from formation of ($S_{C\alpha}$)-**1** or a related species via a rapid net syn addition of ruthenium and deuterium across the carbon–carbon double bond, followed by a rapid

Scheme 4-5. A Plausible Route to Formation of Deuterium-Free (*Z*)-MAC During the Catalytic Deuteration of (*E*)-MAC

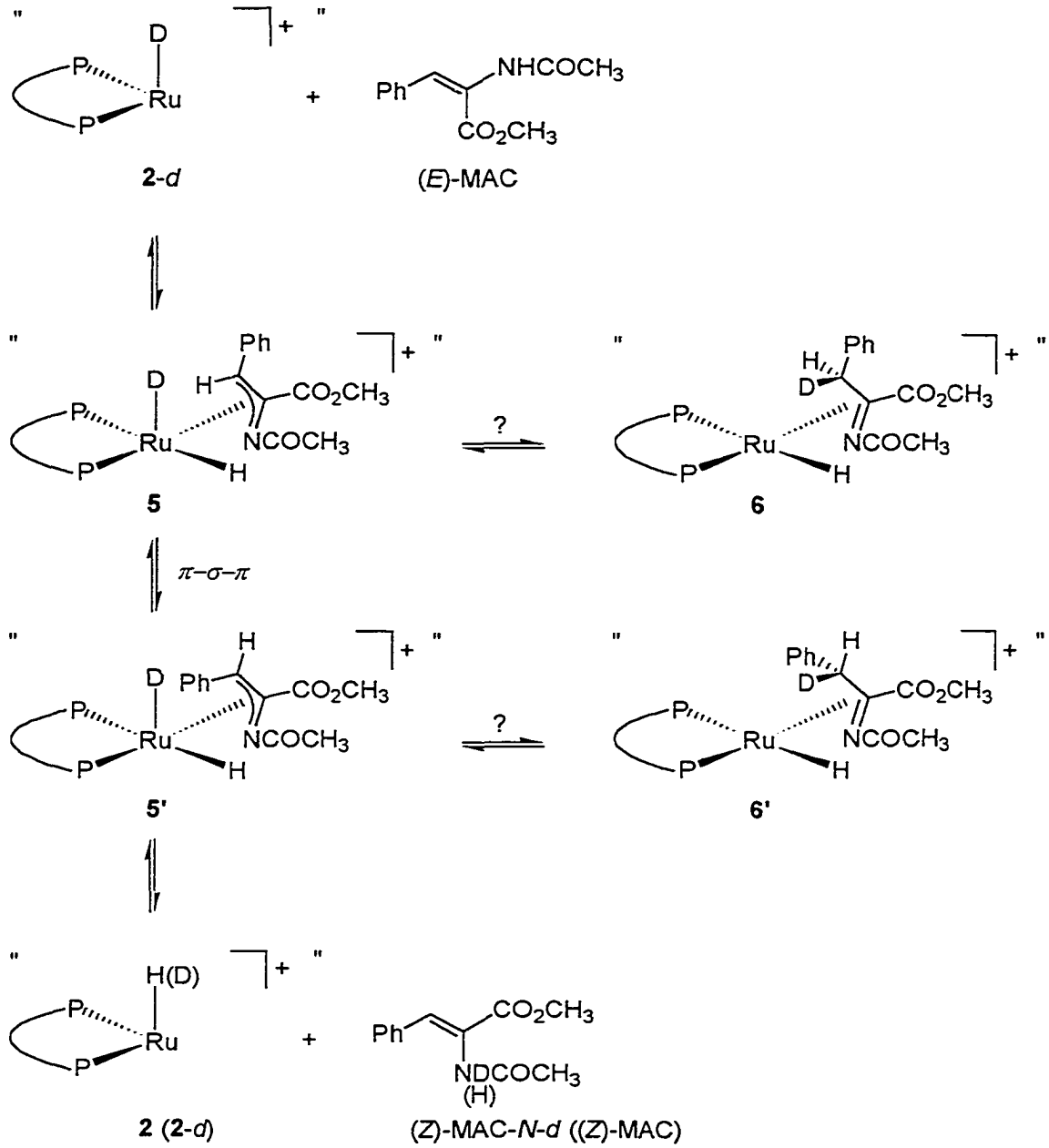

stereoselective β-hydride elimination. It is likely that a further 20% of the product, (*R*,*R* and *S*,*S*)-MAC(H)$_2$-α,β-d_2, also resulted from such a sequence of steps. It is therefore concluded from the product distributions of the catalytic deuteration of (*E*)-MAC and (*Z*)-MAC in acetone that the sum of the stereoselectivities and regioselectivities of the

reversible formation of ($S_{C\alpha}$)-**1** and its hydrogenolysis equals the overall stereoselectivity and regioselectivity of the catalytic hydrogenation.

One of the minor products of the catalytic deuteration of (*E*)-MAC, (*R,S* and *S,R*)-MAC(H)$_2$-α,β-d_2 (4%), likely arose from the direct deuteration of (*E*)-MAC without prior isomerization to (*Z*)-MAC (Scheme 4-4, left, deuteriolysis of ($S_{C\alpha}$,$S_{C\beta}$)-β-d_1-**1**). Of the remaining minor products of the catalytic deuteration of (*E*)-MAC, it is speculated that MACH$_2$-α-d_1 (2%) resulted from deuteriolysis of ($S_{C\alpha}$)-**1** or from reaction of HD gas with (*E*)-MAC catalyzed by **2**. (*R,R* and *S,S*)-MAC(H)$_2$-β-d_2 (1%) and MAC(H)$_2$-β,β-d_2 (4%) likely arose from solvolysis of the ruthenium–carbon bond in ($S_{C\alpha}$,$R_{C\beta}$ and $R_{C\alpha}$,$S_{C\beta}$)-β-d_1-**1** and β,β-d_2-**1**, respectively, by adventitious water.

Methanol as the Solvent. The catalytic deuteration of (*Z*)-MAC was carried out in methanol to determine the ratio of solvolysis to hydrogenolysis during catalysis in this protic solvent. As shown in eq 4-8, the product distribution was (*R,R* and *S,S*)-MAC(H)$_2$-

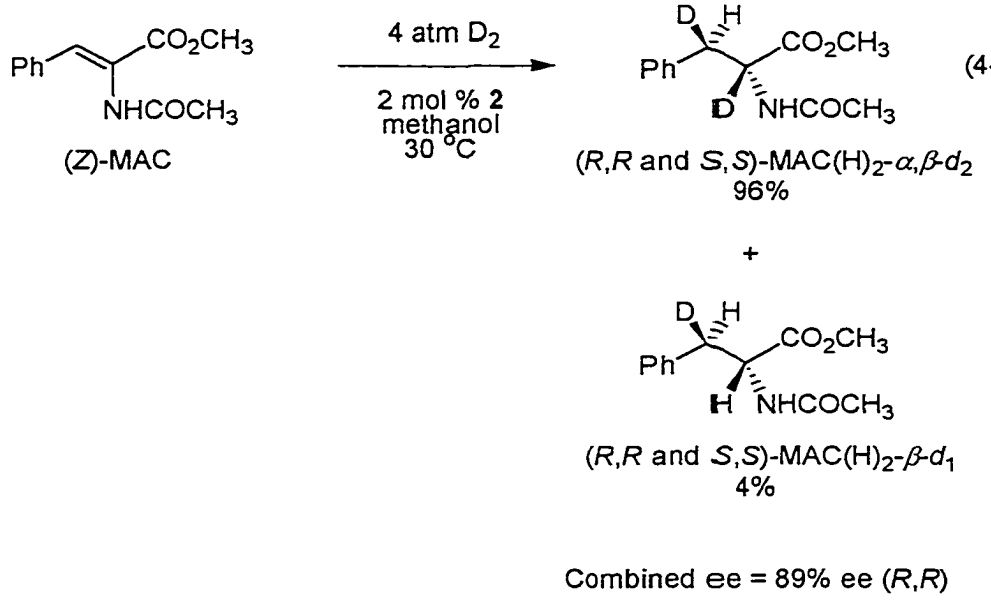

(4-8)

α,β-d_2, 96%; and (*R,R* and *S,S*)-MAC(H)$_2$-β-d_1, 4% (combined ee = 89% (*R,R*)). The low percentage of MAC(H)$_2$ with hydrogen at the α-position shows that solvolysis of the ruthenium–carbon bond is *not* a major pathway of the catalytic hydrogenation in methanol. The 96% relative abundance of (*R,R* and *S,S*)-MAC(H)$_2$-α,β-d_2 also shows that little H–D

exchange occurs between nitrogen and the α-and β-carbon centers during the catalytic hydrogenation. This is evidence against involvement of an amido-allyl (**5** or **5'**; Scheme 4-5) or a related species. Although the catalyst does effect H–D exchange between dideuterium gas and the N–H group of MAC(H)$_2$ and (by extension) likely of (*Z*)-MAC, any deuterium substitution at nitrogen that arose from such a process would immediately H–D exchange with the methanol solvent, effectively maintaining a proton at nitrogen throughout the catalytic hydrogenation.

The stoichiometric hydrogenolysis of ($S_{C\alpha}$)-**1** slowed as the reaction proceeded in acetone (eq 4-2), but went to completion in methanol. In methanol solvent, the rate of the stoichiometric hydrogenolysis was similar to the TOF of the catalytic hydrogenation.[6] The stoichiometric deuteration of ($S_{C\alpha}$)-**1** was carried out in methanol (eq 4-9) to investigate the origins of this discrepancy in behavior between acetone and methanol solvents. Figure

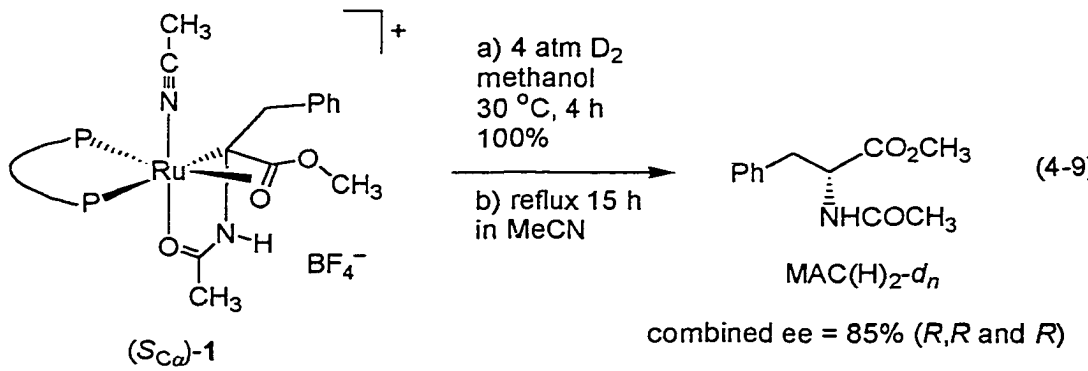

(4-9)

4-4 shows the distribution of organic products from the stoichiometric deuteriolysis of ($S_{C\alpha}$)-**1** in methanol ((*R*,*R* and *S*,*S*)-MAC(H)$_2$-α,β-d_2, 58%; MAC(H)$_2$-α-d_1, 5%; (*R*,*R* and *S*,*S*)-MAC(H)$_2$-β-d_1, 16%; and MAC(H)$_2$, 21%). The combined ee was 85% (*R*,*R* and *R*), which was similar to the catalytic hydrogenation in methanol (87% (*R*)). Only the *R*,*R* and *S*,*S* diastereomers of MAC(H)$_2$-α,β-d_2 were detected, showing that β-elimination within ($S_{C\alpha}$)-**1** proceeds by the same stereoselectivity as that observed in acetone. The ratio of (*R*,*R* and *S*,*S*)-MAC(H)$_2$-α,β-d_2 to MAC(H)$_2$-α-d_1 (ca. 12:1) also indicates that the reversible formation of ($S_{C\alpha}$)-**1** was faster than deuteriolysis of the ruthenium–carbon bond. The MAC(H)$_2$ (21%) and (*R*,*R* and *S*,*S*)-MAC(H)$_2$-β-d_1 (16%) resulted from

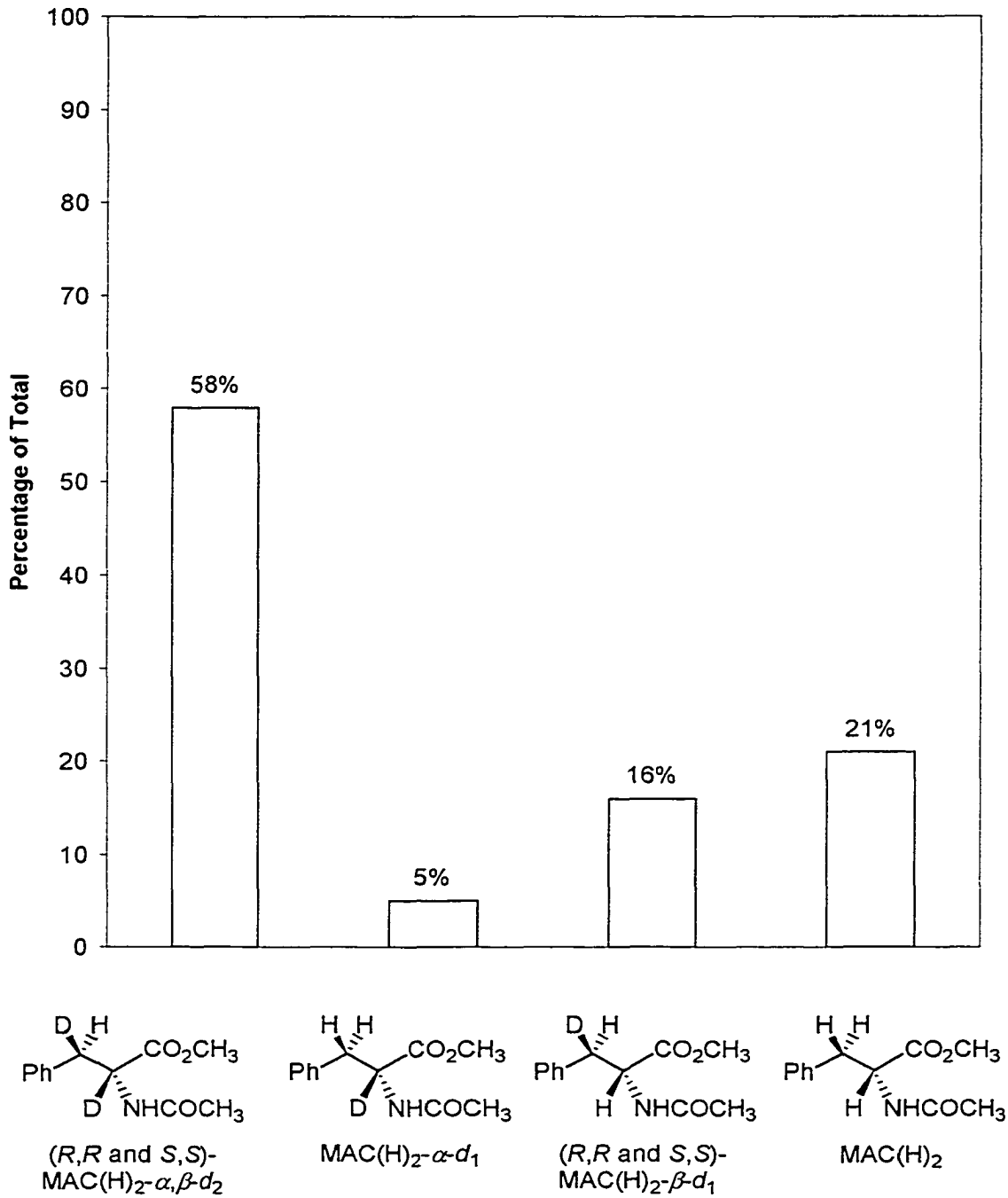

Figure 4-4. The distribution of MAC(H)$_2$-d_n isotopomers from the deuteriolysis of ($S_{C\alpha}$)-**1** in methanol.

solvolysis of the ruthenium–carbon bond in ($S_{C\alpha}$)-**1** and in ($S_{C\alpha}$,$R_{C\beta}$)-β-d_1-**1**, respectively. The total amount of MAC(H)$_2$ and (R,R and S,S)-MAC(H)$_2$-β-d_1 (37%) is likely a direct indication of the amount of solvolysis that occurred under these conditions because control experiments show that **2** does not catalyze the H–D exchange between dideuterium gas and methanol at an appreciable rate. At this stage, it is concluded that the similarity of rates for the stoichiometric hydrogenolysis in methanol and for the catalytic hydrogenation in methanol is coincidental, and is not of mechanistic significance.

Unlike the reaction in acetone solution, the stoichiometric hydrogenolysis of ($S_{C\alpha}$)-**1** in methanol solution was not significantly inhibited even by the addition of a 20-fold excess of MeCN. The reasons why the stoichiometric hydrogenation of ($S_{C\alpha}$)-**1** is not appreciably inhibited by MeCN in methanol solution likely relate to the ability of ($S_{C\alpha}$)-**1** to undergo solvolysis in methanol to generate MAC(H)$_2$. As solvolysis likely proceeds by protonation of the ruthenium center in ($S_{C\alpha}$)-**1**, it is not significantly inhibited by MeCN because protonation of a metal center does not require a vacant coordination site.[24] Whatever their origins, the relative susceptibilities of the stoichiometric hydrogenolysis of ($S_{C\alpha}$)-**1** to inhibition by MeCN in acetone and in methanol solution do not appreciably influence the catalytic hydrogenation as the TOF is higher in acetone than in methanol, at least 980 turnovers can be achieved in acetone, and the catalytic hydrogenation in methanol solution *does not* proceed via solvolysis of a ruthenium–carbon bond.

Conclusions

This work is the first mechanistic study of a ruthenium–BINAP-catalyzed hydrogenation to be complimented by a solid-state structure of a possible intermediate with a prochiral substrate group bonded to ruthenium. It is concluded from the results of this study that the stereoselectivities and the regioselectivities of the rapid and reversible formation of ($S_{C\alpha}$)-**1** and its conversion to MAC(H)$_2$ (via irreversible hydrogenolysis of the ruthenium–carbon bond) summate to give the stereoselectivity and regioselectivity of the catalytic hydrogenation. It is also concluded that solvolysis of the ruthenium–carbon bond

is a minor (<4%) pathway of the catalytic hydrogenation in methanol solvent, and that the presence of MeCN in the system does not contribute to the enantioselection of the catalytic reaction. Although ($S_{C\alpha}$)-**1** is the only detectable species in solution during the catalytic reaction at room temperature, the data from this study do not distinguish between whether ($S_{C\alpha}$)-**1** is a catalytic intermediate or a species in equilibrium with the true catalytic intermediate. Further, a direct comparison between the stoichiometric and catalytic rate data are complicated by both the accumulation of MeCN that occurs in solution during the stoichiometric hydrogenolysis, and the ability of ($S_{C\alpha}$)-**1** to undergo solvolysis in methanol. Both of these processes do not occur during the catalytic hydrogenation. A kinetic study to investigate these issues is underway in this laboratory.

Experimental Section

Materials. Gases and solvents were purified as outlined in Chapter 2. (*Z*)-Methyl-4-benzaloxazolone,[25] (*E*)-MAC,[26] [Ru((*R*)-BINAP)(1–3:5,6-η-C_8H_{11})(MeCN)]-BF_4,[7] ($S_{C\alpha}$)-**1**,[6] [Ru((*R*)-BINAP)(H)(η^6-(*rac*)-MAC(H)$_2$)]BF_4,[6] and [Ru((*R*)-BINAP)(H)-(η^6-(*S*)-MAC(H)$_2$)]BF_4[6] were prepared using established procedures. (*Z*)-MAC, (*rac*)-MAC(H)$_2$, and (*S*)-MAC(H)$_2$ were obtained by methods described in Chapter 2. Florisil (60–100 mesh) was supplied by Fisher Scientific.

Measurements. All instrumentation used were as described in Chapter 2 unless stated otherwise. ^{2}H NMR spectra were recorded using a Bruker AM-400 spectrometer operating at 61.4 MHz. The chemical shifts for ^{2}H are reported in parts per million (δ) relative to external tetramethylsilane and were referenced to signals of the residual deuterium in the protiated solvent. Electron-impact high-resolution mass spectra (HRMS (EI)) of organic compounds were recorded on a Kratos MS50 spectrometer.

Syntheses. All techniques used were as described in Chapter 2.

(A) (*Z*)-MAC-CO_2CD_3. A 1 M sodium methoxide-d_3 solution (prepared from sodium (73.8 mg, 3.21 mmol) and methanol-d_4 (3 mL)) was added to a stirred suspension of (*Z*)-methyl-4-benzaloxazolone (459.7 mg, 2.46 mmol) in benzene (5 mL) at room

temperature. The resulting pale yellow solution was allowed to stir for 5 min, after which the solution was acidified with aqueous 0.1 M hydrochloric acid. The slightly opaque benzene layer was extracted with methylene chloride (3 × 10 mL) and washed with water (3 × 20 mL). The organic layer was dried over anhydrous magnesium sulfate, filtered, and evaporated to give a white solid. Yield: 226.4 mg (41%). ^{1}H NMR (400.1 MHz, $CDCl_3$, 50 °C): δ 2.00 (br s, 3H, NHCOC*H*$_3$), 7.30 (m, 5H), 7.45 (br s, 2H). ^{2}H{^{1}H} NMR (61.4 MHz, $CDCl_3$, 50 °C): δ 3.80 (s, CO_2CD_3). ^{13}C{^{1}H} NMR (100.6 MHz, $CDCl_3$, 50 °C): δ 22.8 (br s, NHCO*C*H$_3$), 124.9 (quaternary), 128.5 (methine), 129.4 (methine), 129.7 (methine), 132.5 (br s, methine), 133.7 (quaternary), 165.9 (*C*O$_2$CH$_3$), 169.4 (br s, NH*C*OCH$_3$). The methoxy ^{13}C resonance appears at δ 52.4 ppm for (*Z*)-MAC. HRMS (EI): *m/z* 222.1083 (M^+, exact mass calcd for $C_{12}H_{10}D_3NO_3$ 222.1084). Anal. Calcd for $C_{12}H_{13}NO_3$: C, 65.74; H, 5.98; N, 6.39. Found: C, 65.39; H, 5.93, N, 6.19.

General Procedure for Catalytic Hydrogenations. The apparatus and procedures used, including identification, purification, and determination of the ee and absolute configuration of the product (MAC(H)$_2$), were as described in Chapter 2 for the hydrogenation of (*Z*)-MAC. Catalytic hydrogenations were, typically, allowed to react for 48 h to ensure complete conversion of (*Z*)-MAC to MAC(H)$_2$.

General Procedure for Catalytic Deuterations. Reactions were performed in a manner similar to that described for catalytic hydrogenations with the following exceptions: (1) the catalyst and substrate were dissolved in the appropriate solvent under an atmosphere of argon gas and subjected to 3 freeze–pump–thaw cycles prior to backfilling with dideuterium gas to the desired levels; and (2) the reactions were initially stirred under dynamic pressure (15 min), followed by static pressure for the remainder of the reaction. The relative proportions of isotopomers in the product mixture were determined via NMR spectroscopy and HRMS (EI). The ABX spin system in the ^{1}H NMR spectrum for the α- and β-protons of MAC(H)$_2$ were assigned by comparison to the reported assignments established for *N*-acetylphenylalanine, the acid analog of MAC(H)$_2$ (Figure 4-5).[3h] Each isotopomer was quantified by integrating the signals of the protons, using the methoxy signal as an internal standard. The amount of deuterium substitution at each position was obtained from ^{2}H{^{1}H} NMR spectra or deduced from the proton signals

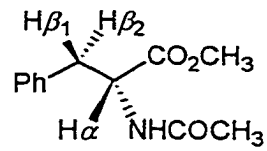

Figure 4-5. Designations used for the ABX spin system in the ^{1}H NMR spectrum of MAC(H)$_2$.

in the ^{1}H{^{2}H} NMR spectrum by subtraction if the signals in the ^{2}H{^{1}H} NMR spectrum overlapped and could not be deconvoluted. The presence of MAC(H)$_2$-d_n (n = 0–3) was confirmed by the parent ion peaks in the mass spectrum. Of the eight possible isotopomers of MAC(H)$_2$-d_n (n = 0–3), only seven were observed during the course of this investigation (MAC(H)$_2$, (*R*,*R* and *S*,*S*)-MAC(H)$_2$-β-d_1, MAC(H)$_2$-α-d_1, MAC(H)$_2$-β,β-d_2 , (*R*,*S* and *S*,*R*)-MAC(H)$_2$-α,β-d_2, (*R*,*R* and *S*,*S*)-MAC(H)$_2$-α,β-d_2, and MAC(H)$_2$-α,β,β-d_3). Of these seven isotopomers, six were identified and quantified by their ^{1}H{^{2}H} NMR spectra. The seventh isotopomer, MAC(H)$_2$-β,β,β-d_3 was identified by HRMS (EI), and its relative amount was determined from the methoxy internal standard signal after subtracting the contributions from the other isotopomers. The ^{1}H{^{2}H} NMR spectrum of each isotopomer was in accord with line patterns predicted by substitution of the appropriate proton(s) by deuteron(s) in the assigned ABX system of MAC(H)$_2$. For example, (*R*,*R* and *S*,*S*)-MAC(H)$_2$-α,β-d_2 was idenified by its proton signal (δ 3.03 (s, 1H, Hβ_2)) which showed the absence of coupling to other protons and which was shifted slightly upfield from the Hβ_2 signal for nondeuterated MAC(H)$_2$.[27] Similarly, (*R*,*R* and *S*,*S*)-MAC(H)$_2$-β-d_1 was identified by its proton signals (δ 3.03 (d, $^3J_{H\alpha-H\beta_2}$ = 6.0 Hz, 1H, Hβ_2) and δ 4.85 (dd, $^3J_{H\alpha-H(NH)}$ = 8.0 Hz, $^3J_{H\alpha-H\beta_2}$ = 6.0 Hz, 1H, Hα). The other isotopomers were identified in the same manner. Identifications were confirmed by ^{1}H{^{2}H, broad band; ^{1}H, selective} NMR experiments. The combined ee and absolute configuration of the products for each mixture of isotopomers was determined using the aforementioned procedure. NMR spectroscopic data for MAC(H)$_2$: ^{1}H (400.1 MHz, CDCl$_3$, 25 °C): δ 1.93 (s, 3H, NHCOC*H*$_3$), 3.03 (dd, $^2J_{H\beta_1-H\beta_2}$ = 14.0 Hz, $^3J_{H\alpha-H\beta_2}$ = 6.0

Hz, 1H, Hβ_2), 3.11 (dd, $^2J_{H\beta_1-H\beta_2}$ = 14.0 Hz, $^3J_{H\alpha-H\beta_1}$ = 6.0 Hz, 1H, Hβ_1), 3.68 (s, 3H, CO_2CH_3), 4.85 (d of apparent t, $^3J_{H\alpha-H(NH)}$ = 8.0 Hz, $^3J_{H\alpha-H\beta_1}$ = $^3J_{H\alpha-H\beta_2}$ = 6.0 Hz, 1H, Hα), 6.27 (br d, N*H*COCH$_3$), 7.08 (d, $^3J_{H-H}$ = 7.0 Hz, 2H, *o*-C$_6$*H*$_5$), 7.24 (m, 3H, *m*- and *p*-C$_6$*H*$_5$). $^{13}C\{^1H\}$ (100.6 MHz, $CDCl_3$, 25 °C): δ 22.8 (NHCO*C*H$_3$), 37.6 (*C*H$_2$CH, Cβ), 52.1 (CO$_2$*C*H$_3$), 53.1 (CH$_2$*C*H, Cα), 126.9 (*C*$_6$H$_5$), 128.4 (*C*$_6$H$_5$), 129.0 (*C*$_6$H$_5$), 135.9 (*i*-*C*$_6$H$_5$), 169.7 (NH*C*OCH$_3$), 172.1 (*C*O$_2$CH$_3$).

General Procedure for Hydrogenolysis and Deuteriolysis of ($S_{C\alpha}$)-1. Reactions were performed in a manner analogous to that described above for catalytic hydrogenations and deuterations with the exception that the concentrations of ($S_{C\alpha}$)-**1** were 10 mM. Typical reaction times were 4 h (in methanol) and 24 h (in acetone), after which time all volatile components were removed under reduced pressure. The remaining residue was refluxed in MeCN under an atmosphere of argon gas overnight (ca. 15 h), followed by evaporation under reduced pressure. The solid residue was washed with ethyl acetate and the solution was passed through a column of Florisil to remove residual ruthenium–BINAP species. Removal of the solvent on a rotary evaporator yielded pure MAC(H)$_2$, which was analyzed without further purification. The ee's of the products and their distributions of deuterium were determined using the aforementioned procedures.

Substrate Equilibrium with ($S_{C\alpha}$)-1. In a 5-mm NMR tube, (*Z*)-MAC-CO$_2$CD$_3$ (5.8 mg, 2.6 × 10^{-5} mol) and ($S_{C\alpha}$)-**1** (9.9 mg, 9.2 × 10^{-6} mol) were dissolved in a mixture of CD_2Cl_2 (0.1 mL, used to ensure complete dissolution of ($S_{C\alpha}$)-**1**) and acetone-d_6 (0.5 mL). The sample was immediately placed in a thermostated NMR probe (T = 35 °C) and monitored by ^{1}H NMR spectroscopy. The extent of the reaction was determined by the ratio of the methoxy signals of ($S_{C\alpha}$)-**1** and (*Z*)-MAC (singlets at δ 4.0 and δ 3.8, respectively), using a benzylic proton of ($S_{C\alpha}$)-**1** as internal standard (doublet at δ 4.2). $^{31}P\{^1H\}$ NMR spectroscopy indicated that the only ruthenium species present in the reaction mixture was ($S_{C\alpha}$)-**1** and ($S_{C\alpha}$)-**1**-CO$_2$CD$_3$.

References and Notes

(1) For reviews, see: (a) Ratovelomanana-Vidal, V; Genêt, J. -P. *J. Organomet. Chem.* **1998**, *567*, 163–171. (b) Genêt, J. P. In *Reductions in Organic Synthesis: Recent Advances and Practical Applications*; Abdel-Magid, A. F., Ed.; ACS Symposium Series 641; American Chemical Society: Washington, DC, 1996; Chapter 2. (c) Ager, D. J.; Laneman, S. A. *Tetrahedron: Asymmetry* **1997**, *8*, 3327–3355. (d) Noyori, R. *Acta Chem. Scand.* **1996**, *50*, 380–390. (e) Kumobayashi, H. *Recl. Trav. Chim. Pays-Bas* **1996**, *115*, 201–210. (f) Akutagawa, S. *Applied Catalysis A: General* **1995**, *128*, 171–207. (g) Noyori, R. *Asymmetric Catalysis in Organic Synthesis*; Wiley: New York, 1994. (h) Noyori, R. *Tetrahedron* **1994**, *50*, 4259–4292. (i) Takaya, H.; Ohta, T.; Noyori, R. In *Catalytic Asymmetric Synthesis*; Ojima, I., Ed.; VCH: New York, 1993; Chapter 1. (j) Takaya, H.; Ohta, T.; Mashima, K. In *Homogeneous Transition Metal Catalyzed Reactions*; Moser, W. R., Slocum, D. W., Eds.; Advances in Chemistry Series 230; American Chemical Society: Washington, DC, 1992; Chapter 8. (k) Noyori, R. *CHEMTECH* **1992**, *22*, 360–367. (l) Noyori, R. In *Organic Synthesis in Japan Past, Present, and Future*; Noyori, R., Ed.; Tokyo Kagaku Dozin: Tokyo, 1992; pp 301–307. (m) Noyori, R. *Science* **1990**, *248*, 1194–1199. (n) Noyori, R.; Takaya, H. *Acc. Chem. Res.* **1990**, *23*, 345–350. (o) Noyori, R. *Chem. Soc. Rev.* **1989**, *18*, 187–208. (p) Noyori, R.; Kitamura, M. In *Modern Synthetic Methods 1989*; Scheffold, R., Ed.; Springer–Verlag: Berlin, 1989; pp 115–198. For recent examples see: (q) Doucet, H.; Ohkuma, T.; Murata, K.; Yokozawa, T.; Kozawa, M.; Katayama, E.; England, A. F.; Ikariya, T.; Noyori, R. *Angew. Chem., Int. Ed. Engl.* **1998**, *37*, 1703–1707. (r) Ohkuma, T.; Koizumi, M.; Doucet, H.; Pham, T.; Kozawa, M.; Murata, K.; Katayama, E.; Yokozawa, T.; Ikariya, T.; Noyori, R. *J. Am. Chem. Soc.* **1998**, *120*, 13529–13530.

(2) For representative examples of mechanistic investigations of hydrogenations catalyzed by ruthenium–BINAP complexes, see: (a) Shaharuzzaman, M.; Braddock-Wilking, J.; Chickos, J. S.; Tam, C, N,; Silva, R. A. G. D.; Keiderling, T. A. *Terahedron: Asymmetry* **1998**, *9*, 1111–1114. (b) Chen, C.-C.; Huang, T.-T.; Lin, C.-W.; Cao, R.; Chan, A. S. C.; Wong, W. T. *Inorg. Chim. Acta* **1998**, *270*, 247–251. (c) Chan, A. S. C.;

Chen, C. C.; Yang, T. K.; Huang, J. H.; Lin, Y. C. *Inorg. Chim. Acta* **1995**, *234*, 95–100. (d) Brown, J. M.; Rose, M.; Knight, F. I.; Wienand, A. *Recl. Trav. Chim. Pays-Bas* **1995**, *114*, 242–251. (e) Brown, J. M. *Chem. Soc. Rev.* **1993**, 25–41. (f) Chan, A. S. C.; Laneman, S. A.; Miller, R. E. In *Selectivity in Catalysis*; Davis, M. E., Suib, S. L., Eds.; ACS Symposium Series 517; American Chemical Society: Washington, DC, 1993; Chapter 2. (g) Kawano, H.; Ikariya, T.; Ishii, Y.; Saburi, M.; Yoshikawa, S.; Uchida, Y.; Kumobayashi, H. *J. Chem. Soc., Perkin Trans. 1* **1989**, 1571–1575.

(3) The mechanism for the enantioselective hydrogenation of (*Z*)-MAC catalyzed by rhodium–bis(phosphine) complexes is well documented: (a) Giovannetti, J. S.; Kelly, C. M.; Landis, C. R. *J. Am. Chem. Soc.* **1993**, *115*, 4040–4057. (b) Landis, C. R.; Halpern, J. *J. Am. Chem. Soc.* **1987**, *109*, 1746–1754. (c) Brown, J. M.; Chaloner, P. A.; Morris, G. A. *J. Chem. Soc., Perkin Trans. 2* **1987**, 1583–1588. (d) Halpern, J. *Science* **1982**, *217*, 401–407. (e) Brown, J. M.; Chaloner, P. A. *J. Am. Chem. Soc.* **1980**, *102*, 3040–3048. For enantioselective reductions of α-aminoacrylic acid derivatives by dideuterium gas catalyzed by rhodium–bis(phosphine) complexes, see: (f) Burk, M. J.; Feaster, J. E.; Nugent, W. A.; Harlow, R. L. *J. Am. Chem. Soc.* **1993**, *115*, 10125–10138. (g) Scott, J. W.; Keith, D. D.; Nix, G., Jr.; Parrish, D. R.; Remington, S.; Roth, G. P.; Townsend, J. M.; Valentine, D., Jr.; Yang, R. *J. Org. Chem.* **1981**, *46*, 5086–5093. (h) Detellier, C.; Gelbard, G.; Kagan, H. B. *J. Am. Chem. Soc.* **1978**, *100*, 7556–7561. (i) Koenig, K. E.; Knowles, W. S. *J. Am. Chem. Soc.* **1978**, *100*, 7561–7564.

(4) (a) King, S. A.; DiMichele, L. In *Catalysis of Organic Reactions*; Scaros, M. G., Prunier, M. L., Eds.; Marcel Dekker: New York, 1995; Vol. 62, pp 157–165. (b) Saburi, M.; Takeuchi, H.; Ogasawara, M.; Tsukahara, T. Ishii, Y.; Ikariya, T.; Takahashi, T.; Uchida, Y. *J. Organomet. Chem.* **1992**, *428*, 155–167. (c) Ohta, T.; Takaya, H.; Noyori, R. *Tetrahedron Lett.* **1990**, *31*, 7189–7192.

(5) (a) Ashby, M. T.; Khan, M. A.; Halpern, J. *Organometallics* **1991**, *10*, 2011–2015. (b) Ashby, M. T.; Halpern, J. *J. Am. Chem. Soc.* **1991**, *113*, 589–594.

(6) Wiles, J. A.; Bergens, S. H.; Young, V. G. *J. Am. Chem. Soc.* **1997**, *119*, 2940–2941.

(7) Complex **2** is a well-defined catalyst system for a variety of transformations, including the hydrogenation of olefins: Wiles, J. A.; Lee, C. E.; McDonald, R.; Bergens, S. H. *Organometallics* **1996**, *15*, 3782–3784.

(8) These TOFs were determined by setting up and taking down the pressure reactor as quickly as possible during a hydrogenation. Their values are therefore to be taken as approximate. Reaction conditions: 2 mol % **2**; [**2**] = 2.6 mM; stir rate = 1100 rpm; $T = 30$ °C; pressure of dihydrogen gas = 4 atm.

(9) All reactions were carried out under reaction-rate-limiting conditions to eliminate gas–liquid mass-transfer effects. For a study describing gas–liquid mass transfer affecting enantioselectivity, see: Sun, Y.; Landau, R. N.; Wang, J.; LeBlond, C.; Blackmond, D. G. *J. Am. Chem. Soc.* **1996**, *118*, 1348–1353.

(10) The differences between the conditions under which the spectrum was recorded and the optimum conditions for the catalytic hydrogenation resulted from the technical difficulties in carrying out such a reaction in a typical NMR tube.

(11) A small amount (ca. 8%) of one other species was detected in the $^{31}P\{^1H\}$ NMR spectrum of the catalytic mixture recorded after cooling to –40 °C ($^{31}P\{^1H\}$ NMR ($(CD_3)_2CO$, 161.9 MHz): δ 39.4 (d, $^2J_{P-P}$ = 23.5 Hz, 1P), 55.4 (d, $^2J_{P-P}$ = 23.5 Hz, 1P)). This species is present in similar amounts in the $^{31}P\{^1H\}$ NMR spectrum recorded at –40 °C of isolated and purified ($S_{C\alpha}$)-**1**. It is likely that this species is the opposite diastereomer (($R_{C\alpha}$)-**1**) in equilibrium with ($S_{C\alpha}$)-**1**. See Chapter 2 (Experimental Section) for ^{13}C and ^{15}N NMR spectroscopic data.

(12) Complex ($S_{C\alpha}$)-**1** typically comprised 80–90% of the ruthenium-containing species in these solvents under these conditions. The other complexes present were mainly a mixture of [Ru((*R*)-BINAP)(H)(η^6-MAC(H)$_2$)]BF_4 and a species which is tentatively assigned as [Ru((*R*)-BINAP)(H)(η^6-(*Z*)-MAC)]BF_4. In these complexes, MAC(H)$_2$ and (*Z*)-MAC are bonded to ruthenium as η^6-arene ligands.

(13) These values were determined by ^1H NMR spectroscopy. Analysis of this mixture by $^{31}P\{^1H\}$ NMR spectroscopy confirmed the presence of ($S_{C\alpha}$)-**1** (35%), **3** (65%), and a number of unidentified species (quantities too low to accurately quantify).

These unidentified species are most likely decomposition products of **3** that generate uncoordinated $MAC(H)_2$.

(14) Joshi, A. M.; James, B. R. *Organometallics* **1990**, *9*, 199–205.

(15) No dissociation of MeCN from ($S_{C\alpha}$)-**1** was observed at room temperature.

(16) All isotope substitution patterns of $MAC(H)_2$-d_n were assigned by comparison of their ^1H and ^2H NMR spectra to those of *N*-acetylphenylalanine. See reference 3h and the Experimental Section for details.

(17) For all reductions with dideuterium gas in acetone, a portion of the product was deuterated at nitrogen. In general, there was an approximate correlation between the extent of deuteration at nitrogen and the length of time the reaction was exposed to dideuterium gas in the presence of **2**. Only an approximate correlation could be obtained because H–D exchange was rapid upon exposure to even trace amounts of water. Control experiments in which $MAC(H)_2$ was exposed to 2 mol % **2** under dideuterium gas in acetone showed that **2** catalyzes the H–D exchange between the N–H bond of $MAC(H)_2$ and dideuterium gas. Deuteration at nitrogen is most likely a side reaction which is not part of the hydrogenation mechanism of (*Z*)-MAC catalyzed by **2**.

(18) An NMR tube containing a –80 °C argon-saturated acetone solution of **2** was quickly ejected from a cooled (–80 °C) NMR probe, injected with an excess of dideuterium gas through a rubber septum, shaken for ca. 15 s, and quickly returned to the probe. NMR spectra recorded at –80 °C indicated **2**-*d* was the only ruthenium species formed in solution, with concomitant formation of HD gas.

(19) Miessler, G. L.; Tarr, D. A. *Inorganic Chemistry*; Prentice Hall: Englewood Cliffs, NJ, 1991; pp 397–398.

(20) Assuming for the sake of argument that β-hydride elimination did not occur during the deuteration of (*E*)-MAC, the absolute configuration of the $MAC(H)_2$-α,β,β-d_3 resulting from deuteration of (*E*)-MAC-β-d_1 would depend on the enantioselectivity of the catalyst toward (*E*)-MAC.

(21) (a) Bergens, S. H.; Noheda, P.; Whelan, J.; Bosnich, B. *J. Am. Chem. Soc.* **1992**, *114*, 2121–2128. (b) Bergens, S. H.; Noheda, P.; Whelan, J.; Bosnich, B. *J. Am. Chem. Soc.* **1992**, *114*, 2128–2135.

(22) Other explanations include reaction via the small amount of HD gas generated by reaction of **2** with D_2, and insertion of (Z)-MAC into the ruthenium–hydride bond of **2** via the opposite regiochemistry (with ruthenium at the β-olefinic carbon and hydrogen at the α-olefinic carbon) followed by deuteriolysis of the ruthenium–carbon bond. Reaction with HD gas cannot be ruled out, but it is unlikely because the HD gas generated by reaction of **2** with D_2 amounts to ca. 2% of the D_2 in the reactor, and because the concentration of **2** relative to **2**-*d* is probably quite low.

(23) Another possibility, which is not ruled out, is that the intrinsic face selectivity of the hydrogenation toward (*E*)-MAC and (*Z*)-MAC are the same.

(24) (a) Crabtree, R. H.; Quirk, J. M.; Fillebeen-Khan, T.; Morris, G. E. *J. Organomet. Chem.* **1979**, *181*, 203–212. (b) Ashworth, T. V.; Singleton, J. E.; de Waal, D. J. A.; Louw, W. J.; Singleton, E.; van der Stok, E. *J. Chem. Soc., Dalton Trans.* **1978**, 340–347. See also, electrophilic attack of $HgBr_2$ on $Cp^*Os(CO)(PMe_2Ph)Me$: Sanderson, L. J.; Baird, M. C. *J. Organomet. Chem.* **1986**, *307*, C1–C4.

(25) Herbst, R. M.; Shemin, D. In *Organic Syntheses*; Blatt, A. H., Ed.; Wiley: New York, 1943; Collect. Vol. 2, pp 1–3.

(26) Vineyard, B. D.; Knowles, W. S.; Sabacky, M. J.; Bachman, G. L.; Weinkauff, D. J. *J. Am. Chem. Soc.* **1977**, *99*, 5946–5952.

(27) The deuterium-induced isotope effects on ^1H nuclear shieldings were typically 8 ppb (β-upfield shift) and 10 ppb (α-upfield shift) per deuterium. For a review of isotope effects on chemical shifts, see: Hansen, P. E. In *Annual Reports on NMR Spectroscopy*; Webb, G. A., Ed.; Academic Press: London, 1983; Vol. 15, pp 105–234.

Chapter 5†

The First Structure Determination of a Diastereomeric Hydrido–Olefin Putative Intermediate in Catalytic Enantioselective Hydrogenation

Introduction

The hydrogenation of prochiral olefins is the most studied and developed enantioselective catalytic reaction to date.[1] Despite hundreds of publications describing these reactions, little is known about the true structures of their diastereomeric catalytic intermediates. For example, a recent report[2] from this research group described the first X-ray structure determination of a diastereomeric putative catalytic intermediate (a catalyst–alkyl complex) of the same absolute configuration as the hydrogenation product.[3,4] The complex, [Ru((*R*)-BINAP)((*S*)-MAC(H))(MeCN)]BF_4 (**1**), forms upon reaction (both during the catalytic hydrogenation and under stoichiometric conditions) between the substrate MAC and the catalyst [Ru((*R*)-BINAP)(H)$(MeCN)_n(sol)_{3-n}$]BF_4 (**2**; n = 0–3, sol = acetone, methanol, or THF, depending on reaction medium).[5] Complex **2** was designed for this mechanistic study because ruthenium is the most commonly used metal in enantioselective olefin hydrogenations, because BINAP is among the most commonly used ligands, and because MAC is the most commonly used (benchmark) substrate. In previous work on this system it was shown that formation of **1** is rapid and reversible and that **1** is the only detectable catalyst species in solution during the catalytic hydrogenation of MAC.[5a] Since the formation of **1** (product) is rapid and reversible under catalytic conditions, the Curtin–Hammett principle[6] dictates that the structure and abundance of **1** provides no information about the structure and abundance of the major diastereomeric olefin adduct ([Ru((*R*)-BINAP)(H)(MAC)(MeCN)]BF_4, reactant) formed

---

† Reproduced with permission from Wiles, J. A.; Bergens, S. H. *Organometallics* **1999**, *18*, 3709–3714. Copyright 1999 American Chemical Society.

by reaction of MAC with **2**. There are 20 diastereomers of this olefin–catalyst adduct in which the olefin and hydride occupy mutually cis coordination sites and in which MAC is bonded through the olefin and amide groups (there are more diastereomers if ester coordination is considered). It was therefore imperative to determine which of these diastereomers form in order to understand how the stereochemical forces evolve during the catalytic hydrogenation. This chapter describes low-temperature NMR experiments that determine the structure of the major olefin–catalyst adduct and that monitor the diastereomeric olefin–hydride insertion reaction to generate **1**.

Results and Discussion

Characterization of the Active Catalyst. The active catalyst **2** is generated by hydrogenation of the precursor [Ru((*R*)-BINAP)(1–3:5,6-η-C_8H_{11})(MeCN)]BF_4 (**3**) in acetone, methanol, or THF.[5] NMR spectra of **2** recorded at –40 °C in THF-d_8 show it exists as a mixture of [Ru((*R*)-BINAP)(H)(MeCN)(THF-d_8)$_2$]BF_4 (**4**), ca. 50%; [Ru((*R*)-BINAP)(H)(MeCN)$_2$(THF-d_8)]BF_4 (**5**), ca. 25%; and [Ru((*R*)-BINAP)(H)(THF-d_8)$_3$]BF_4 (**6**), ca. 25%.[7,8] These species were labeled with Me$C^{15}N$ by ligand exchange between the precursor **3** and Me$C^{15}N$. The magnitudes of $^2J_{P-H}$ (28–42 Hz) shows that the hydride occupies a coordination site cis to both phosphorus centers in **4**–**6**. $^2J_{P-N}$ was not observed in **4**-Me$C^{15}N$, while $^2J_{N-H}$ was (18.5 Hz), showing that the Me$C^{15}N$ and hydrido ligands occupied the mutually trans coordination sites cis to the phosphorus centers[9] (Scheme 5-1). A similar analysis of [Ru((*R*)-BINAP)(H)(Me$C^{15}N$)$_2$(THF-d_8)]BF_4 (**5**) shows that one Me$C^{15}N$ ligand was trans to the hydride and the other was cis to the hydride.[10] These complexes rapidly exchange MeCN and THF at room temperature. To determine which of **4**, **5**, or **6** is the active catalyst is a somewhat diffuse issue for three reasons: first, exchange of MeCN between these species at room temperature is rapid; second, it has been shown previously that removal of MeCN from the catalyst system has no effect on the ee of the catalytic hydrogenation; third, all the species in this mixture react

Scheme 5-1. Formation of the Olefin–Catalyst Adduct *si*-7 at Low Temperature and Its Conversion to 1

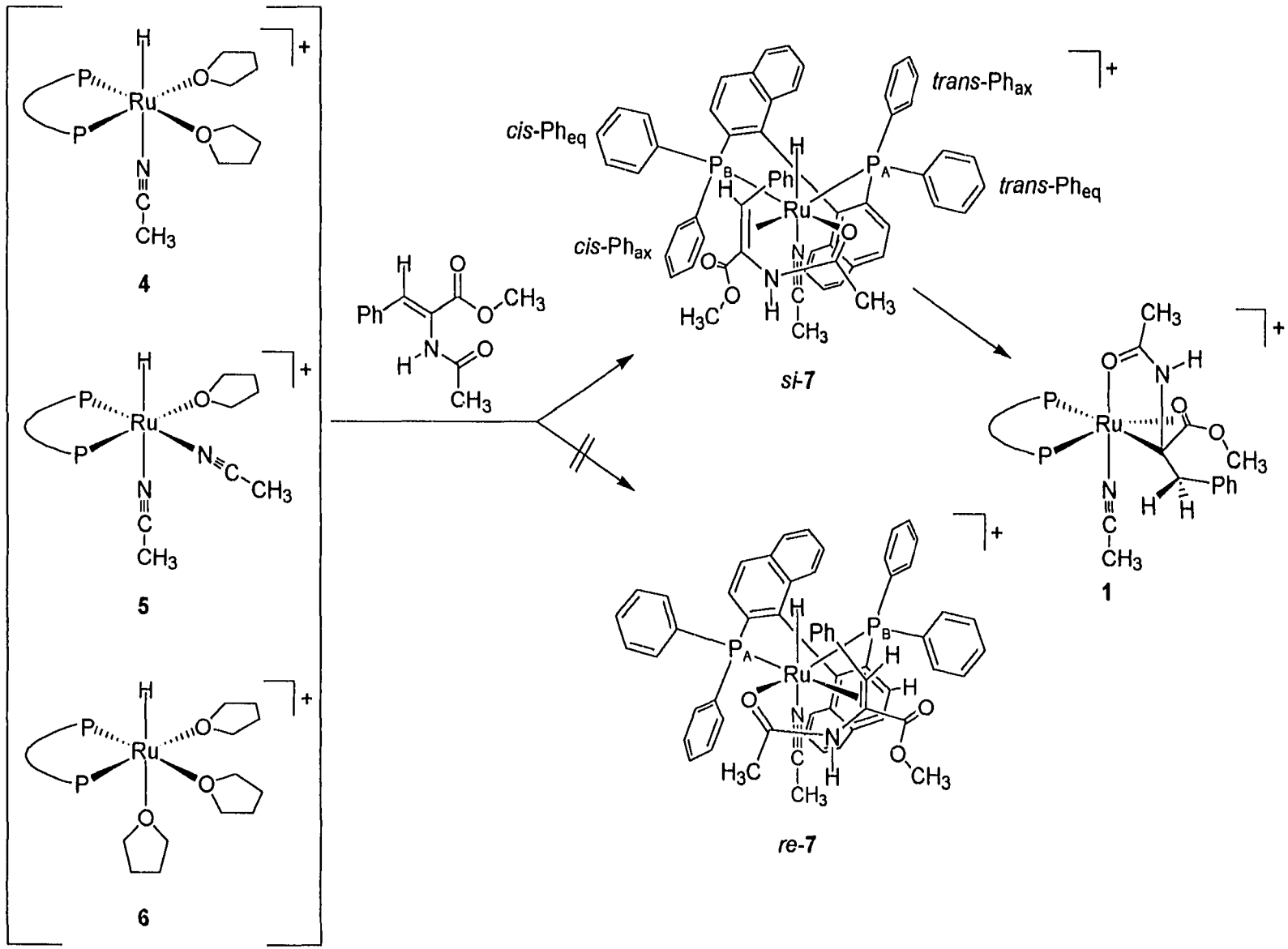

quickly with MAC at room temperature to quantitatively form the insertion product **1**.[2,5] Nevertheless, the active catalysts in this hydrogenation are likely **4** and **6** because **5** must dissociate one MeCN ligand to accommodate the bidentate substrate MAC. Further, stoichiometric reaction between **6** and MAC at room temperature forms the η^6-arene adduct [Ru((*R*)-BINAP)(H)(η^6-MAC)]BF_4, suggesting that the active catalyst is **4**. Regardless, the active catalyst will be referred to as **2** to accommodate these possibilities.

Interception and Characterization of a Transient Intermediate. Reaction of **2** with one equiv of MAC in THF-d_8 at –40 °C over 1 h forms the diastereomeric catalyst–olefin adduct [Ru((*R*)-BINAP)(H)(MAC)(MeCN)]BF_4 (**7**) as major product (Figure 5-1). The structure and absolute configuration of this complex was determined as follows. The phosphorus–hydride coupling constants ($^2J_{P_A-H}$ = 34.5 and $^2J_{P_B-H}$ = 21.5 Hz) show that the hydride is cis to both phosphorus centers in this complex. The magnitude of the nitrogen–hydride coupling constant ($^2J_{N-H(trans)}$ = 10.0 Hz) in the Me$C^{15}N$-labeled isotopomer of **7**, along with the absence of observable phosphorus–nitrogen coupling, shows that the hydrido and MeCN ligands are trans to one another and that they occupy coordination sites cis to both phosphorus centers. Labeling MAC with ^{13}C at the olefinic positions shows an upfield shift (versus uncoordinated MAC) and phosphorus–carbon coupling for each olefin carbon signal in the $^{13}C\{^1H\}$ NMR spectrum of **7** (Cβ (terminal): $\Delta\delta$ = –64.9, $J_{P_A-C(trans)}$ = 17.5 Hz; Cα (internal): $\Delta\delta$ = –46.4, $J_{P_A-C(trans)}$ = 3.5 Hz), confirming that the olefin group is bonded to ruthenium at a coordination site trans to one of the phosphorus centers (P_A) and cis to the other (P_B). Labeling the carbonyl carbon centers in MAC with ^{13}C shows a downfield shift and phosphorus–carbon coupling of the amide carbonyl signal ($\Delta\delta$ = +9.9, $J_{P_A-C} = J_{P_B-C}$ = 2.5 Hz), and a downfield shift ($\Delta\delta$ = +8.9) without observable phosphorus–carbon coupling for the ester carbonyl signal. MAC therefore acts as a bidentate ligand in **7** with the olefin and O-bonded amide groups occupying coordination sites on ruthenium trans to the phosphorus centers (Scheme 5-1). MAC commonly displays this bonding mode in rhodium and iridium complexes.[3,11]

The insertion product **1** resulted from addition of the hydrido ligand to Cβ (terminal olefin carbon) and addition of ruthenium to Cα of MAC with the *S* absolute configuration at the ruthenium-bonded carbon.[2] Apart from those structural features

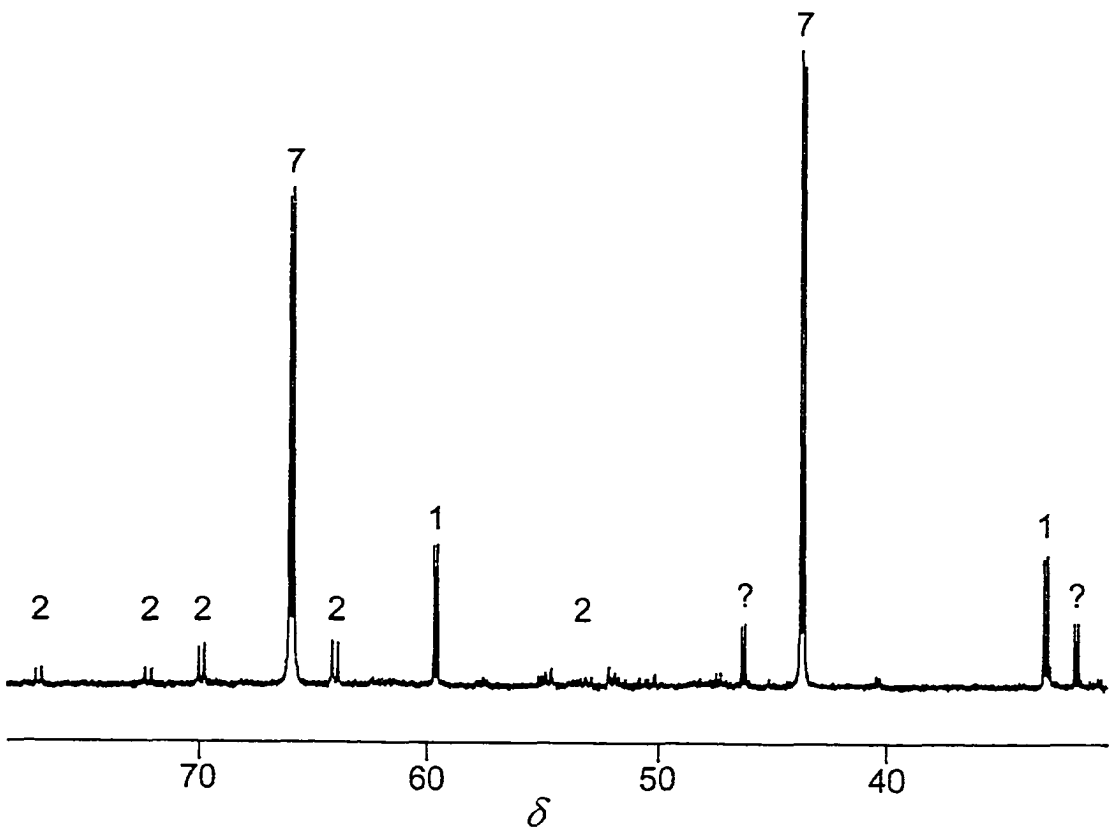

Figure 5-1. $^{31}P\{^{1}H\}$ NMR spectrum (161.9 MHz, THF-d_8, –40 °C) of a mixture containing **7** (75%), **1** (13%), and **2** (6%) recorded 1 h after mixing at –40 °C. A small quantity of an unidentified non-hydrido species (**?**; 6%) was also present in the mixture.

already established, two further conditions must be fulfilled for the olefin–catalyst adduct **7** to be an intermediate between the active catalyst **2** and the insertion product **1**. First, Cβ of MAC and the hydrido ligand must be on the same side of the ruthenium–bis(phosphine) plane. If not, the olefin–hydride insertion reaction in **7** would produce the opposite regiochemistry of **1**, with ruthenium at Cβ. This would rule out **7** as an intermediate between **2** and **1**. Second, the olefin group must be bonded to ruthenium through the *si* enantiotopic face (Scheme 5-1) for olefin–hydride insertion to lead to **1** (the absolute configuration at Cα of MAC(H) in **1** was crystallographically determined[2] as *S*). ^{1}H NOE difference spectra[12,13] at –40 °C showed that irradiation of the hydrido signal from **7** resulted in negative NOE (–3%) of the olefinic hydrogen (Hβ) signal,[14] confirming that the hydrido ligand and Cβ are on the same side of the ruthenium–bis(phosphine) plane. Scheme 5-1 shows the two possible structures of **7** which are consistent with these structural data. They are diastereomers that differ by which enantiotopic olefin face is coordinated to ruthenium and by which phosphorus center is cis to the coordinated olefin. In *si*-**7**, the substituents on the phosphorus center (P_B) cis to the coordinated olefin are disposed with the naphthalene (Nap) ring adjacent (on the same side of the ruthenium–bis(phosphine) plane) to Cβ and with the axial phenyl (*cis*-Ph_{ax}) group adjacent to the methoxy group of the ester (Scheme 5-1). In *re*-**7**, the substituents on the phosphorus center (P_B) cis to the coordinated olefin are disposed with the Ph_{ax} group adjacent to Cβ and with the Nap ring adjacent to the methoxy group of the ester. ^{1}H NMR signals from these groups did not overlap with others[15] and provided an unambiguous assignment of the structure as follows.

A ^{31}P–^{1}H HETCOR experiment, confirmed by selective ^{1}H{^{31}P} NMR experiments, showed that each phosphorus center is coupled to three ortho aromatic proton signals, one for each *o*-Ph and one the *o*-Nap ring (Figure 5-2). That the signals for the ortho protons on the phenyl rings are not separated shows that rotation around the phosphorus–phenyl bonds is rapid on the NMR timescale at –40 °C.[16] The signals for the phosphorus centers cis and trans to the coordinated olefin were assigned by ^{13}C labeling of MAC at the olefinic positions (vide supra). The cis phosphorus (P_B) was coupled to ortho protons at δ 8.22, 7.52, and 6.84. The trans phosphorus (P_A) was coupled to ortho

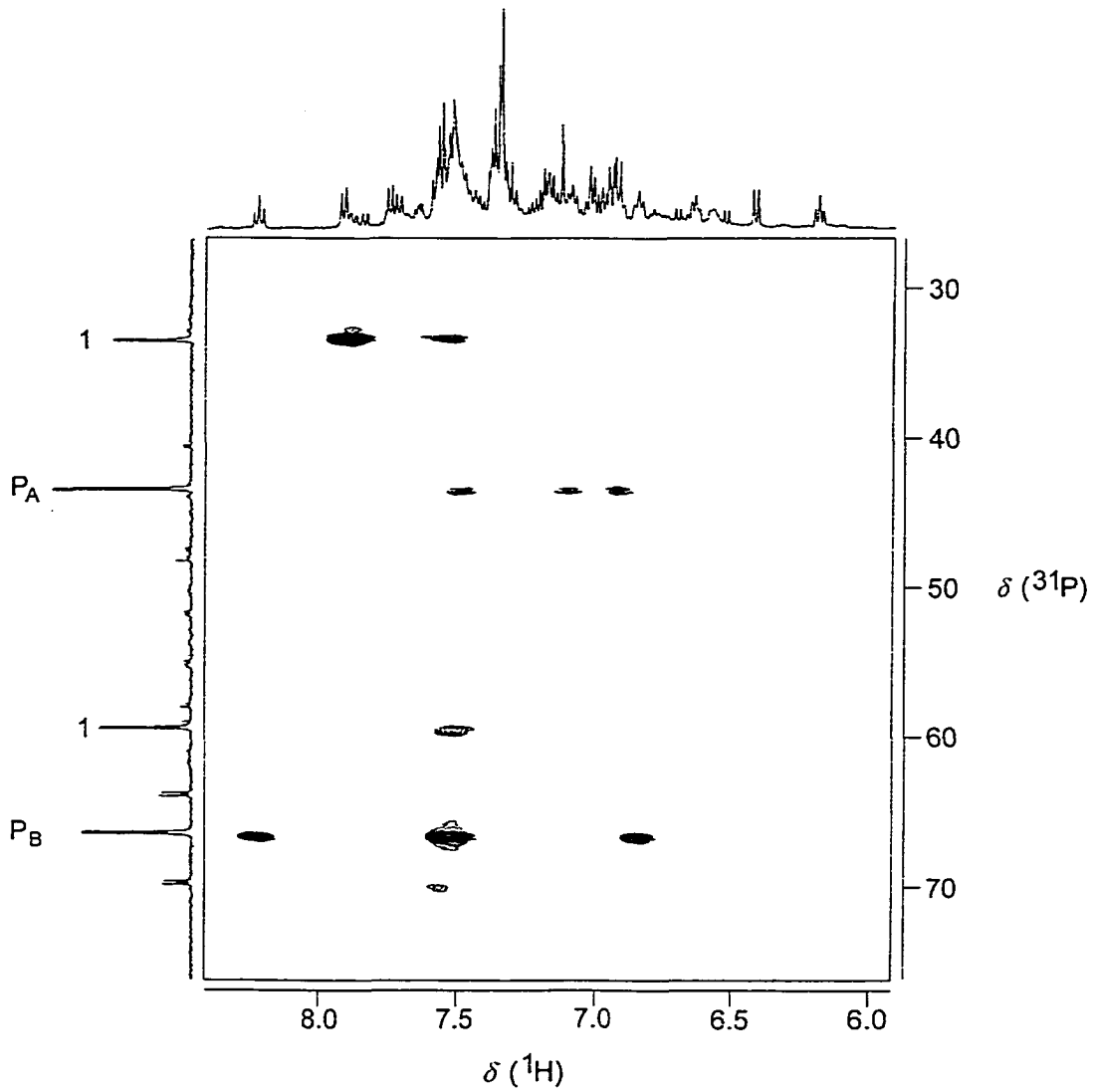

Figure 5-2. Section of the ^{31}P–^{1}H HETCOR NMR spectrum (499.8 MHz, THF-d_8/CD_2Cl_2 (2:1 v/v), –40 °C) of **7** showing three ortho-type protons associated with each ^{31}P resonance. The assignments for P_B are as follows (low field to high field): *o*-Nap, *o*-Ph_{eq}, and *o*-Ph_{ax}.

protons at δ 7.51, 7.10, and 6.92. The signal at δ 8.22 (t, $^3J_{P-H} = {}^3J_{H-H} = 8.5$ Hz) is from *o*-Nap on P_B (H_{Nap}). It is a one-proton signal (by comparison to the integrated intensity of Hβ), and it is coupled to a one-proton signal from the *m*-Nap proton (δ 7.91, d, $^3J_{H-H}$ = 8.5 Hz), which was determined by selective $^1H\{^1H\}$ and ^1H–^1H COSY NMR experiments. Irradiation of the H_{Nap} signal caused a –8% enhancement of the olefinic Hβ signal and a –4% enhancement of the hydrido signal, showing that the hydride, Hβ, and H_{Nap} are on the same side of the ruthenium–bis(phosphine) plane (Figure 5-3). Consistent with this assignment is that irradiation of the methoxy group caused –2% enhancement for the signal at δ 6.62 (t, $^3J_{H-H}$ = 8.0 Hz), which is ascribed to the para proton on the *cis*-Ph_{ax} group. The *cis*-Ph_{ax} ring is on the opposite side of the ruthenium–bis(phosphine) plane with regard to the *cis*-Nap ring. Irradiation of the H_{Nap} signal caused enhancement of *cis*-*o*-Ph_{eq} protons, but not *cis*-*o*-Ph_{ax} protons.

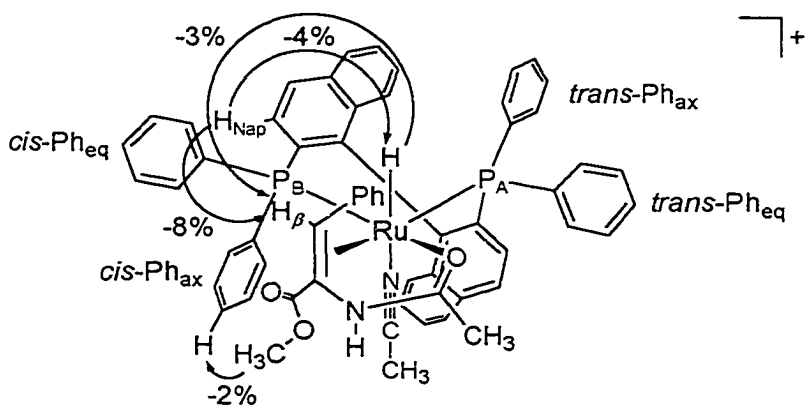

si-7

Figure 5-3. Observed NOE values that were used to determine the structure and absolute configuration of *si*-7.

These correlations are not possible in *re*-7 and therefore unambiguously show that MAC is coordinated by the *si*-olefin face in 7 with the correct regiochemistry for olefin–hydride insertion to form **1**. It is therefore concluded that *si*-7 is a diastereomeric intermediate between the active catalyst **2** and the insertion product **1**. Other correlations

could be found which affirm this structure assignment of *si*-7, but these are considered to be ambiguous because the proton signals involved were overlapped by other aromatic proton signals.

Preliminary kinetic investigations show *si*-7 undergoes first-order olefin–hydride insertion to directly form **1** ($k \approx 1.0 \times 10^{-4}$ s^{-1} at –20 °C) without detection of further intermediates by $^{31}P\{^{1}H\}$ NMR spectroscopy.

Conclusions

Despite that all enantioselective catalytic hydrogenations of olefins must involve diastereomeric hydrido–olefin intermediates, *si*-7 is the first example of such a putative intermediate to be observed and structurally characterized. Since the alkyl complex **1** (product) forms under Curtin–Hammett conditions during the catalytic hydrogenation, it was impossible before this study to predict the stereochemistries and the distribution of the hydrido–olefin diastereomers (reactant(s)) formed by reaction of the active catalyst **2** with MAC. That *si*-7 is the only olefin–catalyst adduct formed in detectable amounts, and that it *is* the immediate predecessor to **1** (of correct regio- and stereochemistry), allowed this direct structural and kinetic study of an olefin–hydride insertion reaction as part of a diastereomeric pathway for an enantioselective olefin hydrogenation. The most direct pathway for the observed first-order transformation of *si*-7 into **1** is olefin–hydride insertion (via hydride migration) followed by rotation around the Ru–Cα bond to result in coordination of the amide carbonyl trans to MeCN and the ester carbonyl trans to P_B. It is notable that *si*-7 and **1** are of the same absolute configuration as the major product enantiomer of the catalytic hydrogenation and that the sequence of reactions involving **2**, *si*-7, and **1** is the most detailed structural observation to date of a diastereomeric pathway in enantioselective catalytic hydrogenation (Scheme 5-2).

Scheme 5-2. Proposed Major Diastereomeric Pathway for the Enantioselective Hydrogenation of MAC Catalyzed by 2

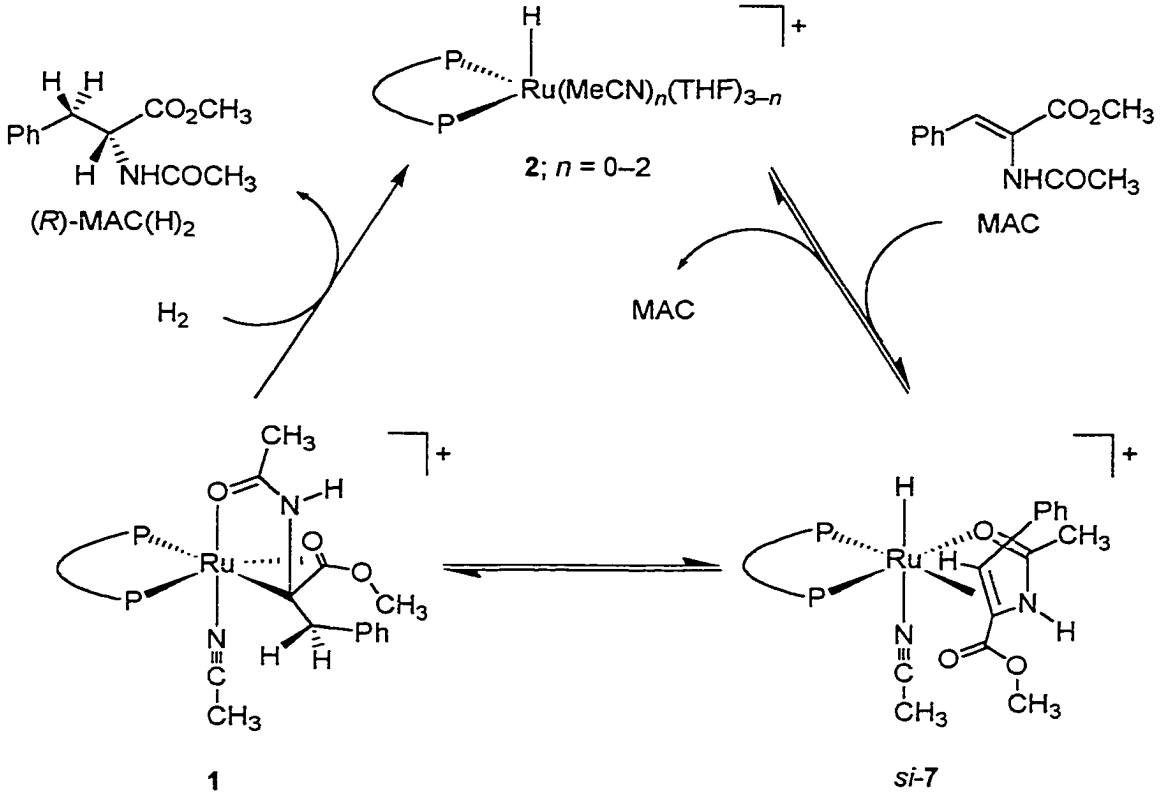

Experimental Section

Materials. Gases and solvents were purified as outlined in Chapter 2. All reagents were used as received from Aldrich unless stated otherwise. The synthesis of **3**-MeC^{15}N was accomplished using the method described in Chapter 2. Isotope-labeled derivatives of MAC were prepared via methanolysis[5a,17] of the corresponding oxazolones[18] using appropriately labeled glycine, benzaldehyde, and methanol as reagents. The exception was MAC-*1'*-^{13}*C*, which was prepared via methanolysis of the oxazolone derived from *N*-acetyl-*1'*-^{13}*C*-glycine (obtained via hydrolysis of ethyl *N*-acetyl-*1'*-^{13}*C*-glycinate) as outlined below.

Measurements. All instrumentation used were as described in Chapter 2 unless stated otherwise. ^{2}H and ^{19}F NMR spectra were recorded using a Bruker AM-400 spectrometer operating at 61.4 MHz and at 376.5 MHz, respectively. Two-dimensional NMR spectra were recorded using a Varian Unity 500 spectrometer (^{1}H at 499.8 MHz and ^{31}P at 202.4 MHz). The chemical shifts for ^{1}H and ^{2}H are reported in parts per million (δ) relative to external tetramethylsilane and were referenced to residual solvent signals. The chemical shifts for ^{19}F and ^{31}P are reported in parts per million (δ) relative to external trichlorofluoromethane and external 85% phosphoric acid, respectively. Electron-impact high-resolution mass spectra (HRMS (EI)) were recorded using a Kratos MS50 spectrometer.

Syntheses. All techniques used were as described in Chapter 2.

(A) Ethyl *N*-Acetyl-*1'*-^{13}*C*-glycinate. Triethylamine (7.1 mL, 0.051 mol) was added dropwise to a stirred suspension of glycine ethyl ester hydrochloride (3.55 g, 0.025 mol) in methylene chloride (150 mL) at -10 °C under an atmosphere of argon gas. The reaction mixture was stirred at –10 °C for 1 h, and then acetyl-*1*-^{13}*C* chloride (1.8 mL, 0.025 mol) was added dropwise. The resulting mixture was stirred at –10 °C for 1 h, and then it was allowed to warm to room temperature and to stir for an additional 1 h. The suspension was evaporated to dryness, and the product was extracted from the solid with benzene (200 mL). Yield after recystallization (benzene/*n*-pentane): 3.30 g (90%). ^{1}H NMR (400.1 MHz, $CDCl_3$, 25 °C): δ 1.28 (t, $^{3}J_{H-H}$ = 7.0 Hz, 3H, $CO_2CH_2CH_3$), 2.04 (d, $^{2}J_{C-H}$ = 6.0 Hz, 3H, CH_3CONH), 4.02 (dd, $^{3}J_{H-H}$ = 5.5 Hz, $^{3}J_{C-H}$ = 3.0 Hz, 2H, $NHCH_2CO_2$), 4.21 (q, $^{3}J_{H-H}$ = 7.0 Hz, 2H, $CO_2CH_2CH_3$), 6.09 (br, 1H, N*H*). $^{13}C\{^{1}H\}$ NMR (100.6 MHz, $CDCl_3$, 25 °C): δ 14.1 (s, $CO_2CH_2CH_3$), 22.9 (d, $^{1}J_{C-C}$ = 51.5 Hz, CH_3CONH), 41.4 (s, $NHCH_2CO_2$), 61.5 (s, $CO_2CH_2CH_3$), 170.2 (s, CH_3CONH), 170.5 (s, $CO_2CH_2CH_3$). HRMS (EI): *m/z* 146.0772 (M^+, exact mass calcd for $C_5{}^{13}CH_{11}NO_3$ 146.0773).

(B) *N*-Acetyl-*1'*-^{13}*C*-glycine. Concentrated hydrochloric acid (1 mL) was added to a stirred solution of ethyl *N*-acetyl-*1'*-^{13}*C*-glycinate (3.10 g, 0.021 mol) in water (50 mL). The resulting solution was heated (75 °C) with stirring for 16.5 h, and then evaporated to dryness to give a white solid. The solid was washed with dry THF (100

mL), yielding 2.40 g of a mixture containing 67% *N*-acetyl-*1'*-^{13}*C*-glycine and 33% glycine hydrochloride (by ^{1}H NMR and HRMS analyses). This mixture was used without further purification for the preparation of enriched (*Z*)-methyl-4-benzaloxazolone-*2*-^{13}*C*. ^{1}H NMR (400.1 MHz, CD_3OD, 25 °C): δ 1.99 (d, $^2J_{C-H}$ = 6.0 Hz, 3H, CH_3CONH), 3.88 (d, $^3J_{C-H}$ = 4.0 Hz, 2H, $NHCH_2CO_2H$). $^{13}C\{^1H\}$ NMR (100.6 MHz, CD_3OD, 25 °C) δ 22.3 (d, $^1J_{C-C}$ = 50.0 Hz, CH_3CONH), 41.8 (s, $NHCH_2CO_2$), 173.1 (s, $NHCH_2CO_2$), 173.7 (s, CH_3CONH). HRMS (EI): *m/z* 118.0459 (M^+, exact mass calcd for $C_3{}^{13}CH_7NO_3$ 118.0459).

(C) Enriched (*Z*)-Methyl-4-benzaloxazolone-*2*-^{13}*C*. Prepared according to established procedures[18] using the above mixture of 67% *N*-Acetyl-*1'*-^{13}*C*-glycine and 33% glycine hydrochloride as starting material. Yield: 25%. ^{1}H NMR (400.1 MHz, $CDCl_3$, 25 °C): δ 2.41 (d, $^2J_{C-H}$ = 8.0 Hz, 3H, CH_3), 7.15 (s, 1H, olefinic C*H*), 7.44 (m, 3H, C_6H_5), 8.08 (m, 2H, C_6H_5). $^{13}C\{^1H\}$ NMR (100.6 MHz, $CDCl_3$, 25 °C): δ 15.7 (CH_3), 128.9 (C_6H_5), 131.1 (C_6H_5), 131.4 (Cβ, olefinic *C*H), 132.1 (C_6H_5), 132.6 (C-4, quaternary olefin), 133.1 (*i*-C_6H_5), 166.1 (C-2), 167.8 (C-5, carbonyl). HRMS (EI): *m/z* 188.0665 (M^+, exact mass calcd for $C_{10}{}^{13}CH_9NO_2$ 188.0667).

(D) Enriched MAC-*1'*-^{13}*C*. Prepared according to established procedures[5a,17] using the above enriched (*Z*)-methyl-4-benzaloxazolone-*2*-^{13}*C* as starting material. Yield after flash column chromatography on neutral alumina (methylene chloride) followed by recrystallization (methylene chloride/*n*-pentane): 35%. ^{1}H NMR (400.1 MHz, THF-d_8/CD_2Cl_2 (2:1 v/v), –40 °C): δ 2.02 (d, $^2J_{C-H}$ = 6.0 Hz, 3H, $NHCOCH_3$), 3.74 (s, 3H, CO_2CH_3), 7.14 (s, 1H, olefinic C*H*), 7.36 (m, 3H, *m*- and *p*-C_6H_5), 7.57 (d, $^3J_{H-H}$ = 7.0 Hz, 2H, *o*-C_6H_5), 9.15 (s, 1H, N*H*$COCH_3$). $^{13}C\{^1H\}$ NMR (100.6 MHz, THF-d_8/CD_2Cl_2 (2:1 v/v), –40 °C): δ 22.9 (d, $^1J_{C-C}$ = 49.0 Hz, $NHCOCH_3$), 52.8 (CO_2CH_3), 127.7 (Cα, quaternary olefin), 129.3 (C_6H_5), 129.9 (C_6H_5), 130.5 (C_6H_5), 130.8 (Cβ, olefin), 134.7 (*i*-C_6H_5), 166.6 (C-1, CO_2CH_3), 170.3 (C-1', $NHCOCH_3$). HRMS (EI): *m/z* 220.0929 (M^+, exact mass calcd for $C_{11}{}^{13}CH_{13}NO_3$ 220.0929).

(E) 2-MeC^{15}N. Prepared as described previously[5] using **3**-MeC^{15}N (>95% ^{15}N-enriched) as starting material. Complex **2**-MeC^{15}N exists at –40 °C as a mixture of **4**, **5**, and **6** (see the Results and Discussion for relative proportions in THF-d_8). **4**: ^{1}H NMR

(400.1 MHz, THF-d_8/CD_2Cl_2 (6:1 v/v), –40 °C): δ –13.10 (m, overlapping with **5**, 1H, Ru*H*), 2.68 (br s, 3H, C*H*$_3$C^{15}N–Ru), 6.0–8.5 (aromatic, overlapping with **5** and **6**). ^{31}P{^{1}H} NMR (161.9 MHz, THF-d_8/CD_2Cl_2 (6:1 v/v), –40 °C): δ 71.8 (d, overlapping with **5**, $^2J_{P-P}$ = 49 Hz, 1P), 81.1 (d, $^2J_{P-P}$ = 49 Hz, 1P). ^{15}N NMR (40.5 MHz, THF-d_8/CD_2Cl_2 (6:1 v/v), –40 °C): δ 211.3 (d, overlapping with **5**, $^2J_{N-H(trans)}$ = 18.5 Hz, CH$_3$C^{15}*N*–Ru). **5**: ^{1}H NMR (400.1 MHz, THF-d_8/CD_2Cl_2 (6:1 v/v), –40 °C): δ –13.10 (m, overlapping with **4**, 1H, Ru*H*), 1.84 (s, 3H, C*H*$_3$C^{15}N–Ru), 2.12 (s, 3H, C*H*$_3$C^{15}N–Ru), 6.0–8.5 (aromatic, overlapping with **4** and **6**). ^{31}P{^{1}H} NMR (161.9 MHz, THF-d_8/CD_2Cl_2 (6:1 v/v), –40 °C): δ 71.9 (apparent t, overlapping with **4**, $^2J_{P-P}$ = $^2J_{P-N}$ = 42 Hz, 1P), 76.4 (d, $^2J_{P-P}$ = 42 Hz, 1P). ^{15}N NMR (40.5 MHz, THF-d_8/CD_2Cl_2 (6:1 v/v), –40 °C): δ 199.5 (d, $^2J_{P-N(trans)}$ = 39.0 Hz, CH$_3$C^{15}*N*–Ru), 211.3 (d, overlapping with **4**, $^2J_{N-H(trans)}$ = 18.5 Hz, CH$_3$C^{15}*N*–Ru). **6** ([Ru((*R*)-BINAP)(H)(THF-d_8)$_3$]BF$_4$): ^{1}H NMR (400.1 MHz, THF-d_8, –40 °C): δ –19.45 (br, Ru*H*), 6.0–8.5 (aromatic, overlapping with **4** and **5**). ^{31}P{^{1}H} NMR (161.9 MHz, THF-d_8, –40 °C): δ 74.1 (br d, $^2J_{P-P}$ = 50.0 Hz, 1P), 82.0 (br, 1P). **6** ([Ru((*R*)-BINAP)(H)]$_2$(BF$_4$)$_2$, major): ^{1}H NMR (400.1 MHz, THF-d_8/CD_2Cl_2 (6:1 v/v), –40 °C): δ –9.53 (dd, $^2J_{P-H}$ = 42.0 Hz, 30.0 Hz, 2H, Ru*H*), 4.2–6.0 (br m, 10 H, bridging aromatic), 6.0–8.5 (aromatic, overlapping with **4**, **5**, and **6**). ^{31}P{^{1}H} (161.9 MHz, THF-d_8/CD_2Cl_2 (6:1 v/v), –40 °C): δ 51.5 (d, $^2J_{P-P}$ = 42.0 Hz, 1P), 54.9 (d, $^2J_{P-P}$ = 42.0 Hz, 1P).

(F) *si*-7. In a 5-mm NMR tube, appropriately labeled **3** (1 equiv, typically ca. 25 mg) was partially dissolved in a mixture of THF-d_8 (0.50 mL) and CD_2Cl_2 (0.15 mL) under an atmosphere of argon gas. The tube was flushed with dihydrogen gas and shaken at room temperature for 5 min causing the original yellow solution to change to orange. The solution was bubbled with argon gas, then cooled to –78 °C, and transferred via cannula to another NMR tube containing an argon saturated solution of appropriately labeled MAC (1 equiv) in CD_2Cl_2 (0.1 mL) at –78 °C. The tube was briefly removed from the cooling bath, quickly shaken, and immediately placed in a –40 °C bath for 1 h before NMR analysis. ^{1}H NMR (400.1 MHz, THF-d_8/CD_2Cl_2 (2:1 v/v), –40 °C): δ –7.48 (dd, $^2J_{P_A-H}$ = 34.5, $^2J_{P_B-H}$ = 21.5 Hz, 1H, Ru*H*), 1.34 (s, 3H, NHCOC*H*$_3$), 1.92 (s, 3H,

CH_3CN), 2.96 (br s, 3H, CO_2CH_3), 3.74 (apparent t, $^3J_{P_A-H} = {}^3J_{P_B-H} = 4.0$ Hz, 1H, Hβ), 6.2–8.2 (aromatic, see the Results and Discussion for signals that could be assigned with certainty), 9.83 (s, 1H, N*H*COCH$_3$). $^{13}C\{^1H\}$ NMR (100.6 MHz, THF-d_8/CD_2Cl_2 (2:1 v/v), –40 °C): δ 65.9 (d, $^2J_{P_A-C} = 17.5$ Hz, Cβ), 81.3 (d, $^2J_{P_A-C} = 3.5$ Hz, Cα), 175.5 (s, *C*O$_2$CH$_3$), 180.2 (br apparent t, $^3J_{P_A-C} = {}^3J_{P_B-C} = 2.5$ Hz, NH*C*OCH$_3$). $^{31}P\{^1H\}$ NMR (161.9 MHz, THF-d_8/CD_2Cl_2 (2:1 v/v), –40 °C): δ 43.1 (d, $^2J_{P-P} = 24.0$ Hz, 1P, P_A), 66.3 (d, $^2J_{P-P} = 24.0$ Hz, 1P, P_B). ^{15}N NMR (40.5 MHz, THF-d_8/CD_2Cl_2 (2:1 v/v), –80 °C): δ 202.5 (d, $^2J_{N-H(trans)} = 10.0$ Hz, CH$_3$C^{15}*N*–Ru). ^{19}F NMR (376.5 MHz, THF-d_8/CD_2Cl_2 (2:1 v/v), –40 °C): δ –152.1 (s, 20%, $^{10}BF_4^-$), –152.2 (s, 80%, $^{11}BF_4^-$).

References and Notes

(1) (a) Noyori, R. *Asymmetric Catalysis in Organic Synthesis*; Wiley: New York, 1994; pp.16–94. (b) Takaya, H.; Ohta, T.; Noyori, R. In *Catalytic Asymmetric Synthesis*; Ojima, I., Ed.; VCH: Weinheim, 1993; pp.1–39. For recent examples see: (c) Burk, M. J.; Bienewald, F.; Harris, M.; Zanotti-Gerosa, A. *Angew. Chem., Int. Ed. Engl.* **1998**, *37*, 1931–1933. (d) Doucet, H.; Ohkuma, T.; Murata, K.; Yokozawa, T.; Kozawa, M.; Katayama, E.; England, A. F.; Ikariya, T.; Noyori, R. *Angew. Chem., Int. Ed. Engl.* **1998**, *37*, 1703–1707. (e) Jiang, Q.; Jiang, Y.; Xiao, D.; Cao, P.; Zhang, X. *Angew. Chem., Int. Ed. Engl.* **1998**, *37*, 1100–1103. (f) Ohkuma, T.; Koizumi, M.; Doucet, H.; Pham, T.; Kozawa, M.; Murata, K.; Katayama, E.; Yokozawa, T.; Ikariya, T.; Noyori, R. *J. Am. Chem. Soc.* **1998**, *120*, 13529–13530. (g) Ratovelomanana-Vidal, V.; Genêt, J.-P. *J. Organomet. Chem.* **1998**, *567*, 163–171.

(2) Wiles, J. A.; Bergens, S. H.; Young, V. G. *J. Am. Chem. Soc.* **1997**, *119*, 2940–2941.

(3) For mechanistic studies of rhodium(bis(phosphine))–enamide systems, see: (a) Kless, A.; Börner, A.; Heller, D.; Selke, R. *Organometallics* **1997**, *16*, 2096–2100. (b) Sun, Y.; Landau, R. N.; Wang, J.; LeBlond, C.; Blackmond, D. G. *J. Am. Chem. Soc.* **1996**, *118*, 1348–1353. (c) Bircher, H.; Bender, B. R.; von Philipsborn, W. *Magn. Res. Chem.* **1993**, *31*, 293–298. (d) Chinn, M. S.; Eisenberg, R. *J. Am. Chem. Soc.* **1992**, *114*, 1908–1909. (e) Landis, C. R.; Halpern, J. *J. Am. Chem. Soc.* **1987**, *109*, 1746–1754. (f) Brown, J. M.; Chaloner, P. A.; Morris, G. A. *J. Chem. Soc., Perkin Trans. 2* **1987**, 1583–1588. (g) Brown, J. M.; Chaloner, P. A.; Morris, G. A. *J. Chem. Soc., Chem. Commun.* **1983**, 664–666. (h) Halpern, J. *Science* **1982**, *217*, 401–407. (i) Brown, J. M.; Chaloner, P. A. *J. Chem. Soc., Perkin Trans. 2* **1982**, 711–719. Some structural details were obtained of diastereomeric rhodium(III)–alkyl–hydrido species which occur after the enantioselective step: (j) Ramsden, J. A.; Claridge, T. D. W.; Brown, J. M. *J. Chem. Soc., Chem. Commun.* **1995**, 2469–2471. (k) Brown, J. M.; Chaloner, P. A. *J. Chem. Soc., Chem. Commun.* **1980**, 344–346. The minor olefin–catalyst diastereomer in these systems has been studied by isotope labeling: (l) Brown, J. M.; Murrer, B. A. *J. Chem. Soc.,*

Perkin Trans. 2 **1982**, 489–497. (m) Brown, J. M.; Chaloner, P. A. *J. Am. Chem. Soc.* **1980**, *102*, 3040–3048. (n) Brown, J. M.; Chaloner, P. A. *J. Chem. Soc., Chem. Commun.* **1979**, 613–615; by using Iridium analogs: (o) Armstrong, S. K.; Brown, J. M.; Burk, M. J. *Tetrahedron Lett.* **1993**, *34*, 879–882. (p) Brown, J. M.; Maddox, P. J. *Chirality* **1991**, *3*, 345–354. (q) Brown, J. M.; Maddox, P. J. *J. Chem. Soc., Chem. Commun.* **1987**, 1276–1278. (r) Alcock, N. W.; Brown, J. M.; Derome, A. E.; Lucy, A. R. *J. Chem. Soc., Chem. Commun.* **1985**, 575–578; and by calculations: (s) Giovannetti, J. S.; Kelly, C. M.; Landis, C. R. *J. Am. Chem. Soc.* **1993**, *115*, 4040–4057. (t) Bogdan, P. L.; Irwin, J. J.; Bosnich, B. *Organometallics* **1989**, *8*, 1450–1453. (u) Brown, J. M.; Evans, P. L. *Tetrahedron* **1988**, *44*, 4905–4916. For a preliminary structural account of two diastereomeric rhodium(III)–dihydrido intermediates in the enantioselective hydrogenation of dimethyl itaconate, see: (v) Harthun, A. ; Kadyrov, R.; Selke, R.; Bargon, J. *Angew. Chem., Int. Ed. Engl.* **1997**, *36*, 1103–1105.

(4) For studies of ruthenium systems, see: (a) Shaharuzzaman, M.; Braddock-Wilking, J.; Chickos, J. S.; Tam, C, N,; Silva, R. A. G. D.; Keiderling, T. A. *Tetrahedron: Asymmetry* **1998**, *9*, 1111–1114. (b) Fehr, M. J.; Consiglio, G.; Scalone, M.; Schmid, R. *New. J. Chem.* **1998**, 1499–1504. (c) Chen, C.-C.; Huang, T.-T.; Lin, C.-W.; Cao, R.; Chan, A. S. C.; Wong, W. T. *Inorg. Chim. Acta* **1998**, *270*, 247–251. (d) Haack, K.-J.; Hashiguchi, S.; Fujii, A.; Ikariya, T.; Noyori, R. *Angew. Chem., Int. Ed. Engl.* **1997**, *36*, 285–288. (e) Mezzetti, A.; Tschumper, A.; Consiglio, G. *J. Chem. Soc., Dalton Trans.* **1995**, 49–56. (f) Brown, J. M.; Rose, M.; Knight, F. I.; Wienand, A. *Recl. Trav. Chim. Pays-Bas* **1995**, *114*, 242–251. (g) Chan, A. S. C.; Chen, C. C.; Yang, T. K.; Huang, J. H.; Lin, Y. C. *Inorg. Chim. Acta* **1995**, *234*, 95–100. (h) Brown, J. M. *Chem. Soc. Rev.* **1993**, 25–41. (i) Chan, A. S. C.; Laneman, S. A.; Miller, R. E. In *Selectivity in Catalysis*; Davis, M. E., Suib, S. L., Eds.; ACS Symposium Series 517; American Chemical Society: Washington, DC, 1993; Chapter 2. (j) Saburi, M.; Takeuchi, H.; Ogasawara, M.; Tsukahara, T.; Ishii, Y.; Ikariya, T.; Takahashi, T. *J. Organomet. Chem.* **1992**, *428*, 155–167. (k) Ashby, M. T.; Khan, M. A.; Halpern, J. *Organometallics* **1991**, *10*, 2011–2015. (l) Ashby, M. T.; Halpern, J. *J. Am. Chem. Soc.* **1991**, *113*, 589–594. (m) Ohta, T.; Takaya, H.; Noyori, R. *Tetrahedron Lett.* **1990**, *31*, 7189–7192. (n) Kawano, H.; Ikariya,

T.; Ishii, Y.; Saburi, M.; Yoshikawa, S.; Uchida, Y.; Kumobayashi, H. *J. Chem. Soc., Perkin Trans. 1* **1989**, 1571–1575. (o) James, B. R.; Wang, D. K. W. *Can. J. Chem.* **1980**, *58*, 245–250.

(5) (a) Wiles, J. A.; Bergens, S. H. *Organometallics* **1998**, *17*, 2228–2240. (b) Daley, C. J. A.; Wiles, J. A.; Bergens, S. H. *Can. J. Chem.* **1998**, *76*, 1447–1456. (c) Wiles, J. A.; Lee, C. E.; McDonald, R.; Bergens, S. H. *Organometallics* **1996**, *15*, 3782–3784.

(6) Seeman, J. I. *Chem. Rev.* **1983**, *83*, 84–134.

(7) Complex **6** exists in equal proportions as a mixture of [Ru((*R*)-BINAP)(H)-(THF-d_8)$_3$]BF_4 and the η^6-arene bridged dimers [Ru((*R*)-BINAP)(H)]$_2$(BF_4)$_2$. The presence of the dimers was deduced from the signals in the range δ 4.2–6.0 in the ^{1}H NMR spectrum, which are from the hydrogen atoms on the bridging phenyl rings. The signals for the dimers appear in the range δ 40–60 in the ^{31}P{^{1}H} NMR spectrum (Figure 5-1). The phenyl-bridged dimers can be prepared in higher relative concentrations by hydrogenation of **3** in CD_2Cl_2.

(8) A related chiral hydrido–solvent complex of ruthenium(II) has been crystallographically characterized: (a) Currao, A.; Feiken, N.; Macchioni, A.; Nesper, R.; Pregosin, P. S.; Trabesinger, G. *Helv. Chim. Acta* **1996**, *79*, 1587–1591. Three ruthenium–hydrido complexes of BINAP ([RuH((*R*)-BINAP)$_2$](PF_6), [RuH(η^2-H_2)((*R*)-BINAP)$_2$](PF_6), and RuHCl((*R*)- or (*S*)-BINAP)$_2$) have been previously characterized: (b) Tsukahara, T.; Kawano, H.; Ishii, Y.; Takahashi, T.; Saburi, M.; Uchida, Y.; Akutagawa, S. *Chem. Lett.* **1988**, 2055–2058. (c) Kawano, H.; Ishii, Y.; Kodama, T.; Saburi, M.; Uchida, Y. *Chem. Lett.* **1987**, 1311–1314. (d) Ikariya, T.; Ishii, Y.; Kawano, H.; Arai, T.; Saburi, M.; Yoshikawa, S.; Akutagawa, S. *J. Chem. Soc., Chem. Commun.* **1985**, 922–924.

(9) This geometry was confirmed by comparison to *fac*-[Ru((*R*)-BINAP)(H)-(MeC^{15}N)$_3$]BF_4 (**8**), in which two signals in the ^{15}N NMR spectrum are coupled to phosphorus, but not to the hydride, while the remaining signal is coupled to the hydride, but not to the phosphorus centers. NMR data for **8**: ^{1}H (400.1 MHz, THF-d_8/CD_2Cl_2 (6:1 v/v), –40 °C): δ –13.58 (d of apparent t, $^2J_{P-H(cis)}$ = 24.5 Hz, $^2J_{N-H(trans)}$ = 18.5 Hz, 1H, Ru*H*), 1.75 (d, $^3J_{N-H}$ = 2.0 Hz, 3H, C*H*$_3$C^{15}N–Ru), 1.79 (d, $^3J_{N-H}$ = 2.0 Hz, 3H, C*H*$_3$C^{15}N–

Ru), 2.16 (d, $^3J_{N-H}$ = 2.0 Hz, 3H, $CH_3C^{15}N$–Ru), 6.0–8.4 (aromatic). $^{31}P\{^1H\}$ (161.9 MHz, THF-d_8/CD_2Cl_2 (6:1 v/v), –40 °C): δ 63.6 (apparent t, $^2J_{P-P} = {}^2J_{P-N(trans)}$ = 39.0 Hz, 1P), 69.6 (apparent t, $^2J_{P-P} = {}^2J_{P-N(trans)}$ = 39.0 Hz, 1P). ^{15}N (40.5 MHz, THF-d_8/CD_2Cl_2 (6:1 v/v), –40 °C): δ 196.4 (d, $^2J_{P-N(trans)}$ = 39.0 Hz, $CH_3C^{15}N$–Ru), 196.9 (d, $^2J_{P-N(trans)}$ = 39.0 Hz, $CH_3C^{15}N$–Ru), 208.4 (d, $^2J_{N-H(trans)}$ = 18.5 Hz, $CH_3C^{15}N$–Ru)). For a similar analysis, see: Chan, A. S. C.; Halpern, J. *J. Am. Chem. Soc.* **1980**, *102*, 838–840.

(10) Only one of the two possible diastereomers of **5** was observed. The absolute configuration of the complex was not determined.

(11) (a) Bender, B. R.; Koller, M.; Nanz, D.; von Philipsborn, W. *J. Am. Chem. Soc.* **1993**, *115*, 5889–5890. (b) McCulloch, B.; Halpern, J.; Thompson, M. R.; Landis, C. R. *Organometallics* **1990**, *9*, 1392–1395. (c) Chan, A. S. C.; Pluth, J. J.; Halpern, J. *J. Am. Chem. Soc.* **1980**, *102*, 5952–5954. (d) Brown, J. M.; Chaloner, P. A.; Glaser, R.; Geresh, S. *Tetrahedron* **1980**, *36*, 815–825. (e) Chan, A. S. C.; Pluth, J. J.; Halpern, J. *Inorg. Chim. Acta* **1979**, *37*, L477–L479.

(12) NOE methods have been used previously in the structure determinations (including absolute configuration) of organometallic complexes containing prochiral substrates. For recent examples, see: (a) Pregosin, P. S.; Trabesinger, G. *J. Chem. Soc., Dalton Trans.* **1998**, 727–734. (b) Krafft, M. E.; Yu, X. Y.; Wilson, L. J. *Organometallics* **1998**, *17*, 2076–2088. (c) Motoyama, Y.; Murata, K.; Kurihara, O.; Naitoh, T.; Aoki, K.; Nishiyama, H. *Organometallics* **1998**, *17*, 1251–1253. (d) Steinhagen, H.; Reggelin, M.; Helmchen, G. *Angew. Chem., Int. Ed. Engl.* **1997**, *36*, 2108–2110.

(13) THF-d_8 solutions containing CD_2Cl_2 (THF-d_8:CD_2Cl_2 = 2:1 v/v) were employed to increase the solubility of **3** in the preparation of **2**.

(14) Typically, solutions of **7** contained traces of excess MAC. The methoxy signal for excess (uncoordinated) MAC in the ^1H NMR spectra of these mixtures obscured the signal for Hβ of **7**, which required the use of MAC-CO_2CD_3 to obtain unambiguous NOE data.

(15) There was significant overlap of the signals for the aromatic protons in the ^1H NMR spectrum of **7** (see Figure 5-2).

(16) This was also shown at room temperature for [Pd((*R*)-BINAP)(η^3-allyl)]CF_3SO_3, where η^3-allyl = β-pinene allyl and exo-methylene cyclopentene allyl: (a) Pregosin, P. S.; Rüegger, H.; Salzmann, R.; Albinati, A.; Lianza, F.; Kunz, R. W. *Organometallics* **1994**, *13*, 5040–5048. (b) Rüegger, H.; Kunz, R. W.; Ammann, C. J.; Pregosin, P. S. *Magn. Reson. Chem.* **1991**, *29*, 197–203. Note that the correlations between P_A and the ortho aromatic protons are weaker than those for P_B. The weaker correlations indicate that the signals from the ortho aromatic protons at P_A are broadened (these signals overlap with other aromatic proton signals). This broadening shows that rotation around the P_A–C_{phenyl} bond is slower at –40 °C than around the P_B–C_{phenyl} bond. These experiments were not optimized to observe correlations within the minor components in solution.

(17) Cativiela, C.; Diaz de Villegas, M. D.; Melendez, E. *Tetrahedron* **1986**, *42*, 583–589.

(18) Herbst, R. M.; Shemin, D. In *Organic Syntheses*; Blatt, A. H., Ed.; Wiley: New York, 1943; Collect. Vol. 2, pp 1–3.

Chapter 6

Conclusions

Mechanism of Catalytic Hydrogenation. This mechanistic study represents the most detailed structural observation of a diastereomeric pathway in enantioselective catalytic hydrogenation. The proposed mechanism for the major (observed) diastereomeric pathway, that is responsible for production of the major product enantiomer, is shown below (Scheme 6-1). The catalytic cycle is entered with activation of the catalyst precursor, [Ru((*R*)-BINAP)(1–3:5,6-η-C_8H_{11})(MeCN)]BF_4 (**1**), by reaction with dihydrogen gas in weakly coordinating solvents (acetone, methanol, or THF) to generate cyclooctane and the active ruthenium–hydrido catalyst [Ru((*R*)-BINAP)$(MeCN)_n(sol)_{3-n}$]-BF_4 (**2**; n = 0–3, depending on reaction medium). Complex **2** then rapidly reacts with the substrate MAC to generate the catalyst–substrate adduct **3**. Complex **3** undergoes rapid olefin–hydride insertion to generate the ruthenium–alkyl complex **4**. Both the initial reaction of MAC with **2** and the subsequent olefin–hydride insertion reaction to form **4** are rapid and reversible, as determined by deuterium-labeling studies. The final step, which completes the catalytic cycle, is hydrogenolysis of the ruthenium–alkyl bond of **4** to liberate the hydrogenation product (*R*)-$MAC(H)_2$ and to regenerate the catalyst **2**. This hydrogenolysis step is both enantioselective and turnover-limiting. Unlike the ruthenium–BINAP system studied by Halpern and Noyori (where the enantioselective step followed the turnover-limiting step[1]), a detailed kinetic study of this system may provide information about the enantioselective step and the origins of enantioselection for hydrogenations catalyzed by ruthenium–BINAP complexes. This study has also demonstrated that for this system, unlike the mechanism proposed by Halpern and Noyori, heterolytic cleavage of dihydrogen gas is not operative and that solvolysis (or protonolysis) of the ruthenium–alkyl bond is a minor (<4%) pathway of the catalytic hydrogenation in methanol solvent. It should also be noted that the distinct difference between the mechanism proposed in the present study and that of the catalytic

Scheme 6-1. Proposed Major Diastereomeric Pathway for the Enantioselective Hydrogenation of MAC Catalyzed by 2

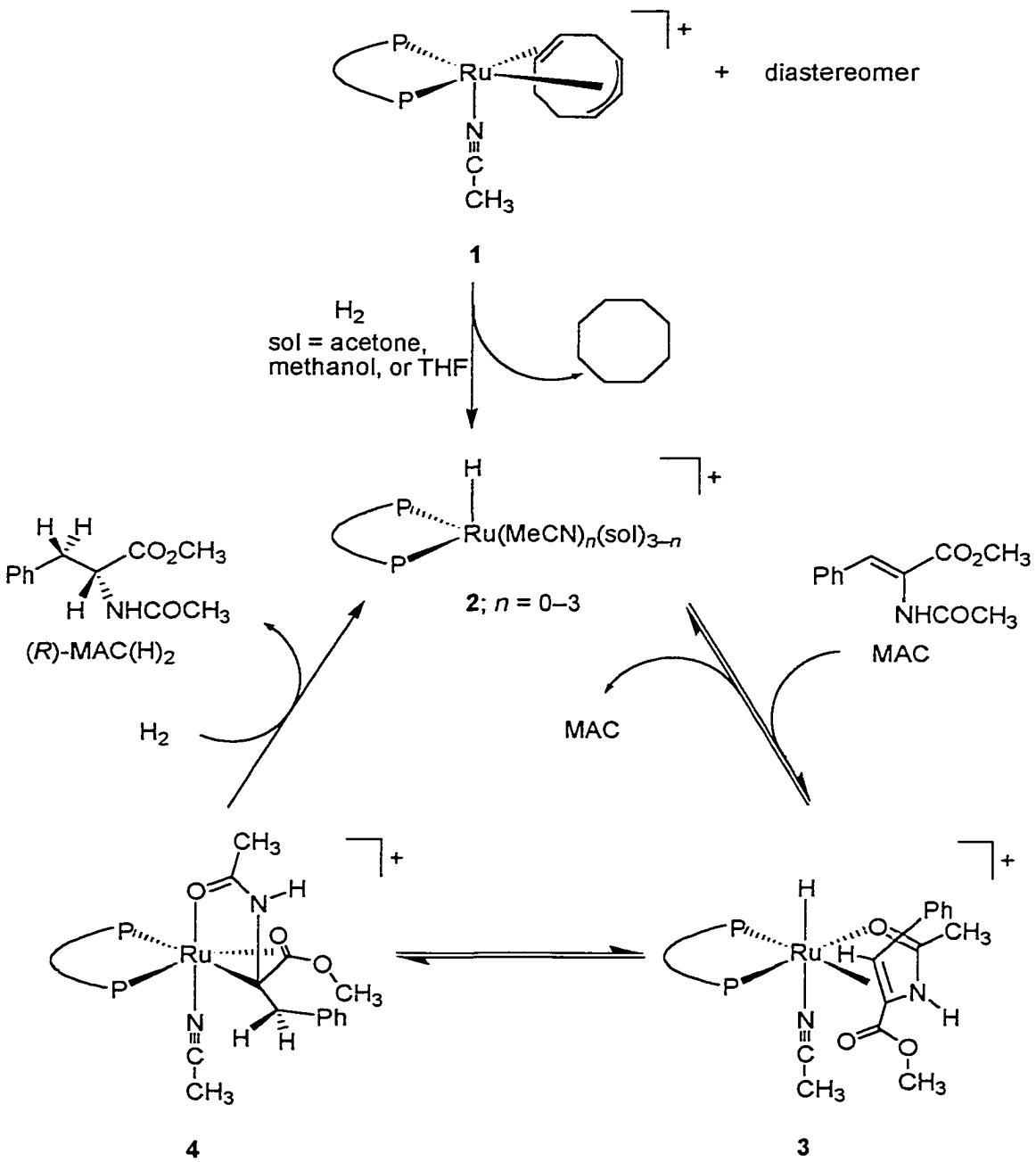

hydrogenation of MAC when using [Rh((*R*,*R*)-DIPAMP)(MeOH)$_2$]BF$_4$ as the catalyst is that the major diastereomeric substrate–adduct leads to the major product enantiomer, whereas the minor diastereomeric substrate–adduct leads to the major product enantiomer

for the rhodium system. Further, formation of **4** is effected by a reversible olefin–hydride insertion step; the corresponding step in the rhodium–((*R*,*R*)-DIPAMP)-catalyzed process is irreversible.[2]

Although the proposed mechanistic pathway (involving reversible formation of ruthenium–alkyl species followed by hydrogenolysis of a ruthenium–carbon bond in which the carbon center is stereogenic) has been postulated for ruthenium–BINAP catalyzed enantioselective hydrogenation,[3] this study represents the first instance where such putative catalytic intermediates have been intercepted, fully characterized, and studied to establish their relevance to the catalytic cycle. The results from the isotope-labeling and stereochemical studies of these putative intermediates demonstrate that the stereo-selectivities and regioselectivities of the rapid and reversible formation of **3** and **4**, and the conversion of **4** to (*R*)-MAC(H)$_2$ (via irreversible hydrogenolysis of the ruthenium–carbon bond) summate to give the stereoselectivity and regioselectivity of the catalytic hydrogenation. These data strongly support the intermediacy of **3** and **4** in the catalytic reaction; however, it has yet to be determined that the rate of hydrogenolysis of **4** is no slower than the catalytic hydrogenation under similar reaction conditions.[4] If this stoichio-metric rate requirement is satisfied, then, combined with the results obtained from the X-ray crystallographic, low-temperature NMR spectroscopic, catalytic and stoichiometric isotope-labeling, and catalytic rate studies, it can be confidently stated that **3** and **4** are true catalytic intermediates. It cannot be conclusively stated, however, because the proposed intermediates may be in equilibrium with the true intermediates that react to generate the products. A direct comparison between the stoichiometric and catalytic rate data, however, are complicated by both the accumulation of MeCN, which occurs in solution during the stoichiometric hydrogenolysis of **4** (reaction of **2** with MAC(H)$_2$ to give MeCN and [Ru((*R*)-BINAP)(η^6-MAC(H)$_2$)]BF$_4$), and the ability of **4** to undergo solvolysis in methanol. Both of these processes do not occur during the catalytic hydrogenation. It should be noted, however, that formation of complex **4** was rapid relative to the overall rate of the catalytic hydrogenation, that **4** is the predominant species in solution during catalysis, and that the rates of catalytic reaction when using **2** and **4** as the catalysts are similar. Regardless, **3** and **4** constitute the first examples of putative

ruthenium–BINAP catalytic intermediates that each contain a substrate that is bonded to the ruthenium center through the prochiral group of the substrate.[5] Further, **3** is the first diastereomeric hydrido–olefin intermediate to be fully characterized in catalytic enantioselective hydrogenation—a necessary intermediate in all catalytic hydrogenations.

Rewards of Mechanistic Studies. The benefits of mechanistic studies reach far beyond satisfying academic curiosities. The purpose of such studies, ultimately, is to expose the underlying principles of enantioselective catalysis that will allow the rational design of catalysts with tailored selectivities. Despite the intense study of transition-metal-based enantioselective catalysis during the past 30 years, there is little predictive understanding of how steric and electronic factors specifically contribute to enantioselection. In fact, it was only through the present study that the critical bonding interactions of the prochiral substrate group to a ruthenium catalyst were first learned. Moreover, this study has provided important guidelines that facilitated the development of highly reactive catalysts for an industrial process. The following briefly describes a portion of our two-year industrial collaboration with workers at Firmenich S.A., a fragrance and flavor company based in Switzerland, that involved the development of new chiral catalysts and enantioselective reactions.[6]

The target molecule **5**, produced by Firmenich under the tradename Hedione®, is an important synthetic fragrance component that is the dihydro derivative of natural methyl (*Z*)-jasmonates (Scheme 6-2). Patented by Firmenich in 1960[7] as an inexpensive

Scheme 6-2. Jasmonoid Compounds of Importance in the Fragrance Industry

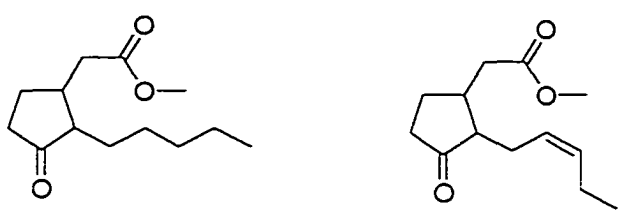

5
Hedione®

methyl (*Z*)-jasmonate

replacement for jasmine oil,[8] Hedione® is present in many commercial fragrances. Since 1970, Firmenich has commercialized a close-to-equilibrium mixture of Hedione® (ca. 4000 tons year^{-1}) that contains ca. 10% (*rac*)-**6** and ca. 90% (*rac*)-**7** (Scheme 6-3). It is

Scheme 6-3. Components of Hedione®

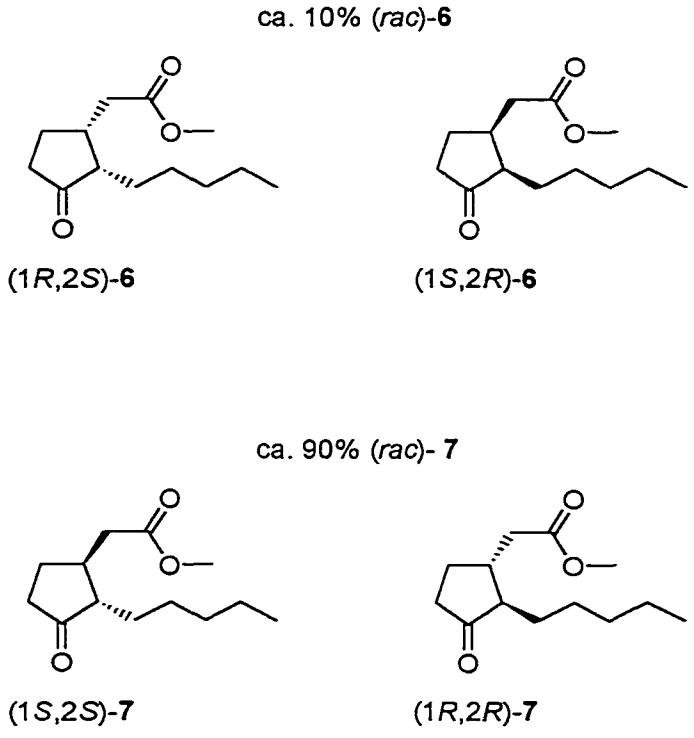

prepared by the aldol condensation of cyclopentanone with pentanal and subsequent isomerization to **8**, followed by Michael addition of dimethyl malonate to **8** and subsequent dealkoxycarbonylation (Scheme 6-4).[9] Evaluation of the four stereoisomers of Hedione® established that (1*R*,2*S*)-**6** has the lowest odor threshold (by several orders of magnitude) and it possesses the distinct jasmine note (a sweet floral fragrance). It is, therefore, desirable to prepare mixtures, known as Hedione® HC, that contain increased amounts of the cis isomer (1*R*,2*S*)-**6**. The use of the *high-cis* product Hedione® HC is limited, however, because (1*R*,2*S*)-**6** epimerizes outside the 5.5–6.5 pH range to give (1*R*,2*R*)-**7**.

Scheme 6-4. Industrial Synthesis of Hedione®

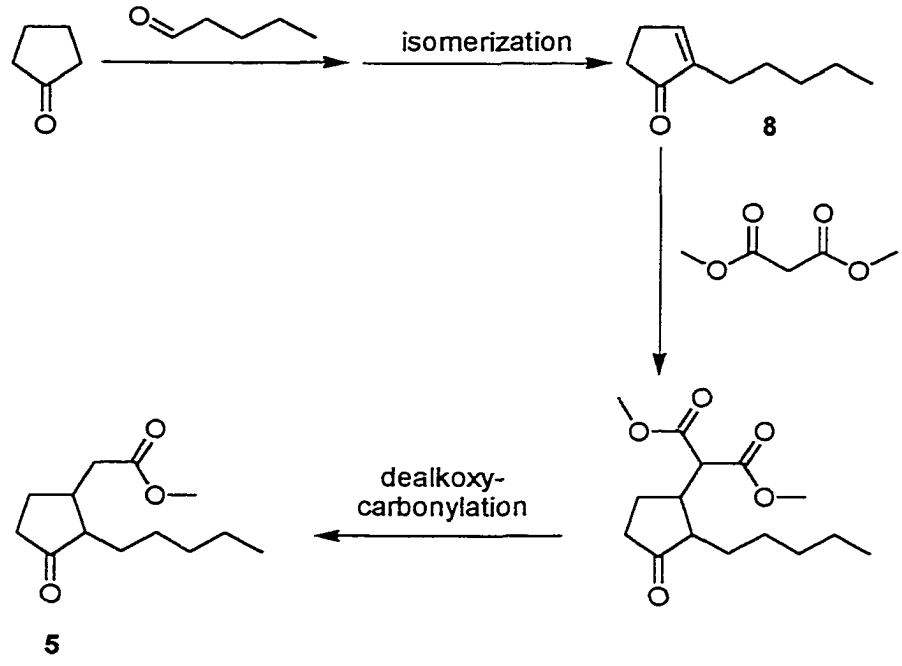

The jasmanoid chemistry of Firmenich has moved from natural jasmine oil to the synthetic variant Hedione® and, more recently, to Hedione® HC—presently a mixture of ca. 70% (*rac*)-**6** and ca. 30% (*rac*)-**7** prepared by fractional distillation of Hedione.® The following discusses the stereoselective preparation of the active isomer (1*R*,2*S*)-**6**—the next milestone of Hedione® chemistry.

The most direct synthetic route to (1*R*,2*S*)-**6** is enantioselective hydrogenation of the tetrasubstituted olefinic precursor **9** under neutral pH conditions (eq 6-1). This

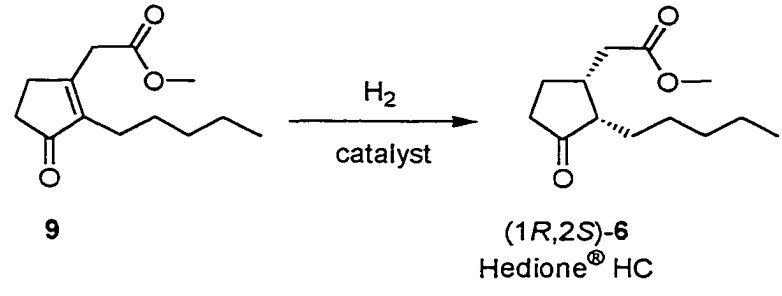

(6-1)

approach is particularly attractive because generation of two of the inactive stereoisomers

of Hedione® (7) is prevented since reduction of olefinic substrates catalyzed by homogeneous transition-metal complexes generally proceeds via syn addition of dihydrogen gas. Known homogeneous catalysts used for enantioselective hydrogenation of olefins, however, do not effect the hydrogenation of **9**, including conventional catalysts of the form [Rh(bis(phosphine))(sol)$_2$]BF$_4$. There are, in fact, few examples of homogeneous enantioselective hydrogenation of tetrasubstituted olefins in the literature.[10] Historically, tetrasubstituted olefins have presented a challenge for known homogeneous hydrogenation catalysts (low reactivity and selectivity), presumably because the steric hinderance of these substrates lowers their ability to bind to the catalyst. It was essential, therefore, that a new catalyst system, with higher reactivity, be developed for the hydrogenation of **9**.

Through the design of a well-defined catalyst precursor, **1**, and identification of the subsequent active catalyst **2**, this research group, in collaboration with workers at Firmenich, has been able to design a general route to chiral ruthenium complexes capable of catalyzing the enantioselective hydrogenation of **9**. Work from this laboratory has shown that **2** is an effective hydrogenation catalyst that exhibits high enantioselectivity; however, the presence of the strongly coordinating MeCN ligand compromises the TOF of this catalyst system and precludes its use in an industrial process. A catalyst system similar to **2**, but containing only weakly coordinating solvento ligands (no MeCN) was envisaged. Ideally, a very weakly coordinating solvent, such as methylene chloride, should be used to prevent competing coordination of the solvent and substrate to the catalyst. Such a catalyst system also requires synthetic flexibility to permit the incorporation of several different chiral bis(phosphine) ligands for rapid screening and optimization of the hydrogenation process.

It was previously established by Chaudret and co-workers[11] that protonation of [Ru(COD)(COT)] by stoichiometric amounts of HBF$_4$·Et$_2$O at low temperature immediately generated thermally unstable [Ru(H)(COD)(COT)]BF$_4$ (**10**). These workers also reported that addition of excess monodentate ligands (L = H$_2$O, MeCN, or phosphines) to **10** at low temperature, followed by warming to room temperature generated [Ru(L)$_3$(1–5-η-C$_8$H$_{11}$)]BF$_4$ and cycloocta-1,3-diene. In this laboratory, it was

found that addition of 1 equiv of (*R*,*R*)-Me-DuPHOS to a solution of **10** in methylene chloride at –78 °C, followed by warming to room temperature generated [Ru((*R*,*R*)-Me-DuPHOS)(H)(COT)]BF_4 (**11**) and COD (eq 6-2). Complex **11** was isolated as an analytically pure crystalline solid in high yield (>80% isolated; quantitative by NMR), and it was fully characterized by X-ray diffraction, NMR spectroscopy, mass spectrometry,

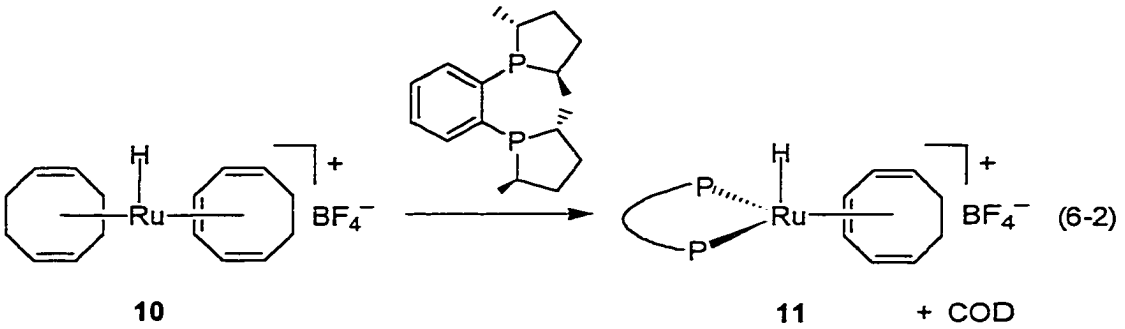

and elemental analyses. Likewise, reaction of **10** with (*R*)-(*S*)-JOSIPHOS, (*R*)-BINAP, and (*R*)-TolBINAP generated [Ru((*R*)-(*S*)-JOSIPHOS)(H)(COT)]BF_4 (**12**; eq 6-3), [Ru((*R*)-BINAP)(1–5-η-C_8H_{11})]BF_4 (**13**; eq 6-4),[12] and [Ru((*R*)-TolBINAP)(1–5-η-C_8H_{11})]BF_4 (**14**; eq 6-4), respectively, as major products. Complexes **11–14** reacted with

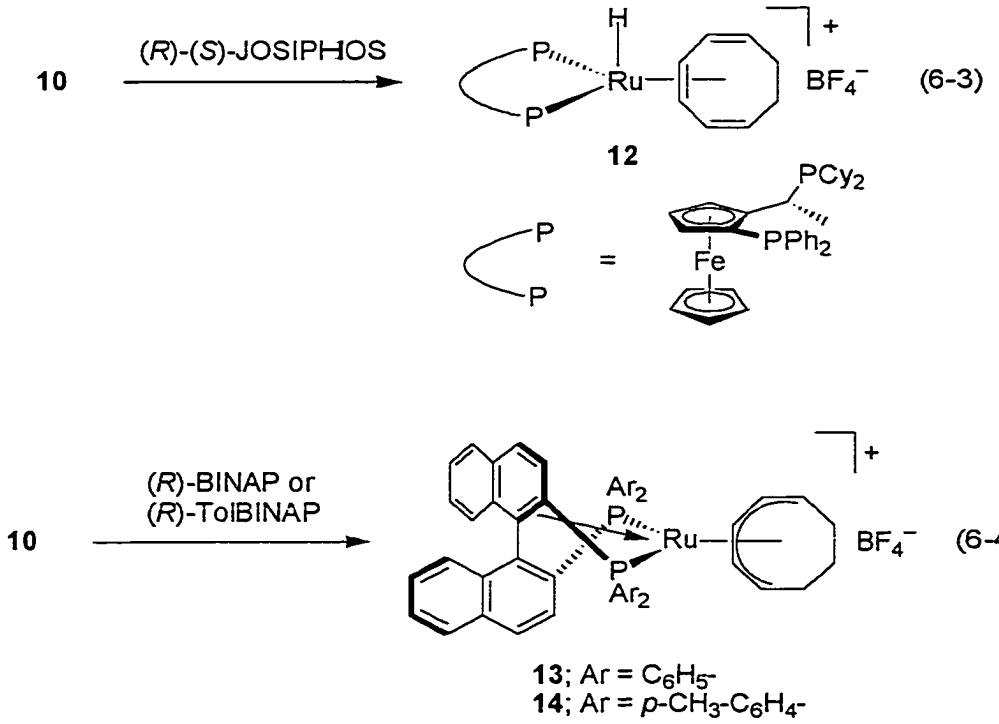

dihydrogen gas in weakly coordinating solvents to generate highly reactive catalysts of the form [Ru(bis(phosphine))(H)(sol)$_3$]BF$_4$ with concomitant formation of cyclooctane. This method is the first versatile synthetic route to prepare catalysts of the form [Ru(bis(phosphine))(H)(sol)$_3$]BF$_4$ that contain structurally and electronically diverse chiral bis(phosphines). These complexes can be easily prepared in high yield and stored as the catalyst precursors [Ru(bis(phosphine))(H)(COT)]BF$_4$ or [Ru(bis(phosphine))(1–5-η-C$_8$H$_{11}$)]BF$_4$. The preparation of the starting ruthenium complex ([Ru(COD)(COT)]), the catalyst precursors, and the active catalysts constitute the first synthetic route for ruthenium that closely parallels that of the highly successful rhodium synthesis of Schrock and Osborn[13] ([Rh(diene)$_2$]$^+$ (diene = COD or NBD), [Rh(bis(phosphine))(diene)]$^+$, and [Rh(bis(phosphine))(sol)$_2$]$^+$, respectively). The limitation of the ruthenium synthesis is the availability of [Ru(COD)(COT)] (30–50% yields by literature methods[14]); nevertheless, this methodology will still provide a rapid and effective means for screening ruthenium–(bis(phosphine)) catalysts in industrial and academic environments to the degree that [Rh(bis(phosphine))(sol)$_2$]$^+$ catalysts are used today.

The effectiveness of the catalyst precursors **11–14** for the hydrogenation of **9** was evaluated by co-workers at Firmenich. Through optimization of the hydrogenation process, (1*R*, 2*S*)-**6** can now be produced in 90% ee with >99:1 *cis*-selectivity when the ruthenium–((*R*)-(*S*)-JOSIPHOS) catalyst is used in methyl *t*-butyl ether solvent (T = 30 °C, 90 atm H$_2$, MTBE:substrate = 10:1, TOF $\approx$ 3 min^{-1}, TON = 2000).

In addition to the development of highly reactive catalysts for an industrial process, this project has provided a platform for further catalyst development. Preliminary experiments have shown that the ruthenium–hydrido catalysts discussed in this thesis are precursors to chiral ruthenium–alkylidene complexes that are promising catalysts for asymmetric olefin metathesis reactions.[15] Chiral variants of Schrock's metathesis catalyst ([Ph(CH$_3$)$_2$CCH=Mo=N(2,6-(*i*-Pr)$_2$C$_6$H$_3$)(OCMe(CF$_3$)$_2$)$_2$];[16] Scheme 6-5) and their use in asymmetric ring-closing metathesis (ARCM) have been described;[17] however, these complexes, unlike the successful metathesis catalyst of Grubbs ([Cl$_2$(PCy$_3$)$_2$Ru=CHPh];[18] Scheme 6-6), are thermally sensitive, highly air-sensitive, and intolerant of many functional groups that are important in organic synthesis. Although chiral alkylidene complexes of

Scheme 6-5. Schrock's Catalyst and Its Chiral Variants

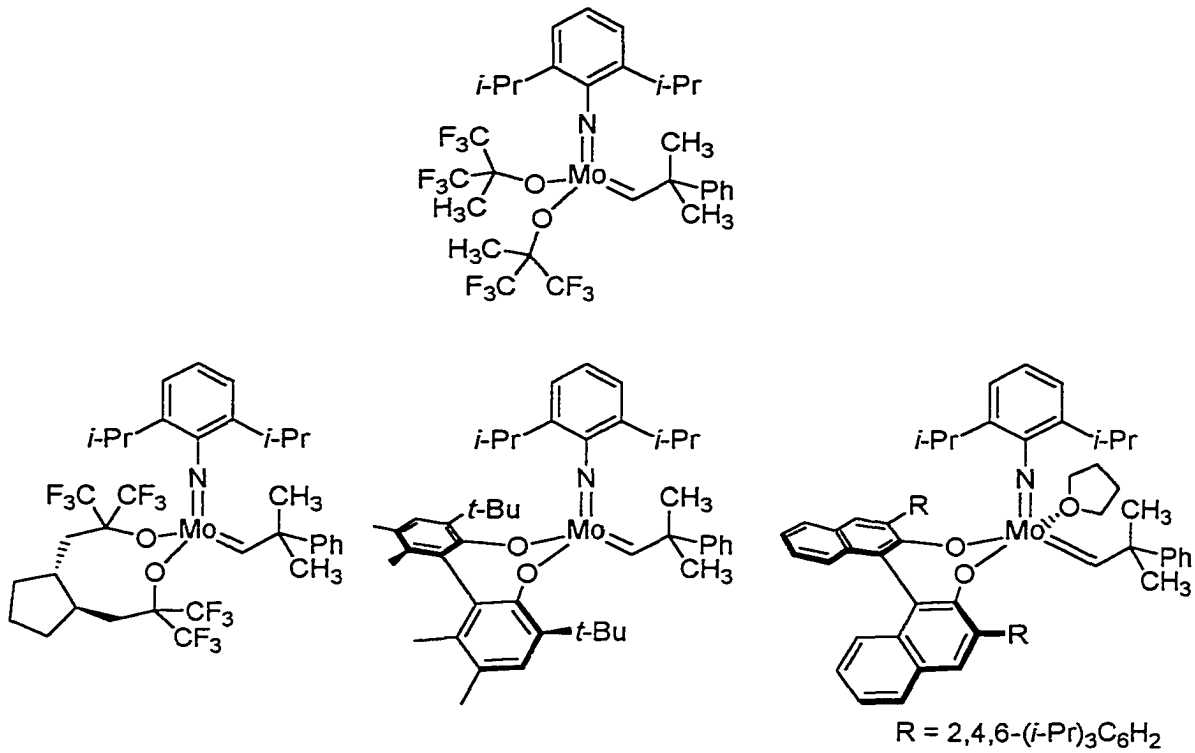

Scheme 6-6. Grubbs' Catalyst

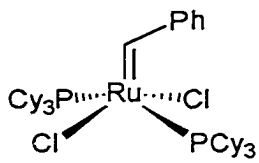

ruthenium are known, these complexes, prepared directly from Grubbs' catalyst by Herrmann and co-workers, contain chiral monodentate *N*-heterocyclic carbene ligands (eq 6-5).[19] It is appreciated in catalyst design that bidentate ligands, in general, are required for high enantioselectivity; therefore, it is desirable to prepare catalysts of well-established chiral bis(phosphine) ligands. Only recently have ruthenium–alkylidene complexes of achiral bis(phosphines) appeared in the literature,[20] but chiral variants have not followed. It was discovered in this laboratory that, using the method of Wilhelm et al.,[21] [Ru=CH–CH=CMe_2(Cl)((*R*)-BINAP)(MeCN)]BF_4 (**15**)[22] can be prepared in high yield by the rapid

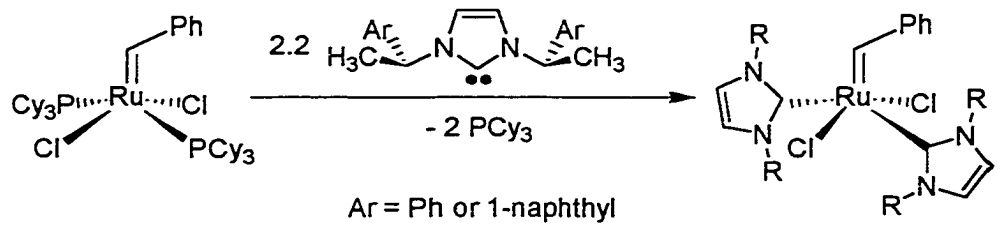

(6-5)

reaction of **2** with 3-chloro-3-methyl-1-butyne (eq 6-6). Complex **15** is the first ruthenium–alkylidene complex of a chiral bis(phosphine). Although the use of **15** as a catalyst in asymmetric olefin metathesis reactions has not yet been evaluated, preliminary experiments have indicated that it is an active ring-opening metathesis catalyst for the polymerization of NBD.

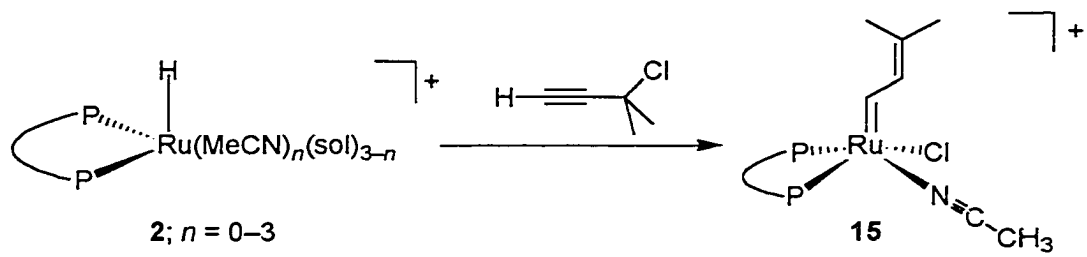

2; n = 0–3 **15**

(6-6)

Future Mechanistic Studies. The present mechanistic study strongly implies that the hydrogenation of MAC catalyzed by **2** is operating under Curtin–Hammett conditions, and that the hydrogenolysis of the ruthenium–carbon bond of **4** is both the enantioselective step and the turnover-limiting step. The hydrogenolysis is responsible for the observed enantioselection (the difference in Gibbs energies of the diastereomeric transition states) and TOF (limited by the slowest step in the catalytic cycle) for the catalytic hydrogenation. It follows that an examination of the hydrogenolysis step is required to determine the influence of **4** on the enantioselectivity of the catalytic reaction. If the rate of the stoichiometric hydrogenolysis of **4** is similar to the TOF of the catalytic hydrogenation, then all of the available data will support the intermediacy of **4** in the catalytic hydrogenation of MAC. Difficulties in studying the hydrogenolysis reaction, however, have been discussed earlier regarding the accumulation of MeCN in solution during hydrogenolysis of **4**—an event that does not occur during the catalytic hydrogenation. To circumvent this draw-

back, it is conceivable that the catalyst precursor containing no MeCN, [Ru((*R*)-BINAP)(1–5-η-C_8H_{11})]BF_4, be used. Preliminary experiments, however, have shown that the only ruthenium species detected by $^{31}P\{^1H\}$ NMR spectroscopy in solution under catalytic conditions are the η^6-arene complexes [Ru((*R*)-BINAP)(H)(η^6-MAC)]BF_4 and [Ru((*R*)-BINAP)(H)(η^6-MAC(H)$_2$)]BF_4.[23] No detectable quantities of a species structurally related to **4** were observed under these conditions. Another possibility that will prevent the formation of MeCN during the stoichiometric hydrogenolysis is the elimination of the phenyl group in MAC(H)$_2$ (which displaces MeCN) by using [Ru((*R*)-BINAP)(MAA(H))(MeCN)]BF_4 or [Ru((*R*)-BINAP)(MAA(H))(sol)]BF_4. Using [Ru((*R*)-BINAP)(MAA(H))(MeCN)]BF_4, that consists of a 72:28 mixture of diastereomers of opposite absolute configuration at their respective α-carbons, also presents the possibility of studying the hydrogenolysis step of both diastereomeric pathways. Characterization of the minor diastereomer would represent the first instance where the structures of both diastereomers have been experimentally determined for an enantioselective catalytic reaction. These structures could serve as approximate models of the diastereomeric transition states in an attempt to determine the origins of enantioselectivity.

It was proposed in Chapter 4 that dissociation of MeCN from **4**, to generate an unsaturated 16-electron species that is receptive towards dihydrogen gas, is the turnover-limiting step in the catalytic cycle. This proposal was supported by the increase in the rate of the catalytic hydrogenation when MeCN was removed from the system and by the decrease in the rate of the stoichiometric hydrogenolysis caused by the accumulation of MeCN during the reaction. We recently found in preliminary experiments that addition of 10 equiv of $MeC^{15}N$ to a solution of **4** in acetone at room temperature resulted in slow exchange of the MeCN ligand for $MeC^{15}N$. No exchange was detected by $^{31}P\{^1H\}$ NMR spectroscopy after 0.5 h and only ca. 60% exchange had occurred after 7h. In comparison, one turnover in the catalytic hydrogenation of MAC in acetone solvent at 30 °C occurs in ca. 1 min. These results suggest that an unsaturated species is required for reaction with dihydrogen gas, and that it is formed through a pathway not involving dissociation of MeCN (possibly through dissociation of the amido or the ester carbonyl

groups of the MAC(H) ligand of **4**). This issue should be further explored in future studies.

The hydrogenolysis of **4** should also be studied using *para*-enriched dihydrogen gas. The advantage of using *para*-dihydrogen gas is that signals in the ^{1}H NMR spectra of hydrogenated products are enhanced by up to 10^5. Such enhancements allow detection of even very minor components in a reaction mixture.[24] These conditions may allow the detection and spectroscopic structure determinations of low concentration intermediates in the catalytic hydrogenation (or in the stoichiometric hydrogenolysis) such as dihydrido complexes. These species were not detected in the present study using conventional NMR spectroscopic methods. It is also well known that reversible addition of *para*-enriched dihydrogen gas to transition-metal complexes in solution causes equilibration of the ortho and para forms (ca. 3:1 at room temperature). An ortho–para interconversion occurring under catalytic or stoichiometric conditions could be interpreted as evidence for the presence of a low concentration dihydrido complex.[2b]

References and Notes

(1) (a) Ashby, M. T.; Halpern, J. *J. Am. Chem. Soc.* **1991**, *113*, 589–594. (b) Ohta, T.; Takaya, H.; Noyori, R. *Tetrahedron Lett.* **1990**, *31*, 7189–7192.

(2) (a) Landis, C. R.; Halpern, J. *J. Am. Chem. Soc.* **1987**, *109*, 1746–1754. (b) Brown, J. M.; Canning, L. R.; Downs, A. J.; Forster, A. M. *J. Organomet. Chem.* **1983**, *255*, 103–111.

(3) Kawano, H.; Ikariya, T.; Ishii, Y.; Saburi, M.; Yoshikawa, S.; Uchida, Y.; Kumobayashi, H. *J. Chem. Soc., Perkin Trans. 1* **1989**, 1571–1575.

(4) A kinetic study of the hydrogenolysis of a ruthenium–carbon bond was previously undertaken: Joshi, A. M.; James, B. R. *Organometallics* **1990**, *9*, 199–205.

(5) For X-ray structure determinations of putative ruthenium–BINAP intermediates in enantioselective hydrogenation of α,β-unsaturated carboxlic acids, see: (d) Chen, C.-C.; Huang, T.-T.; Lin, C.-W.; Cao, R.; Chan, A. S. C.; Wong, W. T. *Inorg. Chim. Acta* **1998**, *270*, 247–251. (e) Ashby, M. T.; Khan, M. A.; Halpern, J. *Organometallics* **1991**, *10*, 2011–2015. These studies showed that the prochiral olefin groups were not bonded to the ruthenium centers in these complexes.

(6) Rautenstrauch, V. Presented at An International Symposium on Chirality, Cambridge, UK, 5–7 September 1999.

(7) Fráter, G.; Bajgrowicz, J. A.; Kraft, P. *Tetrahedron* **1998**, *54*, 7633–7703.

(8) Ohloff, G. *Scent and Fragrances: The Fascination of Odors and their Chemical Perspectives*; Springer–Verlag: Berlin, 1994; pp 151–154.

(9) Bauer, K.; Garbe, D.; Surburg, H. *Common Fragrance and Flavor Materials: Preparation, Properties and Uses*, 2nd ed.; VCH: Weinheim, 1990; p 71.

(10) (a) Troutman, M. V.; Appella, D. H.; Buchwald, S. L. *J. Am. Chem. Soc.* **1999**, *121*, 4916–4917. (b) Lightfoot, A.; Schnider, P.; Pfaltz, A. *Angew. Chem., Int. Ed. Engl.* **1998**, *37*, 2897–2899. (c) Sawamura, M.; Kuwano, R.; Ito, Y. *J. Am. Chem. Soc.* **1995**, *117*, 9602–9603. (d) Schmid, R.; Broger, E. A.; Cereghetti, M.; Crameri, Y.; Foricher, J.; Lalonde, M.; Müller, R. K.; Scalone, M.; Schoettel, G.; Zutter, U. *Pure Appl. Chem.* **1996**, *68*, 131–138. (e) Burk, M. J.; Gross, M. F.; Martinez, J. P. *J. Am. Chem. Soc.*

1995, *117*, 9375–9376. (f) Cabeza, J. A.; Cativiela, C.; Diaz de Villegas, M. D.; Oro, L. A. *J. Chem. Soc., Perkin Trans. 1* **1988**, 1881–1884. (g) Hayashi, T.; Kawamura, N.; Ito, Y. *Tetrahedron Lett.* **1988**, *29*, 5969–5972.

(11) (a) Bouachir, F.; Chaudret, B.; Dahan, F.; Agbossou, F.; Tkatchenko, I. *Organometallics* **1991**, *10*, 455–462. (b) Bouachir, F.; Chaudret, B.; Tkatchenko, I. *J. Chem. Soc., Chem. Commun.* **1986**, 94–96.

(12) See Chapter 2 for the alternative synthesis of **13**.

(13) Schrock, R. R.; Osborn, J. A. *J. Am. Chem. Soc.* **1971**, *93*, 2397–2407.

(14) Frosin, K.-M.; Dahlenburg, L. *Inorg. Chim. Acta* **1990**, *167*, 83–89 and references therein.

(15) Schuster, M.; Blechert, S. *Angew. Chem., Int. Ed. Engl.* **1997**, *36*, 2037–2056.

(16) Schrock, R. R.; Murdzek, J. S.; Bazan, G. C.; Robbins, J.; DiMare, M.; O'Regan, M. *J. Am. Chem. Soc.* **1990**, *112*, 3875–3886.

(17) (a) Zhu, S. S., Cefalo, D. R., La, D. S., Jamieson, J. Y., Davis, W. M., Hoveyda, A. H., Schrock, R. R. *J. Am. Chem. Soc.* **1999**; *121*, 8251–8259. (b) Alexander, J. B.; La, D. S.; Cefalo, D. R.; Hoveyda, A. H.; Schrock, R. R. *J. Am. Chem. Soc.* **1998**, *120*, 4041–4042. (c) Fujimura, O.; Grubbs, R. H. . *J. Am. Chem. Soc.* **1996**, *118*, 2499–2500.

(18) (a) Schwab, P.; Grubbs, R. H.; Ziller, J. W. *J. Am. Chem. Soc.* **1996**, *118*, 100–110. (b) Schwab, P.; France, M. B.; Ziller, J. W.; Grubbs, R. H. *Angew. Chem., Int. Ed. Engl.* **1995**, *34*, 2039–2041. (c) Nguyen, S. T.; Johnson, L. K.; Grubbs, R. H. *J. Am. Chem. Soc.* **1992**, *114*, 3974–3975.

(19) (a) Weskamp, T.; Kohl, F. J.; Hieringer, W.; Gleich, D.; Herrmann, W. A. *Angew. Chem., Int. Ed. Engl.* **1999**, *38*, 2416–2419. (b) Weskamp, T.; Schattenmann, W. C.; Spiegler, M.; Herrmann, W. A. *Angew. Chem., Int. Ed. Engl.* **1998**, *37*, 2490–2493.

(20) (a) Hansen, S. M.; Volland, M. A. O.; Rominger, F.; Eisenträger, F.; Hofmann, P. *Angew. Chem., Int. Ed. Engl.* **1999**, *38*, 1273–1276. (b) Hansen, S. M.; Metz, M.; Rominger, F.; Hofmann, P. *Chem. Eur. J.* **1999**, *5*, 557–566.

(21) Wilhelm, T. E.; Belderrain, T. R.; Brown, S. N.; Grubbs, R. H. *Organometallics* **1997**, *16*, 3867–3869.

(22) ^{1}H NMR (400 MHz, acetone-d_6, 25 °C): δ 9.62 (d, $^3J_{H-H}$ = 12.5 Hz, 1H, Ru=CH–C*H*=C(CH$_3$)$_2$), 15.80 (apparent q, $^3J_{H-H}$ = $^3J_{P-H}$ =12.5 Hz, 1H, Ru=C*H*–CH=C(CH$_3$)$_2$). ^{31}P{^{1}H} NMR (161.9 MHz, acetone-d_6, 25 °C): δ 43.5 (d, $^2J_{P-P}$ = 40.5 Hz, 1P), 44.7 (d, $^2J_{P-P}$ = 40.5 Hz, 1P). ESI-MS (pos): *m/z* 868.2 ((M – BF$_4$)$^+$, exact mass calcd for $C_{51}H_{43}ClNP_2Ru$ 868.2).

(23) Selected NMR spectroscopic data for [Ru((*R*)-BINAP)(H)(η^6-MAC)]BF$_4$: ^{1}H (400 MHz, acetone-d_6, 25 °C): δ –9.16 (dd, $^2J_{P-H}$ = 40.5, 30.0 Hz, 1H, Ru–*H*). ^{31}P{^{1}H} (161.9 MHz, acetone-d_6, 25 °C): δ 50.6 (d, $^2J_{P-P}$ = 44.0 Hz, 1P), 51.3 (d, $^2J_{P-P}$ = 44.0 Hz, 1P).

(24) (a) Morran, P. D.; Colebrooke, S. A.; Duckett, S. B.; Lohman, J. A. B.; Eisenberg, R. *J. Chem. Soc., Dalton Trans.* **1998**, 3363–3365. (b) Harthun, A.; Kadyrov, R.; Selke, R.; Bargon, J. *Angew. Chem., Int. Ed. Engl.* **1997**, *36*, 1103–1105. (c) Harthun, A.; Selke, R.; Bargon, J. *Angew. Chem., Int. Ed. Engl.* **1996**, *35*, 2505–2507. (d) Duckett, S. B.; Newell, C. L.; Eisenberg, R. *J. Am. Chem. Soc.* **1994**, *116*, 10548–10556. (e) Eisenberg, R.; Eisenschmid, T. C.; Chinn, M. S.; Kirss, R. U. In *Homogeneous Transition Metal Catalyzed Reactions*; Moser, W. R., Slocum, D. W., Eds.; Advances in Chemistry Series 230; American Chemical Society: Washington, DC, 1992; Chapter 4. (f) Eisenberg, R. *Acc. Chem. Res.* **1991**, *24*, 110–116. (g) Eisenschmid, T. C. Ph.D. Thesis, University of Rochester, 1989.. (h) Kirss, R. U.; Eisenschmid, T. C.; Eisenberg, R. *J. Am. Chem. Soc.* **1988**, *110*, 8564–8566.